Universidade de Aveiro Departamento de Ambiente e Ordenamento
2008

Jorge Humberto de Melo Rosa Amorim

Modelação da largada aérea de produtos para combate a incêndios florestais

Numerical modelling of the aerial drop of products for forest firefighting

The cover image shows the retardant concentration isocontours obtained by ADM model over a photograph of an aerial drop (www.wildlandfire.com).
My acknowledgment to Richard T. for his help on this figure.

Universidade de Aveiro Departamento de Ambiente e Ordenamento
2008

Jorge Humberto de Melo Rosa Amorim

Modelação da largada aérea de produtos para combate a incêndios florestais

Numerical modelling of the aerial drop of products for forest firefighting

Dissertação apresentada à Universidade de Aveiro para cumprimento dos requisitos necessários à obtenção do grau de Doutor em Ciências Aplicadas ao Ambiente, realizada sob a orientação científica do Doutor Carlos Borrego, Professor Catedrático do Departamento de Ambiente e Ordenamento da Universidade de Aveiro

Apoio financeiro do POCI no âmbito do III Quadro Comunitário de Apoio pelo financiamento do Projecto INTERFACE (POCI/AMB/60660/2004) e da Comissão Europeia no âmbito dos Projectos ERAS (EVG1-2001-00019) e EUFIRELAB (EVR1-CT-2002-40028).

Apoio financeiro da FCT e do FSE no âmbito do III Quadro Comunitário de Apoio pela Bolsa de Doutoramento com a ref.ª SFRH/BD/11044/2002.

Para a Rita, o Francisco e o David.

o júri

presidente

Doutor José Abrunheiro da Silva Cavaleiro
Professor Catedrático da Universidade de Aveiro

Doutor Domingos Filomeno Xavier Viegas
Professor Catedrático da Faculdade de Ciências e Tecnologia da Universidade de Coimbra

Doutor Paulo Alexandre Martins Fernandes
Investigador Auxiliar da Universidade de Trás-os-Montes e Alto Douro

Doutor Carlos Alberto Diogo Soares Borrego
Professor Catedrático da Universidade de Aveiro (Orientador)

Doutor Casimiro Adrião Pio
Professor Catedrático da Universidade de Aveiro

Doutora Ana Isabel Couto Neto Silva Miranda
Professora Associada da Universidade de Aveiro

Doutora Myriam Alexandra dos Santos Batalha Dias Nunes Lopes
Professora Auxiliar Convidada da Universidade de Aveiro

agradecimentos

Gostaria de expressar a minha gratidão ao Prof. Carlos Borrego pela orientação e apoio no decorrer desta investigação, assim como pela oportunidade e pelos meios que me permitiram realizá-lo.

Por terem partilhado o seu conhecimento e experiência com despretensiosa dedicação estou indubitavelmente em dívida para com o Eng. Ryan Becker e o Eng. Greg Lovellette dos Serviços Florestais dos E.U.A., e para com o Dr. Ian Harman do CSIRO Marine and Atmospheric Research na Austrália.

O meu agradecimento também às seguintes pessoas pelos comentários construtivos, opiniões, sugestões, ou simplesmente dúvidas que, em várias ocasiões, se mostraram fundamentais na orientação do meu trabalho: Prof. Rolf Reitz (University of Wisconsin, US), Dr. Gabriel Katul (Duke University, US), Prof. Robert Meroney (Colorado State University, US), Dr. Harold Thistle (Serviços Florestais, E.U.A.) e Dr. Matt Plucinski (CSIRO, Austrália).

À Dr. Ana Miranda, ao Eng. Ryan Becker e à Cristina compete-me agradecer os valiosos comentários, sugestões e correcções do manuscrito.

Estou certo que sem a ajuda dos meus colegas e amigos do Grupo de Emissões, Modelação e Alterações Climáticas (GEMAC), da Universidade, este trabalho ter-se-ia revelado muito mais difícil. Com a Margarida, Joana, Pedro, Cristina, Anabela, Helena, Myriam, Joana F., Oxana, Richard, Vera, João, Carmen e Pedro C. partilhei o equilíbrio entre as discussões científicas criativas e os reparadores momentos de relaxe.

Estou eternamente grato aos meus pais e irmão por sempre me terem incentivado a ir mais além. À Manela, ao Zé e à Catarina devo o incansável apoio. Gostaria de estender o meu agradecimento a toda a minha família, pelo incondicional apoio no decurso de todas as etapas deste trabalho.

E finalmente à Rita e aos meus filhos Francisco e David, estou certo que todos os agradecimentos não seriam suficientes. Eles foram o motivo e a recompensa deste esforço.

acknowledgments

I would like to express my gratitude to my advisor, Prof. Carlos Borrego, for the guidance and support throughout this research as also for the opportunity and the means to conduct it.

For having sheared their knowledge and experience with unpretentious dedication, I am undoubtedly in debt to Eng. Ryan Becker and Eng. Greg Lovellette from the United States Forest Service, and to Dr. Ian Harman from the CSIRO Marine and Atmospheric Research in Australia.

Also my acknowledgment to the following persons for the several constructive comments, opinions, tips, or just doubts that, in many occasions, were fundamental for the orientation of my research: Prof. Rolf Reitz (University of Wisconsin, US), Dr. Gabriel Katul (Duke University, US), Prof. Robert Meroney (Colorado State University, US), Dr. Harold Thistle (US Forest Service) and Dr. Matt Plucinski (CSIRO, Australia).

To Dr. Ana Miranda, Eng. Ryan Becker and to Cristina I must recognise the helpful comments, suggestions and corrections on the manuscript.

I am certain that without the help of all my colleagues and friends of the Research Group on Emissions, Modelling and Climate Change (GEMAC), at the University, this work would have been much harder. With Margarida, Joana, Pedro, Cristina, Anabela, Helena, Myriam, Joana F., Oxana, Richard, Vera, João, Carmen and Pedro C. I've sheared the equilibrium between the creative scientific discussions and the repairing moments of relax.

I am eternally grateful to my parents and my brother, who always incited me to go further. To Manela, Zé and Catarina I owe the indefatigably support. I want to extend my acknowledgment to my entire family, for the unconditional support throughout all the stages of this work.

And finally to Rita and my sons Francisco and David, I'm sure that all the thanks would not be enough. They were the motive and the reward for this effort.

palavras-chave

Incêndios florestais, combate aéreo, escoamento atmosférico, atomização, modelo numérico, optimização.

resumo

Devido ao aumento da frequência e intensidade, os incêndios florestais de grande dimensão e de interface rural-urbana foram identificados pela Organização Mundial de Saúde como uma das ameaças à segurança e saúde públicas no século XXI. A utilização de meios aéreos no combate a incêndios florestais pode ter, se integrada numa estratégia globalizante e eficiente, um papel importante na protecção humana e do património, particularmente em situações exigindo uma rápida intervenção, como fogos emergentes, zonas montanhosas de difícil acesso, ou áreas de risco. A sua eficácia está, contudo, dependente das características do fogo, das condições atmosféricas e da perícia do piloto.

O presente trabalho tem como objectivo o desenvolvimento e validação de um modelo operacional de simulação da largada aérea de produtos no combate a incêndios florestais. O modelo ADM simula o campo de ventos induzido por uma canópia vegetal, sob a influência de diferentes condições de estabilidade atmosférica. A saída do líquido do tanque é calculada com base na geometria e velocidade de abertura das portas. O diâmetro das gotas formadas pela acção das instabilidades de Rayleigh-Taylor e Kelvin-Helmholtz na superfície do jacto é estimado recorrendo à teoria de estabilidade linear. A distribuição por tamanhos e a velocidade das gotas originadas por atomização secundária baseiam-se em correlações experimentais.

O método Lagrangeano é aplicado na simulação da deposição do produto, durante a qual o coeficiente de arrasto resultante da deformação da gota é calculado com base em relações experimentais dinâmicas. O processo termina com a retenção do líquido pela canópia. Os principais dados de saída do modelo são a distribuição espacial das concentrações no solo e o comprimento e área dos diferentes níveis de concentração.

O processo de validação inclui a análise estatística dos resultados através da comparação do perfil vertical do vento simulado com valores medidos em florestas de pinheiro e eucalipto e da comparação dos resultados do ADM com ensaios de largada à escala real realizados com um sistema de descarga convencional (em Marselha, França) e um sistema de caudal constante (em Marana, Arizona, E.U.A.). A análise permitiu inferir um bom desempenho do modelo na vasta gama de condições testadas. A forma da mancha de deposição no solo revela as mesmas características observadas nos dados medidos. O valor médio do erro quadrado normalizado médio para a estimativa dos comprimentos das manchas de cada um dos níveis de concentração é de 0.01, sendo de 0.03 no caso das áreas ocupadas por esses mesmos níveis. Todos os parâmetros estatísticos revelaram um claro cumprimento dos requisitos impostos pelos critérios de aceitabilidade de modelos numéricos.

keywords

Forest firefighting, aerial drop, canopy-induced flow, breakup, numerical model, optimization.

abstract

Due to their increase in frequency and severity, large wildland fires and wildland-urban interface fires have been identified by the World Health Organization as one of the threats to public health security in the 21st century. Within this framework, aerial firefighting can play, if integrated into an efficient global strategy, an important role towards the protection of human lives and patrimony, particularly in situations requiring a rapid intervention, such as emerging fires, inaccessible mountainous areas, or highly risk areas. The efficiency of aerial means is, however, extremely dependent on fire characteristics, atmospheric conditions and pilot expertise.

The objective of the current work is the development and validation of an operational model for the simulation of the aerial drop of firefighting products. The Aerial Dropping Model ADM simulates the vegetative canopy-induced wind flow, under varying atmospheric stability conditions. Vertical turbulent fluxes are calculated through a set of modified flux-profile relationships valid in the atmospheric roughness sublayer. The efflux of liquid from the aircraft tank is calculated based on tank geometry and door-opening rate. The size of droplets formed by Rayleigh-Taylor and Kelvin-Helmholtz instabilities acting on the surface of the jet is estimated applying linear stability theory. The size distribution and velocity of the droplets formed by secondary breakup is based on experimental correlations. A Lagrangian approach is applied to the simulation of the deposition of the spray cloud, during which dynamical drag laws account for droplet shape deformation. The process ends with the canopy retention of the spray cloud. Main outputs are the spatial ground distribution of concentrations, and the line length and area per coverage level.

The validation process includes the statistical analysis of modelling results by the comparison of the computed vertical wind profile with values measured in pine and eucalypt forests and the comparison of ADM outputs against a set of real scale drop tests conducted using a conventional delivery system (at Marseille, France) and a constant flow delivery system (at Marana, Arizona, US). From the investigation of model performance, good accuracy was obtained for the wide range of input conditions tested. Ground pattern shape shows the features observed in measured data. The average normalised mean squared error for the estimation of line lengths is 0.01, and 0.03 for the prediction of areas occupied per coverage level. All the statistical metrics are clearly within the limits imposed by the model acceptance criteria.

Due to its operational characteristics this tool can potentially be used in training activities with firefighters; or in testing the effectiveness of new firefighting chemicals or delivery systems, complementing the data obtained from real scale drop tests.

Table of contents

Acronyms

ABL	Atmospheric boundary layer
ACRE	Additifs Chimiques Rheologie Evaluation. EC research project ENV4-CT98-0729
ADM	Aerial Dropping Model
APP	Ammonium polyphosphate $(NH_4PO_3)_n$
AS	Ammonium sulfate $(NH_4)_2SO_4$
BLS	Boundary-Layer Stripping model
CEREN	Centre d'Essais et de Recherche de l'Entente, France
CFD	Computational Fluids Dynamics
CGS	Centimetre-gram-second system of units
CPU	Central processing unit
DAP	Diammonium phosphate $(NH_4)_2HPO_4$
DSD	Droplet size distribution
DSS	Decision support system
EC	European Commission
EPA	US Environmental Protection Agency
ERAS	Extension Retardant Application System. EC research project EVG1-2001-0019
ETAB	Enhanced Taylor Analogy Breakup model
ETAGS	Experimental Tank and Gating System program
FAO	Food and Agriculture Organization of the United Nations
FT	Fire-Trol
GIS	Geographic information system
gpc	US gallons per 100 square feet (aprox. 0.4 litres per square meter)
GPS	Global positioning system
GUI	Graphical user interface
HADM	High-Altitude Drop Mechanization study
IFR	Instantaneous flow rate
ISL	Inertial sublayer
JICF	Jet in crossflow
JRC	EC's Joint Research Centre
KH	Kelvin-Helmholtz instability
LAI	Leaf area index

LEMTA	Laboratoire d'Energétique et de Mécanique Théorique et Appliquée, France
LES	Large eddy simulation
LWF	Large wildland fires
MAP	Monoammonium phosphate $NH_4H_2PO_4$
MOST	Monin-Obukhov Similarity Theory
NS	Navier-Stokes equations
NTUA	National Technical University of Athens, Greece
PATSIM	Pattern Simulation model
PC	Phos-Chek
pdf	Probability distribution function
RAM	Retardant Application Model
RAM	Random access memory
RANS	Reynolds-averaged Navier-Stokes equations
RSL	Roughness sublayer
RT	Rayleigh-Taylor instability
SDTF	Spray Drift Task Force
SI	International System of Units
SMD	Sauter mean diameter
TAB	Taylor Analogy Breakup model
UA	University of Aveiro, Portugal
US	United States of America
USDA-FS	US Forest Service
VMD	Volume median diameter
VOF	Volume-of-Fluid
WHO	World Health Organization
WUI	Wildland-urban interface
2DVD	2D-Video-Distrometer
3D	Tridimensional

Notation

a	Acceleration, $m.s^{-2}$
a or $a(z)$	Leaf area density, $m^2.m^{-3}$
a, b	Droplet dimensions (polar radius and equatorial radius), mm
a_1, a_2	Empirical constants (incoming solar radiation calculation), $W.m^{-2}$
$a_1, a_2, a_3, b_1, b_2, b_3, b_4$	Empirical constants (dynamical drag model), —
A_E or A_p	Effective area of discharge, m^2
AR	Aspect-ratio, —
Bo	Bond number $\left(\rho g L^2/\sigma\right)$, —
Bo	Bowen ratio, —
b_1, b_2	Empirical coefficients (total incoming solar radiation calculation), —
B_0	Proportionality constant (fluid breakup modelling), —
C	Empirical constant (flow rate calculation), $kg.m^{-4}$
C	Concentration of product at ground, $l.m^{-2}$ or gpc
c_1, c_2, c_3	Empirical constants (net radiation calculation), $W.m^{-2}.K^{-4}$, $W.m^{-2}$, —
c_D	Drag coefficient, —
c_p	Specific heat capacity of dry air, $J.kg^{-1}.K^{-1}$
C_{RT}, C_τ	RT breakup time constants, —
C_u, C_v	Empirical coefficients in droplets velocity (secondary breakup) , —
d	Average bias, $m.s^{-1}$ or m or m^2
d or d_t	Displacement height, m
D_c	Diameter of the droplet formed by primary breakup, m
D_{cc}	Diameter of the droplet formed by secondary breakup, m
D_L	Droplet diameter, m or mm
D_{mm}	Mass mean diameter, m or mm
D_V	Equivalent vent diameter, m
D_{10}	Arithmetic mean diameter, m or mm
D_{30}	Volume mean diameter, m or mm
D_{32} or SMD	Sauter mean diameter, m or mm
e	Ellipticity, —
f	Drag factor, —
f	Fraction of droplets considered (primary breakup), —
f_t	Correction factor for secondary breakup time, —
$FAC2$	Factor of two, —
FB	Fractional bias, —

F_D	Kinematic canopy drag, N
g	Gravitational acceleration, $m.s^{-2}$
h	Canopy average height, m
H	Sensible heat flux, $W.m^{-2}$
H	Total hydraulic head, m
H_a	Dropping height, m
H_T, L_T, W_T	Tank dimensions (height, length and width), m
H_m	Meteorological parameters measurement height, m
k	Von Karman's constant, —
K	Wavenumber, m^{-1}
k_1, k_2	Empirical erosion constants, undetermined
l	Mixing length, m
L	Characteristic length, m
L	Obukhov length, m
L_c	Canopy-drag length scale, m
L_D, W_D	Tank's doors dimensions (length and width), m
$L1$, $L2$	Parameters for the analysis of droplet drift, m
$LAI(z)$	Leaf area index for a given height, $m^2.m^{-2}$
LAI	Cumulative LAI at ground, $m^2.m^{-2}$
m, n	Fluid parameters (power law model for non-Newtonian fluids), $Pa.s^n$, —
MG	Geometric mean bias, $m.s^{-1}$ or m or m^2
Mo	Morton number $\left(g\mu_G^4\lvert\rho_L-\rho_G\rvert/\rho_G^2\sigma^3\right)$, —
MMD	Mass median diameter, mm
n	Fractional opaque cloud cover, —
n	Number of measured profiles, —
N	Number of droplets produced by breakup, —
$NMSE$	Normalized mean squared error, —
Oh	Ohnesorge number $\left(\mu/\sqrt{\sigma\rho L}\right)$, —
p	Wind profile power-law exponent, —
P	Pressure, Pa
q	Dispersion parameter for the Rosin-Rammler distribution, —
r	Pearson correlation coefficient, —
r'	Surface albedo for the sun on the meridian, —
$r(\phi_s)$	Surface albedo as a function of solar elevation angle, —
R	Total incoming solar radiation, $W.m^{-2}$
Re	Reynolds number (UL/ν), —

R_n	Net radiation, W.m^{-2}
R_p, L_p, V_p	Fluid parcel dimensions (radius, length and volume), m, m, m^3
R_0	Incoming solar radiation at ground level for clear skies, W.m^{-2}
s	Elastic strain of the fluid, —
s	Standard deviation of the root-normal distribution
s or S	Surface area, m^2
T	Ambient temperature, K
t	Time, s
Ta	Taylor number $\left(Oh_L\sqrt{We_G}\right)$, —
t_b	Total time for secondary breakup, s
t_d	Deformation time, s
t_α	Door opening time, s
u, v, w	Fluid velocity components in Cartesian coordinates, m.s^{-1}
u_*	Friction velocity, m.s^{-1}
U	Fluid velocity, m.s^{-1}
U_a	Aircraft velocity, m.s^{-1}
U_h	Wind velocity at canopy top, m.s^{-1}
U_m	Wind velocity measured at height H_m, m.s^{-1}
U_r	Relative velocity between fluids, m.s^{-1}
U_{rim}	Normal velocity due to rim expansion (secondary breakup), m.s^{-1}
$U(z)$	Wind velocity at height z, m.s^{-1}
$V_{atomized}$	Volume of liquid atomised in the current time-step, m^3
VG	Geometric variance, m^2.s^{-2} or m^2 or m^4
V_L	Volume of fluid dropped, m^3
V_x	Accumulated volume of fluid deposited along the x-axis, l
w_A	Acceleration-dominated velocity, m.s^{-1}
w_B	Bernoulli velocity, m.s^{-1}
w_E	Velocity of efflux, m.s^{-1}
We	Weber number $\left(\rho U^2 L/\sigma\right)$, —
w_t	Fluid velocity at the top, m.s^{-1}
x, y, z	Cartesian coordinates, m
z_0 or z_{0m}	Roughness length, m
z_*	Height of the RSL, m

α	Door opening angle, º or rad
β	Canopy parameter, —
β_N	Canopy parameter in neutral conditions, —
$\dot{\gamma}$	Shear rate, s^{-1}
η	Non-Newtonian viscosity, Pa.s
ΔQ	Flow rate of liquid released in a given time-step, $m^3.s^{-1}$
Δt	Time-step, s
Δt	Total release time, s
ΔV	Volume of liquid released in a given time-step, m^3
δ	Liquid film mean thickness, mm
δx	Percentage error, %
ζ	Surface layer scaling parameter, —
θ_a	Aircraft direction (in meteorological coordinates), º
θ_m	Wind direction (meteorological coordinates) measured at height H_m, º
Λ	Wavelength, m
μ	Dynamic viscosity, Pa.s or cP
μ_a	Apparent viscosity, Pa.s
ρ	Mass density, $kg.m^{-3}$
σ	Surface tension, $N.m^{-1}$
σ_{sb}	Stefan-Boltzmann constant, $W.m^{-2}.K^{-4}$
τ	Shear stress, Pa
τ	Reynolds stress, Pa
τ_{KH}, τ_{RT}	Breakup time for KH and RT waves, s
τ_L	Droplet response time, s
ϕ	Shape factor, —
ϕ_m	Stability function for momentum, —
ϕ_s	Solar elevation angle, º
Φ_m	Wind profile similarity function, —
ψ_m	Integrated form of the similarity function, —
Ω	Frequency of the wave, s^{-1}

Overlines

$\hat{X}$	RSL variable
$\overline{X}$	Average value

Superscripts

X'	Fluctuating quantity

Subscripts

X_i	Coordinate direction in Einstein notation (i = 1, 2, 3)
$X_{(i)}$	Current iteration (time-step)
$X_{(i-1)}$	Previous iteration (time-step)
X_c	Child droplet from primary breakup
X_{cc}	Child droplet from secondary breakup
X_D	Aircraft tank doors
X_G	Gas phase
X_{KH}	Kelvin-Helmholtz instability
X_L	Liquid phase
X_m	Measured value
$X_{\max}$	Maximum value
X_p	Liquid parcel (parent droplet)
X_r	Relative value
$X_{(real)}$	Real value
X_{RT}	RT Rayleigh-Taylor instability
X_T	Aircraft tank
X_x	Variation in the x-axis
X_0	Initial value

List of figures

List of tables

1. Scope and structure of the work

Fire is an important natural phenomenon in the dynamics of numerous ecosystems, often an essential agent in the maintenance of biodiversity and productivity over time, and also an important and widely used management tool [Heinselman, 1978 in FAO, 2001; FAO, 2007a]. Although existent, the positive impacts of fires are however much less accepted or even perceived than their negative counterparts. Due to the frequency of their occurrence and the magnitude of the effects on environment, health, economy, security and patrimony, forest fires have growingly become a major subject of concern, interest and debate among decision-makers, firefighters, researchers and citizens in general. Reasons beyond this are evident: loss of natural and man-made patrimony, various risks to human health or even loss of human lives, high financial costs; in sum, one of the threats to public health security in the 21st century according to the report recently published by the World Health Organization [WHO, 2007]. For the same reasons, this is also a challenger research topic for scientists involved in each aspect or stage that composes the global scope of fire science, namely: fuel characteristics, fire and smoke behaviour, ecosystems functioning and biodiversity, decision support tools, fire metrology, fire risks and hazards, fire suppression management, wildland urban interfaces management, and socio-economical aspects.

Worldwide attention to the negative facet of wildfire's impacts has been highlighted by a series of extreme fire events that have occurred in Southeast Asia, Australia, North and South America, Russia and Southern Europe [WHO/UNEP/WMO, 1999; FAO, 2001, 2007a; WHO 2007]. According to the statistical data compiled by the European Commission's Joint Research Centre (JRC) [EC, 2007], in the five southern European countries alone (Portugal, Spain, France, Italy and Greece), more than 13 million hectares of forest burned from 1980 to 2006, with an annual average of nearly 500,000 ha. At the global scale, the major satellite data evaluation conducted by the JRC in partnership with several other institutions indicated that in the period from 2000 to 2007 the annual value of area burnt worldwide exceeded 4 million km^2 in three fire years [a] (2001-2, 2003-4 and 2006-7), with a variation between 3.5 million km^2 in 2002-3 and 4.5 million km^2 in 2006-7 [Tansey et al., 2007].

[a] A fire year is defined as the period from the 1st of April to the 31st of March on the following year.

The magnitude of the effects and the worldwide occurrence of the problem alert to the necessity of efficient techniques on the prevention and suppression of forest fires to be adopted and implemented. These should be integrated into a global strategy of fire risk reduction and optimization of firefighting technical means and procedures. In specific situations (such as with emerging fires, inaccessible mountainous areas, when wildfires pose a threat to populations, or in sensible areas requiring a rapid intervention), the aerial drop of firefighting products assumes a significant importance towards the overall efficiency of the firefighting strategy, in particular if integrated with all the means available in the terrain. This was realised by the United States Forest Service (USDA-FS) early in the 1920's when the first attempts at using airtankers in firefighting tasks were started. In these first drops different devices were tested, such as tin cans, surplus fuel tanks, paper bags, hose trailed behind the aircraft, and even oak beer kegs attached to a parachute. Similar drop experiments were performed in New Zealand and Canada in the 1940's and early 1950's using water-filled wax paper bags. These early concentrated load systems proved to be ineffective mainly because of the difficulty inherent to a precise delivery, but also because of the risk to people and structures on the ground due to the falling loads and to the induced spread of embers. The first operational airtanker drops occurred in 1955 (see Figure 1-1), with the retrofitting of surplus military aircraft from the Second World War at a relatively low cost [George et al., 1976; Newstead and Lieskovsky, 1985; George and Johnson, 1990; Pickler, 1994; Robertson et al., 1997a; USDA-FS, 2001; Xanthopoulos, 2003; Oegema, 2004].

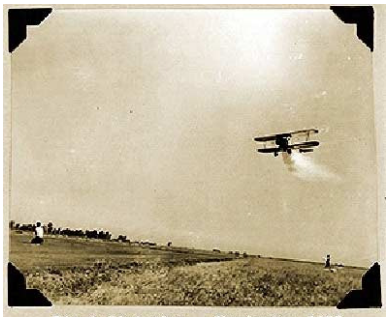

Figure 1-1. The Stearman (Boeing) Model 75 biplane, transformed from a military trainer aircraft used throughout Second World War into a water load airtanker. The first drop on a fire was made during the Mendenhall fire, in the 13th of August 1955, at Mendocino, US [url 1].

Although both the aircraft and the delivery systems used in firefighting operations have realized profound improvements, the efficiency of aerial resources still is, however, highly dependent on the expertise of the pilot in dealing with the complexity of fire behaviour, the aggressive atmospheric conditions (in particular, air flow turbulence), the terrain characteristics and the reduced visibility (see Figure 1-2).

Figure 1-2. Aerial drops facing reduced visibility conditions [url 2].

The design objective of an aerial delivery system is to guarantee an efficient ground coverage under adverse meteorological conditions. However, prior to reaching the target, the behaviour of the liquid is determined by the balance of forces involved. Initially, the relative velocity between the liquid and the gas phases will cause the deflection of the jet column. Simultaneously, the bulk product undergoes a sequence of complex breakup mechanisms that transform it into ligaments and droplets with variable sizes that constitute the spray region with the typical cloud shape visible in Figure 1-3. This process is further complicated by the fact that droplets are formed by a two-stage breakup process, constituted by a primary and secondary breakup, resulting in a wide range of sizes. Moreover, droplet dynamics within the gaseous flow is governed by a number of factors; the importance of each is dependent on the droplet size as well as on the turbulent characteristics of the airflow, the latter intimately dependent on the roughness typology of the surface. The process ends with the gravitational settling of the product, through the penetration and coating of the canopy, as shown in the right image of Figure 1-3.

(a) (b)

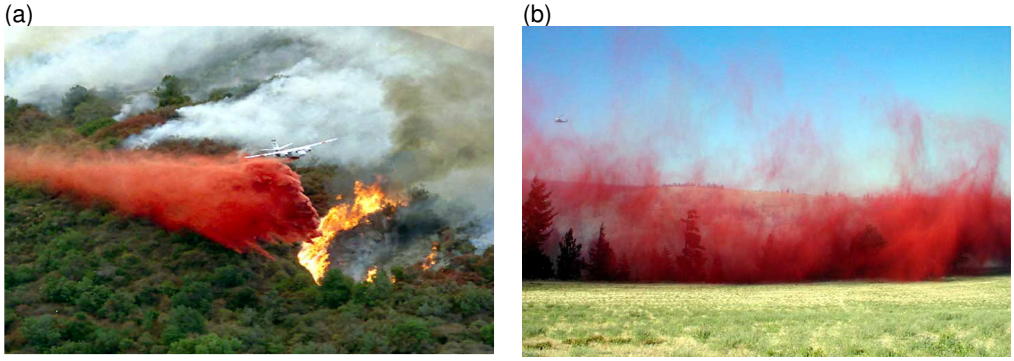

Figure 1-3. (a) The photo of an S-2 drop over an active fire shows the deformation and breakup of the bulk liquid due to the effect of release speed and gravitational acceleration. As the liquid falls, its volume is several times expanded due to air entrainment (copyright by Mike Meadows [url 1]). (b) The trees are wrapped by the falling retardant cloud. Interception mechanisms control the extent of the product penetration (copyright by Zimm. Elk Heights Fire (US), July 31, 2004 [url 1]).

The correct application of the product should guarantee its deposition in the spot and quantity adequate for retarding or extinguishing the fire front, as a way of permitting the subsequent attack by ground resources. However, as the factors that determine the dropping efficiency are numerous, without the use of operational decision support tools this is potentially an operation with unpredictable results, highly conditioned by the skills of the pilot. The use of modelling tools that can aid the pilot's decision on the best way to conduct the drop is of primary importance towards an improved efficiency.

Despite the development of powerful numerical codes for fluid dynamics modelling, associated with the rapid growth of hardware performance, it is generally accepted that although "the parameters affecting drop performance and ground distribution are known, it is still difficult to determine the ground distribution from specific known parameters" [Giménez et al., 2004]. The complexity inherent to the numerical simulation of this process results from a number of factors, namely the rheological behaviour of the product, the outflow of the bulk liquid from the tank, the formation of droplets by a cascade of breakup mechanisms, the interaction with the air flow, or the unsteadiness and quickness of the entire process and the large amounts of liquid involved.

The few numerical models that were developed in this field of application are already too old, or lack validation. Although the USDA-FS have had a distinct leading role on the experimental assessment of the effect of rheology on the overall efficiency, as shown by the several scientific reports published on the subject over the last 50 years (e.g., Andersen et al. [1976], Lovellette [2004]), the most detailed modelling effort dates back to the 70s, when a systematic battery of field trials and laboratorial experiments were conducted in order to establish the basis for the development of the operational model PATSIM [Swanson et al., 1978]. That model is substantially based on empirical concepts, which although resulting from extensive experimental data sets, restricts its application to the range of conditions tested. More recently in Europe, an effort to understand the behaviour of retardant fluids in the atmosphere, as also its impacts on the ecosystems, has been made by a consortium of research teams financed by the European Commission under the scope of the projects ACRE and ERAS. On the modelling topic, however, several questions were left open, namely in what relates to the dynamical transition of the bulk liquid into droplets. Although highly accurate and time-consuming Computational Fluids Dynamics (CFD) numerical codes were tested, a lack in validation with experimental data leaves doubt about the predictive capacity of the developed models.

The research programs that have been conducted worldwide in order to understand the behaviour of firefighting fluids in the atmosphere have lacked the analysis of the

mechanisms that control the aerodynamic breakup of the product, which result in the formation of a combination of large mean droplet sizes, wide size distributions and extreme droplet shapes. Also, the interaction of the liquid with the involving atmosphere, in particular the effect of forest stands on the exchange of momentum and air flow turbulence, and how this impacts the gravitational settling of the spray cloud has been neglected, mainly due to the complex logistics inherent to the measurement of deposition within forest stands. In fact, real scale drops have been made mostly over bare ground, not allowing assessment of effect induced by vegetative canopies. Numerical models have the necessary characteristics for filling these gaps, although the unavailability of experimental data constitutes a problem facing the validation process of the codes. Moreover, the magnitude and extent of the perturbation introduced by the presence of a dense vegetative canopy is intimately dependent on the temporal and spatial evolution of the breakup process, since it determines when and where each newly formed droplet is "injected" into the air stream.

In this context of the urgent necessity of efficient firefighting operations to be adopted, and the unavailability of accurate decision support systems (DSS) for the optimisation of aerial drops, the objective of the current work is to develop and validate the Aerial Dropping Model ADM, an operational model for the simulation of the behaviour of firefighting liquids in the atmosphere, the time and space evolution of the cloud, and the surface wetting pattern. The calculation procedure covers the following main stages:

- Canopy-induced wind flow;
- Outflow of the liquid from the aircraft tank;
- Liquid breakup;
- Shape distortion and dynamic drag of the formed droplets;
- Gravitational settling through spray cloud deposition mechanisms;
- Canopy interception and ground deposition of the spray cloud.

One of the main difficulties encountered during the work relied on the spatiotemporal description of the breakup process, since few experimental data are available for the range of typical flow conditions. An analogy with the studies developed under the scope of fuel injection systems analysis is established, allowing capture of the dynamics of the liquid breakup in the atmosphere. The interaction of the atmosphere with the bulk fluid and the formed droplets, particularly in the presence of vegetative stands, is evaluated. In

order to incorporate the canopy-induced flow effects on the behaviour of the firefighting product, a methodology for the simulation of the response of the wind flow to canopy structure and atmospheric stability is implemented.

The model performance is investigated against real scale measured data. A wide range of input conditions, including delivery system type, flight parameters, meteorological conditions and product characteristics, is tested. Due to its characteristics and capabilities, namely the fast-running code and the friendly-access graphical user interface, this operational tool can potentially be used namely with the following purposes:

- Formation, training and demonstration activities with pilots, aerial resource coordinators, civil protection personnel and ground-firefighters.
- Testing of the effectiveness of new firefighting chemicals and discharge systems, complementing the data obtained from real scale drop tests and laboratorial experiments. The user control over the input parameters allows the effect on ground pattern to be assessed for a wide range of release scenarios, avoiding the natural variability and irreproducibility of field conditions.

The current document is organized as follows. Some aspects related with the occurrence of forest fires in southern European countries are referred in Chapter 2, as also its connection to air pollution episodes and human health outcomes. The types and characteristics of the available products and delivery systems for aerial firefighting are described.

The state-of-the-art from Chapter 3 presents the scientific background on the aerial drop of firefighting products by briefly referring the most important work conducted during the last 50 years on this matter. The spatial and temporal evolution of the breakup process, the physical processes involved, and the interaction of the liquid with the involving gas are interpreted in light of the current understanding of the breakup of liquid jets and droplets in a gaseous medium. Also, some of the most important studies, their achievements and limitations, are referred and briefly analysed. The state of knowledge on the mechanisms involved in the adjustment of a turbulent boundary layer to a vegetative canopy and on the potential drift of free-falling droplets due to the effect of the canopy-induced vertical wind shear is presented.

Chapter 4 describes the structure and mathematical formulation of the developed Aerial Dropping Model ADM. The different modules that compose the numerical tool are

analysed, with emphasis on the discharge module that describes the variation with time of the flow rate of released product; on the wind profile module for the simulation of canopy-induced flows under varying atmospheric stability conditions; and on the breakup module.

In chapter 5, the validation process is described and the results interpreted. This process is composed of three stages:

- The individual validation of the canopy flow module by comparison with vertical wind profiles measured in a pine forest (at North Carolina, US) and in a eucalypt forest (Southeast Australia).
- The individual validation of the discharge module in the description of the liquid outflow from the tank through the comparison with flow rate factory values.
- Intercomparison of ADM model outputs with a set of real scale drop tests performed in Marseille, France, using a conventional delivery system, and in Marana desert, US, with a constant flow delivery system.

The wide range of dropping conditions tested in the validation process (as the rheological properties of the product, or meteorology) allow a detailed analysis of the effects of input parameters on a product's behaviour. This validation process helps contribute to a better understanding of the multiple interrelated phenomena involved.

2. The aerial suppression of forest fires

Although forest fires are a natural phenomenon that exerts a number of relevant benefits to the biological processes occurring in the nature, they have multiple adverse impacts on human security and health and on ecosystems, either at local, regional or even global scales. Within this context, an efficient firefighting system is crucial to the protection of human lives and man-made/natural patrimony, but also to the minimisation of the potential outcomes arising from the exposure of professionals and populations to hazardous concentrations of emitted air pollutants.

During the last 40 years many efforts have been made towards the development of new chemical products and application systems for improving the efficiency of firefighting techniques. At the European level, the Southern countries reveal distinct approaches to the problem and particularly a different use of aerial resources and fire retardants.

2.1. Fire severity in southern Europe

Within the framework of the Global Wildland Fire Network of the United Nations International Strategy for Disaster Reduction, the Food and Agriculture Organization of the United Nations (FAO) recently prepared a global assessment report on fire management [FAO, 2007a]. In this document, which involved a major analysis of satellite data and regional statistics reports, there is scientific evidence that both the frequency and severity of forest fires occurring in the wildland-urban interface (WUI) and large wildland fires (LWF) are increasing, as a response to various factors, namely the increase of fire risk under the influence of climate change and land-uses changes. Fires occurring in the interfaces between agriculture and forestry and between wildland and residential/urban areas, in particular, are pointed out as a major, continuing and potentially increasing threat to human life, health and livelihoods, to economic development, and to the environment [FAO, 2007a].

The complexity and importance of the problem is increased by the multi-spatial dimension of forest fires, exhibited not only through the destructive power of fire but also through the significant amounts of various air pollutants contained in smoke. Especially when occurring in the vicinity of large urban agglomerations, biomass burning events can potentially represent an important public health issue for the affected populations due to the severe degradation of air quality, as recently shown by LWF that have occurred in Southeast Asia, Australia, South America and Russia, but

also in Southern Europe, as in the case of Coimbra, Portugal, in August 2005 (shown in Figure 2-1).

Figure 2-1. Series of images from the Coimbra WUI fire in August 2005. (a) Nocturnal photograph of the fire near the city limits; (b) satellite image from the 24th of August [url 2]; and visual comparison of the city centre (c) during the fires and (d) without smoke.

Consequences on the health of local populations and firefighters can potentially occur due to smoke exposure. Adverse health effects begin with acute, instantaneous eye and respiratory irritation and shortness of breath that can develop into headaches, dizziness, and nausea lasting up to several hours. In particular the personnel involved in firefighting operations can experience acute, subchronic and chronic effects due to frequent and prolonged exposure to unhealthy air pollutant concentrations during daily activity [Brustet et al., 1991; Ward et al., 1993; Miranda et al., 1994, 2005a, b, and 2006; Reinhardt et al., 2001].

On the other hand, notwithstanding that even LWF are limited to some hundreds of hectares, their impacts can be reported far beyond the physical limits reached by fire spread. There is today enough scientific data that support the knowledge that, depending on meteorological conditions, biomass-burning plumes and haze layers can persist in the atmosphere for long periods of time, influencing the chemical and optical characteristics of the atmosphere, as shown by the NASA mission conducted at South Pacific in which 20-day-old smoke plumes were found [Blake et al., 1999]. Several recent research papers have shown that smoke can travel up to 1000 km or more [Browell et al., 1996], having impacts at the continental scale [Conrad and Ivanova

1997; Fearnside, 2000; Wotowa and Trainer, 2000; Dennis et al., 2002; Amiro et al., 2001] or intercontinental scale [Forster et al., 2001; Spichtinger et al., 2001; Fromm and Servranckx, 2003].

A frequently referred and extensively studied extreme smoke event occurred in 1997 as a consequence of the prolonged and uncontrolled forest fires in Indonesia. The continuous burning of about 1 million hectares of forest, plantation and scrub land, only in the period from July to October, was responsible for a dense haze that encompassed a total population of over 200 million people in Indonesia and the neighbouring countries of Malaysia, Philippines, Thailand and Viet Nam [Davies and Unam, 1999; WHO, 2007]. Among the more than 12 million people exposed to critical air quality conditions in Indonesia, it was estimated that there were over 1.8 million cases of bronchial asthma, bronchitis and acute respiratory infection [Dawud, 1999].

In Portugal, as a consequence of the intense 2003 fire season, abnormally high air pollutant concentrations were registered on air quality monitoring stations, several of which were located inside urban areas. At Lisbon, hourly-averaged concentrations of PM_{10} (particles of 10 μm or less in aerodynamic diameter) surpassed the 500 $\mu g.m^{-3}$ (10 times higher than the daily averaged limit value defined by the European Air Quality Legislation) [Miranda et al., 2005b]. An increase in the number of hospital admissions due to respiratory and cardiovascular diseases, and even mortality, was reported. According to the official estimates by national authorities, more than one thousand individuals needed medical assistance as a consequence of smoke inhalation [EC, 2004a; MAI, 2003]. Again in 2005, smoke intoxication was pointed out as one of the most important causes for medical assistance required by an equivalent number of persons [EC, 2006].

The official statistics regarding the number of forest fires and burnt area are systematically compiled and published by the EC through their JRC in the “Forest Fires in Europe” report series. According to these statistical data, an increasing trend in the total number of forest fires occurring in the five Southern European countries has been registered, as represented in the graph from Figure 2-2, even though it is accompanied by a slight tendency of decrease in area burned. Portugal has contributed to the general growth of the number of fires, although the area burned has shown a tendency for increasing in the period from 2000 to 2006 [EC, 2007].

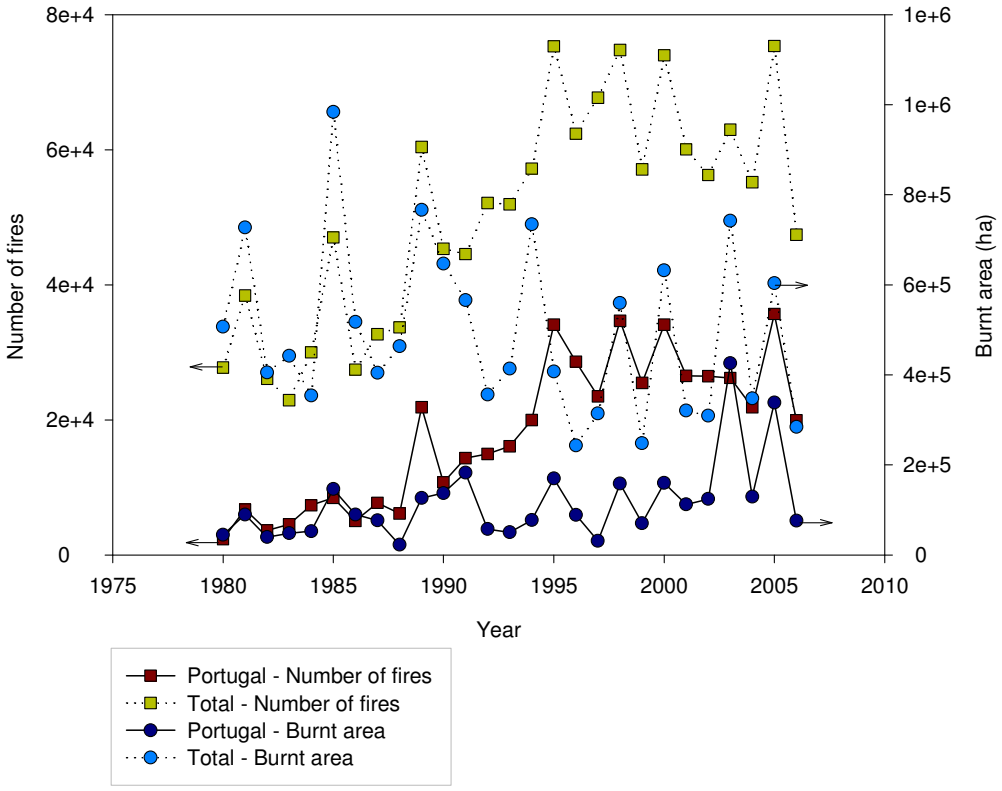

Figure 2-2. Number of fires and burnt area (in ha) in Portugal and in the sum of the five Southern Member States corresponding to the period from 1980 to 2006. A square symbol denotes the annual number of fires and circle the respective burnt area. Full line refers to Portuguese values and dotted to total (sum of the five Southern Member States). Arrows indicate the axis in which the values should be read.

As shown in Figure 2-3, during the period from 1980 to 2006 Portugal has had the leading position in terms of number of fires, with 36% of the total; it is third, after Spain and almost equal with Italy, in terms of area burned, with 23% of the sum of the five countries in the same period [EC, 2007]. Focusing the analysis on the most recent fire seasons, Portugal has increased its relative importance in terms of number of forest fires from 32% of the total in the period between 1980 and 1999 to 44% from 2000 to 2006. Even higher growth was registered compared to the other four countries in terms of burnt area, which increased in Portugal from 17% of the total in 1980-1999 to 42% in 2000-2006. The reason for this increase in area burned in the period from 2000 to 2006 is related to the two particularly severe fire seasons of 2003 and 2005, which are clearly seen in the peaks of Figure 2-2. The summer of 2003 was, in fact, one of the most severe fire seasons of the last decades in Southern Europe, especially in Portugal and France [EC, 2007]. Statistics show that this was by far the worst forest fire season in Portugal since 1980, constituting a major operational challenge for the involved firefighting forces [LBP, 2003]. In comparison with the averaged 7,000 reported fires in the period between 1993 and 2002, in 2003 there was in fact a

decrease to 4,700 fires. However, this was not accompanied by less burnt area. Due to the occurrence of 85 fires with more than 500 ha (representing 86% of the area), the total burnt area was approximately 4 times higher than the annual average for the same period, with more than 425 thousand hectares [DGF, 2003; MAI, 2003]. During the 2005 fire season, both the total area burned and the number of fires were well above the averages for the reporting period in the five European countries, with approximately 88% of the fires and 85% of the total burnt area in Spain and Portugal.

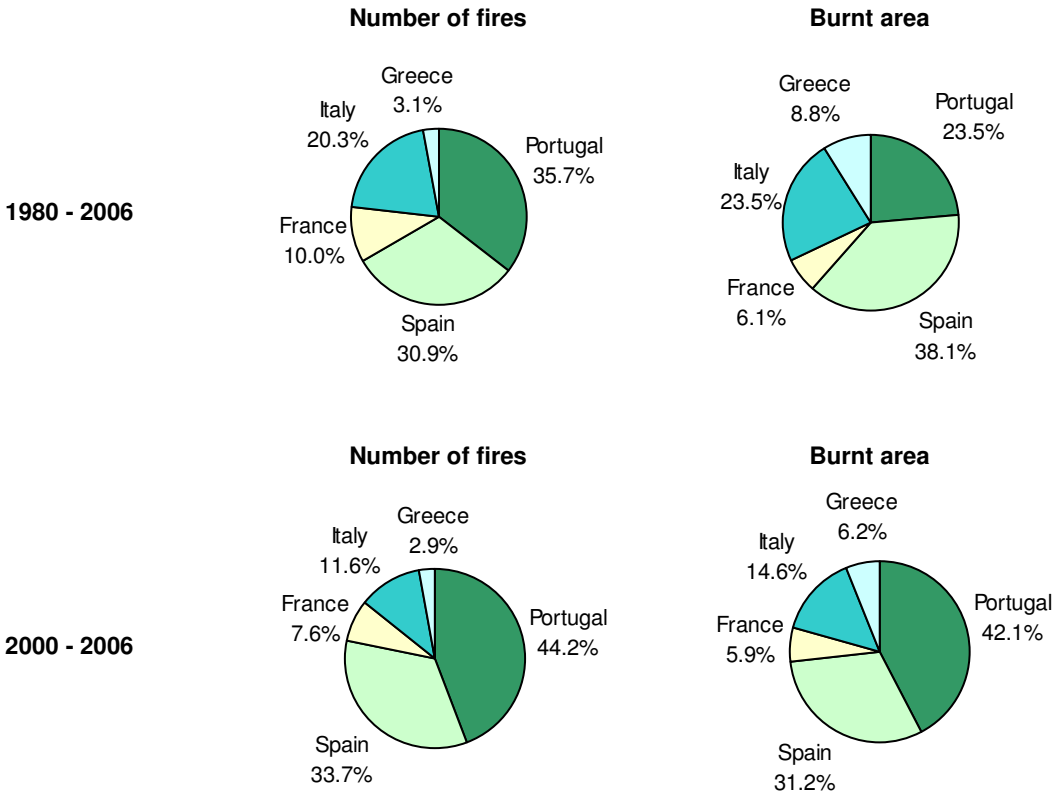

Figure 2-3. Comparative analysis of the number of forest fires and area burned in the five Southern European countries in the periods 1980-2006 and 2000-2006.

The aerial firefighting resources have a special importance in the overall suppression strategy (as it will be analysed in section 2.2). Therefore, the aerial means involved in fire suppression activities are, in general, proportional to the severity of the fire season. In this sense, the total flying time (in number of hours) gives an interesting indication of the engagement of aerial means to a given fire season. In the Portuguese case, the State and private contracted air resources flew an average of 4,900 hours for the period between 2001 and 2006, although with significant differences between fire seasons, as shown in the graph from Figure 2-4, in response to the corresponding fire activity (evaluated in terms of burnt area). Comparatively, the abnormally extensive area burned in 2003 did not have a proportional intervention of aerial resources, most

likely because the upper limit of the response capacity was surpassed. Even in private forest land, there was a decrease in the number of flying hours (227 hours, against the 352 hours in average from 1992 to 2005, and the 700 hours in 1995) and, consequently, on the volume of water dropped (5 times less than in 1995) [CELPA, 2002 to 2007]. In 2005, the entire fleet of aerial means from the State and private sector flew more than 10 thousand hours in prevention, suppression and coordination operations [CEFF, 2007; CELPA, 2006], representing a significant increase comparing to previous years as evidenced in the graphic. Also in Spain, in a response to the high temperatures and absence of precipitation in the territory during the summer of 2005, there was a strong commitment of aerial resources in firefighting operations, surpassing the 9 thousand hours of flying time and nearly 32 thousand drops of water and retardants [MMA, 2006].

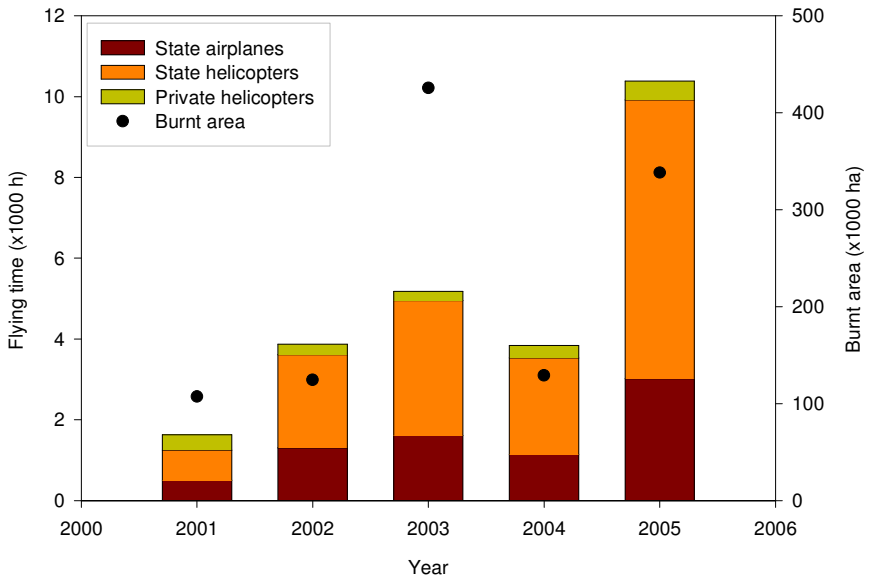

Figure 2-4. Number of hours of flight for the private and State's aircraft, and annual burnt area in the period from 2001 to 2005 [CEFF, 2007; CELPA, 2002 to 2007; CEEMACIF, 2005; DGRF, 2006]. The State's aircraft include the national aerial fleet, the loaned private aerial means and the aircraft from mutual assistance mechanisms.

The efficiency of aerial resources in the sum of firefighting operations conducted in terrain can be assessed at different levels and using distinct evaluation parameters (see, e.g., Barrios and Solé [2004], Plucinski et al. [2007]). In this scope, the relation between the burnt area and the number of flying hours gives some indication of the overall efficiency of aircraft during the season. It should be noted, however, that a wide range of factors contribute to the conditions that determine the fire severity; in particular, the effect of meteorology, prior and during the fire season, although not under the scope of this analysis, is indissociable from the agents intervening and

influencing the suppression effectiveness. At the European scale, the hours of flight during firefighting operations is not consistently and systematically published or compiled. Despite the temporal gaps, the data from the official EC reports on forest fires in Southern Europe from 2001 to 2006 [EC, 2002 to 2007] and National reports [CEEMACIF, 2005; CEFF, 2007; MMA, 2007], were compiled and graphically represented in Figure 2-5 on a comparative basis for Portugal, Spain, France and Italy. The analysis shows that, particularly in 2003, the rate between the number of hectares burned in Portugal and the total flying time was significantly above the other countries, with 82 $ha.h^{-1}$ against 21 $ha.h^{-1}$ in Spain, 8 $ha.h^{-1}$ in France and 7 $ha.h^{-1}$ in Italy. This indicator decreased significantly in Portugal in 2005 (33 $ha.h^{-1}$), although this was the fire season with the second highest value of burnt area since 1980, and particularly in 2006 when a value of approximately 4.3 $ha.h^{-1}$ was reached.

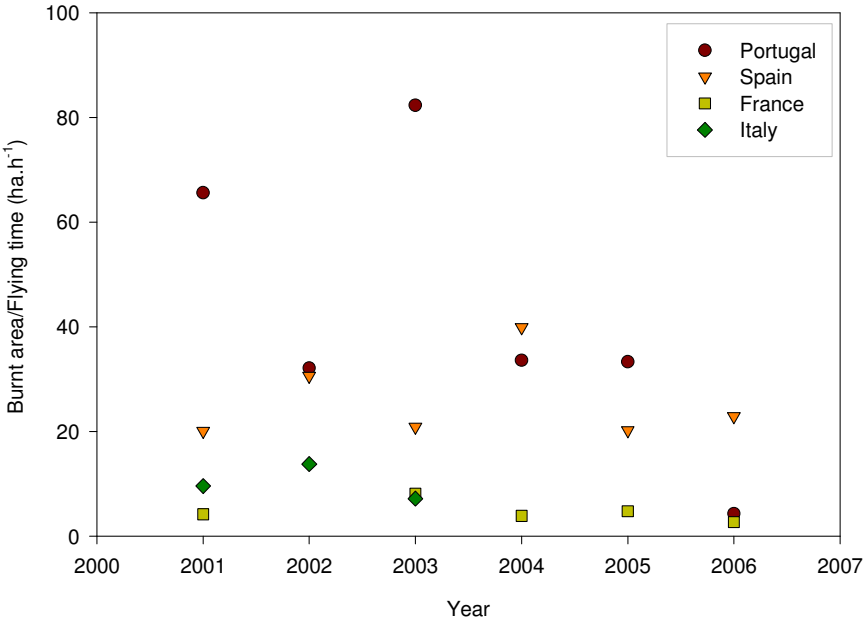

Figure 2-5. Rate between the burnt area and the number of flying hours ($ha.h^{-1}$) between 2001 and 2005 in Portugal, Spain, France and Italy.

The southern European member-states have distinct approaches to the use of aerial means during firefighting operations. In Portugal, the aerial firefighting system is significantly dependent on the loan of private aerial means by the State and on mechanisms of mutual assistance with other member states, activated through the Civil Protection Monitoring and Information Centre (MIC) or under bilateral agreements. Particularly relevant is the bilateral cooperation agreement established in 1992 between the Portuguese Republic and the Kingdom of Spain for technical cooperation and mutual assistance in Civil Protection issues [CEEMACIF, 2005; CEFF, 2006]. In

addition to the firefighting system contracted by the State, and in collaboration with the National Authority for the Civil Protection (ANPC), a group of companies from the Portuguese Paper Industry Association, the AFOCELCA, intervene with a set of hired helicopters in properties that represent nearly 6% of the Portuguese forest [CELPA, 2006]. Each year, the number of aerial means available is around 50, excluding aircraft from other countries.

In Spain, aerial resources have represented a significant part of the firefighting strategy since 1969. Currently more than 60 aircraft, both contracted private resources and those owned by the Ministry of the Environment [Hernández et al., 2007], compose the Spanish fleet. During the period from 1991 to 2004, an average of 18% of the total number of fires in the country saw the intervention of aircraft and helicopters in suppression, transportation, coordination and observation activities [MMA, 2006]. Examples of the intense response of Spanish aerial resources to forest fires are numerous. One can refer to the 5 days fire that occurred in 2001 in Castellón, in which 2.4 million litres of water and flame retardants were dropped by a total of 34 aircraft [EC, 2002], or in 2004 at Minas de Riotinto (Huelva), the third largest wildfire in Spain since 1968, which consumed more than 25,000 hectares of forest, and was suppressed by the intervention of 35 aircraft that flew for more than 766 hours and dropped 7.5 million litres of water [EC, 2005].

Between 1980 and 2006, Greece had the lowest averaged number of fires and the second lowest value of total area burnt in South Europe (see Figure 2-3). With a total of 64 firefighting aircraft, both public and contracted, the aerial fleet available for firefighting purposes has become among the strongest in the world, especially given the size of the territory. This is justified, in part, by its topographical characteristics, but mostly by the large number of islands with a very high fire potential and extremely inhospitable ground firefighting conditions [Sauvagnargues-Lesage et al., 2006].

France has an interesting profile in terms of firefighting resources versus the incidence and extent of forest fires, with 10% of the total of fires between 1980 and 2006 and only 6% of the area burned in the five countries (see Figure 2-3). In this context, France has had a particular interest in the use of retardant products since the first aerial drops of retardants in European territory in 1979 [Calabri, 1983]. As an example, in the years of 2001 and 2003 alone, approximately 2.85 and 5 million litres of retardant products, respectively, were used in France [EC, 2002 and 2004a]. The quick response of aircraft to isolated areas and the use of chemical retardant products to fight fire limits fire spread prior to the arrival of ground forces has been responsible, according to the National authorities, for the efficient suppression of incipient fires and the small number of fires exceeding 5 ha [EC, 2006].

In fact, the use of fire retardants is not very extensive in Europe compared to the US, where an average of 60 million litres per year have been used, mostly from aerial application [Suter, 2000]. While the Canadian market represents approximately 30% of the quantities used in the US, in Europe this rate is only 10% based on the estimates by Oegema [2004]. Depending on the intensity of the fire season, the use of retardants recorded peaks in the US in 2000 and 2002, in Canada in 2003, and in France and Spain in 2003. European countries (especially Italy, Greece and Portugal) have preferred the use of water (dropped with the amphibious aircraft Canadair CL-215 and CL-415).

The most appropriate product to apply should be assessed based on the type of fire, forces involved, efficiency, etc. Also the use of aerial resources should be judiciously evaluated given a number of factors that can potentially limit or prevent its use in particular circumstances (see, e.g., Plucinski et al. [2007]). One of the factors is the high risk associated with the aerial drop of firefighting products, mostly due to the necessity of attaining a correct positioning for the dropping, while maintaining an active avoidance of the nearest obstacles (such as mountains, trees and electric cables) and maintaining control of the aircraft in extremely adverse environmental conditions, including reduced visibility conditions, increased turbulence and thermal updrafts. This fact is obvious from the number of casualties related to aerial operations. According to the JRC's data compilation [EC, 2001 to 2007], 23 deaths of pilots were reported since the year 2000. In Greece, 14 pilots died during firefighting operations from 1973 to 2000 [FAO, 2001; Xanthopoulos, 2007]. In the US, there were 131 fatalities related to aircraft accidents since 1959, representing 21% of the number of firefighters' deaths [NWCG, 1997, 2007a and 2007b].

One of the main advantages of aircraft, and airplanes in particular, is quick access to the fire, in particular in mountainous areas, which are frequently inaccessible to ground forces. The correct application of the product should guarantee its deposition in the spot and quantity adequate for retarding or extinguishing the fire front, as a way of permitting the subsequent attack by ground means. However, the factors that determine the efficiency of this operation are numerous, which is thus highly conditioned by flight characteristics, local meteorological conditions, fire behaviour, and naturally by the expertise of the pilot. The development of operational DSS can potentially increase the efficiency of aerial dropping.

2.2. Aerial delivery systems

A large expansion in the use of airtankers and helitankers has occurred since the first aerial drops in the mid 20th century. The role of aircraft in firefighting operations has seen an increasing prominence in several countries worldwide over the last 50 years, and currently it is present in almost all components of fire management, as shown in Figure 2-6.

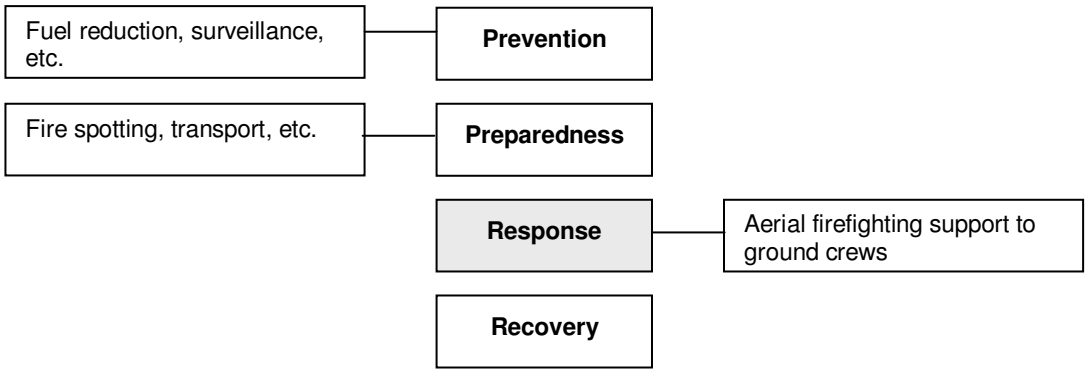

Figure 2-6. Role of aircraft in the fire management process (adapted from Plucinski et al. [2007]).

Aircraft can have distinct roles in the diverse stages of a forest fire (e.g., Barrios and Solé [2004], CEEMACIF [2005]):

- aerial surveillance of under-protected areas;
- fast response to an ignition;
- operation in terrains inaccessible to ground forces (see Figure 2-7);
- delivery of high amounts of water or retardants in short intervals of time;
- transport of firefighters and equipments for ground attack;
- protection, search and rescue of firefighters and at-risk population;
- coordination of the global strategy;
- support to the communications system in hilly areas;
- transmission of aerial images to the coordination centre.

Figure 2-7. Aerial drop from an amphibious aircraft at Sierra da Grova fire (Pontevedra, Spain) [MMA, 2007].

However, the use of aerial means should be evaluated in terms of the aspects that can limit their use, namely (e.g., Barrios and Solé [2004], Vélez [2000]):

- economic: high hourly cost;
- operational: availability and proximity of the needed backup infrastructures;
- technical: the good functioning is conditioned by visibility conditions (in particular, most aircraft can operate only during daylight), meteorology and altitude.

Moreover, there are a number of factors that influence the overall dropping operation effectiveness, namely: delivery system; physical and chemical properties of the firefighting product (particularly its rheological behaviour); and meteorological conditions. Specifically in the case of retardants, these parameters were classified and evaluated in the review by George et al. [1976] and recently by Giménez et al. [2004].

Depending on the characteristics of the fire and the available aerial means, there are two suppression methods:

- direct attack: the water or chemicals are dropped close to the fire edge or directly on an active flame;
- indirect attack: temporary retardant lines are built a considerable distance away from the active edge of the fire. This technique is often required in fast-spreading or high-intensity fires.

Based on the type of product dropped, these operations can be further classified as:

- waterbombing: consists in dropping fresh or sea water, and is mostly effective for large fires, on condition that the water is dropped in large enough quantities and frequently enough for each drop to be made before the effect of the previous drop has dissipated and the fire has reignited. This method is very effective when there are short distances between the source of water and the fire, especially in flat regions.

- fire bombing: corresponds to the dropping of long-term chemical retardants, having a lasting effect against the fire advance, and allowing a considerably lower frequency of drops. This technique is mainly suitable for indirect attack and it is restricted to land-based operations because of the large proportion of chemical in the mix (10% or more). However, the time spent getting to and from the airport is often counterbalanced by the effectiveness of less frequent drops, and by the higher speed of aircraft used for this mission when comparing to CL-215.

There are a number of reasons beyond the preference for a given technique. For instance, Canadian forest land tends to contain plentiful, large, uninhabited lakes with good approach and departure routes for amphibious aircraft, while much US forestland is in high, steep mountainous land with fewer, smaller, less accessible lakes. The amphibious aircraft that dominate Canadian aerial firefighting enable fast, effective continued response to most wildfires in Canadian territory. The same aircraft must travel greater distances in the US to reload, which reduces their efficiency. This has led to the use of aerial tankers as the preferred fire retardant delivery system in the US.

According to the type of product dropped and the technique used during the drop, the characteristics of the aircraft and the delivery systems used vary significantly. The aircraft involved in aerial firefighting operations include fixed-wing multiengine airtankers, fixed-wing single-engine airtankers, helicopters with fixed tanks and helicopters with suspended helibuckets [Suter, 2000]. According to tank capacity, airtankers are classified from type I to type IV. Fire suppression organizations may choose from small agricultural aircraft carrying less than one cubic meter of water or retardant to huge “heavyweight” aircraft such as the Boeing 747, which carries about 80 m^3; the DC-10, with 42 m^3 [R. Becker, pers. communication]; the Ilyushin-76TD [url 3], also with 42 m^3; the Martin Mars amphibious waterbomber [url 4] (see Figure 2-8), with a delivery capacity of 27 m^3; the BV-47/CH-47 “Chinook”, which can carry nearly 12 m^3 in a bucket; and the Erickson helitanker [url 5], with nearly 8 m^3 load capacity.

(a) (b)

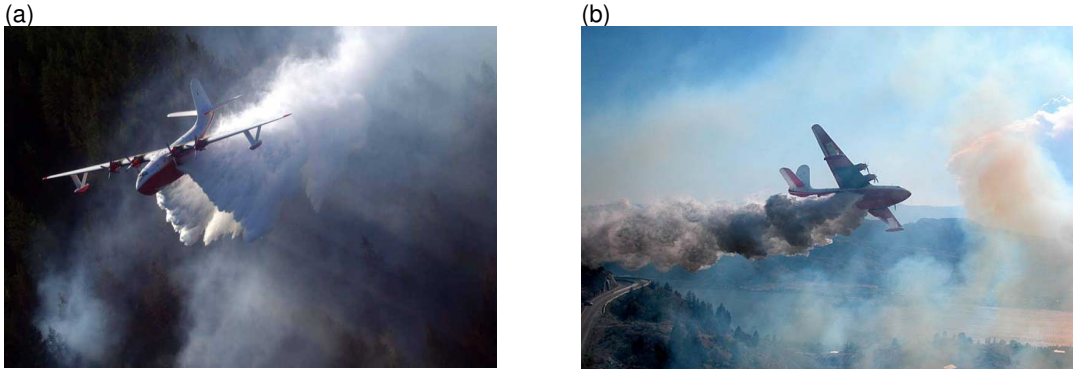

Figure 2-8. Aerial drop of a Martin Mars during real firefighting situations (a: photo by Al Hymers. Ontario, Canada. b: photo by Ian Smith. Osoyoos Fire, British Columbia, Canada. August, 2003 [url 1]).

Helicopters started being used in firefighting later than the airplane. In spite of their higher cost per ton of load delivered to the fire when compared to airplanes, they quickly started gaining acceptance due to their versatility, manoeuvrability and ability to land in relatively small openings [Xanthopoulos, 2003]. Helicopters can drop water, foam or retardant to the fire either from a suspended open-topped collapsible helibucket or from a tank attached to their bottom, and their capacities vary between 0.5 and 10 m^3.

The fixed-wing aircraft used in firefighting operations can be multi-engine, which have typically 6 to 11 m^3 capacity, or single engine, with 1.7 to 3 m^3 capacity and are commonly used to apply agricultural products. There are basically three types of aerial delivery systems used in fixed-wing aircraft by forest firefighting services all around the world [Suter, 2003 and 2006]:

- Conventional Aerial Delivery System: in conventional tanks the retardant load is divided into several compartments that can be released individually or grouped. If multiple compartments are released simultaneously, an increase of both the flow rate and hence the coverage level is obtained. On the other hand, if the release is sequential the length of the drop is increased while maintaining the coverage level of a single compartment release. There are a variety of conventional tanks with different shapes, compartments and capacities.

- Constant Flow Delivery System: the system employs a computer-controlled door system that offers, once the flight crew establishes the flow rate, a constant coverage level over the duration of the drop. The effect of changing the volume released will only change the length of the drop, not the flow rate. The system achieves constant flow by modifying the door opening as the liquid level falls inside the tank. According with the characteristics of the aircraft, there

are several different systems that provide a constant flow at the exit. Examples are the Retardant Aerial Delivery System (RADS II) or the Air Tractor Fire Retardant Delivery System (FRDS).

- Modular Aerial Fire Fighting System (MAFFS): this equipment employs a computer-controlled door system that offers flow rate combinations selected by the flight crew. It was originally designed and developed in 1974 in the US, as a response to a number of catastrophic forest fires burned across Southern California that overwhelmed the airtanker fleet's ability to respond. It is a self-contained reusable delivery system with 11.4 m^3 load capacity that can be loaded onto a military cargo transport, typically a Lockheed C-130 Hercules, which then allows the aircraft to be converted into an airtanker. Five tank modules store the retardant or water under pressure, and guarantee all coverage levels up to 1.6 $l.m^{-2}$. Personnel using MAFFS can make variable drops over the fire, with flow rate preselected at the control module. At maximum flow rate, a MAFFS-equipped C-130 can discharge its entire load in less than seven seconds (see Figure 2-9), and it can be re-loaded and flight-ready in less than seven minutes. The second generation of this system is called MAFFS 2, which holds also 13.6 m^3 and achieves all coverage levels up to 3.2 $l.m^{-2}$.

Figure 2-9. On-board photographs of a MAFFS drop [url 6].

While in the Conventional Aerial Delivery System and in the Constant Flow Delivery System the retardant liquid is released in its bulk form and is then deformed and atomised during the fall; in MAFFS, on the contrary, the product is already atomised at the release due to the pressurized delivery from the nozzles, although droplets can also undergo further breakup due to aerodynamic forces.

Wind flow conditions can potentially reduce the effectiveness of aerial drops, especially when made at high altitudes or using unthickened products. The aircraft company Boeing has under development the Precision Aerial Fire Fighting (PAFF) [url 7], which uses several hundreds of small packages containing a total of more than 60 m^3 of

liquid. These are stacked on cardboard pallets that are dropped from a C-17 as in the aerial delivery of humanitarian aid. Although the system has not yet been submitted to airdrop testing, the objective is to have a computer-aided precise targeting for the aerial drop of firefighting products.

2.3. Types and characteristics of firefighting products

Before analysing the physical phenomena that are behind the aerodynamic breakup and subsequent gravitational settling of the product cloud in the atmosphere, it is important to address the physical and chemical characteristics of the products. Fire retardants are defined as any substance that, by chemical or physical action, reduces or inhibits combustion, thereby slowing or retarding the rate of spread of the flame front [Strickland, 1984], and are commonly found in the form of liquid or slurry applied aerially or from the ground during a fire suppression operation. Under this definition plain water is also a fire retardant, although it is rarely thought as such. More commonly the term is used to refer to a long list of chemical agents that have a more complex retarding effect on the fire than the simple cooling effect of plain water [Xanthopoulos, 2003].

In fact, water is by far the most used firefighting product mainly because of its cost-efficiency, its availability and the known remarkable cooling properties. However, its high surface tension results in a limited ability to coat and wet fuels, which means that only a small proportion of an aerial drop may impact on the fire because of the rapid drainage of the liquid through the fuel bed. Also its natural transparent characteristics enable the radiant energy to heat, dry and ignite fuel particles [Stechishen and Murray, 1988]. Instead, there are basically three classes of wildland firefighting chemicals that are used to increase the ability of water-based firebreaks to contain fire spread, overcoming the problems inherent to the use of just plain water: fire retardants, foam fire suppressants and water enhancers (certain products are sometimes combined to provide the benefits of both) [NIFC, 2007; Oegema, 2004; Xanthopoulos, 2003; USDA-FS 2007a, 2007b and 2007c]. The application rate (in mm) necessary to stop a fire burning through coated fuel is comparatively shown for water and retardant in Figure 2-10.

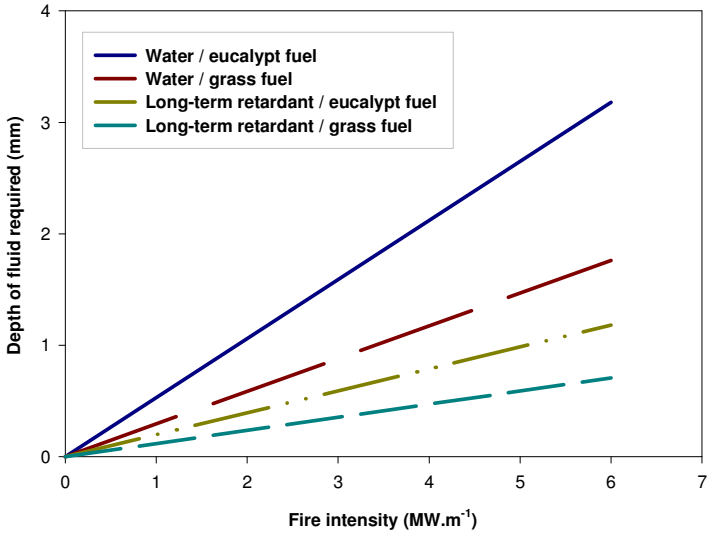

Figure 2-10. Relation between fire intensity in grass and Eucalypt fuel load and the coverage level (depth) of water and long-term retardant required to hold a fire [adapted from Loane and Gould, 1986 in Plucinski et al., 2007].

Beyond cost, another factor contributing to the general preference of fire agencies for the use of water in firefighting aerial operations is related to the potential consequences on ecosystems associated to the application of retardants, which is one of the aspects causing more apprehension among public opinion. Although several works on the environmental effects of retardants have been performed worldwide, the mechanisms through which these products actuate and the complete extent of the expected damages is yet far from completely understood. These impacts are mostly associated to the potentially adverse effects on aquatic ecosystems. Especially when dropped from airplanes, erratic atmospheric conditions and reduced visibility may cause accidental delivery onto streams or lakes. Various studies have documented the retardant toxicity in surface waters through laboratory trials (reviewed by CSIRO [2000] and Giménez et al. [2004]); during field measurements in permanent water bodies and temporary wetlands [Angeler et al., 2005]; or during real firefighting situations [Boulton et al., 2003]. The environmental risk assessment has also covered the potential ecological impacts on soils, plants and fauna; the health risk related to the direct handling of the product, due to contamination of water ways and food chains [Labat, 2003; Labat Environmental, 2007] and as a consequence of the increased emission of particles during combustion [Philpot et al., 1972; Kalabokidis, 2000; Miranda *et al.*, 2006; UA/NTUA/CEREN, 2005]; and the effect on structures and equipment [WFCS, 2007].

Foaming agents specifically designed for wildland fire suppression have been available since 1985, although only since the beginning of the 1990s have foams found an increasing use in wildland firefighting, with the application from aerial or ground application equipment, directly to the fire area to slow or stop combustion. The foams used in wildland firefighting are class A, because their characteristics and behaviour make them appropriate for class A fires (i.e., fires burning wood and other combustible materials, excluding fires burning petroleum products (class B) or metals like magnesium (class D) and fires involving electricity (class C)). Fire suppressant foams depend on the water contained in the mixture to be effective and when that water has evaporated, they are no longer effective. These chemical products contain foaming and wetting agents. The first affect the effectiveness of the aerial drop, the water drain and the adhesion to the fuel surfaces. The wetting agents increase the ability of the drained water to penetrate fuels. Class A foams are provided as foam concentrates that are mixed with water at a ratio that is normally between 0.1 and 1%. Appropriate selection of concentrate dilution and application equipment will yield a range of suppressants from simple solutions and wetting agent (wet foam) for mop-up, through fluid foam for wet line to dry foam to protect fuels (homes, etc.). Through the typical mechanism of action, the foam clings to horizontal and vertical fuels excluding air from the fuel, enveloping the volatile combustible vapour and the fuel interface, and resisting disruption due to wind, heat, and flame.

Retardants are applied ahead of fire to reduce the rate of spread and intensity, although most retardants also act as suppressants if applied directly to the flame. Retardants can be divided into two types according to their characteristics: long-term and short-term.

Short-term retardants and water enhancers are primarily thickeners intended to alter the rheology of the drops, improving the effectiveness of the aerial drops (namely through the minimization of drift) and increasing the adhesion to fuels. Their effectiveness as cooling agents depends on their ability to retain moisture and to keep the fuel wet, since the effect lasts until the water has evaporated. The recent products classified as water enhancers, which are found in the form of firefighting gels and absorbents, can be applied from ground or air. These are especially suited for the protection of structures, due to their increased adhesion to vertical surfaces, although they can also be appropriate for application in vegetation, depending on concentration.

Long-term retardants are flame inhibiting chemicals which through chemical reactions alter the combustion process, decreasing the fire intensity and slowing the advance of the fire, even after the water has evaporated. The active agent is a fertilizer salt mixed into water, which acts as the host medium. These salt solutions are polymeric

compounds that involve some form of phosphate or sulphate in different combination with ammonium. Typical compounds are summarized in Table 2-1. The commercial brands in the last column will be hereafter referred [NWCG, 2000].

Table 2-1. Common active fire retardant salts. *n* is the chain length.

Chemical name	Acronym	Chemical formula	Brand
Monoammonium phosphate	MAP	$NH_4H_2PO_4$	Phos-Chek®
Diammonium phosphate	DAP	$(NH_4)_2HPO_4$	
Ammonium sulfate	AS	$(NH_4)_2SO_4$	
Ammonium polyphosphate	APP	$(NH_4PO_3)_n$	Fire-Trol®

Typical ratios of salt to water are 1:10 by weight. The density of such a mixture can exceed that of pure water by up to about 10%. In the process, the water provides little or no contribution to the retardant effect and is primarily a vehicle to carry the salt through a dripping process that coats the vegetation, aiding in the uniform dispersal of the chemical over the target area. Even after the water has dried, the chemicals maintain a long-term retardant effect until their removal from the fuel by rainfall or other weathering effects. Combustion is reduced by coating the fuel, thus preventing the escape of volatile gases, and by diluting the combustible gases of pyrolysis with noncombustible gases emitted by the retardant in the presence of heat [Calabri, 1983; Giménez et al., 2004; Xanthopoulos *et al.*, 2005].

A colorant such as iron oxide is often added in either long-term or short-term retardants to make the treated area easily distinguishable by firefighters on the ground and by the next pilot as a line is laid out by successive releases. Fugitive colorants, which bleach out over a period of days or weeks when exposed to sunlight, are sometimes used instead of iron oxide. Other compounds can be additionally included in retardant mixtures, as anti-corrosive agents that slow the wear and tear on the delivery equipment, and bactericides or other stabilizing agents. These compounds are expected to have little effect on the cloud formation processes.

The most important additive is the thickening agent that may be added to long-term or short-term retardant mixtures. The thickener increases the viscosity, surface tension, and elasticity of the liquid, thus controlling its breakup [Andersen et al., 1974a and 1974b]. The principal purpose is to make larger droplets that fall more rapidly, and give

a more compact wetting pattern at the surface by reducing the spread due to wind drift and turbulence. The high viscosity may also help the liquid to stick to vegetation surfaces rather than dripping quickly to the ground. Also, the evaporation rates of liquids tend to decrease as viscosity increases, so thickeners increase the effectiveness of short-term retardants.

Guar gum is a thickener commonly used to substantially increase the viscosity of the retardant, e.g. to more than 1000 cP [b] for some long-term fire retardants (comparing with the 0.8 cP viscosity of water at 30 ºC and 1 atmosphere pressure). Adding a thickening agent such as gum reduces droplet drift and promotes strong adherence on fuels. Also a cohesive agent like attapulgite clay has been used as a thickener, although it has a very little thickening effect on the final mixture. By slightly increasing product viscosity, clays give good cohesiveness to the drop and increase retardant coverage level on aerial fuels.

The various products give water-like or gum-like retardants, the latter with varying viscosity, which are more or less advantageous depending on the characteristics of the fire, the types of forest fuels and on the method of dropping. Fire retardants are available in the form of two main commercial brands: Phos-Chek® (PC) [url 8] and Fire-Trol® (FT) [url 9], both with a long list of trade name products available. Originally produced by Monsanto Co. and Chemonics Industries Inc., respectively, both products are currently manufactured by ICL Performance Products [url 10], although FT is available through the subsidiary Astaris Canada Ltd. In Europe, the most common retardant brand is FT, which is commercialized by the French company BIOGEMA S.A. [url 11]. The reason behind the preference of the European Fire Agencies for FT is mainly related with the lower heights at which aerial drops are made when comparing to the US, and thus not requiring the use of a highly thickened product like PC.

Table 2-2 presents laboratory measurements of the mass density, dynamic viscosity and surface tension of water and some common fire retardants.

[b] The SI unit for viscosity is Pa.s, although it is also commonly expressed in the CGS unit system as centipoise (1 cP = 10^{-3} Pa.s).

Table 2-2. Values of mass density (ρ), dynamic viscosity (μ) and surface tension (σ) for water [Pallas and Harrison, 1990] and typical retardant solutions [Andersen et al., 1974a; Van Meter and George, 1981; ACRE, 2000].

Liquid	ρ (kg.m^{-3})	μ (Pa.s)	σ (×10^{-3} N.m^{-1})	Mixture
Water	~1000	1.003×10^{-3} (at 20 ºC) 8.910×10^{-4} (at 25 ºC)	72.86±0.05 (at 20 ºC) 71.99±0.05 (at 25 ºC)	—
Fire-Trol 931		0.13 – 0.16	80.00±0.50 (at 25 ºC)	1:4
Fire-Trol 100		2.07 – 2.49	92.00±2.00 (at 24 ºC)	167 g / 0.5 l water
Phos-Chek XA		1.05 – 1.65	46.30±0.10 (at 22 ºC)	68 g / 0.5 l water

The degree of thickening (ranging from plain water to heavily gum-thickened) is probably the most important factor determining the size of the formed droplets. The chemical (i.e., type of product and mix-ratio) and physical properties (e.g., expansion ratio) of the applied products will ultimately alter the canopy retention, from the extreme behaviour of water, that easily penetrates the canopy and has little ability to adhere to elevated fuels; through foams that, on the contrary, penetrate and coat the fuel particles with a drainage dependent on the level of moisture contained in the fuel; to gum-thickened retardants that easily adhere to fuels. Depending on the concentration of the thickener, the products used in aerial firefighting can be classified as water-like or unthickened products (< 60 cP), low viscosity (60 – 250 cP), medium viscosity (250 – 1000 cP) and high viscosity (> 1000 cP), and thus have distinct application (see Table A-1) [Vandersall, 1994; Robertson *et al.*, 1997a].

Depending on the type and concentration of the thickener in the retardant solution the rheological behaviour of the fluid is significantly affected, as referred. At this level of analysis, the simplest example is brought by water, a Newtonian fluid in nature. In this type of fluids a plot of shear stress (τ) versus shear rate ($\dot{\gamma}$) at a given temperature is a straight line with a constant slope that is independent of the shear rate. The behaviour of a Newtonian fluid is described by Newton's law of viscosity, in which the constant of proportionality, i.e., the slope of the referred straight line, is the dynamic viscosity of the fluid, yielding [Bird et al., 2007]:

$$\tau = \mu \cdot \frac{du}{dz} \qquad \textbf{Eq. 2-1}$$

where the derivative is the velocity gradient perpendicular to the direction of shear (with units of s^{-1}).

In a non-Newtonian fluid, on the contrary, the ratio of the shear stress to the shear rate is not a constant when subjected to a shear deformation. Therefore, the non-Newtonian viscosity (η) is a function of shear rate, which represents the magnitude of the rate-of-strain (or rate-of-deformation) tensor. Various models have been proposed for representing the non-Newtonian viscosity function $\eta(\dot{\gamma})$, from which the most widely used is the power law model described by the Ostwald-de Waele constitutive relationship [Bird et al., 2007]. This simple relation describes the non-Newtonian viscosity curve over the linear portion of the log-log plot of the viscosity versus shear rate according to:

$$\eta = m \cdot \dot{\gamma}^{n-1} \qquad \textbf{Eq. 2-2}$$

where *m* is the consistency parameter (which has units of $Pa.s^n$) and *n* is the dimensionless flow behaviour index, through which the type of fluid can be classified as follows:

$$\begin{cases} n < 1 \Rightarrow \text{Shear - thinning or pseudoplastic (non - Newtonian)} \\ n = 1 \Rightarrow \text{Newtonian} \\ n > 1 \Rightarrow \text{Shear - thickening or dilatant (non - Newtonian)} \end{cases} \qquad \textbf{Eq. 2-3}$$

Basically, this means that in a pseudoplastic fluid the viscosity decreases with increasing shear rate under conditions of shear stress, while in a dilatant fluid the opposite occurs.

From the systematic studies conducted by Andersen et al. [1974a, 1974b and 1976] on the rheology of fire retardants, it was found that FT100, FT931 and PC-XA undergo shear-thinning. This property causes the apparent viscosity of the liquid at the high shear rate experienced by the retardant under aerial dropping conditions to be smaller than that measured at lower shear rates by a conventional viscometer.

However, due to its elastic nature, the effective viscosity of PC-XA, which is a gum thickened product, remains relatively high during breakup, resulting on a relatively large final droplet size. On the other hand, FT100, which is a clay thickened retardant, is non-elastic in nature and consequently exhibits a reduced, shear thinned, viscosity during breakup, resulting on a smaller diameter of the formed droplets. FT931 has a lower apparent viscosity than FT100, but exhibits some elasticity which causes its terminal droplet size to be comparable to that of FT100.

Especially in retardants with viscoelastic characteristics, the non-Newtonian viscosity can be estimated through the apparent viscosity [c] (μ_a) and the recoverable shear (i.e., the elastic strain, *s*) of the fluid by the equation:

$$\eta = \mu_a (1 + s) \qquad \textbf{Eq. 2-4}$$

in which the value of both μ_a and *s* may depend on the shear rate of the liquid while it is undergoing breakup. Based on an extensive series of measurements, a least squares fit was made by Andersen et al. [1974b and 1976] on experimental curves of non-Newtonian viscosity versus shear rate, resulting in the following empirical equation for PC-XA:

$$\eta = 84.19 - 70.43 \cdot \log \dot{\gamma} + 29.3 \cdot (\log \dot{\gamma})^2 - 6.991 \cdot (\log \dot{\gamma})^3 + 0.943 \cdot (\log \dot{\gamma})^4 - 0.0528 \cdot (\log \dot{\gamma})^5 \qquad \textbf{Eq. 2-5}$$

when $1 \le \dot{\gamma} \le 2 \times 10^5\ s^{-1}$.

In the case of FT100, the experimental relation takes the form:

$$\eta = 2.033 - \log^{-1}\left[2.033 - 0.5089 \cdot \log \dot{\gamma} - 0.2292 \cdot (\log \dot{\gamma})^2 + 0.03937 \cdot (\log \dot{\gamma})^3\right] \qquad \textbf{Eq. 2-6}$$

in the range: $10 \le \dot{\gamma} \le 6 \times 10^4\ s^{-1}$, and

$$\eta = 184 \cdot \dot{\gamma}^{-0.746} \qquad \textbf{Eq. 2-7}$$

when $1 \le \dot{\gamma} \le 10\ s^{-1}$.

Finally, the expression for the viscosity of FT931 was defined as:

$$\eta = \log^{-1}\begin{bmatrix} 1.6974 - 1.7974 \cdot \log \dot{\gamma} + 0.8718 \cdot (\log \dot{\gamma})^2 - \\ 0.2567 \cdot (\log \dot{\gamma})^3 + 0.02898 \cdot (\log \dot{\gamma})^4 \end{bmatrix} \qquad \textbf{Eq. 2-8}$$

which is valid for the following range of shear rate: $10 \le \dot{\gamma} \le 10^4\ s^{-1}$.

The limit of applicability of the above-mentioned experimental correlations is given in terms of the range of operating shear rate for which the measurements were conducted. These equations are valid for the type and composition of the specific fluid

[c] The apparent viscosity is the viscosity value obtained by applying the viscometer equations used in obtaining the viscosity of a Newtonian fluid to measurements of a non-Newtonian fluid.

solution analysed, in particular the degree of thickening, since the apparent viscosity of the retardant increases with the thickener concentration, as shown in Figure 2-11.

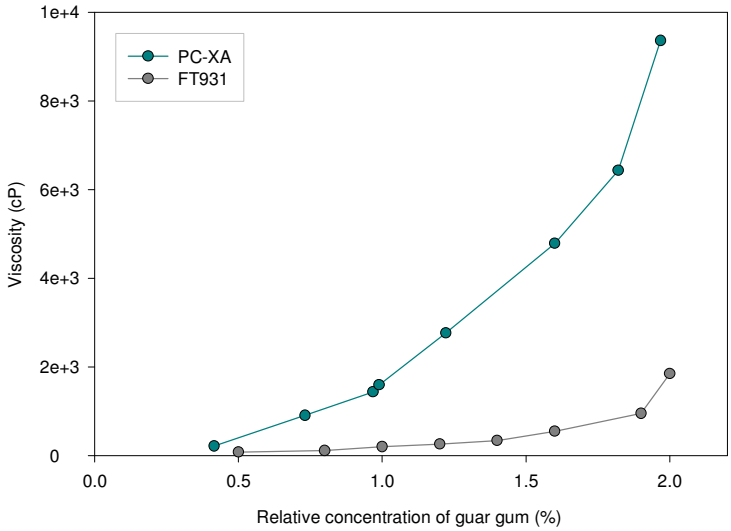

Figure 2-11. Measured apparent viscosity as a function of guar gum concentration in PC-XA (68.39 g per 500 ml water) [Andersen et al., 1976] and FT931 (280 g per 780 ml water) [ACRE, 2000].

At the present state of knowledge, few studies have been focused on the variation of non-Newtonian viscosity with the shear rate in fire retardants used for aerial firefighting. As the available information is scarce, or it is protected by the manufacturers, a detailed laboratorial analysis on the subject should be undertaken, particularly in the case of fluids exhibiting elastic properties (as PC), as a stimulus to an increased accuracy in the numerical modelling of fluids breakup.

3. State-of-the-art

During an aerial drop the liquid goes through a complex sequence of dynamic mechanisms. The first stage starts with the release of the firefighting product from the tank. Depending on the number of tank compartments opened simultaneously and the type of delivery system, the time for total efflux can typically take between 0.5 and 2 s. The geometrical characteristics of the tank and the doors' opening rate shape the emerging fluid at the first milliseconds of the drop. As a result of the interaction with the strong crosswind induced by the forward movement of the airtanker, the bulk liquid jet will bend and deform through thinning and lateral spreading. At this stage, typical relative velocities between the liquid and the atmosphere are usually in the range from 50 to 70 $m.s^{-1}$. Due to the action of the aerodynamic forces, the liquid breaks up into a cascade of fluid structures that form a spray region with the characteristic cloud shape shown in Figure 3-1. Droplet shape and drag deceleration will influence the deposition mechanisms during this multistage breakup process. It is also during this stage that the newly formed droplets, especially the smaller ones, are more vulnerable to wind flow characteristics, namely canopy-induced turbulence.

Figure 3-1. Schematic representation [George and Blakely, 1973] and sequence of images of a retardant aerial dropping (copyright by Bruce Weide. Blodgett Fire (US), August 1, 2000 [url 12]).

The complexity involved in the numerical modelling of an aerial drop results mostly from the panoply of dynamic phenomena that intervene in the breakup of the bulk liquid and in the following deposition and drift of the formed droplets, which will ultimately determine the ground pattern characteristics and the coverage of the fuel by the product. This chapter will focus on the studies conducted in this matter and the resulting scientific understanding. In fact, although the knowledge of the breakup

process is of particular importance towards the understanding of the behaviour of the very large mass of fluid falling in the atmosphere, there have been few successful attempts to study (experimentally or numerically) in detail the complex breakup process that firefighting products (especially retardants) undergo in the atmosphere. On the other hand, the dynamical interaction between the newly formed droplets and the atmospheric flow field establishes the balance of forces involved in the calculation of the trajectory, and thus can be of prime importance towards the final ground deposition.

3.1. Breakup mechanisms

The process of aerodynamic breakup of a large mass of firefighting product in the atmosphere constitutes a multistage process. When subjected to a crossflow, the primary breakup of a liquid jet column occurs, leading to the production of ligaments and large droplets that subsequently originate a spray region due to secondary breakup of the droplets, as shown in Figure 3-1 and Figure 3-2. The primary breakup at the surface of non-turbulent and turbulent liquids yields drops that are intrinsically unstable to secondary breakup [Wu et al., 1991 and 1992], supporting the classical description that atomization occurs by primary breakup of the fluid jet into drops due to several types of instabilities, followed by secondary breakup of the newly formed drops according to different mechanisms due to the interaction with the flow (e.g., Hsiang and Faeth [1995]). As a result of the breakup process, the retardant/water cloud is constituted by two distinct regions, the column of the jet and the spray, and a transition one that gathers all the ligaments or fragments that are originated from the breakup of the jet into droplets, in agreement with the schematic representation in Figure 3-2. The spray region is constituted by a near field (or dense spray) and a far field spray region.

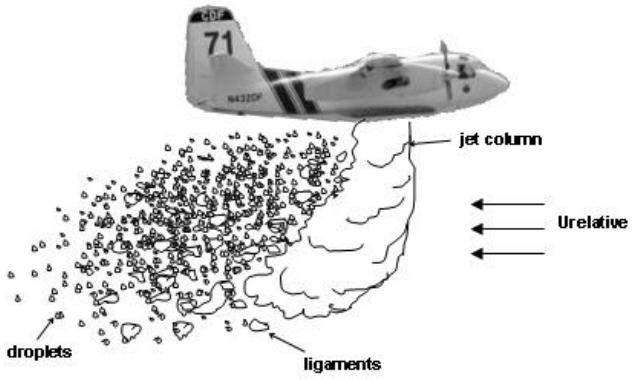

Figure 3-2. Schematic representation of the cascade of fluid structures originated by the breakup of a liquid jet into a crossflow of air (adapted from Wu et al. [1997]).

The primary breakup of liquid jet and the following secondary breakup of the formed droplets will be analysed with more detail in sections 3.1.1 and 3.1.2, respectively. Central to many of the studies on fluids breakup is the use of dimensionless numbers as a privileged tool to capture the balance of forces involved and thus to understand the complex hierarchy of mechanisms involved. A good review on their applicability can be found in McKinley [2005a and 2005b]. Some of the most relevant dimensionless groups governing the instabilities involved in the breakup of jets and droplets are presented in Table 3-1. The subscripts L and G stand for the liquid and the gaseous phases, respectively. The fluids system can be characterised through the knowledge of the following parameters: velocity (U), mass density (ρ), dynamic viscosity (μ), surface tension (σ) , a characteristic length (L) and the acceleration of gravity (g).

Table 3-1. Dimensionless groups with relevance at the analysis of the breakup of firefighting products in the atmosphere. Note: only the dimensionless groups most frequently applied in the work are listed.

Name	Definition	Interpretation
Weber	$We = \frac{\rho U^2 L}{\sigma}$	$\frac{\text{inertial force}}{\text{surface tension force}}$
Reynolds	$Re = \frac{UL}{\nu}$	$\frac{\text{inertial force}}{\text{viscous force}}$
Ohnesorge	$Oh = \frac{\mu}{\sqrt{\sigma \rho L}} = \frac{\sqrt{We_L}}{Re_L}$	$\frac{\text{viscous force}}{\text{surface tension force}}$
Morton	$Mo = \frac{g\mu_G^4 \lvert\rho_L - \rho_G\rvert}{\rho_G^2 \sigma^3}$	$\frac{\text{viscous force}}{\text{surface tension force}}$
Bond	$Bo = \frac{\rho g L^2}{\sigma}$	$\frac{\text{gravity force}}{\text{surface tension force}}$

The Weber number (We) relates the forces that the liquid experiences and its surface tension, characterizing the type of breakup that the jet can be involved in, and thus it is one of the most relevant dimensionless groups in the current analysis. The importance of viscosity is known to increase with the Ohnesorge number (Oh) [Hirahara and Kawahashi, 1992; Joseph *et al.*, 1999], which accounts for the strength of the viscous stress relative to the surface tension force. The larger is Oh, the larger is the breakup time of the liquid [Garcia and Castellanos, 1999]. The Reynolds number (Re) prescribes the relative magnitudes of inertial and viscous forces in the system, while

the Froude number (*Fr*; not shown in the table) those of inertial and gravity forces and the Bond number (*Bo*) those of gravity and surface tension. The importance of surface tension relative to gravity and viscous stresses is thus given by the relative magnitudes of the Weber, Froude, Bond and Reynolds numbers.

Other dimensionless groups are important in this analysis. The Taylor number (*Ta*), for instance, will be used in the linear stability theory applied to the primary breakup of the liquid jet (see section 4.5). It combines, according to the definition by Reitz [1987], the *Oh* and the *We* numbers, although other definitions are available in the literature. The Morton number (*Mo*) and the Eötvös number (*Eo*) are commonly used in the characterization of the shape of droplets, most frequently as a function of *Bo*. While the *Mo* number characterizes the importance of viscous to surface tension forces, the *Eo* number gives the rate of buoyancy force versus surface tension force.

Specifically in the case of non-Newtonian fluids, the most frequently cited dimensionless groups are the Weissenberg number (*Wi*), which gives the relative importance of elastic stresses with respect to viscous stresses in bulk flows of non-Newtonian fluids; or the elasticity number (*El*), that relates the magnitudes of inertial stresses and elastic stresses given by the *Re* and the *Wi* numbers.

3.1.1. Primary breakup of the liquid jet

The breakup of a liquid jet emanating into another fluid has been studied for more than a century, most probably starting with the seminal contribution of Savart in 1833, who showed the formation of a succession of main and satellite droplets. Other scientists continued the study of jet breakup dynamics, namely Plateau, Rayleigh [1879] and Lenard in the second half of the 19th century and Weber in 1931 (for more details see the reviews on the breakup of liquid jets by Lin and Reitz [1998], Eggers [1997 and 2006] and Eggers and Villermaux [2008]). Since these pioneering works, the research on the breakup of liquid jets and droplets has been largely stimulated by the extensive industrial and non-industrial applications involving sprays, as in the automotive and pharmaceutical industries, fire suppression and agriculture activities. Typical applications include the processes of coating, painting, cooling or injection of different types of fluids, as fuel in direct injection combustion engines or ink in printers. Table 3-2 presents some relevant and recent studies on the breakup of liquid jets on airflows.

The earliest studies on jets breakup involved characterizing basic flow-field properties important for engineering applications, such as jet penetration and trajectory. In the past thirty years, the development of new laboratorial equipments and techniques has allowed a better understanding of the jet dynamics, focusing on specific aspects as the analysis of the effects of momentum ratio, injection angle, skew angle, jet geometry,

multiple jets and swirl [Plesniak and Cusano, 2005]. For simplicity, most of the theoretical, experimental and numerical studies on jets breakup have been conducted with still gases or coaxial gas flows. The behaviour of liquid jets in air crossflows (JICF), as in the case of the aerial drop of firefighting liquids, is much more complex due to progressively changes along the trajectory [Ryan, 2006]. Due to this fact, JICF studies are usually made for the simplest situation that considers the injection through circular injection holes normally oriented to the crossflow. The few studies focusing on the effect of the injection angle and exit geometry on the breakup processes have demonstrated that the jet penetration decreases with increasing injection angle [Fuller et al., 2000] and that the mixing increases, implying that the penetration decreases, as the jet aspect ratio (AR) increases [Krothapalli et al., 1981].

Table 3-2. Examples of experimental studies on the injection of circular and rectangular liquid jets into distinct types of airflows.

Jet type	Reference
Liquid jet in still gas	Wu et al. [1992 and 1995], Wu and Faeth [1993, 1995], Sallam et al. [1999]
Liquid jet in coaxial gas flow	Hoyt and Taylor [1977], Lasheras and Hopfinger [2000], Inamura et al. [2001], Varga et al. [2003], Marmottant and Villermaux [2004], Kim et al. [2006]
Jet in crossflow (JICF)	Sherif and Pletcher [1989], Margason [1993], Holdeman [1993], Vich and Ledoux [1997], Wu et al. [1997], Mazallon et al. [1999], Birouk et al. [2003]
Rectangular turbulent jet (RTJ)	Krothapalli et al. [1981], Lozanova and Stankov [1998], Yu and Girimaji [2005]

The wide range of experimental conditions tested in the studies reported in literature have shown that the breakup regimes observed are mainly controlled by the *We* number, which relates, as referred, the forces that the liquid experiences with its surface tension. When there is a velocity gradient between the liquid and the gas the drag force produced distorts the jet's shape and eventually breaks it. Based on the *We* numbers for the liquid and the gas it is thus possible to establish the type of breakup regimes involved, which have been classified as column, transition and bag breakup (although the terminology used sometimes varies according to the author). The criteria

for predicting the onset of the different breakup regimes of a liquid jet in a crossflow are summarized in Table 3-3.

Table 3-3. Weber number ranges for the different breakup regimes of a liquid jet in a crossflow.

Breakup regime	Weber number range		Reference
	Liquid	Gas	
Column	141 – 315	1 – 7	Birouk et al. [2003]
	< 250	~ 7	Vich and Ledoux [1997]
Transition	149 – 939	3 – 9	Birouk et al. [2003]
Bag	323 – 1119	4 – 14	Birouk et al. [2003]
	> 250	~ 8	Vich and Ledoux [1997]

In Figure 3-3, images of a viscous liquid (oil) jet breakup due to the action of an air crossflow are presented. With the increase of the cross airflow and the jet velocities, column breakup regime shown in images (a) and (b) evolutes to bag breakup in (c) and (d), in which liquid bags-like are formed and detach from the jet column and breakup into droplets of various dimensions. The increase in the cross airflow velocity in (d), associated to the lower concurrent injection velocity of the jet, induces an earlier bending of the jet and a lower transverse penetration. The similitude of jet behaviour found in bag type regime with the shape of a water/retardant cloud during an aerial drop is evident. In cases (c) and (d), the spray region constituted by the small particles [d] stripped from the jet is also influenced by the wake structures originated by the preceding jet column. This type of turbulent phenomenon is generated by the windflow boundary layer around the jet, which forms vortices attaching to the lee side of the jet that become the wake structures. The jet fluid penetrates the wake structures to an increasing depth with increasing velocity ratio [Fric and Roshko, 1994; Kelsot et al., 1996; Smith and Mungal, 1998; Camussi et al., 2002; New et al., 2003; Plesniak and Cusano, 2005].

[d] The definition of particle covers a wide range of solid and fluid structures. According to Loth [2000], it can be defined as an unattached body in a flow whose motion is primarily controlled by convection and/or gravity forces. Therefore, it can take the form of a solid particle (e.g., dust or soot) or a fluid particle (e.g., droplet or bubble).

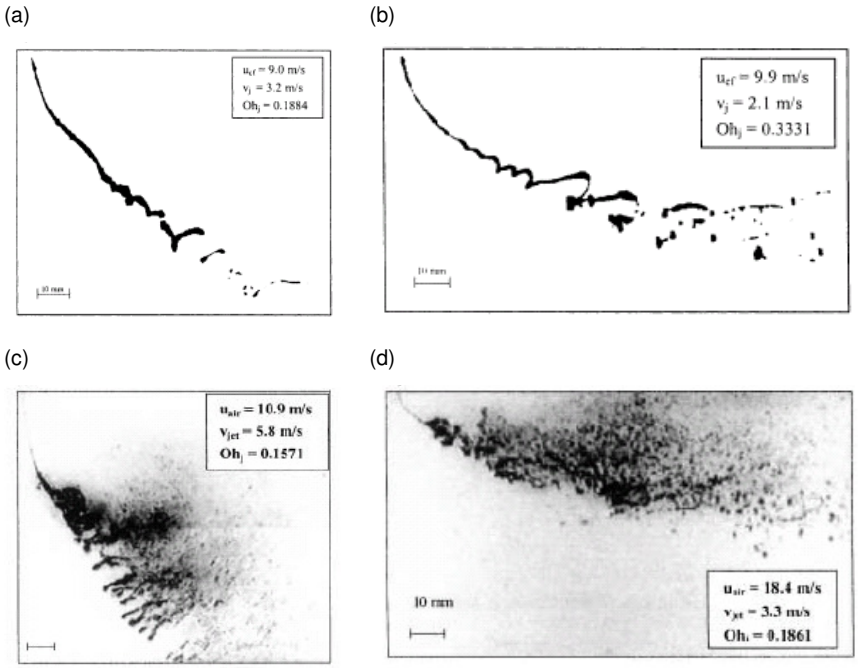

Figure 3-3. Different regimes of jet breakup in crossflow: column type in (a) and (b) images and bag type in (c) and (d) [Birouk et al., 2003]. u_{cf} and u_{air} indicate the *x*-axis component of the airflow velocity; v_j and v_{jet} the vertical velocity of the jet and Oh_j the Ohnesorge number of the jet.

Specifically in the aerial dropping of firefighting products, the primary breakup of the jet is characterised by the interaction of two major mechanisms (as represented in Figure 3-2): one is related to the bending and fracture of the jet column, the other is the continuous stripping of droplets from the bulk liquid surface due to wave instabilities, known as surface breakup. The balance of aerodynamic drag, liquid inertia, gravity, surface tension, and viscous forces induces both deflection and deformation of the jet column. Deflection leads to a curved liquid-jet profile that will break and fragment the column into large segments near the point of curvature due to the growth of wave instabilities. Small droplets are entrained in the near-wall region owing to the wake flow that develops behind the liquid column [Linne et al., 2005]. During the process, deformation increases the frontal cross section of the jet column and increases the drag, which leads to surface stripping of smaller ligaments and fragments directly from the column. The same forces cause secondary breakup of ligaments and fragments into droplets, which may breakup even further before being deposited or eventually evaporated.

Rayleigh [1879] was the first to show that the breakup of a jet is the consequence of hydrodynamic instability, demonstrating that a circular cylindrical liquid jet is unstable with respect to disturbances of wavelengths larger than its diameter. Not despite the fluids considered, the same type of hydrodynamic instabilities govern the breakup of droplets from a jet (e.g., Storr and Behnia [1999], Nicolas [2002], Bang et al. [2003],

Abe et al. [2004 and 2006]). This is shown, as an example, in Figure 3-4 for the cases of a molten jet into water and a retardant jet in the atmosphere. The resemblance between both situations is obvious.

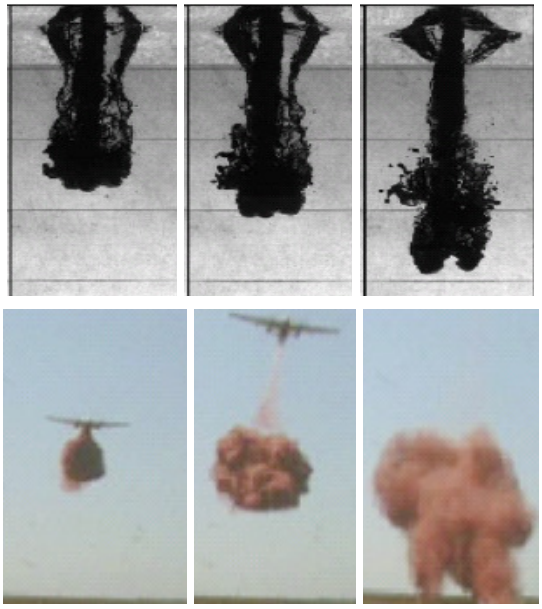

Figure 3-4. Sequential images taken during the injection of a molten jet into water [Abe et al., 2006] and of a retardant dropping during Marseille 2000 aerial drops [Giroud et al., 2002].

The breakup of liquid jets due to aerodynamic forces is a result of a competing mechanism between hydrodynamic instabilities, such as Rayleigh-Taylor (RT) and Kelvin-Helmholtz (KH), occurring on the liquid-gas interface (e.g., Tanner [1998, 2003], Reitz and Bracco [1982], Raju [2005], Abe et al. [2006]). The RT instability is due to inertia of the denser fluid opposing the system acceleration in a direction perpendicular to the interface of the denser fluid. The KH instability is caused by the viscous forces due to the relative motion of the fluids in the direction parallel to the interface.

In an aerial drop, these two types of amplifying instabilities cause the wind stripping of droplets with varying dimensions from the surface of the jet of firefighting liquid, and subsequently also promote the secondary breakup of the formed droplets. RT instabilities preferably occur on the front surface of the jet column and KH instabilities on the side surfaces. The typical jet shapes resulting from the action of these instabilities are shown, as an example, in Figure 3-5 for the case of retardant and Figure 3-6 for water.

(a) (b)

Figure 3-5. Observation of Rayleigh-Taylor and Kelvin-Helmholtz instabilities formed in the surface of a retardant jet (image a: copyright by Al Golub. AT aircraft on Pedro Fire (US), July 2006 [url 1]; image b: url 9).

On a qualitative perspective, a similar behaviour occurs during the aerial drop of water, as seen in Figure 3-6. However, the distinct properties of the liquid (as density, viscosity and surface tension), and particularly its Newtonian behaviour, will have an effect on the sizes of the droplets originated.

Figure 3-6. Similar behaviour from previous figure but with a water drop (Martin-Mars on the Jordan Creek fire (US), August 1998 [url 1]).

The complexity involved in the numerical modelling of the behaviour of firefighting products in the atmosphere significantly increases due to the non-Newtonian characteristics of retardants, according to which the viscosity changes with the applied shear stress, as mentioned. This behaviour is a result of the thickener usually present in the solution, which is added as a way to increase viscosity and consequently the terminal size of the droplets produced by aerodynamic breakup. It was previously shown by Andersen et al. [1974a, 1974b and 1976] that due to the effect of the thickener, the effective viscosity, which results from both viscosity and elasticity, contributes to the control of the aerodynamic breakup characteristics of the liquid while undergoing shear and to its final droplet size.

For the current state of knowledge, the complex dynamical effects of non-Newtonian behaviour on breakup are, however, incompatible with the desired characteristics of a fast-running operational model of aerial dropping. Moreover, although many fluids used in practical atomization applications are non-Newtonian, the outcomes on breakup are not totally understood and quantified, and most of the studies have been focused on low-speed jets in stagnant media. Research has found that in particular for a viscoelastic fluid, the properties of the non-Newtonian liquid jet tend to enhance the initial growth of disturbances with small amplitudes as compared to Newtonian jets with the same Ohnesorge number. Although an increased deformation is observed, the non-Newtonian liquid behaviour leads to a retardation of breakup and to the formation of a structure of drops connected by thin filaments, despite the initially enhanced disturbance growth rates [Yarin, 1993 in Brenn et al., 2000]. However, the increase of the liquid viscosity dampens disturbance waves on non-Newtonian liquid jets drastically, and at high liquid viscosity the growth rate of non-Newtonian liquid jets is close to that of Newtonian ones [Brenn et al., 2000].

3.1.2. Secondary breakup of droplets

In terms of secondary breakup analysis, most of the early literature on the breakup of droplets was focused on the study of Newtonian liquids in subsonic airstreams. The use of shock tubes and a series of measuring techniques offered the possibility to study different breakup regimes of both Newtonian (usually water or diesel oil) and non-Newtonian droplets, under high subsonic and supersonic conditions. Reviews on the atomization of droplets can be found in the papers by Pilch and Erdman [1987], Hsiang and Faeth [1992], Hwang et al. [1996], and Joseph et al. [1999].

The paper by Pilch and Erdman [1987] is still a reference on the study of the dependence of breakup regimes on the *We* number, as schematically represented in Figure 3-7. Since this work, the threshold *We* for each regime or the existence of some of the mechanisms have been discussed (see, e.g., Joseph *et al.* [1999]). There is, however, a general consensus that the main mechanisms responsible for the secondary breakup of droplets are bag, shear and catastrophic breakup. Additionally, when two or more droplets interact, collisional breakup can eventually be induced, which has been identified as a limiting factor to maximum drop size in natural rain (e.g., Pruppacher and Klett [1997]). The collision between two droplets can be classified according to four different regimes: bounce, coalescence, reflexive separation and stretching separation. Research has shown that the binary collision of equal-sized droplets typically occurs for *We* numbers under 100 (e.g., Ko and Ryou [2005]).

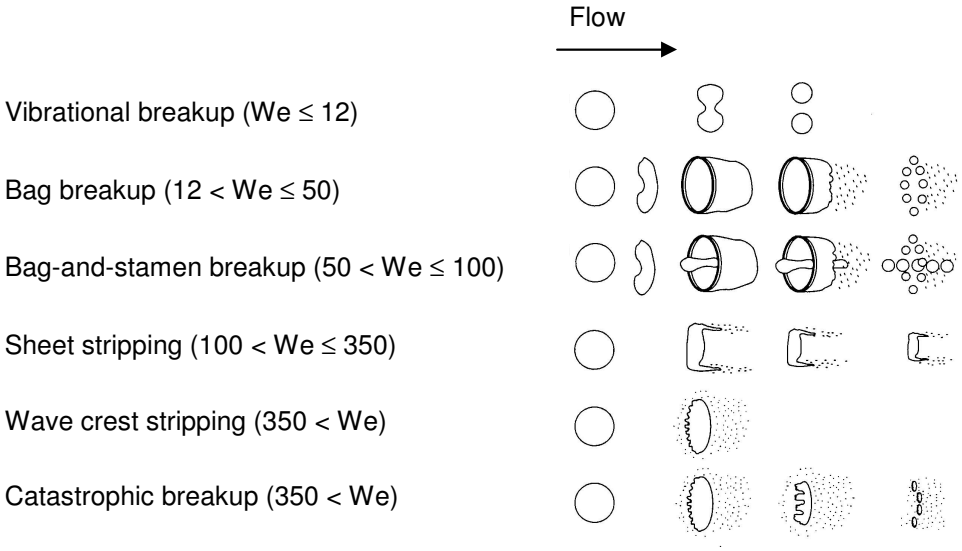

Figure 3-7. Schematic representation of water drops breakup mechanisms according to Pilch and Erdman [1987]. Particularly in bag breakup, several stages are represented: droplet deformation, bag growth, bag burst and rim breakup.

As in the primary breakup, the *We* number is also one of the most relevant dimensionless numbers, indicating the type of breakup that a droplet can be involved in. The minimum critical *We* number, which represents the most stable droplet diameter below which no breakup is possible, increases with the viscosity of the droplet. This dependence is usually expressed through the *Oh* number, as seen in Figure 3-8.

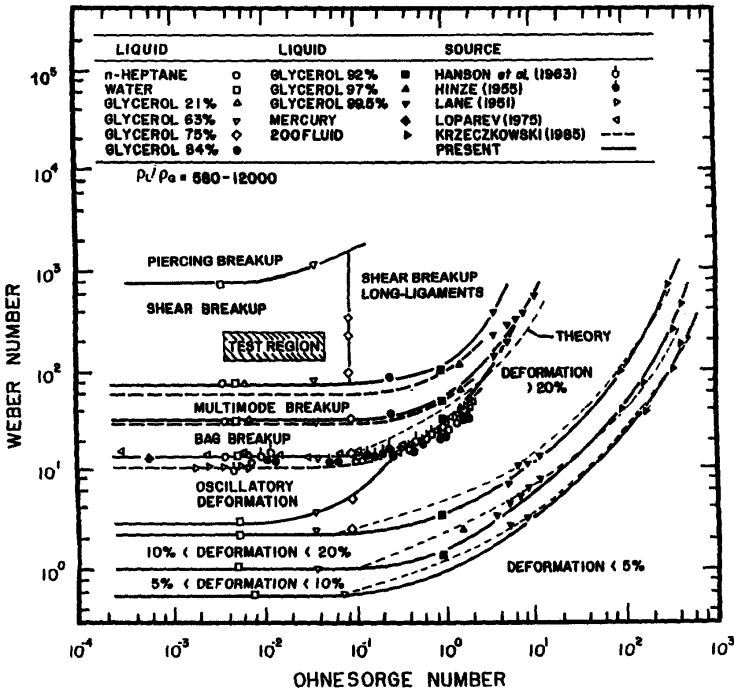

Figure 3-8. Droplet deformation and breakup regime map from shock-wave studies [Chou et al., 1997].

In 1974 the USDA-FS performed a number of shock tube studies in order to obtain high speed photographic coverage of the behaviour of water and retardant droplets in the air flow [Andersen et al., 1974a and 1974b]. Some example images of the breakup of a FT931 droplet when injected into a crossflow with different velocities are shown in Figure 3-9. Not despite the coarse resolution of the photos, their importance relies on the fact that, to the knowledge of the author of the present study, these were the only laboratorial analysis of the aerodynamic breakup of retardant droplets ever made.

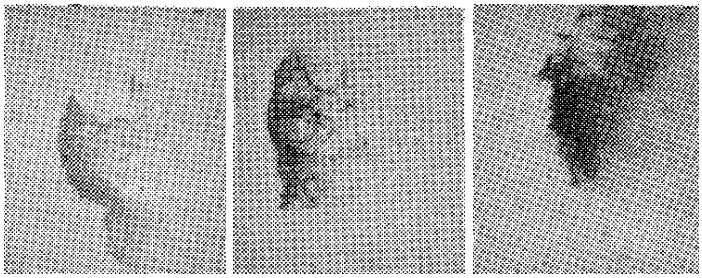

Figure 3-9. Shock tube analysis of the aerodynamic breakup of retardant droplets showing selected frames (6.27, 4.04 and 2.03 ms) from photographic sequences of the aerodynamic breakup of 2-5 mm FT931 droplets into a cross airflow with a velocity of 27, 44.5 and 86.6 m.s^{-1}, respectively [Andersen et al., 1974a].

As in the case of the primary breakup of the liquid jet, also the secondary breakup of the formed droplets is affected, in variable extent, by the non-Newtonian behaviour of the fluid, especially if it exhibits also elastic properties, as PC products usually do. In general, the non-Newtonian characteristics of the fluid are capable of stretching the threshold values for each breakup regime. An example of this was shown by the experimental work by Andersen et al. [1974b], in which the dynamics of a 5.7 mm PC-XA droplet was studied in the shock tube for an air flow velocity of 27.4 m.s^{-1}. For that air speed, although near the minimum limit, a nonelastic drop would typically breakup with the formation of a bag onto many small droplets. In the experiment, the highly elastic characteristics of PC merely deflate the bag without breaking up the drop, evidencing the stabilizing effect that elasticity can confer to a liquid.

This behaviour is confirmed by the work of Arcoumanis et al. [1994] in which the author investigated, using high speed photography and impaction tests, the breakup of droplets of both Newtonian and non-Newtonian fluids in a high speed subsonic air jet. Single droplets with diameters from 2.4 to 3.3 mm were arranged to fall under gravity into a crossflow with velocities up to 360 m.s^{-1}. While the droplets of Newtonian fluids were atomised in the expected manner within three main regimes characterised by the *We* number of the droplet and air jet conditions, similar droplets of non-Newtonian fluids were found not to atomise but to develop under shear and stretching into ligaments of fluid separated from a local region of their surface; these ligaments were

elongated until breakup occurred, though not into small droplets as with the Newtonian fluids. As in the case of PC-XA tests conducted by Andersen et al. [1974a, b], highly viscoelastic fluids (depending on the concentration of the thickener) were found not to breakup even at the maximum jet speed of the tests (360 $m.s^{-1}$). Instead, the subsonic air jet only rotated the droplet in a clockwise direction and caused elongation in the direction of the flow. An increase in the concentration of the thickener contained in the mixture resulted in higher critical speed for a given droplet diameter, showing that thickened droplets require higher speeds and, therefore, higher shear rates to cause breakup. It was shown that the characteristics of non-Newtonian fluids, in particular viscosity, had a great influence on the critical velocity value, with an increase of the critical speed from less than 20 $m.s^{-1}$ to 360 $m.s^{-1}$ due to an increase from 1 to 5%, respectively, on the thickener's concentration.

3.1.3. Droplet size distribution

The rheological behaviour of the product, in conjunction with operating drop parameters (as the aircraft speed and height) and meteorological conditions (particularly, the airflow velocity), determine the droplet size distribution (DSD) at ground. On the development of probability distribution functions (pdf) that adequately describe the size, number, mass and volume distribution of droplets of firefighting products after breakup, distinct approaches have been taken, namely: laboratorial tests [Van Meter and George, 1981], real-scale measurements [Andersen et al., 1976; Schönhuber et al., 2005] and numerical estimates [Andersen et al., 1974a, b, 1976; Van Meter, 1983].

Different empirical distributions [e] have been used to describe the sprays that are commonly found in engineering applications, such as the log-normal [Andersen et al., 1974b], the Rosin-Rammler [Tomé, 2004] or the log-stable [Rimbert and Séro-Guillaume, 2004]. Other distributions are also frequently applied in spray analyses, namely the root-normal, the Nukiyama-Tanasawa, the log-hyperbolic, or the upper-limit. A number of parameters need to be adjusted in order to fit the theoretical distribution to the measured data, and thus it is desirable to characterize

[e] There are basically three distinct methods for providing the distribution of droplets: the empirical method, the maximum entropy method, and the discrete probability function method, although the former is by far the most commonly applied. It involves the curve fitting of a series of data collected with different equipments and operating conditions. The problem inherent to the empirical approach is the difficulty of extrapolating the data to operating regimes outside the experimental range, which can introduce a source of inaccuracy when simulating the droplet size distribution of a spray [Liu, 2000; Babinsky and Sojka, 2002].

a particular DSD by a representative droplet diameter [f] as: the arithmetic mean diameter (D_{10}), the volume mean diameter (D_{30}), the Sauter mean diameter (SMD or D_{32}), the mass median diameter (MMD), the mass mean diameter (D_{mm}) and the volume median diameter (VMD) (e.g., Liu [2000]; Babinsky and Sojka [2002]). The MMD and the VMD represent, respectively, the diameter that divides the spray such that half of the mass or volume has droplets of diameters smaller than the MMD or VMD, and half of the mass or volume has droplets of diameters greater than the MMD or VMD (e.g., Crowe et al. [1998]). Simmons [1977], based on a large number of experimental tests with nozzles, concluded that the ratio of MMD to SMD is always close to 1.2.

In the 1970s, the USDA-FS (e.g., Andersen et al. [1976]) conducted a comprehensive investigation of DSD during real scale drops of distinct fluids. Different measuring methods, including rotating impact devices and high-speed cameras, were tested. Table 3-4 compares the maximum droplet size measured by both the camera and sampler, as well as the mass mean diameter. Due to technical reasons, camera measurements represent a shorter time period than the sampler. In order to be comparable, data analysis is limited to the measuring time of the camera. Thus, only the initial, but usually the most significant, portion of the liquid reaching the surface is considered. Beyond the significant discrepancy found for fluids that atomise into larger droplets (the PC-XA solutions), the experimental results showed conclusively that different droplets sizes are produced by different fluids when dropped under roughly the same conditions.

[f] Mugele and Evans [1951] have generalized the concept of mean diameters, several of which can be calculated by the following general expression:

$$D_{pq} = \left[\frac{\int_0^\infty D^p f(D) dD}{\int_0^\infty D^q f(D) dD} \right]^{\frac{1}{p-q}}$$

where p and q are typically positive integers.

Table 3-4. Experimental results from the USDA-FS study [Andersen et al., 1976] on droplet sizes data obtained by a camera and a rotating sampler (during the camera measuring time). Each row represents a specific drop. Aircraft speed was approximately 67 m.s^{-1}, except for the PC-XA drop marked with an asterisk, which was equal to 93 m.s^{-1}. Camera and sampler number II were in the same location during drops, allowing the comparison of the respective measured values. For the mass mean diameter also the average of the diameters measured by three impact devices in different positions (in and near the effective ground pattern) is presented.

Fluid	Maximum diameter (mm)		Mass mean diameter (mm)		
	Camera	Sampler II	Camera	Sampler II	Average of the 3 samplers
1.6 PC	12.3	10.1	10.8	8.4	6.4 ± 1.5
1.6 PC	10.9	6.3	7.4	4.6	
PC-XA	11.3	9.0	7.7	6.0	4.8 ± 0.9
PC-XA (*)	7.1	5.7	5.9	3.8	4.0 ± 0.9
0.42 PC	8.1	6.5	5.2	3.5	3.6 ± 0.4
FT 100	4.8	—	2.8	—	2.5 ± 0.4
FT 931	5.3	4.3	2.8	3.1	2.3 ± 0.2
Water	2.8	—	1.9	—	2.0 ± 0.4

Table 3-4 also shows that, depending on position, different droplets sizes are measured as indicated by the standard deviation in the last column. Andersen et al. [1976] focused their research also on the spatial distribution of droplets by diameters, showing some evidence that the droplet size may increase in areas of very high ground concentration, and that the sizes are slightly smaller in the initial low concentration region of the pattern than in the subsequent effective high concentration contour. In the absence of wind, droplets size was found to be smaller on the periphery than in the interior of the ground pattern and smaller on the downstream side of the pattern in the presence of wind.

A rotating impact sampler was also used in the measurement of DSD under the scope of the EC project ACRE (see Figure 3-10a). Due to some technical problems, some of the results were, however, inconclusive [Tomé, 2004]. Also a cryogenic technique was tested with the same purpose (see Figure 3-10b). It basically consisted on using liquid nitrogen to freeze droplets before the impaction on the bottom of the recipient in order to allow the subsequent weighting at the laboratory. The low number of samples (one

measuring point in only two drops) did not allow to take statistically based conclusions on droplets sizes.

(a) (b)

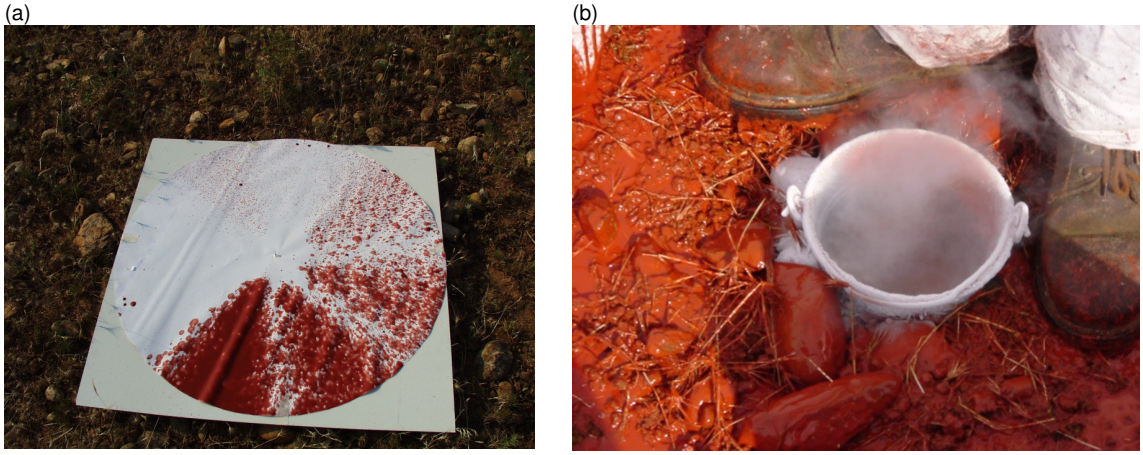

Figure 3-10. Droplets sampling techniques tested during ACRE project.

The correlation between fluid rheological properties and DSD was also analyzed on the laboratorial study by Van Meter and George [1981], in which samples of different firefighting products were injected on a wind tunnel (at a constant air velocity of 18 $m.s^{-1}$) using a specific release mechanism. Droplets diameters were measured after breakup of the main liquid mass using a high-speed camera. Experimental results have shown that as salt content increases or viscosity decreases the shape and position of the drop DSD curve approaches that of water, as can be seen in Figure 3-11. The highest frequency was for 1.4 mm droplets of water. The high narrow peak observed particular in this case, but common to many retardants, indicates a uniform spray with a significant number of droplets of roughly the same size. The attapulgite clay (absence of salt), on the contrary, produced the widest range of sizable frequencies.

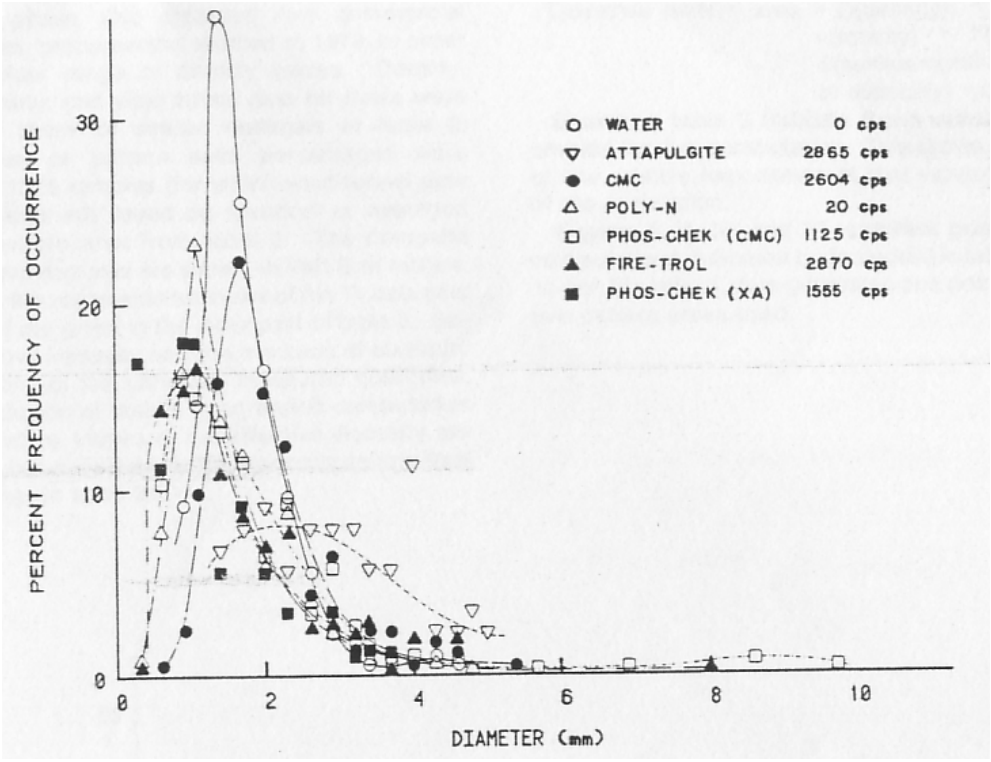

Figure 3-11. Frequency of occurrence of droplets of firefighting liquids by diameter [Van Meter and George, 1981].

The real scale experiments conducted under the scope of the study conducted by Andersen et al. [1976] also indicated that the droplet size increased with the increase in gum thickener concentration (in PC-XA solutions) and with the decrease in aircraft speed. This conclusion was corroborated in the work by Van Meter [1983], in which a computational program was developed that utilized measured values of product density, surface tension, viscosity and elasticity in order to estimate the MMD as a function of the aircraft velocity. The work considered five short-term retardants against only one long-term retardant (PC-XA). From the results it was concluded that the apparent viscosity should be 2 to 10 times more important than the elasticity in determining the effective viscosity and that the MMD is a result of the combined action of the effective viscosity, density and surface tension. However, these results should be interpreted with some caution since the concept and numerical approach were not presented and the results were not validated.

Common to many of the works cited, both at the wind-tunnel or at the field, is the difficulty in capturing the droplet sizes with the needed accuracy. An equipment with potential interest in this field is the 2D-Video-Distrometer (2DVD), which is typically used to measure natural raindrops. The Joanneum Research from the Institute of

Applied Systems Technology, Austria, tested the feasibility of using a 2DVD on the measurement of the number and size distribution of retardant droplets [Schönhuber et al., 2005]. One of the difficulties encountered by the authors was related with the significantly higher number of retardant particles when compared to natural rain. In particular, as most of the data was collected from the periphery of the drops (due to technical reasons), probably the larger droplets typically contained at the center portion of the ground pattern were not considered in the observations [R. Becker, pers. communication]. Nevertheless, there is a great potential on this technique for increasing the knowledge on the size of droplets formed by aerodynamic breakup.

3.2. Field experiments and numerical models

Linear and nonlinear instability theories and computational methods have been used to study the stability and the disintegration of both Newtonian and non-Newtonian liquid jets. The first linear instability analysis for an inviscid cylindrical liquid column in the absence of surrounding gas was carried out by Rayleigh [1879]. A comprehensive review of the linear instability theories for liquid jets is given by Lefebvre [1989] and, more recently, by Lin [2003] and Yoon and Heister [2003].

Reitz and Bracco [1982] applied a stability analysis to the breakup of a liquid jet due to an infinitesimal axisymmetric disturbance using a first order linear theory. The analysis led to the development of a dispersion relationship between the growth rate of the initial perturbation to its wavelength that includes also the physical and dynamical parameters of the liquid jet and the surrounding gas. For the limiting case in which the gas density, the liquid viscosity and the initial jet velocity are neglected, the derived equation reduces to the previous Rayleigh's result for a low-speed inviscid jet. Later, Reitz [1987] generated a set of curve-fits of numerical solutions to the dispersion equation for the maximum growth rate and the corresponding wavelength.

Brenn et al. [2000] applied the linear stability analysis to the particular case of non-Newtonian liquid jets, deriving a dispersion relation for axisymmetric disturbances from the linearized equations of motion and the constitutive equation of the non-Newtonian fluid. This linear theory was shown to describe accurately the growth rate spectra of viscoelastic liquid jets measured in experiments, but in contrast to the analogous theory for Newtonian jets, the theory proved to be inapplicable for calculating the breakup lengths of viscoelastic jets. Also nonlinear analysis has been used to predict the sizes of the main and the satellite drops formed during breakup (e.g., Wang [1968], Nayfeh [1970], Lafrance [1975], Mansour and Lundgren [1990],

Spangler et al. [1995] and Park et al. [2005]). However, these analyses have been focused on the breakup of low-speed jets in stagnant media.

Based on the fundamental mechanisms of atomization a number of atomization models have been developed that can estimate, for a given set of initial injection conditions, critical parameters as the droplets sizes, velocities or temperatures. These models, which have been applied mostly in the simulation of fuel injection systems in the automotive industry, range from linear stability models to detailed numerical models as shown in Table 3-5. Except for the Volume-of-Fluid (VOF) model, the presented bibliographic references regard to the original author of the model, since several works have been published that apply the referred numerical codes (e.g., Lee and Park [2002], Madabhushi [2003], Grover et al. [2004], Raju [2005]). Most of the current spray breakup models for internal combustion engine applications apply the KH-RT hybrid atomization model of Beale and Reitz [1999] or the TAB model, as in the case of KIVA model that has been applied in the simulation of a variety of hydrodynamics problems involving fuel sprays and chemical reactions (e.g., Amsden and Amsden [1993], Torres and Trujillo [2006]). The models from Table 3-5 are also implemented in general-purpose CFD commercial software as KH-RT in FLUENT® and ETAB in STAR-CD®.

Table 3-5. Types of liquid breakup models.

Primary breakup	Secondary breakup	Model	Reference
•		Blob injection model (linear stability theory)	Reitz and Bracco [1982], Reitz [1987], Reitz and Diwakar [1987]
•	•	Boundary-Layer Stripping (BLS)	Khosla and Crocker [2004]
•		Volume-of-Fluid (VOF)	Mashayek and Ashgriz [1993], Rimbert et al. [2002]
	•	Rayleigh-Taylor (RT)	Patterson and Reitz [1998]
	•	Taylor Analogy Breakup (TAB)	O'Rourke and Amsden [1987]
	•	Enhanced Taylor Analogy Breakup (ETAB)	Tanner [1998, 2003]
•	•	Kelvin-Helmholtz/Rayleigh-Taylor hybrid model (KH-RT)	Beale and Reitz [1999]

In the KH-RT model, the primary breakup of the intact liquid core of a diesel jet is predicted with the KH instability model (derived from the blob injection model), and the secondary breakup of the newly formed droplets is then modelled with the KH model in conjunction with the RT accelerative instability model applying the competing mechanism introduced by Su et al. [1996, in Beale and Reitz, 1999]. While in the KH model child droplets are continuously stripped from the parent droplet surface, in the RT model the parent droplet is completely atomized at the instant of breakup.

Breakup models supply the initial conditions for spray dispersion computations. In spite of the importance of atomization, the mechanisms of breakup are still not well understood, increasing the difficulty of providing the necessary drop size, velocity and trajectory data. In particular, few have been the successful attempts to study, both experimentally or numerically, the complex process in which firefighting products (especially retardants) undergo when exposed to aerodynamic breakup, and the consequences on size distribution of drops and final ground deposition.

The first and most detailed study on the breakup of firefighting liquids was undertaken by the Shock Hydrodynamics Division, from the Whittaker Corporation (California, US), under contract to the Intermountain Forest and Range Experiment Station of the USDA-FS. These works were published in a number of reports in the mid 70's [Andersen et al., 1974a, 1974b and 1976]. Although some preliminary tests with liquid jets were conducted then, these experiments were mainly focused on the secondary breakup of retardant droplets for different inflow velocities (see Figure 3-9). This assessment was part of a systematic, comprehensive and extensive study on the aerial application of firefighting products, especially retardants, conducted by the USDA-FS since the late 50's. This broad investigation, focusing on many aspects related to the quality, effectiveness and application of firefighting products, involved the performance of numerous experimental real-scale drop tests, which consist on the dropping of different types of liquids over a regularly spaced array of sampling cups as shown in Figure 3-12. Drop testing is still a common practice on the evaluation of retardant effectiveness, although modern equipments allow to improve the accuracy of the measurements [Davis, 1959; George and Blakely, 1973; George, 1975; Andersen et al., 1976; George and Johnson, 1990; Robertson et al., 1997b; Suter, 2000; Lovellette, 2004]. Most drop pattern studies have been conducted in open areas, such as airport runways, and under low wind conditions. These have been known as "bare ground pattern studies" after Robertson et al. [1997a]. In fact, few have been the studies considering the effect of canopy interception. Examples include the works by Stechishen [1976], Rawson [1977], Newstead and Lieskovsky [1985] and Robertson et al. [1997a]. Field trials have been also complemented by static testing [Blakely et al.,

1982; Lovellette, 2005], laboratorial measurements [Andersen et al., 1974a and 1974b; Van Meter, 1983], as well as wind tunnel experiments [Van Meter and George, 1981].

Figure 3-12. Airtanker dropping water over a grid of cups during a drop test [Suter, 2000].

The extensive set of data compiled and analysed during the High-Altitude Drop Mechanization (HADM) Study conducted by Honeywell Corporation under contract to the USDA-FS, supported the development of a model capable of predicting retardant ground patterns over a range of aircraft velocities and altitudes [Swanson and Helvig, 1973 and 1974]. One of the characteristics of the original code was the employment of a steady-state Bernoulli equation for the temporal variation of the flow rate of product exiting from the tank based on the work by MacPherson [1967, in Swanson et al., 1975]. However, measured data on actual fluid flow rates obtained at the end of HADM program suggested that the subroutine used to predict flow rate from tank geometry was not entirely accurate, mostly because most tanks were acceleration-dominated rather than steady-state in their flow, and that the predictive capability of the model was substantially improved when measured flow rates were used instead. This work culminated with the development in 1975 of the retardant ground pattern operational model PATSIM (PATtern SIMulation) [Swanson et al., 1975]. In 1977 the model was refined through an improved subroutine to predict flow rate by choosing between limit conditions of steady-state (Bernoulli) or acceleration-dominated flow based on tank geometry, door-opening rate and vent parameters [Swanson et al., 1977]. Because of the significance of flow rate in determining pattern formation and distribution, an Experimental Tank and Gating System (ETAGS) Program was initiated in 1974 with the objective of obtaining a more definitive understanding on the effect of aircraft tank and gating characteristics on retardant ground pattern formation. According to Swanson et al. [1978], the results of the ETAGS tests and subsequent analysis showed certain deficiencies in the ability of PATSIM program to account for all aspects of tank performances, stressing the need for a more physically based concept namely through the inclusion of the breakup mechanism.

PATSIM model, which is still a reference in the simulation of retardant aerial drops, uses an algorithm consisting of four distinct sections. First the model calculates the marginal downrange distribution by breaking the volume discharged from the tank into small increments based on the temporal evolution of flow rate and on aircraft velocity. Secondly the program generates the marginal cross range distribution as a function of altitude and retardant type. The empirical marginal range distribution derived in the two first stages consists on a coarse approach to the complex physical process of breakup. Next, the model calculates the ground response pattern from the distributions, and finally it gives the concentration, area and lengths according to various coverage levels [George and Johnson, 1990].

In Europe, the first systematic investigation on the utilisation of retardants in the fire prevention and suppression was started in 1998 with ACRE project ("Additifs Chimiques Rheologie Evaluation"), financed by the European Commission. This innovative project was dedicated to the study of the rheological characteristics of fire retardants and the development of operational guidelines for the aerial application. It involved the set up of a series of real scale drop tests in Marseille, willing to analyse the effect of rheology on ground pattern. In the scope of ACRE, the University of Aveiro (UA) developed the Retardant Application Model (RAM) [Tomé and Borrego, 2002], which applies the empirical concept of the atomization introduced in PATSIM, and adds some improvements namely at the level of the wind flow description. In a subsequent study, the CFD model FLUENT was applied by Tomé [2004] in order to evaluate the impact of the two-way coupling between the particulate and the carrier phases on the flow field and, consequently, on the deposition of the cloud. However, the spatiotemporal evolution of the breakup process was again described by the empirical law implemented in PATSIM.

In 2001, the ERAS Project ("Extension Retardant Application System") was started. It had a wider scope of analysis, covering the aerial and ground application of retardants and the assessment of the environmental impact on water, soil and air. Under the scope of ERAS, a research team from the "Laboratoire d'Energétique et de Mécanique Théorique et Appliquée" (LEMTA), France, applied a Volume-of-Fluid (VOF) method available in FLUENT commercial package to the simulation of the retardant breakup and deposition [LEMTA, 2005; Rimbert et al., 2002]. In this approach the volume fraction of liquid in each cell is calculated using an Eulerian approach. The results weren't, however, compared with measured data. LEMTA's work on the numerical simulation of forest firefighting by aerial means culminated with the mathematical derivation of a set of closures for modelling two-phase flows [Séro-Guillaume and Rimbert, 2005]. However, and according to the authors, some of the coefficients in the closure relations are unknown, and thus need to be determined by experimental

procedures or, more probably, by numerical approaches. Although innovative, the developed method is hardly applicable given the limitations brought by the required previous determination of a series of fundamental variables. Its applicability on the specific case of retardants is not presented and the accuracy of the approach needs further study and validation.

Also under the scope of ERAS, the team from the UA focused on the improvement of RAM model, namely with its integration with a GIS-based graphical interface for a friendly user access [Amorim et al., 2006]. These developments were in the genesis of the present work. RAM model results were intercompared with measured values from Marseille experiments, revealing some of the problems inherent to the simplicity of the numerical approach implemented in the code.

An interesting example on the potential use of aerial dropping models as a DSS is given by the fire growth simulation model FARSITE [Finney, 1998]. It uses spatial information on topography and fuels along with meteorological data and incorporates the existing models for surface fire, crown fire, spotting, post-frontal combustion, and fire acceleration into a two-dimensional fire growth model. A specific module of aerial attack allows to allocate a set of air resources to the specific fire being simulated by the model. The software does not simulate the dropping; instead, the user is responsible for providing realistic performance parameters, as the length of effective retardant pattern for different coverage levels. The user can also give the cost per drop, allowing to estimate the overall cost of the operation. The type of information given by the model, as the efficiency of the aerial means, the time needed for the operation and the involved costs, is potentially useful to professional wildland fire planners and managers.

Based on the developments from the numerical simulation of deposition and drift in agricultural and forestry aerial application of pesticides, Teske et al. [1999] developed, under contract to the USDA-FS, the FireDrop model for the prediction of the ground deposition distribution of fire retardant released from helicopters. The model applies an inverse back-calculation program to optimize the values of the four driving model parameters: droplet volume median diameter, droplet size slope, incremental release height, and spray width. A forward-calculation program applies the Lagrangian trajectory model AgDRIFT [Teske et al., 1997] to the calculation of the ground deposition patterns using the previously fitted parameters as inputs.

Table 3-6 summarizes the most important numerical models on the aerial drop of retardants.

Table 3-6. Time chart on the development of models for the aerial drop of retardants from aircraft.

Model	Characteristics	Reference
PATSIM	Empirical breakup module. Simplified wind flow.	Swanson et al. [1975, 1977 and 1978]
FireDrop	Intended for helicopters releases.	Teske et al. [1999]
Fluent (VOF method)	Attempt to describe the breakup process. No validation.	Rimbert et al. [2002]
Fluent (Lagrangian method)	2-way coupling analysis. No validation.	Tomé [2004]
RAM	Applies the PATSIM's empirical breakup module. Lagrangian trajectory. Graphical interface.	Tomé and Borrego [2002], Amorim et al. [2006]
FARSITE	DSS for fire growth simulation. User defined coverage levels. No drop modelling capabilities.	Finney [1998]

In fact, and notwithstanding the specificities of each situation, there is some analogy on the physics underlying the aerial application of pesticides and fertilisers (shown in Figure 3-13) and the aerial drop of retardants. Main differences arise from the significantly lower release height (typically around between 2.5 and 7 m) and smaller size of the drops (VMD ≅ 140 μm) due to the use of pressurized atomizers.

Figure 3-13. Aerial spraying of pesticides over crop fields [url 13, url 14].

Several studies (e.g., SDTF [1997]) on the drift of aerial sprays used for agricultural purposes, in particular those conducted by the Spray Drift Task Force (SDTF) in cooperation with the US EPA Office of Pesticide Programs, have shown the importance of droplets diameter distribution, release height and atmospheric conditions on general efficiency of the application. The numerical models for the application of pesticides with aerial means, which intend to minimise the lost of product due to the drifting action of the wind and thus improve the efficiency and decrease the impacts over the ecosystem, have known significant advances during the last years. The most important models in this field are the FSCBG ("Forest Service Cramer-Barry-Grim") [Teske et al., 1993], the PKBW ("Picot Kristmanson Basak-Brown Wallace") [Picot e Kristmanson, 1997] and the AgDRIFT/FS ("Agricultural Drift") [Teske et al., 1997; Bi et al., 2000].

3.3. Vegetative canopy-induced flows

Due to the vertical extent, biomass content, and roughness of forests the physical and chemical properties of the overlying atmospheric boundary layer (ABL) are markedly modified (e.g., Oke [1987], Stull [1988], Garratt [1992], Kaimal and Finnigan [1994], Finnigan [2000]). While the atmospheric flows near the land surface resemble a rough-wall boundary layer, in the presence of a vegetative canopy the flow develops important characteristics of a mixing layer [Raupach et al., 1996; Finnigan, 2000; Marshall et al., 2002; Poggi et al., 2004]. In particular, the turbulence in the roughness sublayer (RSL) is characterised by the presence of distinct coherent structures generated near the top of the canopy [Finnigan and Shaw, 2000]. As a result, many of the characteristic properties of the RSL differ from those of a boundary layer and resemble more those of a plane mixing layer [Raupach et al., 1996].

The characteristics of the wind flow are thus intimately related to the surface roughness. A significant number of field measurements and small-scale experiments have shown that an inadequate description of surface properties can lead to large differences between modelled and measured fluxes [Wesely and Hicks, 2000]. As in the case of real scale dropping tests that have been systematically conducted over bare ground, also the dropping models developed so far (see Table 3-6) do not consider the effect of roughness on the vertical wind shear and particularly the mechanisms through which vegetative canopies can potentially modify the breakup of the liquid and the motion of droplets within the surface layer. In order to understand the influence of vegetative canopies on the wind flow some fundamental characteristics of the ABL should be referred.

The ABL is the turbulent region adjacent to the Earth's surface directly influenced by the effects of the surface. Because the main airflow characteristics (as the velocity, air temperature or moisture) exhibit different height dependent features the ABL is vertically structured into several conceptual layers and sublayers, as schematically shown in Figure 3-14 (e.g., Stull [1988], Garratt [1992], Kaimal and Finnigan [1994]). The ABL depth, which is typically about 10% of the troposphere height, can have 1 to 3 km during daytime depending on the mechanical and buoyant mixing and synoptic scale motions. At the top of the ABL the stable entrainment zone is a boundary between the turbulence in the mixed layer and the streamlined flow of the free atmosphere. Usually, the lowest 10% of the daytime ABL, in which the properties of the airflow reveal their greatest gradients, is called the surface layer. Over very rough surfaces (e.g., forests or urban areas) the surface layer can be further divided into an inertial sublayer (ISL) and a RSL.

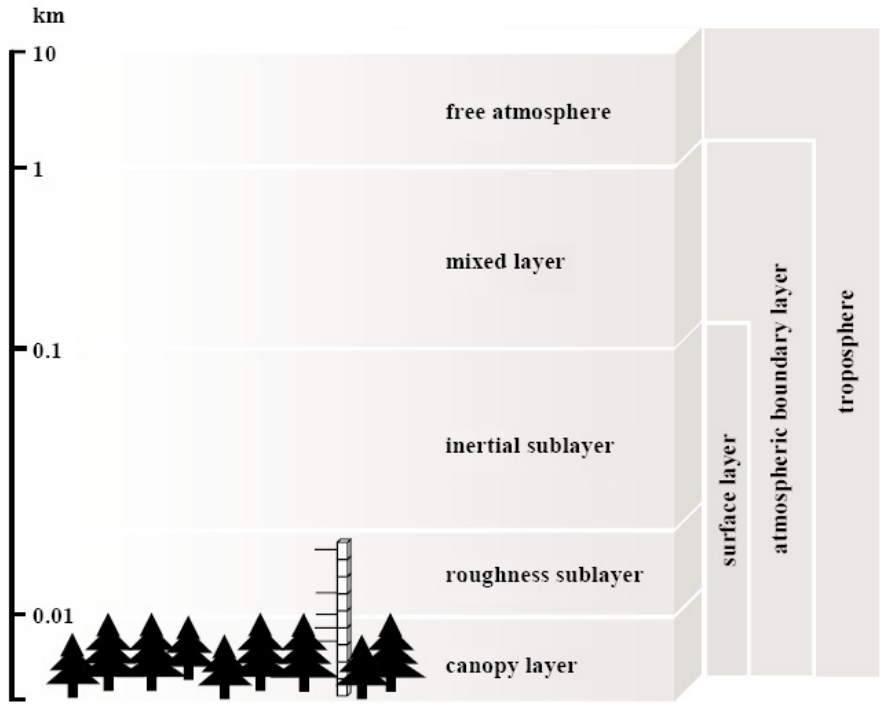

Figure 3-14. Daytime structure of the troposphere over a forest showing the different structured layers [Moncrieff et al., 2000 in Schindler, 2004].

The RSL is the layer immediately above the roughness elements where these individual elements have a direct effect on the characteristics of the airflow. Main characteristics of the RSL are horizontally and vertically varying flux densities. Furthermore, wake turbulence caused by the roughness elements and thermal effects enhance turbulence in the RSL over the turbulence in the ISL. Eddy diffusion coefficients are increased above their logarithmic values encountered in the ISL.

Observations indicate that the depth of the RSL is between two to three times the height of the vegetation. Additionally, a canopy layer forms near the ground, with a depth that is roughly the mean height of the roughness elements [Garratt, 1992].

Due to the fact that forests cover about 30% of the dry land area [FAO, 2007b], biosphere-atmosphere interactions, and in particular the behaviour of flows over and through plants canopies, have been subject of research at different spatial scales and in numerous fields, such as hydrology, ecology, climate system modelling and various engineering branches. The beginning of modern forest meteorology can probably be attributed to the first scientific works of Ebermayer in 1873, Metzger in 1893 and Voeikov in 1894, which were mainly focused on the qualitative analysis of the behaviour of winds in forests [Reifsnyder, 1973; Gayev, 2007]. In 1932, Prandtl, the pioneer of aerodynamics and the first to define the boundary layer, also noticed a significant change in the air properties in its movement through a tall vegetative canopy, identifying a logarithmic behaviour of the flow above the canopy, typical of the turbulent flow regime over a roughness surface [Businger, 1959]. However, nothing was known about the motion within the roughness elements. Intensive investigations on the nature of within-canopy turbulence were started in the early 60s (e.g., Inoue [1963], Uchijima and Wright [1964], Cionco [1965], Wright and Lemon [1966] and Cowan [1968]).

The link between the classical studies on surface boundary layers and the structure of within-canopy turbulence resulted from early observations and theoretical considerations. The majority of these first experimental works were dedicated to observations of the mean wind speed profile within uniform stands, while turbulence intensity and turbulent fluxes of heat or momentum were much less investigated due to the technical complexity involved. An extensive number of measurements on different types of canopies has been the basis for the overall understanding of turbulence structure in vegetation canopies. Measurements have been made on natural stands and on model forests represented by artificial plastic trees and on corn and wheat models of both stiff and flexible crops using arrays of pegs and flexible plastic strips (see Table A-2). Excellent reviews of flow and turbulence in plants canopies can be found in Raupach and Thom [1981] and, more recently, in Finnigan [2000].

The presence of tree trunks, branches, stems and leaves or needles in a forest produces a barrier to air flow caused by form drag and skin friction which reduces the under-forest flow velocities substantially compared with wind speeds which occur above the canopy. Momentum is absorbed from the wind not just at the ground surface but through the whole depth of the canopy as aerodynamic drag on the plants. Surface layer streamlines are displaced vertically, flow beneath the canopy is driven by shear

from the flow above the canopy, and maximum winds occur at the top of the average height of the vegetation (*h*). Mean wind speeds typically decrease within the canopy as one approaches the ground to about 20% of the treetop wind values. Turbulence just above and within a plant canopy results from the distribution of sources and sinks of momentum and scalars within the plant canopy. This source and sink distribution causes a variation in the time averaged moments of velocities and scalars. Turbulence levels beneath the canopy may be similar to those found at ground level over small roughness surfaces (5-15%), but are significantly less than those which can occur in the strong shear which occurs above the canopy roof (20-40%) [Meroney, 2004]. Consequently, although a logarithmic velocity profile is still observed above the canopy, its apparent origin has moved to a level near the top of the plants, which is called the displacement height (*d*), as can be seen in Figure 3-15. The parameter *d* depends on the way the drag force is distributed through the foliage and this in turn depends on the structure of the mean wind and turbulence within the canopy.

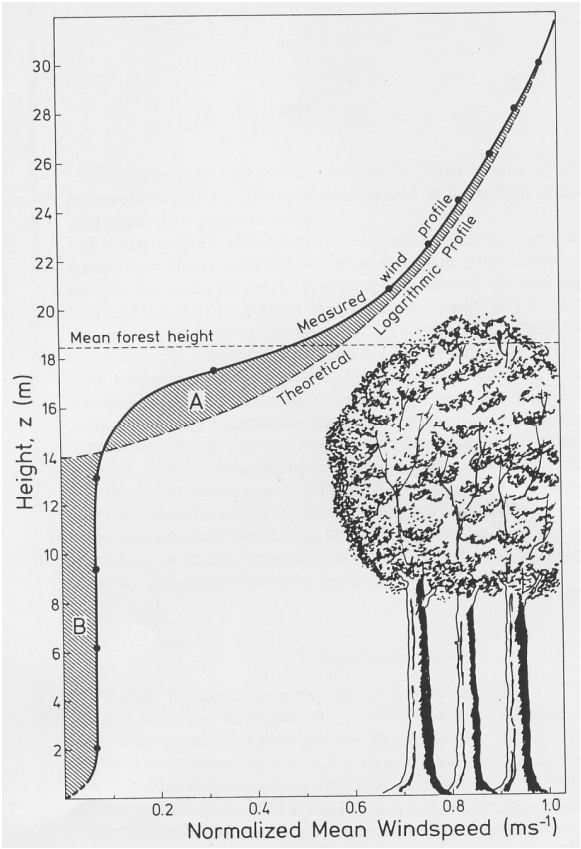

Figure 3-15. Comparative representation of vertical mean wind profiles within and above a plantation of *Pinus sylvestris* in near-neutral stability conditions [De Bruin and Moore, 1985]. The solid line is a measured profile, with the characteristic inflection near the canopy top. The dashed line shows the extrapolated log profile given by Eq. 3-2, which becomes zero at a height $z = d + z_0$ where *d* is the displacement height (in this case equal to 12.7 m) and z_0 the roughness length (equal to 1.28 m). The condition of mass conservation imposes that *d* is chosen such that the log profile, extrapolated to $z \approx 14$ m, transports the same amount of mass as the actual wind profile, as indicated by equal areas A and B.

One of the most typical universal features of the turbulent exchange between plant canopies and the atmosphere is the inflexion of the mean wind speed profile at the canopy top, which is caused by the aerodynamic drag on the plant elements and this is determined by the density of the foliage. The inflexion point corresponds to a hydrodynamic instability, which initiates large coherent structures that are major contributions to the turbulent air mass exchange between tall plant canopies and the atmosphere [Finnigan and Brunet, 1995 in Finnigan, 2000; Raupach et al., 1996; Brunet and Irvine, 2000; Finnigan, 2000].

Wind profiles just above and within plant canopies differ systematically from the typical logarithmic law. Instead, the mean wind speed decreases very strongly at the top of the canopy while the velocity gradient is almost zero in the mid-canopy. An inversion of this gradient may occur in the low-canopy, revealing that a jet can potentially exist in the trunk space due to the low leaf area density. Assuming the forest to be a homogeneous medium with a uniform leaf area density, an exponential profile can be derived. This exponential decrease fits the empirical data rather well, at least close to the canopy top.

For thermally neutral conditions, steady-state flow over horizontally bare soil can be described by the well-known logarithmic law (e.g., Monin and Yaglom [1971]):

$$U(z) = \frac{u_*}{k} \ln\left(\frac{z}{z_0}\right) \qquad \textbf{Eq. 3-1}$$

where $U(z)$ is the horizontal velocity at height z; u_* is the friction velocity for a bare soil, which is given by $\sqrt{\tau/\rho}$, with τ the Reynolds stress and ρ the air density [g], and thus expresses the turbulent surface stress; k is the von Karman's constant taken to be 0.41 and z_0 the roughness length of a bare soil ($z_0 \approx 0.1$ m for general land surfaces [Garratt, 1992]).

For vegetative surfaces, the wind profile above tall vegetation under neutral atmospheric conditions given by Eq. 3-1 can be approximated to:

$$U(z) = \frac{u_*}{k} \ln\left(\frac{z-d}{z_0}\right) \qquad \textbf{Eq. 3-2}$$

[g] In the wind flow analysis, the subscript *G* indicating the gaseous phase when referring to the fluid's properties (as mass density and velocity) is omitted.

where d is the displacement height (or zero-plane displacement), the mean height in the vegetation on which the bulk aerodynamic drag acts [Thom, 1971], and z_0 expresses in this case the capacity of the canopy to absorb momentum ($z_0 \approx 1$ m for tall crops and forests [Garratt, 1992]). According to this expression, the wind speed is zero at height $z = d+z_0$, as shown by Figure 3-15, which also coincides with the mean level of momentum absorption [Jackson, 1981]. However, the logarithmic profile cannot be extrapolated that far downwards. For the non-neutral atmosphere, Eq. 3-1 and Eq. 3-2 were modified by Businger et al. [1971] in order to cope with stability effects. Experimental evidence (e.g., Wilson et al. [1982]; De Bruin and Moore [1985]; Sellers et al., [1986]) indicates that in the RSL above a vegetative surface there is a departure of the wind profile from that predicted by the logarithmic relationship, giving values that are greater than those observed as previously shown in Figure 3-15.

Despite that a great research effort has been made in order to numerically describe the canopy-induced flows, and their implications on turbulent transport and dispersion, a complete time-dependent solution of the exact Navier-Stokes (NS) equations for high-Reynolds number turbulent flows is unlikely to be attainable in the near future. Different closure methods have been proposed in order to deal with this issue. Since the 1960s, the gradient-diffusion theory, or *K*-theory, has been used to study air mass exchange between the Earth's surface and the atmosphere over tall plant canopies as shown in Table 3-7. The proposed profiles use first order closure models that specify an eddy diffusivity, *K*, and a drag coefficient to describe the portion of the mean wind profile beneath the forest ceiling for constant foliage distribution. Beginning in the 1970s, higher-order turbulence closure models and Lagrangian diffusion models have made possible to study not only mean wind velocity speed within and above tall plant canopies but also the statistical characteristics of canopy turbulence. Large eddy simulation (LES) models have also contributed to extend the knowledge about plant canopy turbulence.

Table 3-7. Canopy turbulence closure models.

Turbulence closure	Reference
K-theory	Monin and Yaglom [1971], Thom et al [1975], Raupach [1992], Harman and Finnigan [2007]
Higher-order models	Wilson and Shaw [1977], Meyers and Paw U [1986], Wilson [1988], Liu et al. [1996], Katul and Albertson [1998], Ayotte et al. [1999], Leuning [2000], Finnigan and Shaw [2000]
LES	Shaw and Schumann [1992], Su et al. [1998]

3.4. Summary

Resuming, the review on the state-of-the-science of the numerical modelling of aerial dropping provides the following main conclusions:

- Dropping models can play an important role on the efficiency of firefighting operations, especially if integrated on a DSS that covers other parameters as meteorology, terrain, vegetation, fire progression, available firefighting resources, etc.

- The most systematic and detailed study on the aerodynamic breakup of firefighting products dates back to the 1970s. An analogy can be established with some studies performed since, namely at the levels of the experimental analysis of the breakup of JICF and the modelling of fuel injection in internal combustion equipments.

- In general, the newer dropping models currently available were not validated with measured values of product concentration at ground. Their conceptual fundaments, based on physical laws or empirical approaches, require further verification.

- The non-Newtonian behaviour of chemical retardants represents an additional complexity to the analysis of the aerodynamic breakup of the liquid. Operational dropping models have neglected these effects due to computational time constraints. However, also detailed numerical schemes as VOF have had difficulty in describing the involved dynamical processes with the required accuracy. Moreover, laboratorial work has been focused mostly on the study of Newtonian fluids, especially in the case of the primary breakup of jets.

- The effect of wind flow over the breakup and trajectory of the liquid droplets has been neglected. Especially in the presence of dense vegetative canopies, characterized by an intense exchange of momentum with the atmosphere, its impact should be assessed following the example from pesticides' drift studies. The percentage in volume of fine droplets present in the wide range of diameters originated by secondary breakup of firefighting products is significant, and increases when water or pressurized discharge systems (as MAFFS) are used. Lower droplets diameters make the spray cloud more susceptible to drift and thus increase the importance of vegetative canopy-induced flows on ground pattern.

These aspects are discussed along the current work and constitute the basis for the development of the Aerial Dropping Model ADM.

4. Aerial Dropping Model development

The present chapter presents the development of the Aerial Dropping Model ADM, describing the general structure, the input and output data and the different modules that constitute this numerical tool. The numerical approaches to the implicit phenomena are analysed.

4.1. General structure and input/output data

The model is divided into six modules, as represented in Figure 4-1, each of them representing a stage in the aerial drop of the liquid. Figure A-1 shows a more detailed scheme of the data used and produced by each module.

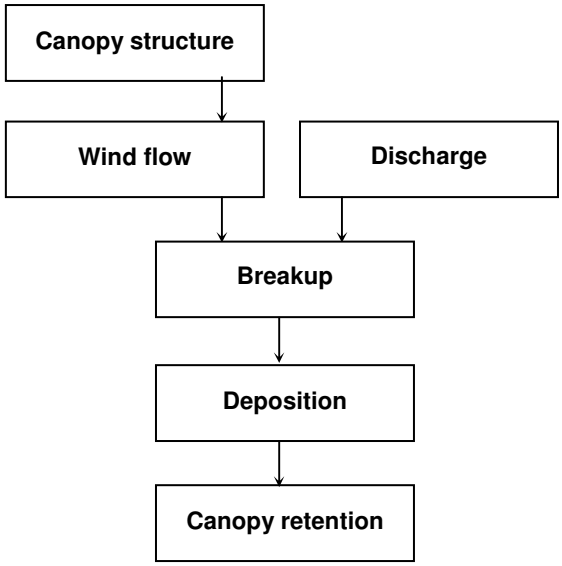

Figure 4-1. General fluxogram of ADM model showing the different modules and data flow.

ADM is written in the Fortran® programming language. If used without the graphical user interface (GUI), it requires only one input file where the user provides all the parameters needed for the simulation. Some of these parameters are already defined as default values that the user can modify or not depending on the information available. The input data shown in Table 4-1 can be categorized as follows: product characteristics, flight parameters, meteorological conditions and canopy characteristics. The main output data is the ground pattern of liquid, which is given in the format of liquid concentration per computational cell in a file with .dat extension. This file can then be represented with any 2D surface mapping and contouring

software. When using the GUI, the ground pattern is automatically generated at the end of the simulation.

Table 4-1. Input parameters used by ADM model.

	Input parameters	Units
	Canopy module	
—	Tree species	—
h	Canopy height	m
	Wind flow module	
U_m	Measured wind velocity	$m.s^{-1}$
θ_m	Measured wind direction	º
H_m	Measurement height	m
	Discharge module	
H_T	Tank height	m
L_T	Tank length	m
W_T	Tank width	m
D_V	Equivalent vent diameter	m
L_V	Vent length	m
L_D	Door length	m
W_D	Door width	m
α	Door opening angle	º
t_α	Door opening time	s
V_L	Volume dropped	l
ρ_L	Retardant density	$kg.m^{-3}$
	Breakup module	
μ_L	Retardant viscosity	cP
U_a	Aircraft velocity	$m.s^{-1}$
θ_a	Aircraft direction	º
H_a	Dropping height	m
	Canopy retention module	
δ	Film thickness	mm

4.2. Canopy module

Leaves are the active interface for energy, momentum, carbon and water exchange between plants and the atmosphere and, therefore, the leaf area is a key variable in most of the models dealing with the dynamics of heat, mass and momentum between stands of plants and their environment (e.g., Cowan [1968], Cutini et al. [1998]). In this context, the leaf area index (LAI) constitutes an important structural characteristic of the forest ecosystem and is one of the most important biophysical parameters on climatic, ecological and agronomical research studies (e.g., Stroppiana et al. [2006]). In current literature LAI is usually defined as one half the total plant area [h] per unit ground surface area (with units in $m^2.m^{-2}$). In fact, there has been some discussion around the most suitable definition for LAI since the original definition by Watson [1947], in particular due to the case of non-flat leaves, which pose some problems when using the projected one-sided plant area concept [Jonckheere et al., 2004].

Methods for in situ LAI measurement can be grouped in two main categories: direct and indirect (for more details see Jonckheere et al. [2004], Weiss et al. [2004], Stroppiana et al. [2006]). LAI, and other biophysical parameters, can be also estimated by using remote-sensing imagery, which is commonly made through vegetation index approach or modelling approach. However, operational algorithms or procedures to convert radiometric measurements into LAI are still under development [Qi et al., 2000]. Because direct and indirect methods are time-consuming and laborious, remote sensing offers the opportunity to monitor the variability of LAI over large scales of time and space [Le Dantec et al., 2000].

The referred studies have shown that the spatial variability of LAI is due to several factors, namely the canopy type (as species composition and age of the stands), site characteristics (nutrient availability and soil typology) and meteorological conditions, thus explaining the seasonal and interannual variation at the stand scale.

In ADM model, default LAI values are available depending on the type of overstorey, i.e., by the knowledge of the specific canopy over which the drop is going to occur the user just selects a typical average value. Alternatively, LAI can be specified by the user. In the Portuguese forest four species are clearly dominant: the maritime pine (*Pinus pinaster* Ait.), the cork oak (*Quercus suber* L.), the eucalyptus (*Eucalyptus globulus* Labill.), and the holm oak (*Quercus ilex* L.). These species represent, respectively, 30%, 22%, 21% and 14% of the total area occupied by forest

[h] The plant area corresponds to the leaf area in the case of deciduous canopies and to the needle area in the case of coniferous canopies.

(according to the National Forest Inventory [DGF, 2001]). The LAI values for each species can vary considerably as can be seen for the pine forest in Table A-3, for which values between 1.6 and 3.5 are referred in literature. The default LAI values shown in Table 4-2 were obtained, in the cases of the pine and eucalypt forests, from the observations by Valente [1999] in Portuguese territory. For the oak canopy type, the default LAI corresponds to the average from the values measured by Quilchano et al. [2008].

Table 4-2. ADM default LAI values for the dominant species in the Portuguese forest.

Canopy classification	Species	*LAI* ($m^2.m^{-2}$)
Resinous	*Pinus pinaster* Ait.	2.7
Evergreen	*Eucalyptus globulus* Labill.	3.2
	Quercus suber L. *Quercus ilex* L.	1.9

Specifically for simulations with North American tree species, ADM applies the method developed by Teske and Thistle [2004], in which an extensive database was created by assembling data for several forests, allowing to define the characteristics of generic deciduous and coniferous trees. The values of LAI and canopy height given in Table 4-3 were obtained by averaging across the observed data. Additionally, this approach allowed generation of average profiles that represent the variation of LAI with height for these two generic canopy categories. This was accomplished by curve fitting the profiles available in literature to a modified Weibull cumulative distribution function that computes the LAI vertical profile through Eq. 4-1:

$$LAI(z) = LAI \cdot \left(\frac{1 - \exp\left[-\left(1 - \frac{z}{h \cdot b} \right)^{c} \right]}{1 - \exp\left[-\left(\frac{1}{b} \right)^{c} \right]} \right) \qquad \textbf{Eq. 4-1}$$

where h is the canopy height, z the height at which the LAI value is computed, LAI is the mean LAI across the entire depth, and b and c are curve fitting constants (defined in Table 4-3).

Table 4-3. ADM default canopy parameters for generic US forests.

Canopy type	*LAI* ($m^2.m^{-2}$)	*h* (m)	*b*	*c*
Generic deciduous	3.29	25.75	0.574	2.230
Generic coniferous	6.12	19.3	0.906	2.145

As it will be seen in the following section, for estimating the wind flow ADM requires only the knowledge of the mean LAI for a given canopy and the respective height. The simple method developed by Teske and Thistle [2004] for computing the vertical profile of LAI is used by the retention model described in section 4.7.

4.3. Wind flow module

The recent proposal by Harman and Finnigan [2007] of a unified theory for the description of the mean wind speed vertical profile in the presence of a vegetative canopy under varying atmospheric stability conditions served as the basis for the development of the ADM wind flow module. It describes the flow inside the canopy and in the RSL through the mixing layer analogy originally proposed by Finnigan [2000].

The coordinate system of the model has its vertical origin (z = 0) located at the canopy top, 'separating' the flow into two vertical layers: a dense horizontally homogeneous canopy on flat terrain and the overlying RSL. In this modified coordinate system the displacement height (d_t) is related to the conventionally defined displacement height (d) through the canopy height (h) according to:

$$d_t = h - d \qquad \textbf{Eq. 4-2}$$

The justification for this deviation from standard practice relies on the fact that for dense canopies almost all the momentum is absorbed as drag on the foliage rather than as stress on the ground. Consequently, no drag is exerted on the underlying substrate and the location of the ground becomes irrelevant to the dynamics. While simplifying the calculation, the core of the analysis is focused at the region of the ABL that directly impacts on the motion of the droplets of firefighting product, i.e., the RSL above the canopy top. Moreover, as noted by the comparative study by Raupach et al. [1986] on the turbulence statistics of different canopies, the normalized mean velocity profiles exhibit a characteristic inflection point at the canopy top, which

separates the standard boundary layer profile observed above the canopy from the roughly exponential profile within the canopy space. This inflexion point, which is known to play a critical role in canopy dynamics, is the location where the physical processes change and thus constitutes the natural choice for the origin of the coordinate system. Moreover, in the variety of canopies analysed by Raupach et al. [1986], the vertical turbulent flux of momentum, $-\overline{u'w'}$ (where *u'* and *w'* are the fluctuating velocities around the mean velocities *u* and *w*), were practically zero at ground level, indicating that all of the horizontal momentum was absorbed by the canopy elements even though some of the canopies in the ensemble were not particularly dense [Finnigan, 2000]. As the model does not recognise the presence of the ground it allows non-zero flow at the ground surface. To force the profile to zero at the ground would require the inclusion of a second boundary layer along the ground surface, which in the present analysis is unnecessary given the reasons above mentioned.

4.3.1. Air flow within the canopy

The time-averaged momentum equation within a vegetative canopy can be written as follows [Belcher et al., 2003; Harman and Finnigan, 2007] [i]:

$$0 = -\frac{1}{\rho}\frac{\partial \tau}{\partial z} - F_D \qquad \textbf{Eq. 4-3}$$

where the first term in the second member represents the turbulent fluxes and the last the kinematic canopy drag.

The turbulence closure for the turbulent fluxes applies the Prandtl's mixing length hypothesis given by (e.g., Garratt [1992]):

$$\tau(z) = \rho \cdot l^2 \left(\frac{dU(z)}{dz} \right)^2 \qquad \textbf{Eq. 4-4}$$

where *l* is the mixing length and $U(z)$ is the mean wind speed at height *z*.

The kinematic canopy drag F_D is associated with a momentum deficit in the wake of the canopy elements that slows the mean flow, which is mathematically expressed as:

[i] For a detailed discussion on the derivation of the momentum equation for adiabatic flow within vegetation see Raupach and Shaw [1982], Raupach et al. [1986], Brunet et al. [1994] and Finnigan [2000].

$$F_D = c_D \cdot a \cdot U^2(z) \qquad \textbf{Eq. 4-5}$$

In this expression, c_D is the drag coefficient, which for simplicity is considered to be constant throughout the depth of the canopy, and a is the leaf area density, a parameter describing the foliage distribution analogous to LAI, that represents the projected one-sided plant area per unit volume of deciduous/coniferous canopies (in $m^2.m^{-3}$) [j].

The concept of canopy drag underlying the present approach was also tested by the author using a higher order turbulence closure model for use in urban air quality applications. The major difference was that it relied on a different method for providing the Reynolds stress, according to which the turbulent viscosity is calculated from the values of the turbulent kinetic energy (K) and its dissipation (ε) given by a $K\varepsilon$ turbulence closure model (for more details see Amorim [2003], Amorim et al. [2004a, b and 2005], Borrego et al. [2003 and 2004], Miranda et al. [2007] and Martins et al. [2008]).

The drag coefficient is, in fact, an important parameter which links canopy architecture with its aerodynamic behaviour. However, the values reported in literature, both from wind tunnel and open field experiments, show a high variability among canopies and a systematic dependence on wind speed, which has generally been justified with the alignment of canopy elements and with the effect of viscous drag [Cescatti and Marcolla, 2004; Novak et al., 2000]. However, in most natural canopies, the product $c_D \cdot a$ is expected to be more constant with height than each of the parameters alone [I. Harman, pers. communication]. A typical drag coefficient of 0.25 is used in the model. LAI, on the other hand, is defined based on the type of canopy (as described in section 4.2).

The inverse of the product $c_D \cdot a$ defines the canopy-drag length scale, denoted as L_c, which is independent of U and determines the efficiency of the canopy to remove momentum from the flow; thus, it is related to the distance required for the adjustment of the boundary layer to the canopy [Finnigan and Brunet, 1995 in Finnigan, 2000; Belcher et al., 2003]. The kinematic canopy drag is then expressed as:

$$F_D = \frac{U^2(z)}{L_c} \qquad \textbf{Eq. 4-6}$$

[j] In literature other notations are also used for indicating the variation of leaf area density with height, namely $LAD(z)$ and $L(z)$.

The LAI is given by the integral of the leaf area density $a(z)$ through the canopy depth h:

$$LAI = \int_{-h}^{0} a(z)dz \qquad \textbf{Eq. 4-7}$$

As the canopy is considered homogeneous:

$$a \approx \frac{LAI}{h} \qquad \textbf{Eq. 4-8}$$

Thus L_c can be approximated from the height of the canopy h and the LAI value as:

$$L_c \approx \frac{h}{c_D LAI} \qquad \textbf{Eq. 4-9}$$

Substituting the turbulent fluxes given by Eq. 4-4 and the canopy drag expressed in Eq. 4-6, the momentum equation then becomes:

$$0 = \frac{d}{dz}\left[l^2 \left(\frac{dU(z)}{dz} \right)^2 \right] - \frac{U^2(z)}{L_c} \qquad \textbf{Eq. 4-10}$$

The vertical wind profile dU/dz within the canopy ($z < 0$) can be described applying the formulation by Inoue [1963 in Harman and Finnigan, 2007]:

$$U(z) = U_h e^{\frac{\beta \cdot z}{l}} \qquad (for\ z < 0) \qquad \textbf{Eq. 4-11}$$

In this expression the coefficient β relates the wind speed at the canopy top, U_h, with the friction velocity, u_*, for the flow in the overlying surface layer, according to:

$$\beta = \frac{u_*}{U_h} \qquad \textbf{Eq. 4-12}$$

where,

$$u_* = \sqrt{\frac{\tau_{(z=0)}}{\rho}} \qquad \textbf{Eq. 4-13}$$

Harman and Finnigan [2007] derived a closure for the calculation of β as:

$$\beta = \frac{\beta_N}{\phi_m(z=0)} \qquad \textbf{Eq. 4-14}$$

In this expression, β_N is the canopy parameter in neutral conditions (which is around 0.3 based on Harman and Finnigan [2007]) and the stability function ϕ_m has the form given in Eq. 4-28.

In order to derive the partial derivative $dU(z)/dz$ in Eq. 4-10 one can consider both L_c and l as constant. With this simplification, the following expression is obtained:

$$\frac{dU}{dz} = \frac{\beta}{l} U(z) \qquad \textbf{Eq. 4-15}$$

The mixing length l is then found to relate with L_c according to:

$$l = 2\beta^3 L_c \qquad \textbf{Eq. 4-16}$$

The displacement height d_t can be interpreted as the mean level of momentum absorption by the canopy, based on the work by Thom [1971] and Jackson [1981]. This yields a method for calculating d_t (where the negative sign arises from the choice of coordinate origin) applying the drag given by Eq. 4-6 and Eq. 4-16 for l, as described below.

$$d_t = \frac{\int_{-\infty}^{0} z \cdot F_D dz}{\int_{-\infty}^{0} F_D dz} = \frac{\int_{-\infty}^{0} \frac{z \cdot U^2(z)}{L_c} dz}{\int_{-\infty}^{0} \frac{U^2(z)}{L_c} dz} = \frac{l}{2\beta} = \beta^2 L_c \qquad \textbf{Eq. 4-17}$$

From Eq. 4-14 and Eq. 4-17 it is possible to obtain the stability dependent polynomial expression for β, which is solved in the model applying the Newton-Raphson method:

$$\begin{cases} \beta_N^{-4}\beta^4 + \frac{\gamma_1 L_c}{L}\beta^2 - 1 = 0 & \text{if } \zeta < 0 \\ \beta_1 L_c \beta^3 + L\beta - \beta_N L = 0 & \text{if } \zeta \geq 0 \end{cases} \qquad \textbf{Eq. 4-18}$$

In this expression, L is the Obukhov length, which is used to characterise the atmospheric stability of the boundary layer, and ζ is a surface layer scaling parameter. Both will be analysed with more detail in section 4.3.2. After having determined the β value, the friction velocity u_* is calculated by applying Eq. 4-12.

4.3.2. Air flow above the canopy

The use of flux-profile relationships is a common practice in many boundary-layer studies, mainly due to the fact that aid in the understanding of turbulent transport and allow the vertical turbulent fluxes to be predicted from the more-easily measured and predicted vertical gradients of the mean profiles. Although the Monin-Obukhov

Similarity Theory (MOST) [Monin and Yaglom, 1971] provides a consistent set of flux-profile relationships for application in the atmospheric surface layer, it has been shown that these fail in a layer extending to several canopy heights [Raupach and Thom, 1981; Garratt, 1992; Högström, 1996]. In order to extend their validity to the RSL different functions have been proposed [Garratt, 1980 and 1983; Raupach, 1992; Cellier and Brunet, 1992; Mölder et al., 1999; Harman and Finnigan, 2007]. Therefore, the wind gradient above the canopy can be written as:

$$\frac{dU}{dz} = \frac{u_*}{k(z+d_t)}\Phi_m(\zeta) \qquad (for\ z>0) \qquad \textbf{Eq. 4-19}$$

Where the similarity function Φ_m depends on the scaling parameter ζ (e.g., Stull [1988], Garratt [1992]), modified due to the change of coordinates to:

$$\zeta = \frac{z+d_t}{L} \qquad \textbf{Eq. 4-20}$$

The Obukhov length *L* can be physically interpreted as being proportional to the height above the surface at which buoyant factors first dominate over mechanical (shear) production of turbulence. In ADM, *L* is estimated similarly to the approach implemented in the meteorological preprocessor AERMET of the air quality dispersion model AERMOD [USEPA, 1999]. This calculation requires the knowledge of the sensible heat flux (*H*). The expression for estimating *H*, which was derived by Holtslag and van Ulden [1983] from the energy balance at the earth's surface for rural sites, depends on the net radiation (R_n) and the Bowen ratio (*Bo*) as follows:

$$H = \frac{0.9R_n}{1+\left(\frac{1}{Bo}\right)} \qquad \textbf{Eq. 4-21}$$

The daytime *Bo* value expresses the ratio between the sensible heat flux and the latent heat flux, and thus gives an indication of surface moisture content. The variation of *Bo* with type of canopy, moisture conditions and season was developed by Paine [1987]. Indicative values are given in Table 4-4 for seasons that are typically characterised by the occurrence of forest fires.

Table 4-4. Indicative values of daytime Bowen ratio for deciduous and coniferous forests by season and moisture conditions.

	Bowen ratio		
Forest / moisture	**Spring**	**Summer**	**Autumn**
Dry conditions			
Deciduous	1.5	0.6	2.0
Coniferous	1.5	0.6	1.5
Average moisture conditions			
Deciduous	0.7	0.3	1.0
Coniferous	0.7	0.3	0.8

The net radiation R_n is estimated from:

$$R_n = \frac{R(1 - r(\phi_s)) + c_1 T^6 - \sigma_{sb} T^4 + c_2 n}{1 + c_3} \qquad \textbf{Eq. 4-22}$$

where R is the total incoming solar radiation; $r(\phi_s)$ the surface albedo as a function of solar elevation angle (ϕ_s); T the ambient temperature; n the fractional opaque cloud cover; σ_{sb} the Stefan-Boltzmann constant; and c_1, c_2 and c_3 are empirical constants (see Table 4-5).

The value for the albedo as a function of solar elevation angle is given by the following empirical expression [Paine, 1987]:

$$r(\phi_s) = r' + (1 - r')\exp\left[-0.1\phi_s - 0.5(1 - r')^2\right] \qquad \textbf{Eq. 4-23}$$

where r' is the albedo for the sun on the meridian, which is specific for the surface characteristics of the site. The albedo is the fraction of total incident solar radiation reflected by the surface back to space without absorption and thus expresses the reflectivity of the surface. Given the necessity of knowing the ϕ_s and r', a default value of 0.12, typical for forests in the period from Spring to Autumn according to Paine [1987], is used in ADM model by default.

R is computed using the following expression from Kasten and Czeplak [1980]:

$$R = R_0\left(1 + b_1 \cdot n^{b_2}\right) \qquad \textbf{Eq. 4-24}$$

with R_0 as the incoming solar radiation at ground level for clear skies and b_1 and b_2 are empirical coefficients [Holtslag and van Ulden, 1983].

The value for the incoming solar radiation for clear skies is estimated by the model as:

$$R_0 = a_1 \cdot \sin(\phi_s) + a_2 \qquad \textbf{Eq. 4-25}$$

where the values for the empirical constants a_1 and a_2 given in Table 4-5.

With the knowledge of the net radiation (R_n) and the Bowen ratio (Bo) it is now possible to estimate the sensible heat flux H (from Eq. 4-21). In this manner, all the information required for calculating the Obukhov length through Eq. 4-26 is known:

$$L = -\frac{\rho c_p T u_*^3}{kgH} \qquad \textbf{Eq. 4-26}$$

where ρ is the density of air, c_p the specific heat capacity of air, T is the ambient temperature (in Kelvin), k the von Karman constant and g the acceleration of gravity.

Table 4-5 summarizes the values for the constants appearing in the calculation of the Obukhov length as described above.

Table 4-5. Summary of constants and respective values used in the estimation of the Obukhov length.

Symbol	Name	Value	Units
ρ	density of dry air	1.2	$kg.m^{-3}$
c_p	specific heat capacity of dry air	1003	$J.kg^{-1}.K^{-1}$
σ_{sb}	Stefan-Boltzmann constant	5.67×10^{-8}	$W.m^{-2}.K^{-6}$
k	von Karman constant	0.41	-
c_1	empirical constants	5.31×10^{-13}	$W.m^{-2}.K^{-4}$
c_2		60	$W.m^{-2}$
c_3		0.12	-
b_1		-0.75	-
b_2		3.4	-
a_1		990	Wm^{-2}
a_2		-30	Wm^{-2}

Returning to Eq. 4-19, the similarity function Φ_m is calculated by the following expression [Harman and Finnigan, 2007]:

$$\Phi_m = \phi_m\left(\frac{z+d_t}{L}\right)\cdot\hat{\phi}_m\left(\frac{\beta(z+d_t)}{l}\right) \qquad \textbf{Eq. 4-27}$$

where the hat indicates a RSL variable and the MOST stability function for momentum (ϕ_m) takes the form [Garratt, 1992; Högström, 1996]:

$$\phi_m(\zeta)=\begin{cases}(1-\gamma_1\zeta)^{-0.25} & \text{if } \zeta<0\\ 1+\beta_1\zeta & \text{if } \zeta\geq 0\end{cases} \qquad \textbf{Eq. 4-28}$$

with γ_1 = 15 and β_1 = 5. The integrated form of the MOST similarity function is [Garratt, 1992]:

$$\psi_m(\zeta)=\begin{cases}2\ln(1+x)+\ln(1+x^2)-2\tan^{-1}(x) & \text{if } \zeta<0\\ -\beta_1\zeta & \text{if } \zeta\geq 0\end{cases} \qquad \textbf{Eq. 4-29}$$

where $x=\phi_m^{-1}$.

For the neutral stability case ($\zeta\to 0$) the MOST similarity functions reduce to the limits of ϕ_m = 1 and ψ_m = 0, with obvious simplifications on the following expressions.

Integrating Eq. 4-19 between $-d_t+z_{0m}$ and z with Φ_m given by Eq. 4-27 gives [Physick and Garratt, 1995; Harman and Finnigan, 2007]:

$$\frac{k}{u_*}U(z)=\ln\left(\frac{z+d_t}{z_{0m}}\right)-\psi_m\left(\frac{z+d_t}{L}\right)+\psi_m\left(\frac{z_{0m}}{L}\right)+\hat{\psi}_m(z) \qquad (\text{for } z>0) \qquad \textbf{Eq. 4-30}$$

z_{0m} is the roughness length associated with the flow in the inertial sublayer and was derived by Harman and Finnigan [2007] as:

$$z_{0m}=d_t\exp\left\{\frac{-k}{\beta}\right\}\exp\left\{-\psi_m\left(\frac{d_t}{L}\right)+\psi_m\left(\frac{z_{0m}}{L}\right)\right\}\exp\{\hat{\psi}_m(z=0)\} \qquad \textbf{Eq. 4-31}$$

As it is shown, z_{0m}, as also d_t in Eq. 4-17, are stability dependent, and to assume constant values (as is common practice) could represent a significant deviation in the predicted wind speed profile. This equation is implicit by nature and is solved in the model applying the bisection method. In this expression, the function $\hat{\psi}_m$ takes the form:

$$\hat{\psi}_m(z)=\int_{z+d_t}^{\infty}\frac{\phi_m\left(\frac{z'}{L}\right)\left[1-\hat{\phi}_m\left(\frac{z'}{l/\beta}\right)\right]}{z'}dz' \qquad \textbf{Eq. 4-32}$$

The $\hat{\phi}_m$ function quantifies the deviation from the standard MOST profiles due to the presence of the canopy. It was formulated by Harman and Finnigan [2007] based on the work by Garratt [1980] as:

$$\hat{\phi}_m(z) = 1 - c_1 \exp\left\{-\beta c_2 \frac{(z + d_t)}{l}\right\} \qquad \textbf{Eq. 4-33}$$

with $c_2 = 0.5$ and c_1 is given by:

$$c_1 = \left[1 - \hat{\phi}_m(z=0)\right]\exp\left\{\frac{c_2}{2}\right\} = \left[1 - \frac{k}{2\beta\phi_m(z=0)}\right]\exp\left\{\frac{c_2}{2}\right\} \qquad \textbf{Eq. 4-34}$$

Knowing that c_1 is fixed with respect to stability then the following simplification applies [Harman and Finnigan, 2007]:

$$c_1 = \left[1 - \frac{k}{2\beta\phi_m(z=0)}\right]\exp\left\{\frac{c_2}{2}\right\} = \left[1 - \frac{k}{2\beta_N}\right]\exp\left\{\frac{c_2}{2}\right\} \qquad \textbf{Eq. 4-35}$$

After some algebra, the integral from Eq. 4-32 gives:

$$\hat{\psi}_m(z) = \begin{Bmatrix} \frac{c_1}{L}\exp\left(\frac{-0.5\beta d_t}{l}\right)\left[\frac{\sigma l^2}{\beta^2}\left(-\exp\left(\frac{-0.5\beta^2 B}{l^2}\right) + \exp\left(\frac{-0.5\beta^2 A}{l^2}\right)\right)\right] + \\ + L\left(E_i\left(\frac{-0.5\beta^2 B}{l^2}\right) - E_i\left(\frac{-0.5\beta^2 A}{l^2}\right)\right) \end{Bmatrix} \qquad \textbf{Eq. 4-36}$$

Where the lower limit of integration A for $z = 0$ is d_t and the upper limit B is approximated as the top boundary of the domain ($50 \times L_c$) and the constant σ is equal to 32 in the unstable case and 10 in the stable one. For positive x, the exponential integral E_i is defined as (e.g., Abramowitz and Stegun [1972]):

$$E_i(x) = \int_{-x}^{\infty} \frac{e^{-t}}{t} dt \quad , x > 0 \qquad \textbf{Eq. 4-37}$$

The Puiseux series of $E_i(x)$ along the positive real axis is given by:

$$E_i(x) = \gamma + \ln x + \sum_{n=1}^{\infty} \frac{x^n}{n \cdot n!} \quad , x > 0 \qquad \textbf{Eq. 4-38}$$

where the Euler's constant, γ, is equal to 0.57721.

As in Eq. 4-36 the argument of the exponential integral is always negative, the mathematical functions in Eq. 4-37 and Eq. 4-38 are not valid. Instead, the expression for $E_i(x)$ in the negative x region is defined by the Cauchy principal value:

$$E_i(x) = -E_1(-x) \quad , x < 0 \qquad \textbf{Eq. 4-39}$$

where E_1 is:

$$E_1(x) = \int_x^{\infty} \frac{e^{-t}}{t} dt \quad , x > 0 \qquad \textbf{Eq. 4-40}$$

The exponential integral function $E_i(x)$ is calculated in the model through Eq. 4-39 applying the approximate solution from Segletes [1998] to the exponential integral in Eq. 4-40. This fit, which has an error of ±0.00511%, is given by:

$$E_1(x) \approx e^{-x} \ln\left\{1 + \frac{1}{x} - \left[\frac{1}{x} - \ln\left(1 + \frac{1}{x}\right)\right] \cdot f(x)\right\} \qquad \textbf{Eq. 4-41}$$

with the function $f(x)$ equal to:

$$f(x) = \frac{x^2 + 4.054x + 6.207\left(1 - e^{-\gamma}\right)}{x^2 + \left(4.054 + \frac{5}{3}\right)x + 6.207\left[1 + \frac{0.5032x}{(1 + 29.3x)^2}\right]} \quad , 0 < x < \infty \qquad \textbf{Eq. 4-42}$$

The referred derivation defines the full set of equations needed for determining the coupled wind profile.

In order to guarantee the accuracy of the computations, the following limits of applicability for unstable and stable conditions should be fulfilled [Harman and Finnigan, 2007]:

$$\begin{cases} \frac{L_c}{L} \geq -\frac{2}{\beta^2} & , L < 0 \\ \frac{L_c}{L} \leq \frac{2.2 \cdot k(1-\alpha)^2}{\alpha^2 \cdot \gamma_2 \cdot \beta} & , L > 0 \end{cases} \qquad \textbf{Eq. 4-43}$$

where $0 < \alpha < 0.8$ and $0 < \gamma_2 < 1$.

4.4. Discharge module

Because of the relevance of flow rate variation in determining the pattern characteristics and coverage levels, an accurate knowledge of the volume of product released per time is needed. The model allows the user to select between three distinct discharge options according to the categories of aerial delivery systems referred in section 2.2. The following information is required in each of the situations:

- Modular Aerial Fire Fighting System (MAFFS): in pressurized delivery system, the following data are requested: flow rate; up to five representative classes of droplets diameters produced by the atomizer; and exit velocity.

- Constant Flow Delivery System: the code requires from the user measured values of the variation with time of volume released (in litres). The model will interpolate the values, if needed, for the necessary time-step of the calculations: 0.02 s.

- Conventional Aerial Delivery System: in this type of systems two possibilities are available. In the first, the user provides an input file with measured values of the variation with time of volume released, as in previous system. If measured flow rate is not available, the code simulates the volume released as a function of time applying the methodology developed during the flow rate studies conducted by the USDA-FS under the scope of ETAGS program [Swanson et al., 1975, 1977 and 1978] (referred in section 3.2). A brief description of the simulation procedure is given above.

ETAGS research has shown that there are basically two types of tanks: those with only minor restrictions and fast doors, in which the fluid continually accelerates out of the tank, and those sufficiently restricted that a steady-state flow is reached and sustained during the discharge. The tank is thus dominated by either steady-state flow or acceleration flow. Moreover, most tanks present both acceleration- and pressure-dominated flows with regions of mixed contribution.

ADM applies the developments on flow rate simulation from Swanson et al. [1977]. From the extensive testing in Swanson et al. [1978] it was shown that the flow rate prediction based on tank geometry and door-opening rate accounted for most aspects of tank flow with significant accuracy.

Without the complexity of dealing directly with the equations governing the vertical flow from the tank, numerical approximations are applied in both flow regimes. In this combined approach, the instantaneous flow rate and new fluid position under both conditions is given by the vertical velocity of efflux (w_E), corresponding to the lower value between the acceleration-dominated velocity (w_A) and the Bernoulli velocity (w_B):

$$w_E = \min\{w_A, w_B\} \qquad \textbf{Eq. 4-44}$$

ETAGS experiments have shown that in unrestricted tanks the flow rate is better described by the acceleration regime alone. In this case, if the doors rate has been

identified by the model as being fast enough not to restrict the outflow, the model does not allow the steady-state case to be applied.

Initial conditions for each calculation are those resulting from the prior computational step. The combined approach for steady-state and acceleration flows applied in the model is explained hereafter.

In a truly free-fall tank, the outflow of the liquid from the aircraft tank will change from acceleration-dominated to steady-state toward the end of discharge. During the opening of the tank doors the ratio of the doors area and the actual (effective) area will progressively approach unity, as it does in most tanks with doors fully open. The acceleration-dominated velocity, also including a pressure-related term, takes the form:

$$w_A = w_E + \Delta t\left(g + \frac{P}{\rho h}\right) \qquad \textbf{Eq. 4-45}$$

where w_E is the efflux velocity in the previous time-step (at t = 0 s $\Rightarrow$ w_E = 0 m.s^{-1}), and the pressure head term, representing the acceleration due to pressure, usually assumes negative values in unpressurized tanks.

The steady-state condition begins with the assumption that, after a given time, the acceleration is negligible and, therefore, the flow is no longer acceleration-dominated but steady-state. Additionally, if one assumes that the vertical flow from the tank is also inviscid, incompressible and irrotational along a streamline, it can be described by the Bernoulli equation, which expresses the difference in velocity between the top surface of the tank and the flow exiting from the bottom. In these conditions, the Bernoulli velocity is then given by:

$$w_B = \sqrt{\frac{2g\rho h + 2P}{\rho} + w_t^2} \qquad \textbf{Eq. 4-46}$$

where g is the acceleration of gravity, ρ the mass density of the liquid, h the fluid height, P the pressure and w_t the velocity at the top of the fluid. Basically, the Bernoulli equation states that the total hydraulic head [k] is constant along a

[k] The total hydraulic head (H) is expressed as the sum of the pressure head (the internal energy of a fluid due to the pressure exerted on the container, $P/\rho g$), the velocity head (the kinetic energy from the motion of the fluid, $U^2/2g$, where U is the liquid velocity) and the elevation head (the relative potential energy in terms of the level of fluid in the reservoir, h).

streamline. This equation also accounts for the effects of pressure build-up due to venting restrictions.

The following input parameters related to the dimensions and characteristics of the tank and gating system are required by the model: tank height (H_T), tank length (L_T), tank width (W_T), equivalent vent diameter (D_V), door length (L_D), door width (W_D), all in meters, plus door opening angle (α) in radians and door opening time (t_α) in seconds. The model accepts two ways of reading the values for the last two parameters. These can be given as a file with α and t_α for a given time interval. The model then interpolates, if needed, the angle for the simulation time-step. The second hypothesis is to give only the maximum angle (α_{max}) and respective time ($t_{\alpha_{\max}}$). In this case, the rate door opening is assumed as constant until t_α, according to:

$$\begin{cases} if\ t < t_{\alpha_{\max}} \Rightarrow \alpha = \dfrac{\alpha_{\max} \cdot t}{t_{\alpha_{\max}}} \cdot \dfrac{3.142}{180.0} \\ if\ t \geq t_{\alpha_{\max}} \Rightarrow \alpha = \alpha_{\max} \cdot \dfrac{3.142}{180.0} \end{cases} \qquad \textbf{Eq. 4-47}$$

where α_{max} and $t_{\alpha_{\max}}$ are thus the values provided by the user.

The area of the doors is calculated from its dimensions as:

$$A_D = L_D W_D \qquad \textbf{Eq. 4-48}$$

And similarly to the tank area:

$$A_T = L_T W_T \qquad \textbf{Eq. 4-49}$$

Thus, the effective area of efflux (A_E) in each time-step results from the knowledge of the angle α between the door and the bottom of the tank, giving:

$$A_E = A_D \sin(\alpha) \qquad \textbf{Eq. 4-50}$$

In the limit, A_E / A_D equals unity with the doors fully open ($\alpha = \pi/2$), as referred.

The vertical displacement of a fluid parcel in each time-step (Δt) is calculated as:

$$\Delta z = w_E \cdot \Delta t \qquad \textbf{Eq. 4-51}$$

And the position for current time step ($z_{(i)}$) is given from the position in the previous ($z_{(i-1)}$) plus the displacement:

$$z_{(i)} = z_{(i-1)} + \Delta z \qquad \textbf{Eq. 4-52}$$

The incremental quantity of retardant released per time-step (ΔV) derives from the calculated velocity of efflux (w_E) and the effective area of efflux (A_E), given by the door-opening rate. The model specifies four different door conditions based on the restriction imposed over the flow: door full open, door rate fast enough not to restrict flow, door rate partially restrictive and door rate restricting flow. These conditions are determined as follows:

Door full open:

$$if\ t \geq t_\alpha \Rightarrow A_E = A_D \qquad \textbf{Eq. 4-53}$$

Door restricting flow:

$$if\ \Delta z > 0.5 W_D \sin(\alpha) \Rightarrow \begin{cases} if\ \alpha > 0.7854 \Rightarrow A_E = A_D \sin(\alpha) \\ if\ \alpha \leq 0.7854 \Rightarrow A_E = A_D \left(\sin(\alpha) + \dfrac{W_D \cdot \cos(2\alpha) \cdot \Delta\alpha}{2 w_E} \right) \end{cases} \qquad \textbf{Eq. 4-54}$$

Door partially restrictive:

$$if\ z > W_D \sin(\alpha) \Rightarrow A_E = A_D \left(1 - \frac{\cos(\alpha)}{2} \right) \qquad \textbf{Eq. 4-55}$$

Door faster than fluid:

$$\text{if } z \leq W_D \sin(\alpha) \Rightarrow A_E = A_D \left(1 - \frac{\Delta t}{2 W_D \tan(\alpha)} \right) \qquad \textbf{Eq. 4-56}$$

The volume of liquid released (ΔV) in a given time-step is thus:

$$\Delta V = A_E \cdot \Delta z \qquad \textbf{Eq. 4-57}$$

The fluid velocity at the top (w_t) is calculated from the velocity at the bottom (exit) of the tank applying the continuity equation:

$$w_t = \frac{w_E A_E}{A_T} \qquad \textbf{Eq. 4-58}$$

which prescribes the conservation of mass for an incompressible flow, where A_E is the exit area and A_T is the tank area (equal to the top area of the fluid).

During fluid discharge, vents at the top of the tank allow the volume of fluid lost to be replaced by the air entry. Typically, the vent area is a restriction usually closed by a

spring-action flapper valve, which induces a negative pressure at the top of the tank due to the pressure drop at the restriction. To include the dynamic effects arising from this negative pressure, and its significance on flow prediction, its value (in Pa) is calculated from the following expression derived from the original expression for the change in pressure across a duct by Eshbach and Souders [1975, in Swanson et al., 1977]:

$$P = \frac{C \cdot \Delta Q^2}{D_V^4} \cdot \frac{V_{air(i-1)}}{V_{air(i)}} \qquad \textbf{Eq. 4-59}$$

where ΔQ is the flow rate for a given time-step ($\Delta Q = \Delta V / \Delta t$), V_{air} represents the volume of air in the tank in the actual ($V_{air(i)}$) and precedent time-step ($V_{air(i-1)}$) and D_V is the equivalent vent diameter. The empirical constant C, equal to 0.101 kg.m^{-4}, accounts for the combination of the constants for air density, mean pressure, friction factor and the universal gas constant from the original equation (for more details see Swanson et al. [1977 and 1978]).

At each computational time-step the model gives the following output data: head height, exit velocity, top velocity, flow rate, volume discharged per time-step, cumulative volume, and pressure.

4.5. Breakup module

As previously referred, the aerodynamic breakup of liquid jets is a two stage process composed by the primary breakup of the jet into large droplets (or globs) and the subsequent secondary breakup of these fluid structures with the formation of the spray cloud, according to the schematic representation from Figure 3-2. The basis for the development of the algorithm implemented in ADM for the primary breakup of the jet derives from the concepts and numerical approaches introduced in the field of fuel spray modelling, especially from the models by Reitz and Diwakar [1987], Reitz [1987] and Beale and Reitz [1999]. Due to the much larger diameter of the firefighting liquid jet comparing to fuel jets in engine combustion systems, some fundamental differences exist. In the case of an aerial drop, the breakup of the large liquid mass into globs is primarily controlled by RT instability, while in fuel spray atomisation models account only for KH waves growth. In the breakup of a firefighting liquid jet, KH instabilities are mainly responsible for the appearance of small drops at the liquid-gas surfaces, due to the high relative velocity. Therefore, ADM introduces a new mechanism for primary breakup, which is governed by a competing mechanism

between RT and KH instabilities, in analogy to Beale and Reitz's [1999] modelling approach for secondary breakup, as it will be described hereafter.

The sizes of the child droplets resulting from primary breakup are obtained in the model through the jet stability theory (see, e.g., Reitz and Bracco [1982] and Lin and Reitz [1998] for details), which establishes that the droplet formation resulting from interfacial instability is controlled by the particular wave which grows the most rapidly. The sizes of the droplets are thus related to the wavelengths of the most unstable waves, known as the most dangerous wavelength. The breakup length, on the other hand, is a measure of the growth rate of the disturbance. The jet stability theory has been extensively applied and validated by several authors within a wide range of operation conditions, evidencing the robustness of the implicit concept (e.g., Beale and Reitz [1999], Lee and Park [2002], Madabhushi [2003], Grover et al. [2004] and Raju [2005]).

As in the original approach by Reitz and Diwakar [1987] and Reitz [1987], instead of assuming an intact liquid at the exit, ADM injects discrete parcels of liquid, also known as blobs, at each computational time-step. These parcels have diameters equal to the effective discharge diameter. Initial conditions for the jet breakup simulation are given by the discharge module described in section 4.4. These are basically the flow rate of liquid, the injection velocity, and the characteristic dimensions of the liquid parcels. As the flow rate varies in time, particularly in the case of conventional discharge systems, the size of the liquid parcels varies in agreement with the volume released during that specific time interval. Parcel dimensions are calculated assuming that the jet has the shape of a cylinder. As the tank gates have a rectangular shape, this is converted to a circular one through the concept of the equivalent diameter, which is defined as the diameter of a round exit with the same area as the original rectangular one (e.g., Yu and Girimaji [2005]), as follows:

$$R_p = \sqrt{\frac{A_p}{\pi}} \qquad \textbf{Eq. 4-60}$$

where R_p is the initial radius of the liquid parcel at the exit; and A_p is equal to the effective area of discharge ($=A_E$), which is dependent on door-open rate, as calculated by the discharge module. The length of the parcel (L_p) for the current time-step is then:

$$L_p = \frac{V_p}{\pi \cdot R_p^2} \qquad \textbf{Eq. 4-61}$$

where V_p is the volume of liquid released in the time-step ($=\Delta V$) given by Eq. 4-57.

Then the model simulates the primary breakup of the injected liquid parcels that represent the jet as follows. The size of the child droplets (R_{KH}) that are stripped from the unstable surface of the jet by KH instability is assumed to scale with the wavelength (Λ_{KH}) of the fastest-growing unstable surface KH wave via a proportionality constant, B_0, defined by Reitz [1987] as 0.61:

$$R_{KH} = B_0 \cdot \Lambda_{KH} \qquad \textbf{Eq. 4-62}$$

The wavelength of the KH instability with the maximum growth rate is calculated from the dimensionless numbers *Oh*, *We* (given in Table 3-1) and Taylor ($Ta = Oh_L We_G^{0.5}$) as follows:

$$\Lambda_{KH} = 9.02 \cdot R_p \cdot \frac{\left(1 + 0.45 \cdot Oh_L^{0.5}\right) \cdot \left(1 + 0.4 \cdot Ta^{0.7}\right)}{\left(1 + 0.87 \cdot We_G^{1.67}\right)^{0.6}} \qquad \textbf{Eq. 4-63}$$

The rate of stripping is then assumed to behave according to the following uniform radius reduction rate of the parent parcel radius:

$$\frac{dR_p}{dt} = -\frac{(R_p - R_{KH})}{\tau_{KH}}, \quad R_{KH} \le R_p \qquad \textbf{Eq. 4-64}$$

Eq. 4-64 is solved applying a fourth-order Runge-Kutta method. The breakup time τ_{KH} of the stripping process is inversely proportional to the product of Λ_{KH} and the frequency of the fastest growing KH wave, Ω_{KH}, via constant B_1, as shown in Eq. 4-65. As the magnitude of B_1 has been concluded to depend upon nozzle design and initial disturbance levels of the spray [Reitz, 1987], several values have been proposed in the literature (e.g. 20 by Reitz [1987], 1.73 by O'Rourke and Amsden [1987], 30 by Patterson et al. [1994]). The B_1 value in the model has been defined as 10.

$$\tau_{KH} = \frac{3.726 \cdot B_1 \cdot R_p}{\Lambda_{KH} \cdot \Omega_{KH}} \qquad \textbf{Eq. 4-65}$$

The expression for Ω_{KH} is given by:

$$\Omega_{KH} = \frac{0.34 + 0.38 \cdot We_G^{1.5}}{(1 + Oh_L) \cdot \left(1 + 0.4 \cdot Ta^{0.6}\right)} \sqrt{\frac{\sigma}{\rho_L \cdot R_p^3}} \qquad \textbf{Eq. 4-66}$$

As can be seen from Eq. 4-63 and Eq. 4-66, the maximum wave growth rate increases and the corresponding wavelength decreases with increasing *We* number (the ratio of the inertial force to surface tension force acting on the jet). The effect of the liquid viscosity (which appears in the *Re* and *Oh* numbers) reduces the wave

growth rate and increases the wavelength significantly as the liquid viscosity increases.

The volume atomised by KH instabilities ($V_{atomized\_KH}$) during current time-step (i) is calculated from the parcel radius (R_p) given by Eq. 4-64 as follows:

$$V_{atomized\_KH_{(i)}} = V_{p_{(i-1)}} - \pi \cdot L_{p_{(i-1)}} \cdot R_{p_{(i)}}^2 \qquad \textbf{Eq. 4-67}$$

The total number of droplets shed by KH instabilities is thus:

$$N_{KH(real)} = \frac{V_{atomized\_KH}}{V_{KH}} \qquad \textbf{Eq. 4-68}$$

where the volume of each droplet is calculated from the previously determined radius (Eq. 4-62):

$$V_{KH} = \frac{4}{3}\pi \cdot R_{KH}^3 \qquad \textbf{Eq. 4-69}$$

In parallel with KH instabilities, also RT waves are growing in the surface of the jet. This type of instability occurs in the interface between two fluids with different densities in a gravitational field. The most dangerous wavelength (Λ_{RT}) of an RT instability, which in this case equals the radius of the child droplets, is expressed as follows [Bellman and Pennington, 1953 in Lee and Park, 2002]:

$$R_{RT} = \Lambda_{RT} = \frac{\pi \cdot C_{RT}}{K_{RT}} \qquad \textbf{Eq. 4-70}$$

In this expression, C_{RT} is an RT breakup time constant defined as 0.3 (values in literature vary in the range 0.2-0.4 [Beale and Reitz, 1999; Lee and Park, 2002]). The wavenumber (K_{RT}) of the fastest-growing RT wave is given by:

$$K_{RT} = \left(\frac{-(g+a)\cdot(\rho_L - \rho_G)}{3\sigma} \right)^{0.5} \qquad \textbf{Eq. 4-71}$$

where g and a are the acceleration in the direction of travel by gravity and drag force, respectively.

Fluids atomisation models in literature apply the RT instability theory only in the case of secondary breakup (e.g., Beale and Reitz [1999], Lee and Park [2002], Madabhushi [2003], Grover et al. [2004], Raju [2005]). In that situation, the droplet splits into small droplets (with a given size distribution) at the breakup time τ_{RT}, which

is given by the ratio between an RT breakup time constant (C_τ) in the range from 1 to 9 and the frequency (Ω_{RT}) of the fastest growing RT wave. This approach, however, reveals some difficulties if transposed to the primary breakup of a large diameter liquid jet since the instant "explosion" of the liquid parcel does not occur. Moreover, the range of Ω_{RT} values, fitted to the breakup of fuel droplets and related to the distance relating the nozzle, has a deep impact on calculations. Instead, ADM applies the liquid erosion law obtained by Swanson et al. [1978] in the extensive ETAGS experiments, and which was integrated on PATSIM model. This expression gives the variation of the volume of liquid atomised as a function of time as follows:

$$V_{atomized\_RT_{(i)}} = \frac{\Delta t \cdot k_2 \cdot e^{(k_1 \cdot t)}}{u_p \cdot V_{p_{(i-1)}}} \qquad \textbf{Eq. 4-72}$$

where u_p is the velocity of the fluid parcel (calculated by the deposition module described in section 4.6) and k_1 and k_2 are empirical erosion constants with values given in Table 4-6, conjointly with the values of the other constants used in the primary breakup stage.

Table 4-6. Values of the constants used by the ADM breakup module.

Constant	Value
B_0	0.61
B_1	10
C_{RT}	0.3
K_1	3.97 (gum-thickened retardants) 4.4 (unthickened products)
K_2	12

The number of droplets produced is then:

$$N_{RT(real)} = \frac{V_{atomized\_RT}}{V_{RT}} \qquad \textbf{Eq. 4-73}$$

In order to optimize the computational run-time only a fraction of the total (real) number of droplets originated by primary breakup mechanisms are tracked during the computation, which is a common practice in the simulation of droplet motion (see, e.g., Crowe et al. [1998]). The number of marker (or representative) droplets is thus given by:

$$\begin{cases} N_{KH} = f_{KH} \cdot N_{KH(real)} \\ N_{RT} = f_{RT} \cdot N_{RT(real)} \end{cases} \qquad \textbf{Eq. 4-74}$$

The coefficients f_{KH} and f_{RT}, defining the fraction of the real number of droplets considered in the computation, were given values of $1x10^{-7}$ and $1x10^{-3}$, respectively, since the number of droplets originated by KH instabilities is much larger (although the volume atomized is smaller). The following limit values were imposed:

$$\begin{cases} \text{if } N < 1 \Rightarrow N = 1 \\ \text{if } N > 10 \Rightarrow N = 10 \end{cases} \qquad \textbf{Eq. 4-75}$$

This computational feature does not have a significant influence on results and balances the need for adequate representation of the spray while keeping the computational time within the restrictions imposed by an operational application.

After the primary breakup of the liquid jet column surface, droplets are subject to secondary breakup. ADM estimates the spatiotemporal evolution of the mechanisms occurring during this stage of the atomisation as a function of experimental correlations based on the Weber and Ohnesorge numbers (e.g., Pilch and Erdman [1987], Madabhushi [2003]). The subscript cc will be used hereafter for indicating the child droplet from secondary breakup.

The characteristic time scale for secondary breakup (t^*) is given by [Ranger and Nicholls, 1969]:

$$t^* = \frac{D_{c0}}{U_r}\sqrt{\frac{\rho_L}{\rho_G}} \qquad \textbf{Eq. 4-76}$$

where U_r is the relative velocity between the droplet and gas, and D_{c0} is the initial diameter of the droplet after being stripped from the jet surface (prior to deformation).

During secondary breakup, the droplet will be deformed into a disk shape, with a consequent increase on frontal diameter and drag coefficient (as it will be calculated by the deposition module in section 4.6). The deformation (or initiation) time (t_d) is given by [Hsiang and Faeth, 1992]:

$$t_d = 1.6 \cdot t^* \cdot f_t \qquad \textbf{Eq. 4-77}$$

where,

$$f_t = \begin{cases} 1 & (Oh < 0.1) \\ \left(1 - \frac{Oh}{7}\right)^{-1} & (Oh \geq 0.1) \end{cases} \qquad \textbf{Eq. 4-78}$$

The correction factor f_t allows an accounting for the effects of liquid viscosity on breakup time. As it was previously referred in section 3.1.2, the effect of higher *Oh* numbers is to increase the time required for a given breakup event to occur.

The total breakup time (t_b), which includes the deformation period, is defined based on the Weber number:

$$t_b = \begin{cases} 6 \cdot t^* \cdot f_t \cdot (We - 12)^{-0.25} & 12 \leq We < 18 \\ 2.45 \cdot t^* \cdot f_t \cdot (We - 12)^{0.25} & 18 \leq We < 45 \\ 14.1 \cdot t^* \cdot f_t \cdot (We - 12)^{-0.25} & 45 \leq We < 351 \\ 0.766 \cdot t^* \cdot f_t \cdot (We - 12)^{0.25} & 351 \leq We < 2670 \\ 5.5 \cdot t^* \cdot f_t & 2670 \leq We \end{cases} \qquad \textbf{Eq. 4-79}$$

At the end of the deformation period, the values of D_c and c_D remain constant and the droplet continues its motion (as determined by the deposition module) until breakup time is attained. At that precise instant ($t = t_b$) secondary breakup occurs by one of the two following mechanisms: bag breakup for Weber numbers lower than 100 and shear breakup for Weber numbers higher than 100, according to the analysis from section 3.1.2.

In the bag breakup regime, a parent droplet parcel is assumed to be broken into five child droplets. The diameters of these formed droplets and their velocities after breakup are calculated as follows. The volumetric distribution of droplets after bag breakup is assumed to follow the root-normal distribution as originally proposed by Simmons [1977] and extensively validated after (e.g., Hsiang and Faeth [1995]), in the form:

$$f(D_{cc}) = \frac{1}{\sqrt{2\pi}s} \exp\left[-\frac{1}{2s^2} \left(\sqrt{\frac{D_c}{MMD}} - 1 \right)^2 \right] \qquad \textbf{Eq. 4-80}$$

According to the study by Simmons [1977], the standard deviation *s* is defined as 0.24 and the mass median diameter (MMD) is given by:

$$MMD = 1.2 \cdot SMD \qquad \textbf{Eq. 4-81}$$

where the Sauter mean diameter (SMD) of the child droplets is calculated as [Schmehl et al., 1998, in Madabhushi, 2003]:

$$SMD = 1.5 \cdot D_{c0} \frac{Oh_L^{0.2}}{(We_{G,corr})^{0.25}} \qquad \textbf{Eq. 4-82}$$

In this expression, $We_{G,corr}$ is the Weber number corrected for high liquid viscosity as follows:

$$We_{G,corr} = \frac{We_G}{1 + 1.077 \cdot Oh_L^{1.6}} \qquad (Oh > 0.1) \qquad \textbf{Eq. 4-83}$$

The velocities of the child droplets are calculated by assuming that after breakup each droplet inherits the parent droplet velocity plus a normal velocity due to the rim expansion during breakup, which has the magnitude [Madabhushi, 2003]:

$$U_{rim} = \frac{5 \cdot D_{c0}}{t_b - t_d} \qquad \textbf{Eq. 4-84}$$

The angle of U_{rim} in the normal plane with the parent droplet trajectory is randomly chosen between 0 and 2π for each of the five child droplets as shown in Figure 4-2. The tridimensional components of velocity are then calculated accordingly.

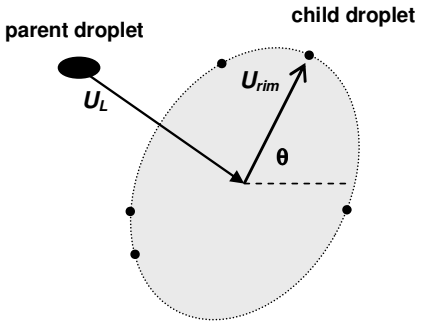

Figure 4-2. Bag breakup of a parent liquid droplet into five child droplets. U_L is the velocity of the parent and U_{rim} the added normal velocity due to rim expansion and θ is the random angle between the two velocities.

When the Weber number is greater than 100, a procedure for the determination of droplet sizes and velocities originated by the shear breakup of the deformed falling liquid droplet is applied. This methodology described hereafter derives from the experimental correlations obtained by Chou et al. [1997].

In each time-step, the mass of droplets formed due to shear breakup is calculated as follows:

$$M_{strip} = 0.42 \cdot \Delta t \cdot \left(\frac{M_c}{t^*} \right) \cdot \exp\left[0.8 \cdot \left(\frac{t_b}{t^*} - 3.5 \right)^2 \right] \qquad \textbf{Eq. 4-85}$$

where M_c is the initial parent droplet mass:

$$M_c = \frac{\pi}{6} \cdot \rho_L \cdot D_c^3 \qquad \textbf{Eq. 4-86}$$

Contrarily to bag breakup, child droplets are continuously stripped from the parent droplet until extinction. The droplet size distribution is fitted with the most widely used in spray studies, the Rosin-Rammler expression, which is defined as the fraction of the total volume of the droplets with diameters smaller than D_c, here given in terms of the MMD [Liu, 2000]:

$$F(D_{cc}) = 1 - \exp\left[-0.693 \left(\frac{D_c}{MMD} \right)^q \right] \qquad \textbf{Eq. 4-87}$$

The dispersion parameter q, with typical values between 1.5 and 4 for most sprays [Lefebvre, 1989], was defined as 3.5. It is a measure for the span of the spreading of droplet sizes, with a large value indicating a spray with very uniform droplet sizes. The MMD is calculated applying Simmons's [1977] relation between MMD and SMD (Eq. 4-81), the latter given as a function of time:

$$\begin{cases} SMD = 2D_c \sqrt{\dfrac{\nu_L \cdot t}{D_{c0}^2}} & (t_b < t_c) \\ SMD = 0.09 \cdot D_{c0} & (t_b > t_c) \end{cases} \qquad \textbf{Eq. 4-88}$$

Finally, the velocity of the secondary child droplets departs from Chou et al. [1997] experiments, according to which the streamwise velocity of the stripped droplets is related to the primary child droplet according to:

$$\begin{cases} u_{cc} = u_c + C_u \cdot u_r \\ v_{cc} = C_v \cdot u_r \end{cases} \qquad \textbf{Eq. 4-89}$$

where the coefficients C_u and C_v take values of 0.37±0.08 and -0.01±0.15, respectively, suggesting that there is appreciable acceleration of the formed droplets in the streamwise direction.

4.6. Deposition module

The overall particle translational equation of motion specifies that the rate of change of the particle linear momentum is equal to the net sum of the forces acting on the particle. In the spray cloud deposition module, the droplet trajectories are simulated by integrating the droplet motion equation in a Lagrangian reference frame. This force balance equates the droplet inertia with the forces acting on the droplet, which in Einstein notation can be written as (e.g., Crowe et al. [1998]):

$$\frac{dU_{Li}}{dt} = \left(\frac{18\mu_G c_D Re}{24\rho_L D_L^2} \right) \cdot \left(U_{Gi} - U_{Li} \right) + g_i \qquad \textbf{Eq. 4-90}$$

Note that the subscript L refers to both the primary and secondary droplets (previously indicated as p, c and cc). In this expression, the first term on the right side relates the drag factor [l] with the response time of the droplet [m]; μ_G is the molecular viscosity of the air; c_D is the drag coefficient; ρ_L and D_L are the density and diameter of the droplet; *Re* is the relative Reynolds number (calculated by Eq. 4-91); U_{Gi} and U_{Li} are the velocity vectors of the continuous phase and the droplet, respectively; and g_i is the acceleration due to gravity.

$$Re = \frac{D_L \left(U_{Li} - U_{Gi} \right)}{\nu_G} \qquad \textbf{Eq. 4-91}$$

For the simplicity of the numerical description of droplet motion, the interaction between the droplet and the surrounding flow is made through the common one-way coupling approach, which involves the transfer of momentum from the continuum phase to the discrete one. With this approach, the wind flow 'shapes' the trajectory of the falling droplet, but the contrary does not occur. Similarly, the model does not solves the mass transfer due to evaporation, which makes it specially indicated for indirect attack (i.e., at some distance from the fire front). Also the effects on the fluid motion due to its non-Newtonian behaviour are not considered. However, the influence of these simplifications on model accuracy should be further investigated.

[l] The drag factor expresses the ratio of the drag coefficient to Stokes drag as follows: $f = (c_D Re)/24$

[m] The kinematic response time of the particle, an important parameter in the characterisation of the flow, is given by [Crowe et al., 1998]: $\tau_L = \left(\rho_L D_L^2 \right) / (18\mu_G)$

Due to the large MMD of the droplets of firefighting liquid (see section 3.1.3), and consequently their inertia, these will behave as nearly unresponsive to turbulent velocity fluctuations. As a consequence, the effects of turbulence on droplet movement are not significant in general, except for the range of smaller diameters that can potentially follow the airflow more closely. Due to the low relative importance of smaller droplets and the interest in maintaining the operational characteristics of ADM, the turbulent fluctuations of the gaseous phase [n], and their effects on particle motion, are not calculated.

Integration in time of Eq. 4-90 yields the velocity of the particle along the trajectory, while the trajectory itself (position of the droplet in each of the Cartesian coordinates) is given by:

$$\frac{dX_i}{dt} = U_{Li} \qquad \textbf{Eq. 4-92}$$

In order to solve Eq. 4-90 and Eq. 4-92, the application of numerical integration methods over discrete time-steps is required. ADM applies a 4th order Runge-Kutta algorithm in order to determine the velocity and position of each particle in each time-step. In order to guarantee the needed accuracy for the trajectory integration in time a 0.02 s time-step is used, which decreases to 0.007s with droplets smaller than 0.2 mm [o].

One of the difficulties in this analysis relies on the calculation of the drag coefficient, c_D, since during the free-fall the droplets of firefighting liquid typically deform into an oblate spheroid, as schematically shown in Figure 4-3, although its horizontal cross section maintains approximately circular.

[n] The instantaneous velocity vectors of the gaseous fluid contain a local time-averaged component plus a fluctuating velocity: $U_{Gi}(t) = \overline{U}_{Gi} + U'_{Gi}(t)$. There are several particle turbulence models available (see, e.g., Pozorski and Minier [1998], Loth [2000]) for calculating the velocity fluctuations of the carrier phase.

[o] One of the limitations inherent to the application of a high-order Runge-Kutta technique is the imposed stability requirement that $\Delta t < 2\tau$. The exponential scheme is a frequently used alternative solution for the integration (e.g., Tomé [2004]). However, it is less accurate and also less numerically stiff [Morgan and Barton, 2000].

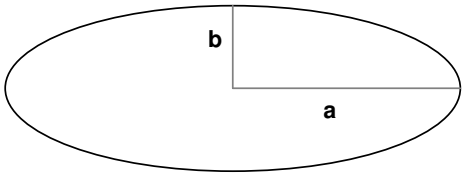

Figure 4-3. Oblate spheroid shape of a liquid droplet during free-fall in the atmosphere. *a* and *b* are, respectively, the equatorial radius and the polar radius.

The importance of deformation depends largely on the size of the droplet, since there is an increasing aspect-ratio [p] with increasing size, as it was shown for both water [Loth, 2000] and retardant droplets [Schönhuber et al., 2005]. In general, when the droplet is roughly at the terminal velocity, according to Loth [2000] deformation can be considered significant for Bond numbers (see Table 3-1) higher than 0.14, i.e., approximately for all droplets above 1 mm. Another important aspect is the viscosity of the liquid as analysed in section 3.1.2. In fact, experimental work (e.g., Hsiang and Faeth [1992]) has shown that as *Oh* increases a progressive delay in the time required for maximum distortion is observed, because viscous forces in the liquid tend to inhibit droplet deformation. Therefore, ADM applies a methodology for the calculation of drag that accounts for the effect of viscosity on droplet deformation, as schematically shown in Figure 4-4.

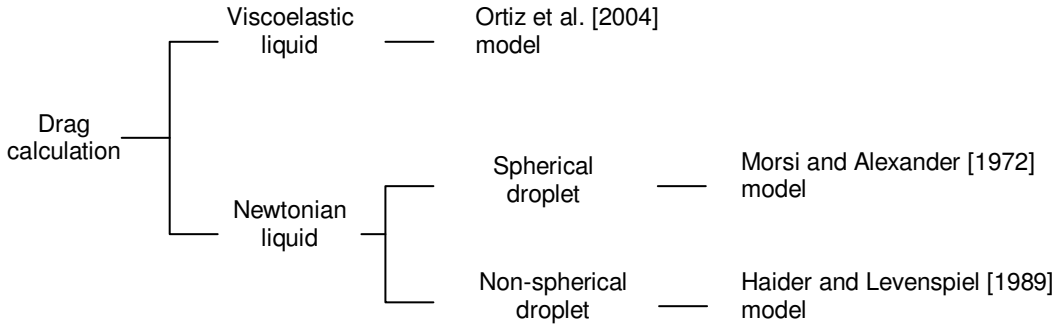

Figure 4-4. Drag calculation models implemented in ADM.

The effect of liquid viscosity on droplet deformation can be significant for *Oh* values above 0.1 (e.g., Hsiang and Faeth [1992]). In that cases ADM applies the experimental correlation by Ortiz et al. [2004] derived from an extensive set of data

[p] The aspect-ratio of a droplet represents the ratio of its height to the width: $AR = b/a$.

for both Newtonian and viscoelastic liquids and a wide range of operating conditions. The function for c_D varies with *Oh* and *We* as follows:

$$c_D = 1.6 + 0.4 \cdot Oh^{0.08} \cdot We^{0.01} \qquad \textbf{Eq. 4-93}$$

In order to evaluate the effect of non-sphericity over the drag of the free-falling firefighting droplets, when $Oh < 0.1$, and thus the viscosity of the liquid does not affect deformation and breakup, ADM incorporates a dynamical drag model that accounts for the effect of droplet shape transformation on c_D. First, the model calculates the increase on droplet frontal diameter during the deformation period as [Hsiang and Faeth, 1992; Madabhushi, 2003]:

$$D_L = D_{L0} \cdot \left(1 + 0.19 \cdot \sqrt{We} \cdot \frac{t}{t_d}\right) \qquad (Oh < 0.1,\ We \leq 100) \qquad \textbf{Eq. 4-94}$$

As this expression is valid for $We \leq 100$, *We* is assumed as 100 in the remaining situations.

Then, ADM applies two distinct approaches in the calculation of c_D for spherical and non-spherical droplets. When dealing with a spherical droplet the model allows that it increases to no greater than 10% beyond the initial diameter, i.e., $D_L \leq 1.1 D_{L0}$. In this case, the Morsi and Alexander [1972] drag model is used. It is one of the most complete in literature, adjusting the function definition frequently over a large range of Reynolds numbers:

$$c_D = a_1 + \frac{a_2}{\mathrm{Re}} + \frac{a_3}{\mathrm{Re}^2} \qquad \textbf{Eq. 4-95}$$

where,

$$a_1, a_2, a_3 = \begin{cases} 0, 18, 0 & 0 < Re < 0.1 \\ 3.690, 22.73, 0.0903 & 0.1 < Re < 1 \\ 1.222, 29.1667, -3.8889 & 1 < Re < 10 \\ 0.6167, 46.50, -116.67 & 10 < Re < 100 \\ 0.3644, 98.33, -2778 & 100 < Re < 1000 \\ 0.357, 148.62, -47500 & 1000 < Re < 5000 \\ 0.46, -490.546, 578700 & 5000 < Re < 10000 \\ 0.5191, -1662.5, 5416700 & Re \geq 10000 \end{cases} \qquad \textbf{Eq. 4-96}$$

For the case in which the diameter increase exceeds more than 10% the original value, i.e., when $D_L > 1.1 D_{L0}$, the model identifies the droplet as non-spherical and

the dynamic drag law from Haider and Levenspiel [1989] (Eq. 4-101) is applied. This approach accounts for variations in the droplet shape through the shape factor:

$$\phi = \frac{s}{S} \qquad \textbf{Eq. 4-97}$$

where s is the surface area of a sphere having the same volume as the droplet and S is the actual surface area of the droplet. S is calculated from the knowledge of the lengths of the semi-major axis (equatorial radius a) and the semi-minor axis (polar radius b) of the droplet, according to the following expression (valid for $0 < b < a$) [Beyer, 1987]:

$$S = 2\pi \cdot a^2 + \pi \frac{b^2}{e} \ln\left(\frac{1+e}{1-e}\right) \qquad \textbf{Eq. 4-98}$$

where e is the ellipticity, defined by:

$$e = \sqrt{1 - \frac{b^2}{a^2}} \qquad \textbf{Eq. 4-99}$$

The length of each axis corresponds to:

$$\begin{cases} a = \dfrac{D_L}{2} \\ b = \dfrac{3 \cdot V_L}{\pi \cdot D_L^2} \end{cases} \qquad \textbf{Eq. 4-100}$$

The c_D is finally calculated as:

$$c_D = \frac{24}{\mathrm{Re}}\left(1 + b_1 \mathrm{Re}^{b_2}\right) + \frac{b_3 \mathrm{Re}}{b_4 + \mathrm{Re}} \qquad \textbf{Eq. 4-101}$$

where the coefficients b_1 to b_4 are given as a function of ϕ as follows:

$$\begin{cases} b_1 = \exp\left(2.3288 - 6.4581\phi + 2.4486\phi^2\right) \\ b_2 = 0.0964 + 0.5565\phi \\ b_3 = \exp\left(4.905 - 13.8944\phi + 18.4222\phi^2 - 10.2599\phi^3\right) \\ b_4 = \exp\left(1.4681 + 12.2584\phi - 20.7322\phi^2 + 15.8855\phi^3\right) \end{cases} \qquad \textbf{Eq. 4-102}$$

Although some works (e.g., Poo and Ashgriz [1991]) have shown that the drag of a spray of closely spaced drops into a turbulent flow is affected by the motion of the preceding droplets, particularly in the region close to the injector where drops flow in the wake of each other, there is currently no sufficient scientific understanding on the

subject and thus these effects are not considered in the present analysis. It is assumed that, at some distance downstream of the injection point, i.e., in the far-field spray region, the mean distance between neighbouring droplets is already sufficient to allow drag coefficients to approach those of a single isolated droplet.

4.7. Canopy retention module

The suppression effectiveness of firefighting products depends both on the amount of material deposited on a unit area of the fuel, and on the amount of fuel coated by the material [Andersen et al., 1974a]. It is thus important to have a prediction of the vertical distribution of product within the canopy. The penetration of retardant into the canopy, the foliar interception (the fraction of fluid contacting the foliage) and the foliar retention (the fraction retained) have been scarcely investigated in the literature (see, e.g., Calogine et al. [2007]). An analogy with rainfall interception studies is therefore established. The vertical distribution of retained liquid is estimated by ADM using the film thickness (h) concept of Grah and Wilson [1944], which gives the liquid depth on the surface of leaves after precipitation has ceased and drainage stopped and thus expresses the limit of retention by the fuels. The model will basically assume that the amount of fluid retained in the tree is then given by an equivalent film thickness uniformly applied over the tree surface area. An approximated value for the variation of volume retained with height is then calculated from the knowledge of the vertical profile of LAI for the specific canopy considered, previously provided by the canopy structure module.

From the temporal evolution of liquid deposition at ground surface the model provides a file with the final ground pattern and calculates the line length and the respective area occupied by a set of predefined coverage levels (see section 5.3 for more details).

4.8. GIS-based graphical user interface

A user-friendly tool was developed that allows the model to be used by firefighters for training purposes. This tool is a GIS-based application used for predicting the ground pattern of firefighting product at any position of a given area of interest according to user-defined parameters. The Graphical User Interface (GUI) includes a variety of tools and functions for spatial operations, which are activated via a number of graphical control elements such as command buttons, text, list and combo boxes, as

shown in Figure 4-5. All the input parameters are defined by the user through a specific menu.

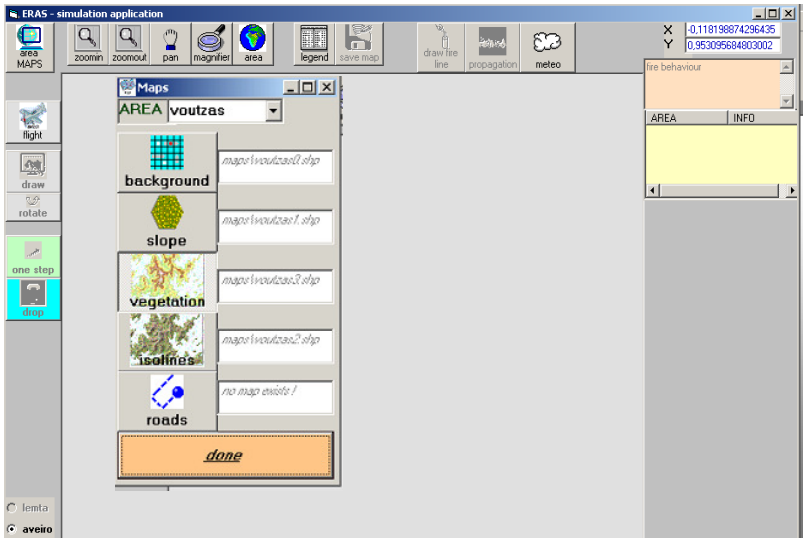

Figure 4-5. A snapshot screen of the GUI graphical elements.

Through the application environment the user is capable of selecting an area of interest from an existing geographical database, as shown in Figure 4-5. Varied information about the specific domain selected can be visualized and manipulated as thematic layers that include topography, roads, vegetation or high resolution satellite imagery. A flight line is then drawn over the map using the computer's pointing device (mouse, or other), while a window shows the topographic profile across the designed flight line as shown in Figure 4-6. At this stage the simulation is ready to be initiated.

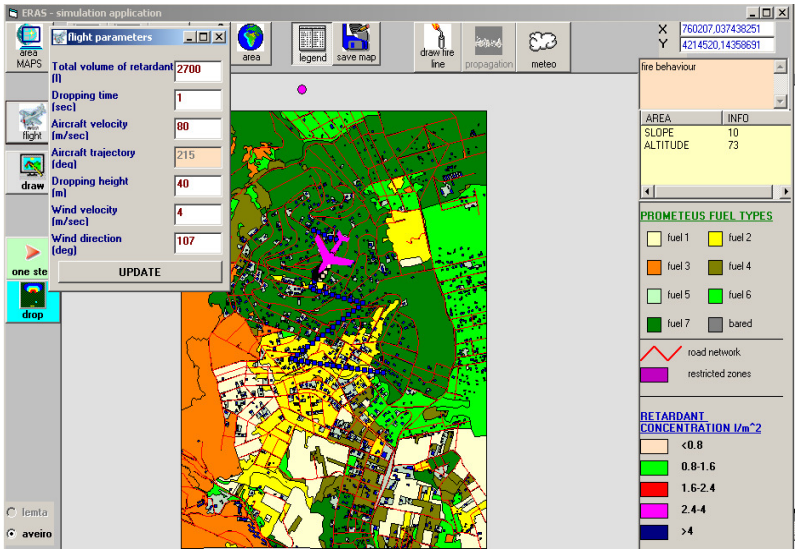

Figure 4-6. Definition of the flight parameters and drawing of the flight-line on the map.

After activating the dropping simulation, an alarm message alerts the user whenever the drop could potentially reach sensitive areas (e.g., residential areas, aquatic systems, etc.). The final result is given as a footprint over the map, as represented in Figure 4-7, which can be exported and stored by the user. The different classes of product concentration are shown with a coloured representation, which provides a clear indication of the effective coverage of the retardant drop.

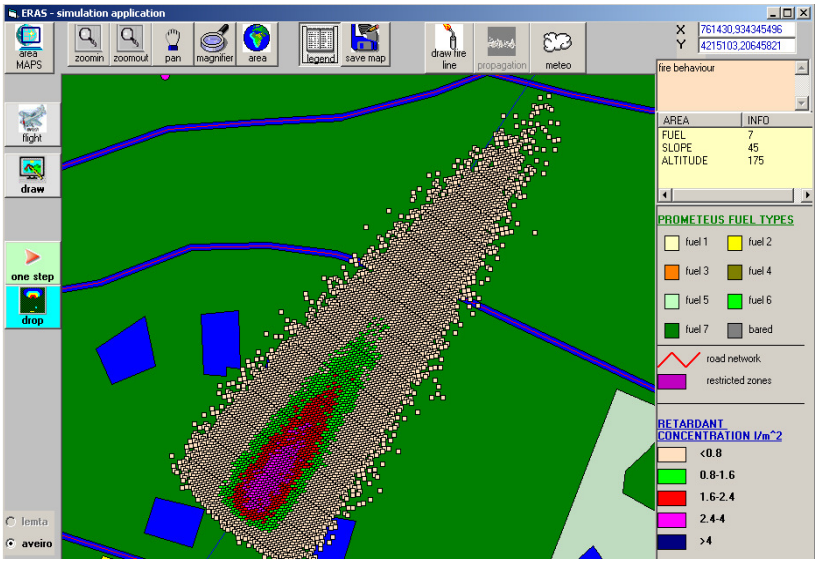

Figure 4-7. Zoom-in image over the simulated dropping pattern showing the colour scale indicating the coverage levels.

The main objective behind the development of the GUI was to provide a friendly access to the tool's capabilities for people with no specialized training. This goal is accomplished through the use of intuitive buttons and procedures. The GUI development resulted from the collaborative work with the Greek company Algosystems, under the EC project ERAS [Amorim et al., 2006].

5. Modelling results analysis and validation

The prime tool for the validation of an aerial drop of a firefighting product is the intercomparison with the spatial distribution (commonly known as ground pattern) of the liquid at ground. Given the purpose of the present work it would be desirable to have, for a particular set of drop tests, measurements of volume of liquid retained by vegetation, remaining concentration at ground and droplets sizes, in parallel with flow rate of the efflux from the aircraft tank, meteorological conditions and canopy description. Unfortunately, and due to the complex logistics involved in the measurement of retention within forest stands, real scale drops have been made almost exclusively over bare ground (see section 3.2). Therefore, the information needed for the validation of ADM in its entire scope is unavailable, at least as an ensemble of data for a particular drop.

In order to compare the simulated values with experimental data as detailed and accurate as possible the evaluation/validation of ADM model consisted of three independent stages. In the first two, the canopy flow and the discharge modules are validated separately and independently from the main model (sections 5.1 and 5.2, respectively). Section 5.3 deals with the validation of ADM model in the application to a set of drops from real scale tests. Although the drops were made over bare ground, excluding the possibility of relating the results with the effects of canopy, they include a detailed collection of measured parameters under the influence of a wide range of operational conditions, namely: various formulations and viscosities of the products dropped, distinct delivery systems, different dropping heights and variable meteorological conditions.

5.1. Canopy flow module validation

The canopy flow module was validated through the intercomparison with meteorological measurements taken at different levels in forests with very distinct characteristics.

The first dataset is from an experimental campaign conducted in the Duke forest (35º98' N, 79º8' W, elevation 163 m), North Carolina, US, from May 25 until June 12, 1997. The site is an even-aged pine forest equipped with a 20 m tall meteorological tower, with 6 levels of measurement, as seen in Figure 5-1. Further site description and analysis of the data are given by Katul et al. [1997] and Katul and Albertson [1998].

Figure 5-1. Measuring site and equipment at the Duke forest [url 15]

The second set of measurements is from an extended campaign at Tumbarumba in the Bago State Forest, south-east Australia, from June 3 to September 13, 2005. The Tumbarumba site (35º39' S, 148º10' E, elevation 1200 m) is a managed, mature eucalyptus forest with a 70 m meteorological mast instrumented at 9 levels that is shown in the photograph of Figure 5-2. For more details see Finnigan and Leuning [2000] and Leuning et al. [2005].

Figure 5-2. View of 70 m instrument mast at the Tumbarumba site and view of forest canopy from the top of the mast [url 16].

The physical and aerodynamic properties of the forests are given in Table 5-1. The drag coefficient (c_D) for each situation was derived from the application of Eq. 4-9.

Table 5-1. Physical and aerodynamic properties of the Duke forest and Tumbarumba site (values taken from Katul et al. [1997], Katul and Albertson [1998], Finnigan and Leuning [2000], Leuning et al. [2005] and Harman and Finnigan [2007]).

Site	Forest	h (m)	LAI ($m^2.m^{-2}$)	c_D	L_c (m)	β_N
Duke	*Pinus taeda* L. (Loblolly Pine)	14 ± 0.5	3.82	0.13	28	0.31
Tumbarumba	*Eucalyptus delegatensis* (Alpine Ash)	40	1.40	0.38	75.47	0.39

Figure 5-3 to Figure 5-5 show the measured and computed normalized vertical profiles of wind velocity for the two considered canopies under different atmospheric stability conditions. In the figures, the parameter *n* indicates the number of profiles used for calculating the mean wind velocity at each height. The velocity was normalized with the friction velocity ($U(z)/u_*$) and the height above ground with the penetration depth (z/L_c).

The distinguishing characteristic of a canopy-induced wind flow is the observed (e.g., Raupach et al. [1986]) inflection point at the canopy top that separates the standard boundary layer profile above the canopy from the approximately exponential profile within the canopy. This feature is captured by the model in all the tests performed, with a good coupling between the flow in both levels. Prior to the analysis of the results, it should be noted that, for simplicity, the model allows non-zero velocity at the ground surface (see section 4.3). This behaviour results from the fact that, as it is considered that almost all the momentum is absorbed as drag on the foliage rather than as stress on the ground (even for not particularly dense canopies as stressed by Raupach et al. [1986]), ADM does not recognise the presence of the ground. In the application to a sparse canopy, however, some drag can be exerted on the underlying substrate. In order to cope with this effect the profile would have to be forced to a zero wind velocity at the ground. Given the purpose of the current version of ADM, which is clearly defined as the numerical modelling of the aerial drop of firefighting products under the influence of a vegetative canopy, the analysis is focused at the RSL, as being the region of the ABL that directly impacts on the breakup and motion of the droplets. Future developments with the objective of giving the model the capability of considering the effect of the wind flow structure inside the canopy air space on the retention of liquid by the leaves and branches would require the inclusion of a second boundary layer along the ground surface.

In neutral stability, the simulated values of mean wind speed closely follow the observed profile through the full depth of the canopy as shown in Figure 5-3. The agreement on the comparison with the values from the Duke forest evidence the flexibility of the model in dealing with the heterogeneity of the canopy structure, as it is the case, although a constant L_c value is assumed. This site is characterised, in particular, by a sparse upper canopy [Katul et al., 1997; Katul and Albertson, 1998], fact that explains the underestimation of the velocity at the highest level within the canopy [Harman and Finnigan, 2007]. The very good performance of the model for the Tumbarumba forest is evident in the agreement between computed and measured values shown in Figure 5-3b. The relevance of this result is even higher considering that the topmost measurement level is nearly 70 m tall, 30 m above the canopy top.

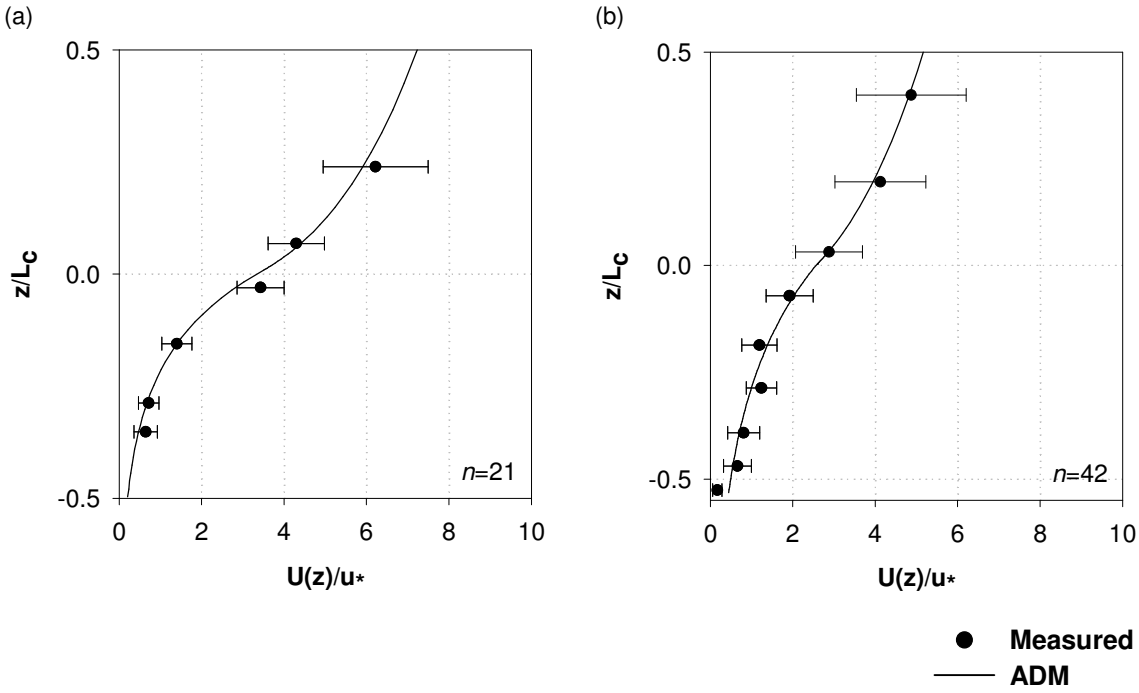

Figure 5-3. Vertical profiles of mean wind speed in near-neutral conditions. Comparison with observations from Duke (a) and Tumbarumba (b) forests. Circles are mean values of normalized mean velocities at different (normalized) heights obtained from averaging *n* measured profiles. Horizontal bars denote ±1 standard deviation from measured values. The zero value in the *y*-axis indicates the canopy top.

In order to evaluate the modelling performance under unstable atmospheric conditions, the model was applied using data collected at Duke and Tumbarumba canopies for varying values of the Obukhov length (L). As shown in Figure 5-4, the estimated profiles are again within the expected accuracy for the model, although an underestimation of wind speed for the highest level above the canopy is noticeable. Apparently this behaviour is not directly dependent on the canopy type or on the L value, since the highest identified differences are from the Duke site in the less

unstable situation and from the Tumbarumba site in the most unstable case. In terms of the intensity of wind velocity, the maximum deviation between model and measurement above the canopy top is approximately equal to the friction velocity, i.e., $U(z \approx 0.25L_c) \approx u_*$. Within the canopy the model response to the drag exerted by leaves and branches on the airflow momentum is very good, when comparing to observations, for the two lowest *L* values (images c and d). On the contrary, the model had some difficulty in coping with the strongly inflected profile measured in the Duke forest (image a). For the Tumbarumba site, image b, there is a general tendency of underestimation inside the canopy, with a maximum deviation equal to $U(z \approx -0.4L_c) \approx 0.5 \cdot u_*$.

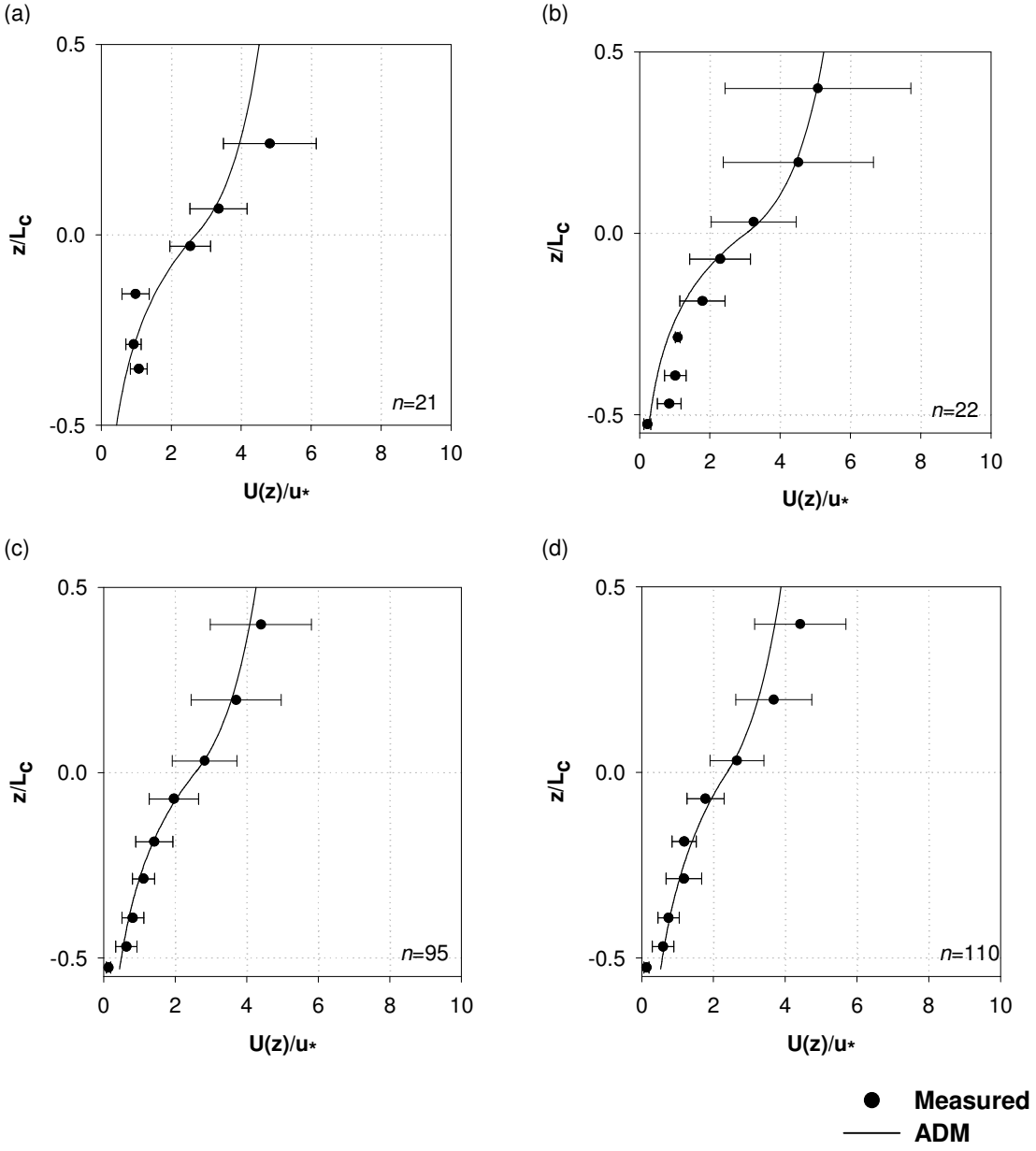

Figure 5-4. Vertical profiles of mean wind speed in unstable conditions. Comparison with observations from Duke forest with *L*=-20 m (a), and from Tumbarumba site with *L* values equal to -52 m (b), -204 m (c) and -444 m (d). From (a) to (d) profiles are progressively more unstable. Note the difference in the number of measurements used in the average.

The model was also applied to the situation of stable stratification. The larger impact, when comparing to unstable conditions, of the RSL on the wind speed profile above the canopy is captured by the model as illustrated in Figure 5-5. This relation derives from the form of $\hat{\psi}_m(z)$ given by Eq. 4-32. There is, however, a disagreement with the observations at the levels under the canopy top, with the model evidencing an underestimating tendency.

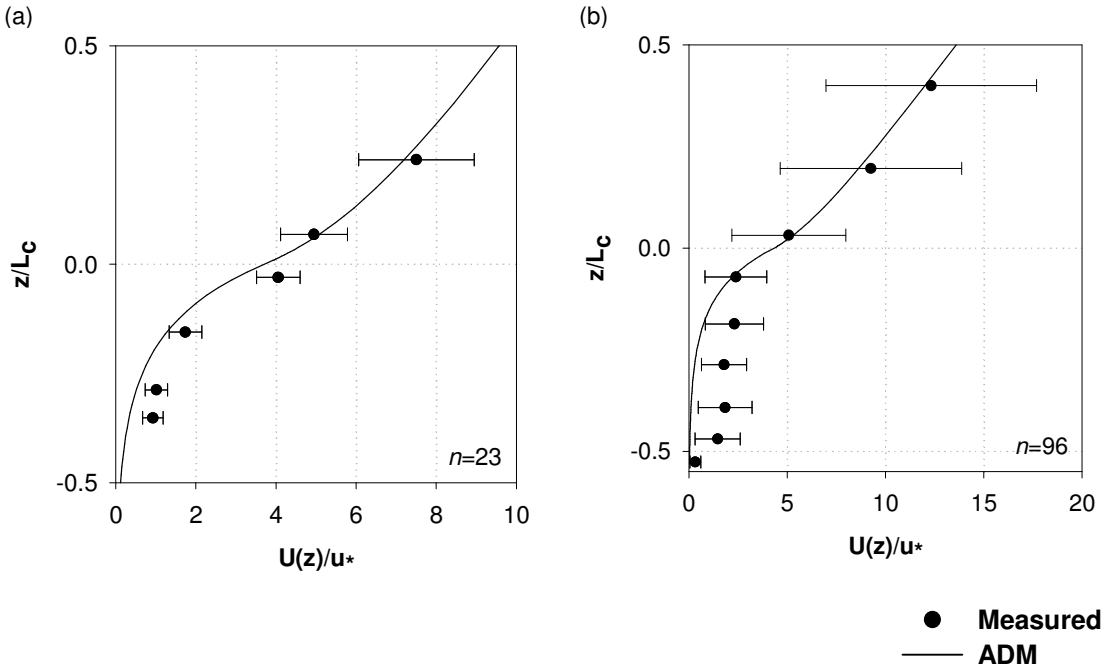

Figure 5-5. Vertical profiles of mean wind speed in stable conditions. Comparison with observations from Duke forest with *L*=54 m (a) and Tumbarumba with *L*=47 m (b). Note the different scale in the *x*-axis.

These results confirm that the consideration of non-neutral conditions represents an additional complexity to the simulation, as was demonstrated in the description of the wind flow module in section 4.3, due to the necessity of dealing with the substantial dependence on stability exhibited by the wind profile within and above the canopy (e.g., Harman and Finnigan [2007]).

The modelling performance was also evaluated applying the statistical metrics defined by ASTM International [2000] and the ones incorporated into the BOOT statistical model evaluation software package [Chang and Hanna, 2005]. The statistical metrics considered were the following: mean bias (*d*), geometric mean bias (*MG*), geometric variance (*VG*), fractional bias (*FB*), normalised mean square error (*NMSE*), Pearson correlation coefficient (*r*) and geometric fraction within a factor of 2 (*FAC2*). The expressions for the calculation of each of these parameters are given in

Table A-4 [q]. As the table shows, all these parameters are linear measures except *MG* and *VG*, which are logarithmic. *NMSE* and *VG* are measures of scatter and reflect both systematic and unsystematic (random) errors. *FB* and *MG* are measures of mean bias and indicate only systematic errors; although as *FB* is based on a linear scale the systematic bias refers to the arithmetic difference between observed and predicted values; the systematic bias in *MG* expresses the ratio between predicted and observed values because it is based on a logarithmic scale. The FB is of particular interest because, being a dimensionless number, it is convenient for comparing results involving different levels. This measure of performance is symmetrical and bounded, with values that range between -2.0 and +2.0 for, respectively, extreme over-prediction and extreme under-prediction. As an indication, an FB equal to -0.67 is equivalent to an over-prediction by a factor of two, while a value of +0.67 denotes an under-prediction by a factor of two.

Although the definition of quality acceptance criteria is dependent on the purpose of the model and on the relevant metrics considered, some indicative threshold values are presented in Table A-4 along with the statistical metrics for the 'perfect' model. In the field of air pollutants dispersion modelling, the following performance measures define an 'acceptable' performance [Chang and Hanna, 2005]:

- the fraction of predictions within a factor of two of observations is about 50% or greater, i.e., $FAC2 > 0.5$;
- the mean bias is within ± 30% of the mean, which can be interpreted in terms of $|FB| < 0.3$ or $0.7 < MG < 1.3$;
- the random scatter is about a factor of two to three of the mean, which means that approximately $NMSE < 1.5$ or $VG < 4$.

From the extensive list of validation metrics available, there is not a single measure that is universally applicable to all conditions. Therefore, the simultaneous analysis of multiple performance measures is the most correct approach for determining the quality of model performance. Each parameter has, in fact, intrinsic characteristics that make it more or less appropriate for application to a given situation. When both measured and computed values vary significantly along the dataset, and although *MG* and *VG* provide a balanced treatment of extremely high and low values, *FAC2* will become the most robust measure, because it is not overly influenced by

[q] The quantification of the error resulting from both bias and scatter is made through the NMSE. The percentage error will be used only in section 5.3.

discrepancies on the magnitude of the properties under analysis. *FB* and *NMSE*, on the other hand, are strongly influenced by this type of feature [Chang and Hanna, 2005].

In order to perform the analysis, the value of wind velocity at the nearest computational cell from each of the measuring levels was considered. For each of the study cases, the paired values of predicted and measured normalized velocities were statistically compared by using the parameters given in Table A-4. Table 5-2 lists the results of the validation procedure. The *NMSE* is between 0.02 and 0.04 except for the last case, evidencing the good agreement between values. The higher *NMSE* for the Tumbarumba site under stability conditions results from the deviation between profiles within the canopy, as previously referred. Nevertheless, the *NMSE* is clearly lower than the maximum of 1.5 defined by the acceptance criterion. The good correlation between predicted and observed values is shown by the high *r*, while the mean bias is kept within reasonable limits as shown by *d* or *MG*, although evidencing an overall under-prediction (positive values).

Table 5-2. Statistical analysis of the ADM results for the measured and computed wind velocities within and above the canopy. D and T stand for Duke and Tumbarumba sites, respectively.

Case	*NMSE*	*r*	*d* ($m.s^{-1}$)	*MG* ($m.s^{-1}$)	*VG* ($m^2.s^{-2}$)	*FB*	*FAC2*
D, *L*=∞	0.02	0.992	0.192	1.11	1.03	0.071	1.000
T, *L*=∞	0.02	0.988	0.086	0.96	1.13	0.044	0.889
D, *L*=-20 m	0.04	0.971	0.157	1.04	1.06	0.071	1.000
T, *L*=-52 m	0.03	0.991	0.294	1.29	1.18	0.141	0.778
T, *L*=-204 m	0.02	0.991	0.107	0.94	1.19	0.058	0.889
T, *L*=-444 m	0.04	0.990	0.102	0.88	1.27	0.058	0.889
D, *L*=54 m	0.04	0.989	0.493	1.50	1.35	0.158	0.833
T, *L*=47 m	0.13	0.989	1.100	3.84	25.7	0.310	0.444

Table 5-3 presents the overall statistical metrics for the complete dataset of measured and simulated values as a whole. Although some tendency of the model to underestimate the wind velocities is known to affect its overall performance, all the metrics indicate a good relation with observations.

Table 5-3. Statistical metrics over the complete dataset of measured and computed wind velocities within and above the canopy. μ and σ represent, respectively, the mean and standard deviation of the data.

Data	μ ($m.s^{-1}$)	σ ($m.s^{-1}$)	*NMSE*	*r*	*d* ($m.s^{-1}$)	*MG* ($m.s^{-1}$)	*VG* ($m^2.s^{-2}$)	*FB*	*FAC2*
Measured	2.52	2.26	0.00	1.000	0.00	1.00	1.00	0.000	1.000
ADM	2.20	2.18	0.06	0.975	0.321	1.28	1.83	0.136	0.825

As the region above the canopy is the most relevant, the statistical metrics were calculated considering only the values above the canopy top. The results are given in Table 5-4 and Table 5-5. The analysis is limited in each simulation to 2 points of comparison (measuring levels) in the Duke case and to 3 in the Tumbarumba case.

Table 5-4. Statistical analysis of the ADM results for the measured and computed wind velocities above the canopy.

Case	*NMSE*	*r*	*d* ($m.s^{-1}$)	*MG* ($m.s^{-1}$)	*VG* ($m^2.s^{-2}$)	*FB*	*FAC2*
D, *L*=∞	0.00	1.000	0.11	1.01	1.00	0.020	1.000
T, *L*=∞	0.01	1.000	0.30	1.12	1.02	0.078	1.000
D, *L*=-20 m	0.03	1.000	0.49	1.12	1.02	0.128	1.000
T, *L*=-52 m	0.01	0.999	0.27	1.09	1.02	0.064	1.000
T, *L*=-204 m	0.01	0.988	0.34	1.12	1.02	0.098	1.000
T, *L*=-444 m	0.03	0.994	0.56	1.19	1.03	0.169	1.000
D, *L*=54 m	0.00	1.000	0.10	1.01	1.00	0.015	1.000
T, *L*=47 m	0.02	0.999	1.06	1.22	1.08	0.127	1.000

As previously, Table 5-5 presents the statistical metrics for the complete dataset.

Table 5-5. Statistical metrics over the complete dataset of measured and computed wind velocities above the canopy.

Data	μ ($m.s^{-1}$)	σ ($m.s^{-1}$)	*NMSE*	*r*	*d* ($m.s^{-1}$)	*MG* ($m.s^{-1}$)	*VG* ($m^2.s^{-2}$)	*FB*	*FAC2*
Measured	4.96	2.24	0.00	1.000	0.00	1.00	1.00	0.000	1.000
ADM	4.54	2.24	0.02	0.981	0.43	1.11	1.03	0.090	1.000

The comparison between the ensemble measurements with the vertical profiles computed by ADM has shown that, in general, the model is capable of simulating the effects of the canopy structure and the wide range of atmospheric stability conditions analysed (*L* between -444 m and 54 m, plus L = ∞ for neutral stability) with a good performance. In particular, an adequate response of the model to the heterogeneous characteristics of the Duke forest, resulting from the prominent variation of leaf density [Katul and Albertson, 1998], has been observed. Particularly under stable atmospheric conditions, improvements on the simulation of mean wind flow within the canopy would permit an increase in the accuracy of simulations.

5.2. Discharge module validation

The performance of the flow rate algorithm was evaluated through the comparison with the available data on the tank and gating system for the Marseille 2000 real scale drop experiments, conducted under the scope of ACRE Project [Giroud et al., 2002; ITRATECH, 1999]. The aircraft was a S2F Turbo Firecat, converted by CONAIR Aviation, which carries approximately 3 m^3 of firefighting product in four compartments containing 0.7 m^3 each, as schematized in Figure 5-6. The tests were based on 1×4 salvo drops, in which the four compartments are released simultaneously.

(a) (b)

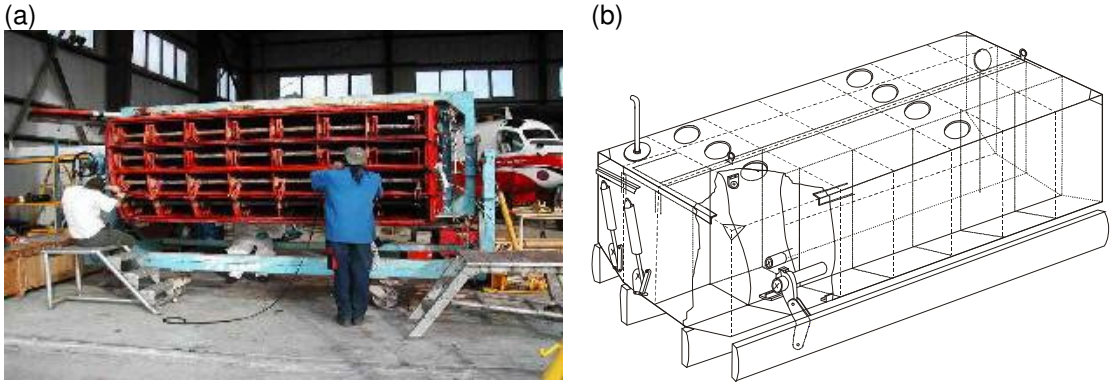

Figure 5-6. (a) Photograph of a S2F CONAIR tank during maintenance operations on the 4 individual compartments [url 17]. (b) 3D scheme of tank configuration showing the opening mechanism of the 4 doors at the bottom [ITRATECH, 1999].

The input parameters needed for calculating the variation of volume discharged with time are presented in Table 5-6. These values were obtained from ITRATECH [1999].

Table 5-6. ADM input parameters related to the geometrical characteristics of each of the CONAIR tanks (tank height H_T, tank length L_T, tank width W_T, equivalent vent diameter D_V, door length L_D, door width W_D, door opening angle α and door opening time t_α).

Input parameter	Tank 1	Tank 2	Tank 3	Tank 4	Unit
H_T	0.843	0.843	0.843	0.843	m
L_T	3.228	3.228	3.228	3.228	m
W_T	0.292	0.322	0.322	0.292	m
D_V	0.197	0.197	0.197	0.197	m
L_D	3.200	3.200	3.200	3.200	m
W_D	0.274	0.265	0.265	0.274	m
α	86	86	86	86	º
t_α	0.21	0.21	0.21	0.21	s

The ADM discharge module was run for three different combinations of compartments opening: 4 single-door drops, 2 two-door salvos, 1 four-door salvo. The comparison with manufacturer's values of total release time (Δt) and peak flow rate (Q_{max}) is shown in Table 5-7 for each of the configurations. ADM values are given for the combined regime in which the model is allowed to choose between the minimum velocity value from Bernoulli regime and acceleration regime, and the default one, in which the model identifies if it is an unrestricted tank and in that case calculates only the acceleration-induced velocity. Output model results with unrestricted tanks are given only by acceleration-dominated regime. Results from the combined regime are given, in this case, just for comparison. It should be noted that the manufacturer's measurement process is not absent from a certain degree of inaccuracy. In particular, the total time for release is dependent on choosing when the release stops, which for tank salvos is actually rather subjective, as sidewall drainage will continue for some time [R. Becker, pers. communication]. The following data comparison should thus be interpreted as indicative, since a comprehensive validation process would require a detailed and accurate set of experimental data.

Table 5-7. Data comparison of total release time (Δt) and peak flow rate (Q_{max}) according to factory (available in ITRATECH [1999]) and model output values for combined regime (for comparison purposes only) and acceleration-dominated flow.

	Manufacturer values		ADM values			
			Combined regime		Acceleration-dominated regime	
Number of compartments released simultaneously	Δt (s)	Q_{max} ($m^3.s^{-1}$)	Δt (s)	Q_{max} ($m^3.s^{-1}$)	Δt (s)	Q_{max} ($m^3.s^{-1}$)
1	0.5	2.177	0.62	2.274	0.56	2.312
2	0.5	4.353	0.62	4.548	0.56	4.624
4	0.5	8.706	0.62	9.176	0.56	9.314

Given the simplicity of the numerical approach to a highly complex outflow of firefighting product when released from the tank, the results obtained can be considered as very satisfactory. ADM shows a reasonable accuracy on the prediction of time for total discharge of the liquid and maximum flow rate attained during the process. The higher value of release time can be associated with a tendency of the algorithm to underestimate the amount of liquid evacuated approximately during the last quarter of time, as identified by the USDA-FS during the extensive validation tests performed under ETAGS program [Swanson et al., 1978]. This is particularly clear in the combined regime, according to which the time for complete evacuation is 0.62 s. A better agreement with manufacturer indicative values is found if the flow is approached to an acceleration-dominated one. In this case, release time is decreased to 0.56 s due to the higher outflow velocities attained during the second half of the time, and consequently the higher peak flow rate values, as can be seen in Figure 5-7, in which ADM results for the time evolution of discharge velocity and door angle at each time-step are shown.

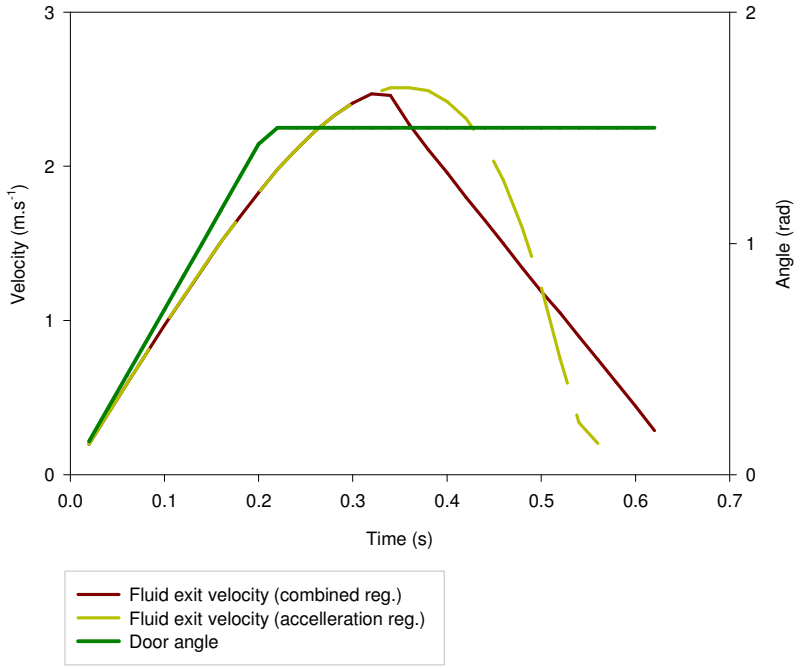

Figure 5-7. Variation with time of outflow velocity of the liquid and door angle for the 1×4 salvo drop configuration Firecat Conair tank.

In all of the configurations, door rate was found to be fast enough not to restrict flow. Maximum aperture (angle of 1.5 radians) is reached after 0.21 s, after which the effective door area equals the value of door area. The inflexion point in the combined regime line, approximately at half the total time of discharge, marks the transition from a free-fall acceleration-dominated regime to a steady-state regime. As the tank was identified by the model as unrestricted, it will not calculate the steady-state Bernoulli velocity, as referred.

Figure 5-8 presents the time evolution of the volume discharged and cumulative volume discharged, according to the acceleration-dominated flow, for the 1×4 salvo drop situation.

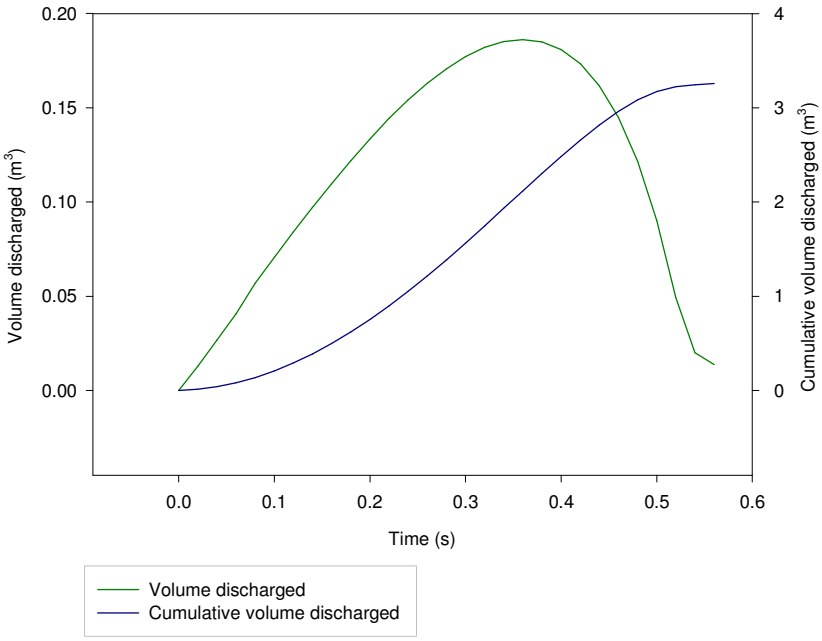

Figure 5-8. Variation with time of volume discharged and cumulative volume discharged for the 1×4 salvo drop configuration Firecat Conair tank.

The flow rate algorithm incorporated in ADM model was originally developed by Swanson et al. [1977]. Extensive measurements with a panoply of tank configurations in Swanson et al. [1978] have demonstrated an acceptable accuracy in most tank and gating systems. This algorithm has shown to fulfil the requirements for integration in the ADM model, in particular because it allows a fast running performance without compromising general modelling accuracy, which was one of the main concerns during the development of the present model. Nevertheless, ETAGS tests have shown that the algorithm had a tendency to underestimate pressure, and that an improved match with measured values is obtained for higher values of the *C* constant in Eq. 4-59, although the final accuracy of the simulated flow rate would be decreased. ADM thus applies the original *C* value.

Although it was not the purpose of this dissertation to go into full detail on the behaviour of the liquid during the gravitational discharge from the tank, a more focused and physically-based study of the phenomena involved, namely through the state-of-the-art capabilities of CFD models, could improve the accuracy of the simulations. Such study should address the analysis, in particular, of the effect of rheology on flow behaviour, thus fulfilling a gap in research on this subject [Dziubiński and Marcinowski, 2005 and 2006]. This approach would require, however, an extensive set of flow rate measured data, similar to the ETAGS program conducted by the USDA-FS in the 70's, in order to validate the numerical approach.

5.3. Dropping model validation with real scale drop tests

ADM model validation consisted of the comparison of the simulated ground concentrations against a set of real scale dropping tests conducted at Marseille, France, and at Marana, Arizona, US, in which different products and delivery systems were used permitting the analysis of model performance within a wide range of conditions, as given in Table 5-8.

Table 5-8. Dropping tests general characterisation.

Location	Delivery system	Product	Viscosity (cP)	Drop height (m)	Wind velocity ($m.s^{-1}$)
Marseille	Conventional (salvo drop)	Fire-Trol (931)	432 – 1430	34 – 45	1 – 7
Marana	Constant flow	Water and Phos-Chek (LV, MV and HV)	152 – 1300	38 – 78	0.5 – 4

As previously referred, both drop trials were conducted over bare ground. Due to the absence of a vegetative canopy, the vertical wind profile has been calculated applying a power-law, which has been applied with acceptable accuracy in non-complex terrain up to a height of about 200 m and thus constitutes a reasonable alternative to the logarithm profile (see Eq. 3-1) that does not requires the determination of the friction velocity. In this case, the wind shear given in Eq. 5-1 is a function of the velocity (U_m) measured at a given reference height (H_m) and of a power exponent (p), which depends on both the atmospheric stability and the surface characteristics, defined as 0.2 (e.g., Irwin [1979]).

$$U(z) = U_m\left(\frac{z}{H_m}\right)^p \qquad \textbf{Eq. 5-1}$$

Each drop trial was categorized according to the following criteria shown in Table 5-9. Viscosity classification is what is currently used by worldwide fire agencies [Vandersall, 1994]; the range for classification of drop height is based on the 45 m imposed as minimum value in the US [Vandersall, 1994]; wind velocity categories derive from the Beaufort scale for land winds; and the relative wind direction uses typical aeronautics terminology. The relative wind direction is the angle in geometric

coordinates between the aircraft trajectory (0º) and the wind. In other words, it indicates the direction to which the wind blows relative to the grid orientation.

Table 5-9. Criteria for classification of drops based on viscosity, drop height, wind velocity and relative wind direction.

Viscosity (cP)		Drop height (m)		Wind velocity ($m.s^{-1}$)		Relative wind direction (º)	
Water-like	<60	Low	<45	Calm	[0, 0.3[	Headwind	[135, 225[
Low	[60, 250[	Medium	[45, 70[	Light air	[0.3, 1.6[	Left crosswind	[225, 315[
Medium	[250, 1000[	High	>70	Light breeze	[1.6, 3.4[	Tailwind	[315, 45[
High	>1000			Gentle breeze	[3.4, 5.5[	Right crosswind	[45, 135[
				Moderate breeze	[5.5, 7.9[		

Real scale drop tests were performed applying the “cup-and-grid” method, which allows quantification of the variation of line length and area occupied by a given coverage level (product concentration) at ground, due to the influence of the delivery system, the flight parameters, the product characteristics, and meteorological conditions. The equipment used consisted of video cameras, global positioning system (GPS) devices and radar altimeters for determining aircraft drop height and drop speed. A meteorological mast equipped with a weather station adjacent to the drop site allowed the monitoring of wind speed, direction and air humidity. The weight of retardant in each cup and the location of each cup within the grid were registered (see Figure 5-9) and a given interpolation method is used to estimate the values between cups [Suter, 2000; Giroud et al., 2002; Lovellette, 2004].

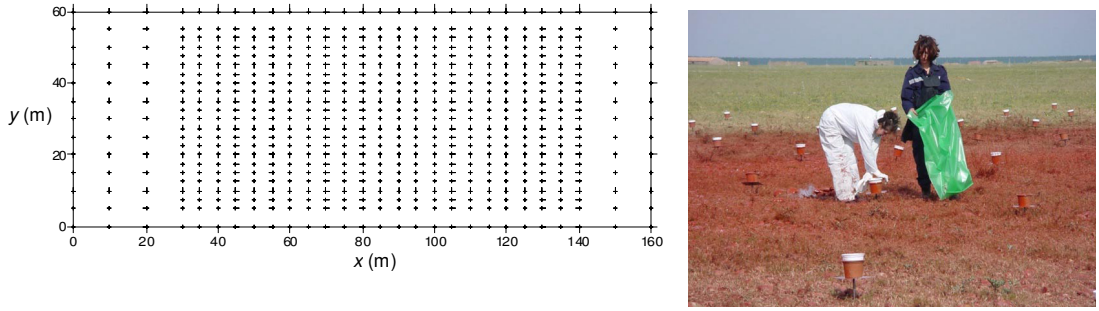

Figure 5-9. Cup grid setting and cup collection during Marseille 2000 aerial drops [Giroud et al., 2002].

The post-processing of the measured ground concentration of product involves the analysis of several "metrics of interest" or "ground pattern responses" in technical terminology. The most important are the line length and the area of each isoconcentration contour, i.e., each concentration level, which thus defines a given range of concentrations. In the US, the following minimum threshold concentrations are defined: 0.25, 0.75, 1.5, 2.5, 3.5, 5.5, 7.5 and 9.5 gpc [r]. In Europe the only drop tests made until present were analysed under the scope of ACRE research project using the following minimum values per class of concentration: 0.8, 1.6, 2.4 and 4 $l.m^{-2}$. However, in order to have a wider comparison, the analysis for the Marseille tests will consider the following coverage levels: 0.5, 0.8, 1, 1.5, 2, 3 and 4 $l.m^{-2}$.

As the coarse measuring grid is usually a source of error on the determination of line lengths and areas, an interpolation method should be applied in the determination of the concentration values between two consecutive measurement cups. In the current work, the measured concentrations are first interpolated to a 1x1 m^2 grid in the Marseille case and to a 1x1 ft^2 in the Marana tests using the Kriging interpolation scheme available in Surfer® software.

Both in Marseille and Marana drop tests the position of the aircraft relating the measuring grid at the exact moment of the opening of the tank doors was not registered. The analysis of results cannot thus be made by the comparison of the spatial distribution of modelled and measured concentrations at ground surface, nor by the statistical analysis of data in each cell. In order to overcome this aspect, the validation procedure involved a three stage process:

- visual comparison of ground pattern shape per contour area;
- calculation of a set of statistical parameters on the computed and measured values of line length and area per coverage level;
- intercomparison of the volume of product deposited along the *x*-axis.

As in section 5.1, the statistical analysis of modelling results involved the calculation of a set of metrics (see Table A-4) commonly applied on state-of-the-art methodologies for the evaluation of model performance [ASTM International, 2000; Chang and Hanna, 2005]. There is not an acceptance criterion available specifically for the aerial dropping models. In this sense, the analysis of results is made by comparing each metric with the threshold minimum and maximum limits commonly

[r] 1 gpc = 1 US gal.100 ft^{-2} = 0.407 $l.m^{-2}$

used in air quality applications. The percentage error, on the other hand, which is hereafter calculated in this study, is evaluated by a maximum 10% (in modulus) according to usual requirements for aerial dropping models performance established by the USDA-FS [R. Becker, pers. communication].

5.3.1. Marseille 2000

The first set of data for ADM validation is from the real scale drops performed in 2000 at Marseille, France, during the ACRE Project (see Figure 5-10). These experiments were conducted in order to analyse the effect of product viscosity on its ground distribution. For detailed description and results see Giroud et al. [2002], ITRATECH [1999] and Picard et al. [2001].

Figure 5-10. Retardant drop during Marseille 2000 tests.

A CDF-S2F Turbo Firecat aircraft, converted by Conair Aviation, was used. The delivery system carries a maximum of 3030 l of water or retardant distributed by four similar compartments. The experiments were based on a 1x4 salvo drop, in which the entire capacity of the tank is dropped at one time. One of the major uncertainties relating the experiments relies on the value of the drop speed. Although a value of 60 $m.s^{-1}$ was predefined there is no register of the real speed attained. The retardant used was gum thickened Fire Trol 931. The spatial distribution of the product concentrations at ground was obtained for each drop using a 160×60 m^2 grid of cups with 10×5 m^2 resolution (see Figure 5-9). In order to complement the analysis of product behaviour in function of viscosity, two digital video cameras provided frontal and lateral images of the droppings. Meteorological parameters (wind direction and velocity, air temperature and humidity) were monitored in continuum during the tests. Table 5-10 shows the parameters used as input data by the model. As in Table 5-9, wind direction is the angle of the wind in geometric coordinates corrected with the grid orientation.

Table 5-10. Drop parameters for the Marseille 2000 drop tests.

Drop number	Product viscosity (cP)	Drop height (m)	Wind velocity ($m.s^{-1}$)	Wind direction (º)
S4L1	432	42.9	1	294
S4L3	432	34.1	1	12
S3L1	637	41.2	7	214
S3L2	720	39.0	7	224
S6L3	1060	45.9	6	159
S6L1	1260	35.5	4	107
S6L2	1430	44.7	4	144

As can be seen in Table 5-10, Marseille 2000 drop trials cover a wide range of conditions:

- retardant viscosity between 432 and 1430 cP;
- meteorological conditions: wind velocities between 1 and 7 $m.s^{-1}$ and variable wind direction.

The drop trials can be classified following the criteria from Table 5-9 as given in Table 5-11.

Table 5-11. Classification of Marseille drop trials based on the predefined criteria.

Drop number	Viscosity				Drop height			Wind velocity				Relative wind direction			
	No viscosity	Low	Medium	High	Low	Medium	High	Light air	Light breeze	Gentle breeze	Moderate breeze	Headwind	Left crosswind	Tailwind	Right crosswind
S4L1			•		•			•					•		
S4L3			•		•			•						•	
S3L1			•		•						•	•			
S3L2			•		•						•	•			
S6L3				•		•					•	•			
S6L1				•	•					•					•
S6L2				•	•					•		•			

Figure 5-11 to Figure 5-17 show the comparison of ground patterns obtained by simulation and measurement for all the test cases analysed. As mentioned, the position of the aircraft at the instant of release was not measured, therefore the locations of the modelled and measured patterns in the grid are not comparable. Generally speaking, ADM allows a good representation of the spatial distribution of product for all the classes of concentrations considered, showing the typical accumulation of product at the front of the pattern as a result of the delivery system type.

Figure 5-11 to Figure 5-14 are specific for medium viscosity products. In particular for the two first cases, Figure 5-11 and Figure 5-12, the model underestimates the accumulation of product at the front of the pattern for the higher concentration level, probably due to an inaccurate estimation of the flow rate of product exiting from the tank. Although the overall shape of the patterns is similar, the observed contours for the higher concentrations (roughly above 3 $l.m^{-2}$) have an elliptic shape that is not present in the model results.

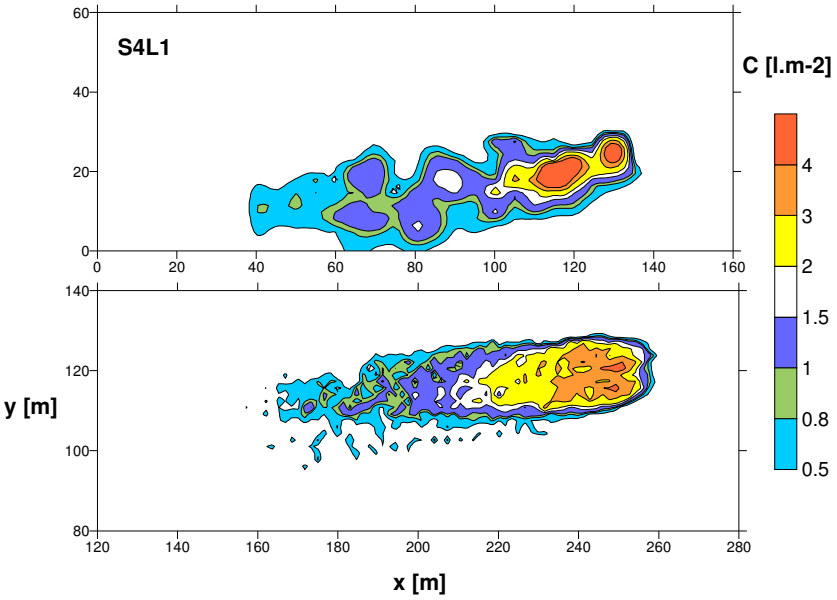

Figure 5-11. Comparison between the measured (up image) and simulated (down image) ground patterns of product concentration for the Marseille 2000 drop test S4L1: medium viscosity, low drop, light air, left crosswind.

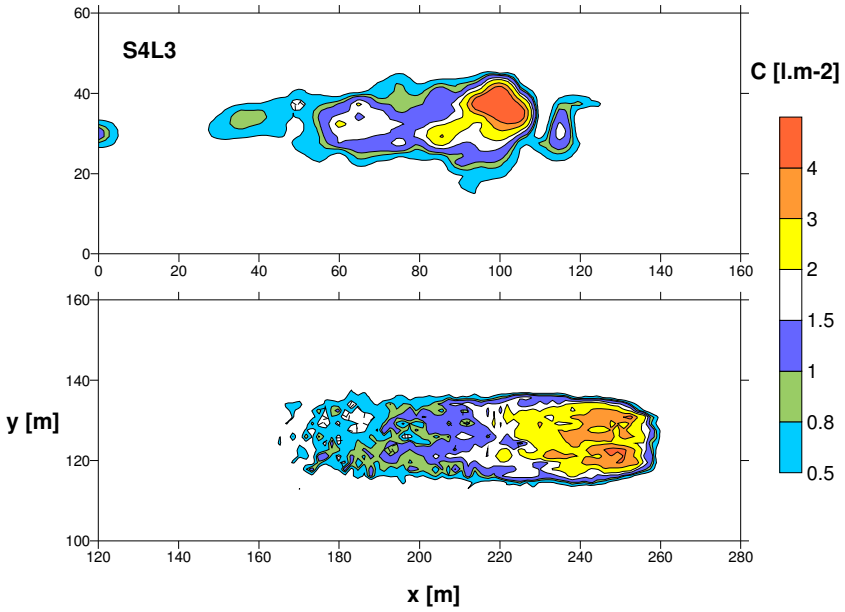

Figure 5-12. Comparison between the measured (up image) and simulated (down image) ground patterns of product concentration for the Marseille 2000 drop test S4L3: medium viscosity, low drop, light air, tailwind.

The patterns shown in Figure 5-13, Figure 5-14, Figure 5-15 and Figure 5-17 show a distinct behaviour of the liquid, evidenced by the narrow configuration, with a lower cross distance at the front and an increased total length, which is mainly a result of the headwind. From the comparison, ADM demonstrates the capability to deal with this effect.

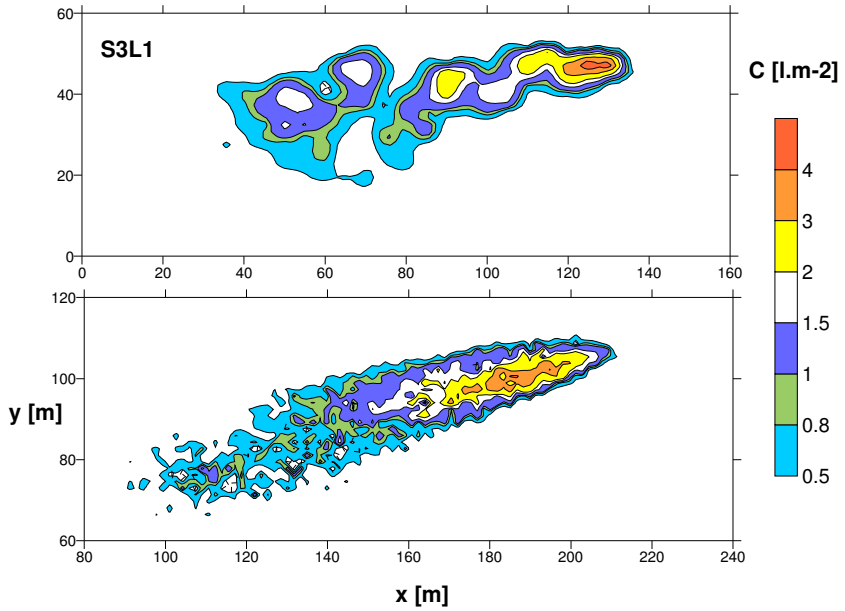

Figure 5-13. Comparison between the measured (up image) and simulated (down image) ground patterns of product concentration for the Marseille 2000 drop test S3L1: medium viscosity, low drop, moderate breeze, headwind.

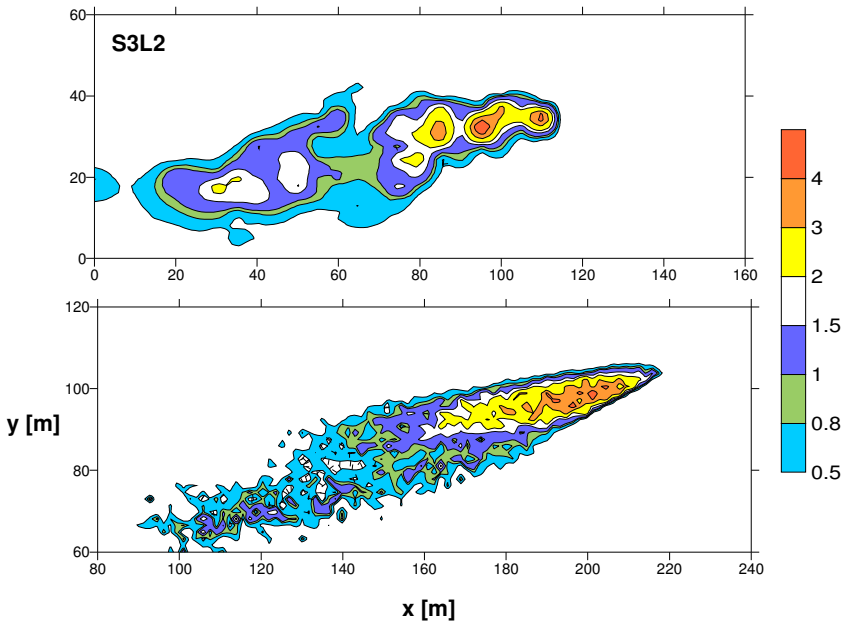

Figure 5-14. Comparison between the measured (up image) and simulated (down image) ground patterns of product concentration for the Marseille 2000 drop test S3L2: medium viscosity, low drop, moderate breeze, headwind.

Figure 5-15 to Figure 5-17 correspond to the high viscosity products. ADM shows an acceptable performance in treating the physics underlying the liquid behaviour for this range of viscosities, at least in terms of final results.

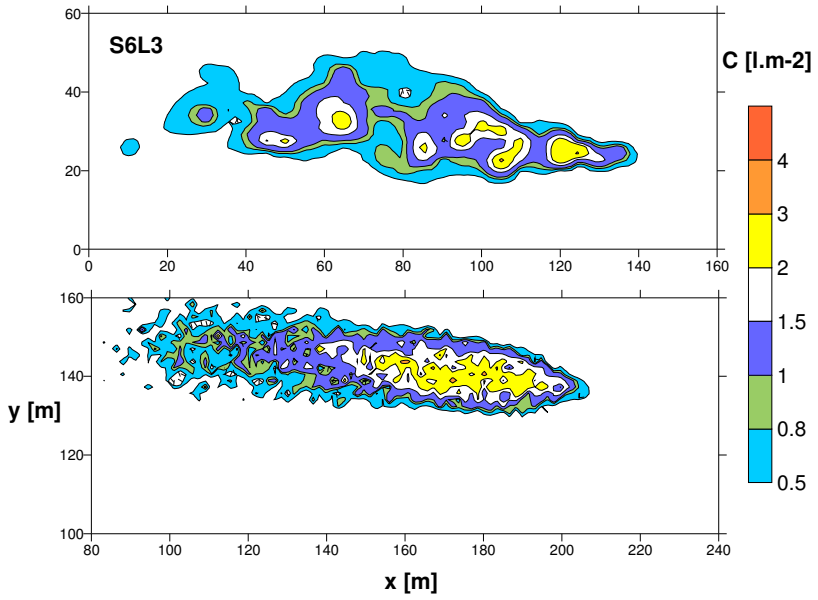

Figure 5-15. Comparison between the measured (up image) and simulated (down image) ground patterns of product concentration for the Marseille 2000 drop test S6L3: high viscosity, medium height drop, moderate breeze, headwind.

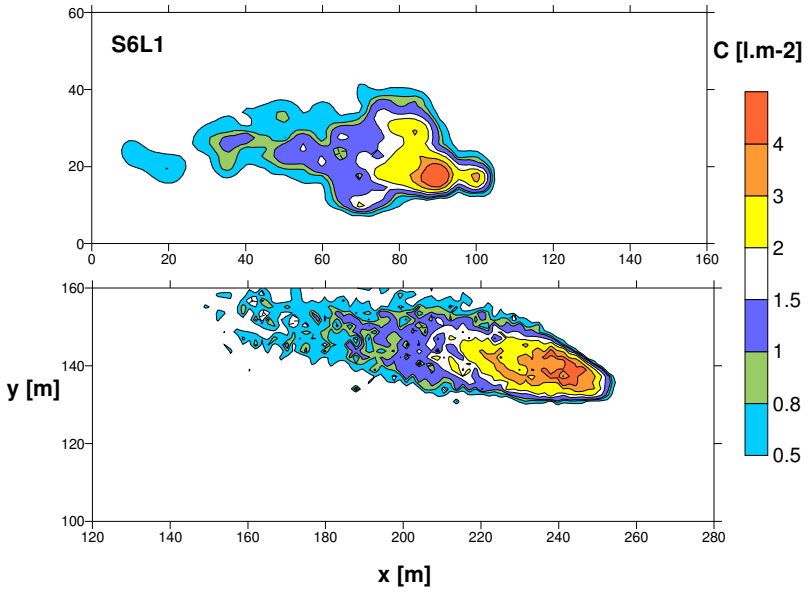

Figure 5-16. Comparison between the measured (up image) and simulated (down image) ground patterns of product concentration for the Marseille 2000 drop test S6L1: high viscosity, low drop, gentle breeze, right crosswind.

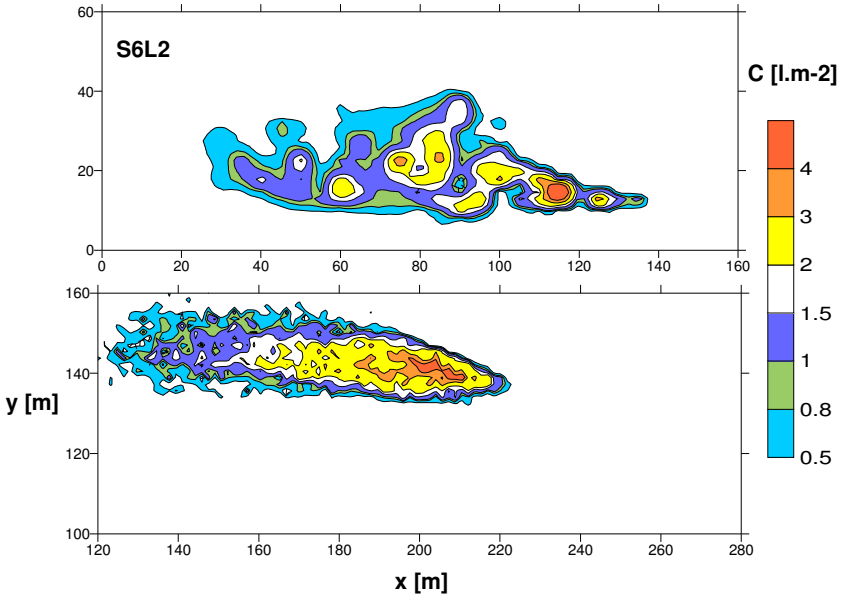

Figure 5-17. Comparison between the measured (up image) and simulated (down image) ground patterns of product concentration for the Marseille 2000 drop test S6L2: high viscosity, low drop, gentle breeze, headwind.

For each of the study cases, the line lengths per coverage level were validated using the statistical metrics given in Table A-4. The results are presented in Table 5-12.

Table 5-12. Statistical analysis of the ADM results for line lengths per coverage level in comparison with the experimental data for the Marseille 2000 drop tests.

Drop number	*NMSE*	*r*	*d* (m)	*MG* (m)	*VG* (m^2)	*FB*	*FAC2*
S4L1	0.010	0.987	1.571	1.19	1.32	0.029	0.857
S4L3	0.011	0.987	-0.571	1.15	1.38	-0.011	0.857
S3L1	0.032	0.972	5.143	1.39	1.75	0.092	0.857
S3L2	0.020	0.983	4.714	1.19	1.09	0.077	1.000
S6L3	0.008	0.993	3.167	1.26	1.23	0.045	0.833
S6L1	0.010	0.996	-4.000	0.92	1.03	-0.080	1.000
S6L2	0.013	0.992	5.000	1.11	1.03	0.077	1.000

Table 5-13 presents the statistical metrics for the complete measured and simulated datasets.

Table 5-13. Statistical metrics of line lengths per coverage level for the overall Marseille 2000 drop tests.

Data	μ (m)	σ (m)	*NMSE*	*r*	*d* (m)	*MG* (m)	*VG* (m^2)	*FB*	*FAC2*
Measured	58.80	36.40	0.000	1.000	0.00	1.00	1.00	0.000	1.000
ADM	56.70	36.50	0.010	0.983	2.12	1.16	1.24	0.037	0.917

From the statistical parameters given in Table 5-12 and Table 5-13 it is possible to conclude that the model exhibits a general good performance, independently from the viscosity of the product, as indicated by the average NMSE of 0.01. In fact, all the metrics are within the defined range of the acceptance criteria (see Table A-4). Both the mean (μ) and standard deviation (σ) over the computed dataset are in close agreement with the measured values, notwithstanding the slight tendency for underestimating the length of the ground patterns given the lower μ (in agreement with the positive value of the mean bias *d*). Apparently there is not an immediate relation between the tendency of the model to underestimate or overestimate the lengths of the contours per class of concentration, although it can be inferred that the model always underestimated lengths in headwind conditions.

The same statistical analysis was performed for the area occupied by each coverage level, as shown in Table 5-14. Although there was a slight decrease on the quality of the results, all the parameters are clearly within the limits defined for the acceptability of model performance.

Table 5-14. Statistical analysis of the ADM results for the area occupied per coverage level in comparison with the experimental data for the Marseille 2000 drop tests.

Drop number	*NMSE*	*r*	*d* (m^2)	*MG* (m^2)	*VG* (m^4)	*FB*	*FAC2*
S4L1	0.029	0.986	-65.71	1.04	1.68	-0.096	0.857
S4L3	0.021	0.986	-28.71	1.33	2.66	-0.047	0.857
S3L1	0.024	0.990	32.50	1.25	1.22	0.055	0.857
S3L2	0.015	0.999	60.14	1.04	1.02	0.080	1.000
S6L3	0.004	0.998	-0.50	1.08	1.10	-0.001	1.000
S6L1	0.011	0.993	-5.00	1.00	1.05	-0.008	1.000
S6L2	0.011	0.995	26.71	0.97	1.08	0.036	1.000

The overall good accuracy of ADM results in terms of area occupied by each concentration contour is reinforced by the analysis of the overall statistical metrics presented in Table 5-15. Also in this case the model maintains a very low NMSE and a good linear correlation between predicted and observed values, demonstrating that the slight tendency of underestimation ($d > 0$) of the ground pattern area has not an important effect on general accuracy. In fact, the mean bias is clearly within the threshold of 30% of the mean imposed by the acceptance criterion as given by the values of FB and MG. These conclusions are strengthened by the analysis of the FAC2 parameter, which states that nearly 94% of the data is within a factor of two of the observations.

Table 5-15. Statistical metrics of areas per coverage level for the overall Marseille 2000 drop tests.

Data	μ (m^2)	σ (m^2)	*NMSE*	*r*	*d* (m^2)	*MG* (m^2)	*VG* (m^4)	*FB*	*FAC2*
Measured	694.96	635.82	0.000	1.000	0.00	1.00	1.00	0.000	1.000
ADM	692.11	621.73	0.020	0.991	2.84	1.09	1.32	0.004	0.938

Figure 5-18 shows the comparison between modelled and measured line lengths per coverage level. The adequate statistical parameter for this analysis is the percentage error (δx), which is equal to 100% times the relative error, i.e., 100% times the difference between the observed and the computed values normalized by the latter [Abramowitz and Stegun, 1972]. The performance goal of the model is to guarantee that, for each level, $|\delta x| < 10\%$. This criterion is fulfilled in most of the situations, although ADM has some difficulty in coping with the apparent higher line length for mid coverage levels (3 and 4 l.m^{-2}) in S3L1, S3L2, S6L3 and S6L2 drops.

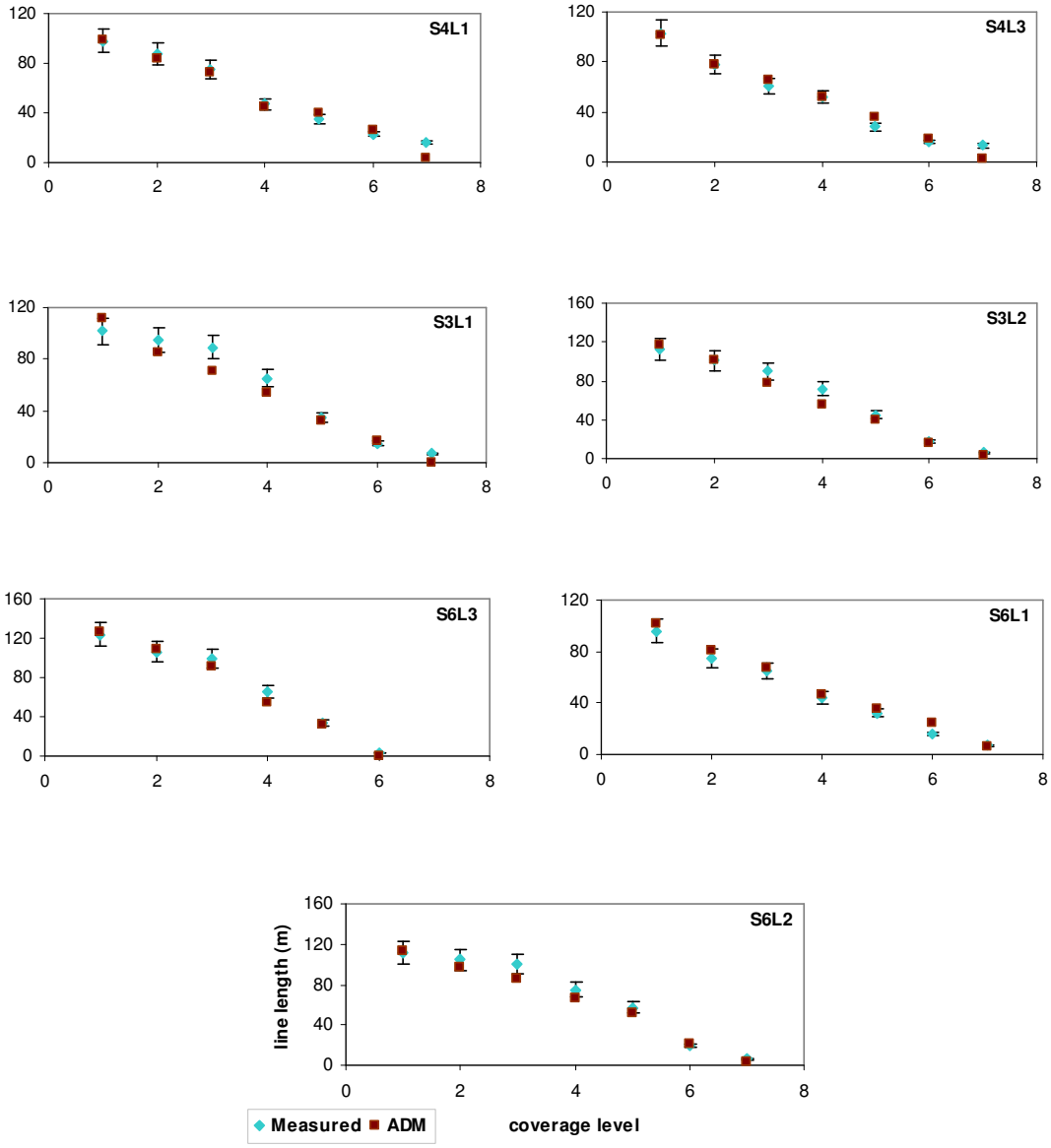

Figure 5-18. Comparison between modelled and measured line lengths per coverage level for the Marseille drops. Vertical error bars indicate a relative error of ± 0.1. The numbers in the *x*-axis represent the 7 coverage levels considered: 0.5, 0.8, 1, 1.5, 2, 3 and 4 l.m^{-2}. Note that the scale indicates the order of each coverage level and not the respective concentration.

Finally, in Figure 5-19 the regression lines for the comparative analysis between measured and simulated line lengths per coverage levels are shown. The underestimation of the length of mid range coverage levels contours is visible in some of the drops. Nevertheless, there is a good correlation between measured and simulated values.

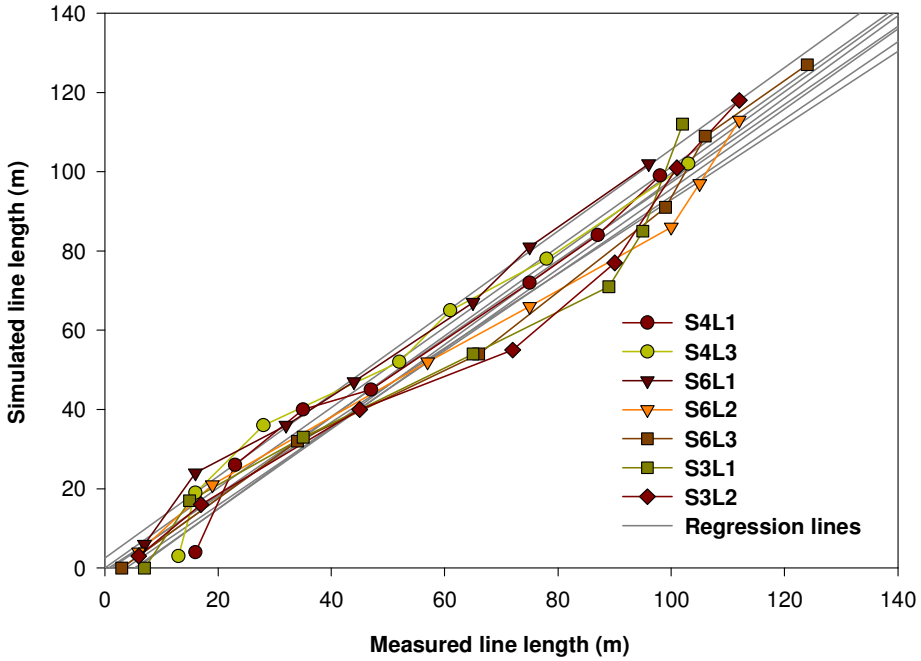

Figure 5-19. Regression analysis of the measured and simulated line lengths for the Marseille drops.

In order to have a simple perception of the spatial variation of the volume deposited at ground, for each cell in the *x*-axis the total volume in the *y*-direction was calculated according to:

$$V_x = V(x) = \sum_y V(y) \qquad \textbf{Eq. 5-2}$$

The various graphs in Figure 5-20 show, for each drop, the comparison between the computed and measured V_x values. The position of the curves in the *x*-axis was adjusted in order to give the best fit (note that the position of the aircraft is unknown, and therefore the position of the pattern in the grid cannot be compared). In general, ADM is capable of showing a distribution similar to the one measured, although in drops S3L1 and S3L2 there is a tendency for overestimating the asymmetry. On the other hand, an underestimation of the maximum value of V_x was found, except for S3L1. The degree of underestimation varies between 3% (S6L3) and 27% (S6L2) of the corresponding maximum volume (with a mean value of 16%).

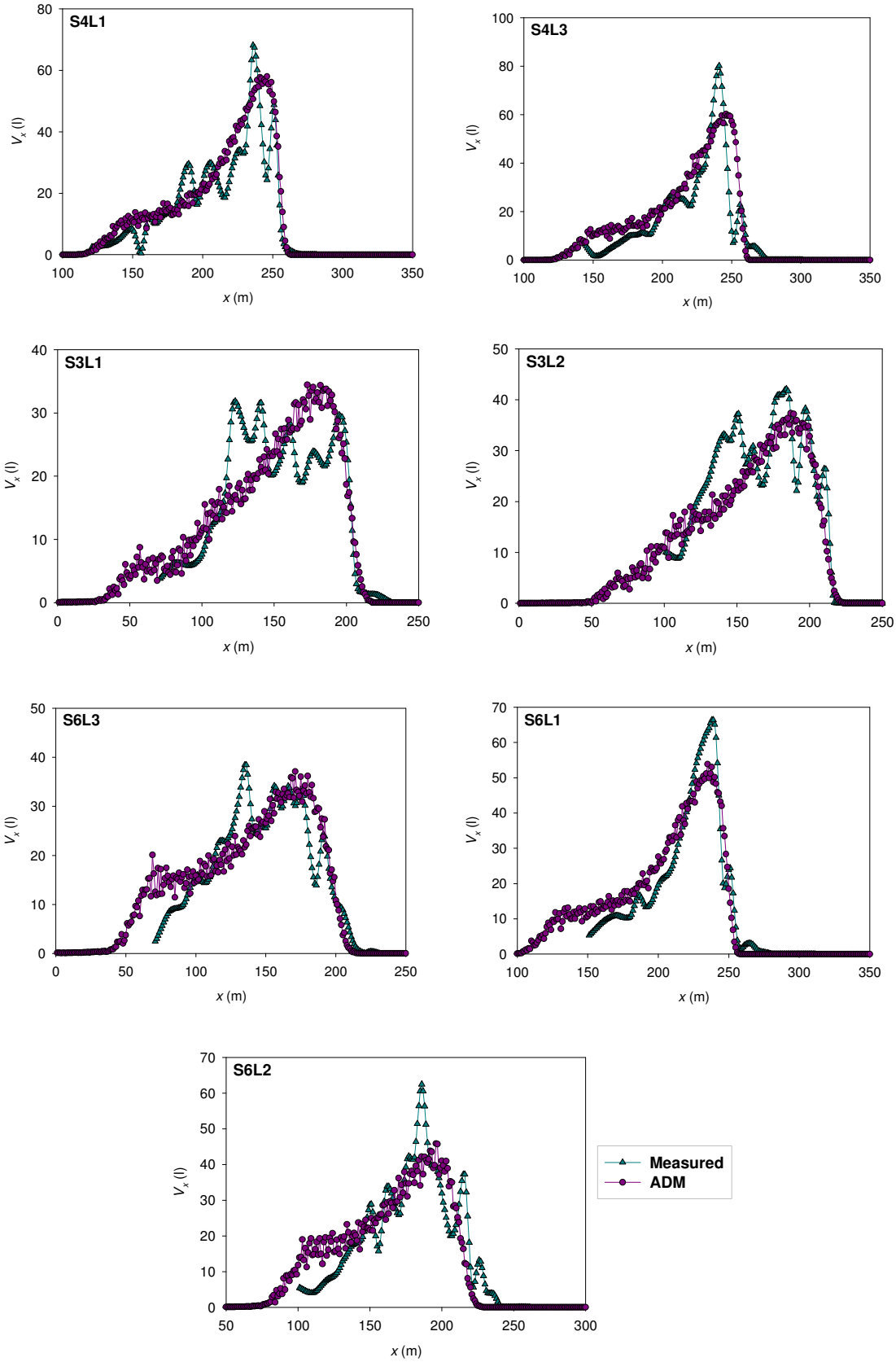

Figure 5-20. Comparison between modelled and measured values of deposited volume along the *x*-axis for the Marseille drops.

As can be seen, due to the time evolution of the flow rate of product in the outflow from the aircraft tanks, the distribution of volumes in the *x*-axis is right-skewed, which is in fact a characteristic of conventional delivery systems. In some cases, as in drops S4L1, S4L3 and S6L1 the distribution is highly skewed to the right, evidencing that a significant amount of product deposits in the last one third of the total length of the pattern.

The Marseille dropping tests have shown that ADM has some flexibility in dealing with the variation of the input conditions without compromising the accuracy of the results. The wide range of viscosities tested has shown that the numerical approach for the aerodynamic breakup of the bulk liquid and the following deposition of the spray cloud obtains the desired pattern of concentrations at ground level. Although the methodology for dealing with the complex process of liquid breakup is specifically suited for fluids exhibiting Newtonian behaviour, apparently the model is capable of numerically describing the phenomena occurring on a simplified basis without prejudice to general performance. Nevertheless, the considered FT products are known to be non-elastic in nature. The simulations for the Marana tests will allow the evaluation of the accuracy of the results with a viscoelastic product.

5.3.2. Marana 2005

Systematic real scale drop tests have been conducted since the 1970's by the USDA-FS with the main purpose of comparing ground deposition response to changes in retardant rheology. The specific data used in this work was obtained in October 2005 at the Marana desert, Arizona, in the US. The grid has 613x105 m^2, with a maximum resolution of 4.6x4.6 m^2. The aircraft used was the CDF S2F-T (see Figure 5-21) also, with a dropping system similar to the one that was tested in Marseille, except that it carries approximately 4500 l and has a constant flow gating system, with two doors that control flow rate and volume released [G. Lovellette, pers. communication]. Contrarily to Marseille tests in which no flow rate values were available (requiring its calculation with the discharge module), reliable data on instantaneous flow rate (IFR) was collected in flight from an on-board data acquisition system. IFR represents the volume difference of adjacent measurements divided by the time separation. Drop height and speed were registered by GPS and photo analysis. Under the scope of the present analysis the following products were considered: water, PC-LV, PC-MV and PC-HV. Fluid density and viscosity were measured in tank samples and in the cups.

Figure 5-21. Water dropping with the CDF S2F-T aircraft tested in Marana.

Table 5-16 presents the input data for the simulation: product characteristics, flight parameters and meteorological conditions. The drops are ordered by increasing viscosity.

Table 5-16. Drop parameters for the Marana 2005 drop tests.

Product	Drop number	Viscosity (cP)	Density ($kg.m^{-3}$)	Volume (m^3)	Average flow rate ($m^3.s^{-1}$)	Drop height (m)	Drop speed ($m.s^{-1}$)	Wind velocity ($m.s^{-1}$)	Wind direction (º)
water	**M128**	1	1000	4.60	1.22	59.44	68.42	2.68	210
	M134	1	1000	4.64	2.04	60.66	67.90	2.68	135
	M183	1	1000	4.59	2.11	88.09	66.36	1.79	130
LV	**M114**	152	1033	4.57	1.15	72.54	69.44	2.68	120
	M112	214	1032	4.60	2.08	37.19	63.79	2.68	120
MV	**M120**	700	1052	4.62	2.23	57.91	70.99	1.79	210
	M110	750	1051	4.62	2.12	54.86	65.84	2.68	125
	M109	800	1055	4.55	1.18	65.84	65.84	3.58	110
HV	**M119**	1250	1078	4.59	1.17	59.44	66.87	0.89	0
	M117	1300	1075	4.63	2.05	77.72	70.99	0.45	20
	M118	1300	1075	4.64	2.12	60.96	66.36	0.89	50

Based on these data, drops were categorized according to the criteria presented in Table 5-17. As can be seen, data are widespread along the different product viscosities, drop heights and meteorological conditions, although a tendency for right crosswind drops is noticeable. Comparing to Marseille, and following the usual procedure at the US, the product was released from much higher altitudes, exceeding the 70 m in three cases; two of them, curiously, using water and a low viscosity product.

Table 5-17. Classification of Marana drop trials based on the predefined criteria.

Drop number	Viscosity				Drop height			Wind velocity				Relative wind direction			
	No viscosity	Low	Medium	High	Low	Medium	High	Calm	Light air	Light breeze	Gentle breeze	Headwind	Left crosswind	Tailwind	Right crosswind
M128	•					•				•		•			
M134	•					•				•		•			
M183	•						•			•					•
M114		•					•			•					•
M112		•			•					•					•
M120			•			•				•		•			
M110			•			•				•					•
M109			•			•					•				•
M119				•		•			•				•		
M117				•			•		•				•		
M118				•		•			•						•

The ground pattern contours for each of the study cases are given in Figure 5-22 to Figure 5-32. The gpc concentration unit used by the USDA-FS in the experiments was retained in order to facilitate the comparison with data from literature. As in Marseille, the position of the aircraft relating the grid at the moment of release was not registered and, therefore, the location of the pattern given by cup measurement and model is again not comparable.

The contours obtained for water dropping are represented in Figure 5-22 to Figure 5-24. In general, the model captures the main aspects that influence the final ground pattern. There is, however, an underestimation tendency on the line length for the first coverage level (i.e., concentration values above 0.75 gpc) that, as expected, influences also the accuracy on the estimation of the area occupied by this concentration class range.

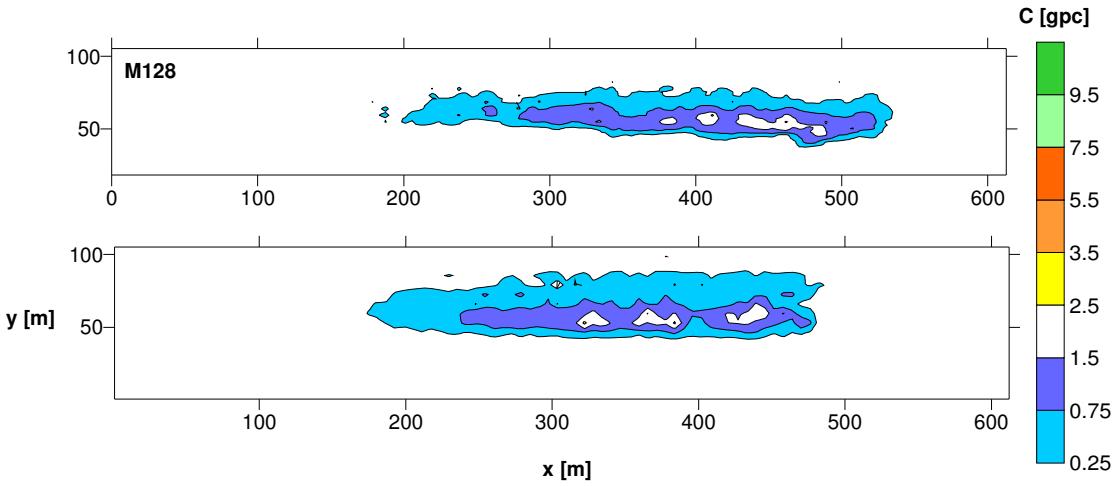

Figure 5-22. Comparison between the measured (up image) and simulated (down image) ground patterns of product concentration for the Marana 2005 drop test M128: water, medium height drop, light breeze, headwind.

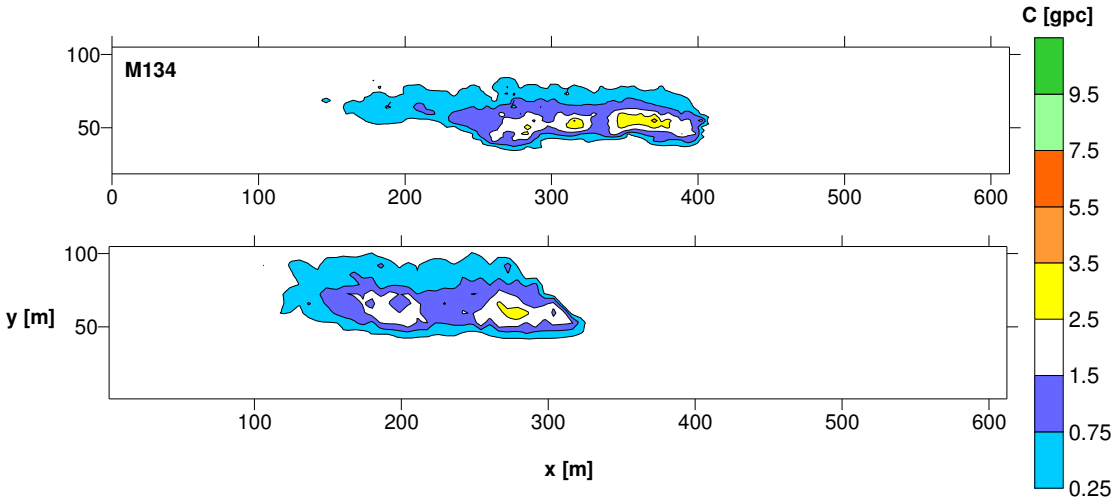

Figure 5-23. Comparison between the measured (up image) and simulated (down image) ground patterns of product concentration for the Marana 2005 drop test M134: water, medium height drop, light breeze, headwind.

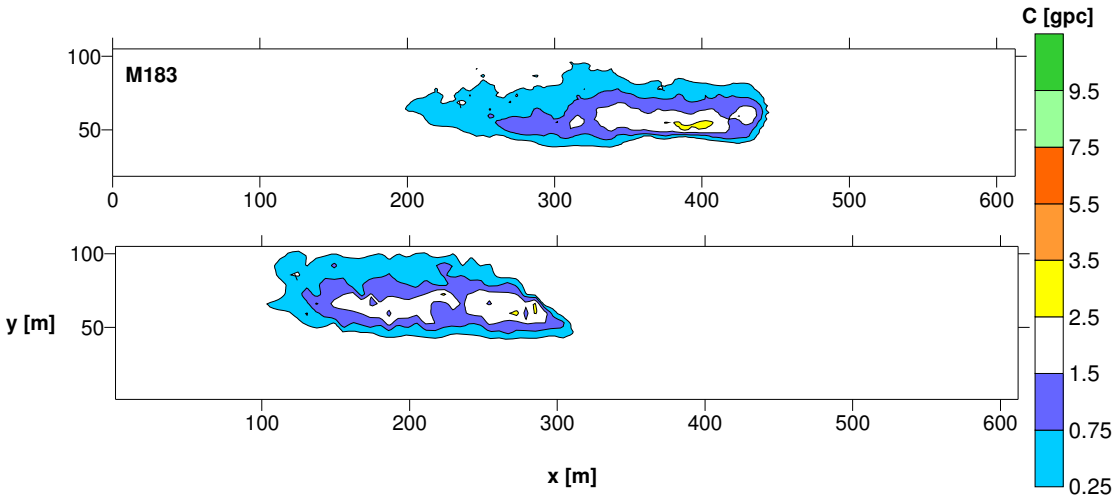

Figure 5-24. Comparison between the measured (up image) and simulated (down image) ground patterns of product concentration for the Marana 2005 drop test M183: water, high drop, light breeze, right crosswind.

The spatial distribution of concentrations at ground for the low viscosity PC products is given in Figure 5-25 and Figure 5-26. There is an acceptable agreement between modelled and measured contours, although the tendency for ADM to underestimate the line lengths for the lower coverage levels, i.e., for values lower than 1.5 gpc, is maintained. As a result of the lower drop height, case M112 is characterised by a much higher maximum concentration, reaching the highest coverage level. This wide distribution of product across all the levels is present also in the modelling results, although ADM tends to under-predict the area occupied, which leads to an increased error when compared to measurements (as will be seen in Table 5-20).

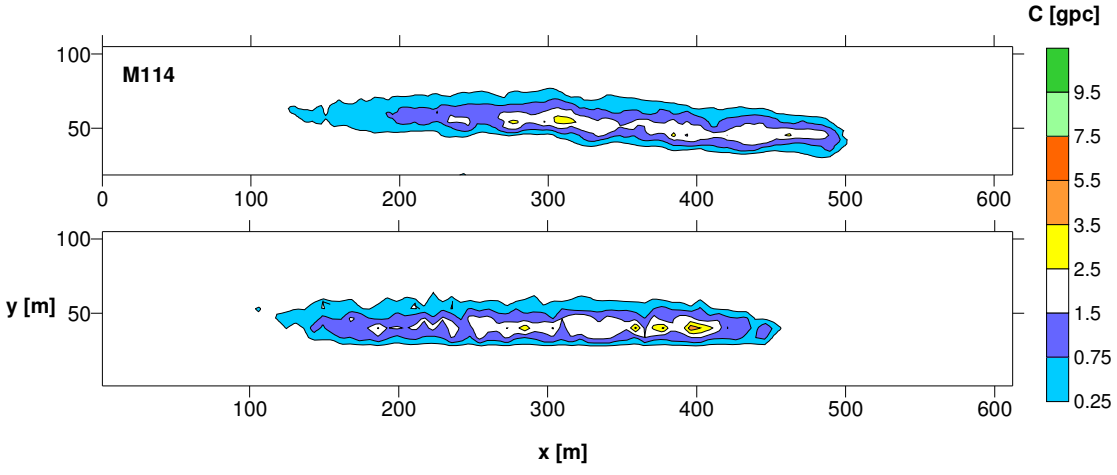

Figure 5-25. Comparison between the measured (up image) and simulated (down image) ground patterns of product concentration for the Marana 2005 drop test M114: low viscosity, high drop, light breeze, right crosswind.

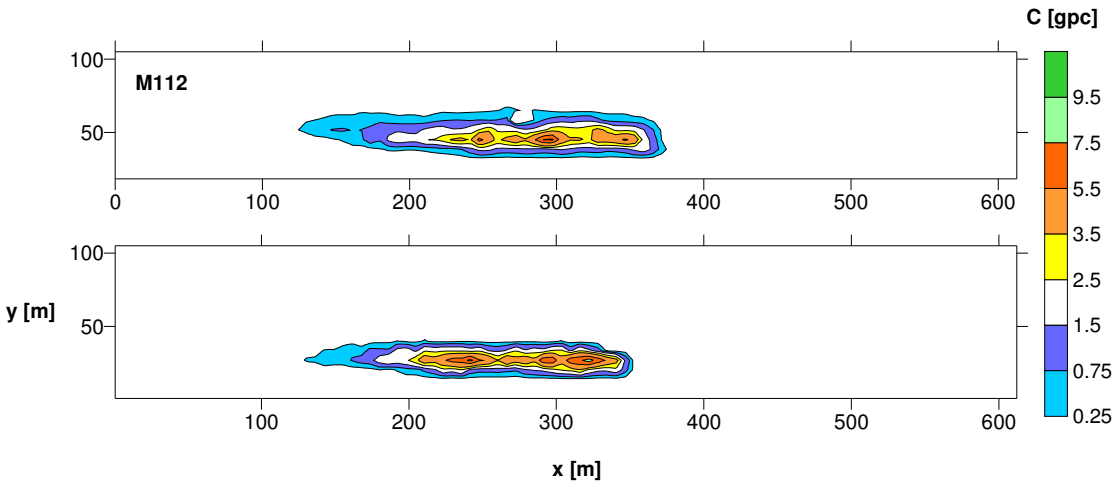

Figure 5-26. Comparison between the measured (up image) and simulated (down image) ground patterns of product concentration for the Marana 2005 drop test M112: low viscosity, low drop, light breeze, right crosswind.

The results for medium viscosity products are shown in Figure 5-27 to Figure 5-29. In general, the model provided an acceptable performance in dealing with the conditions simulated.

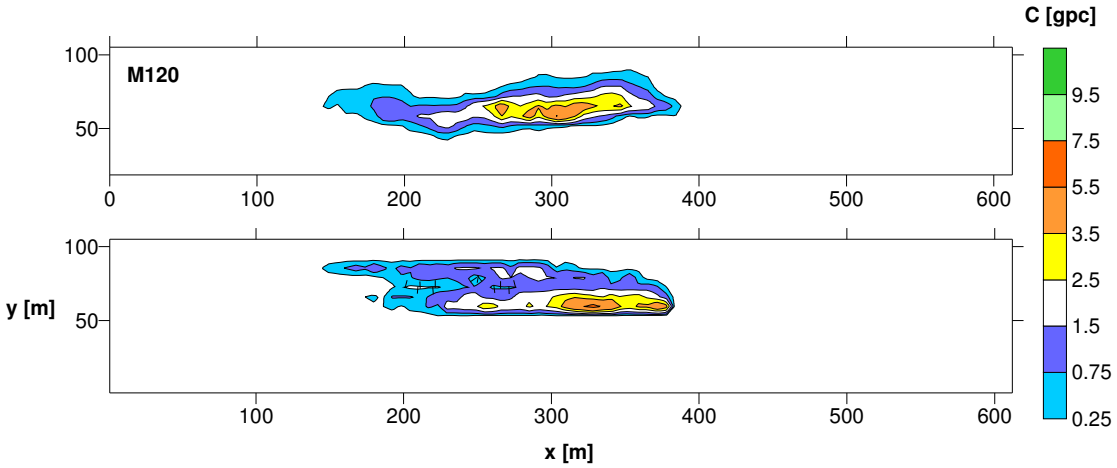

Figure 5-27. Comparison between the measured (up image) and simulated (down image) ground patterns of product concentration for the Marana 2005 drop test M120: medium viscosity, medium height drop, light breeze, headwind.

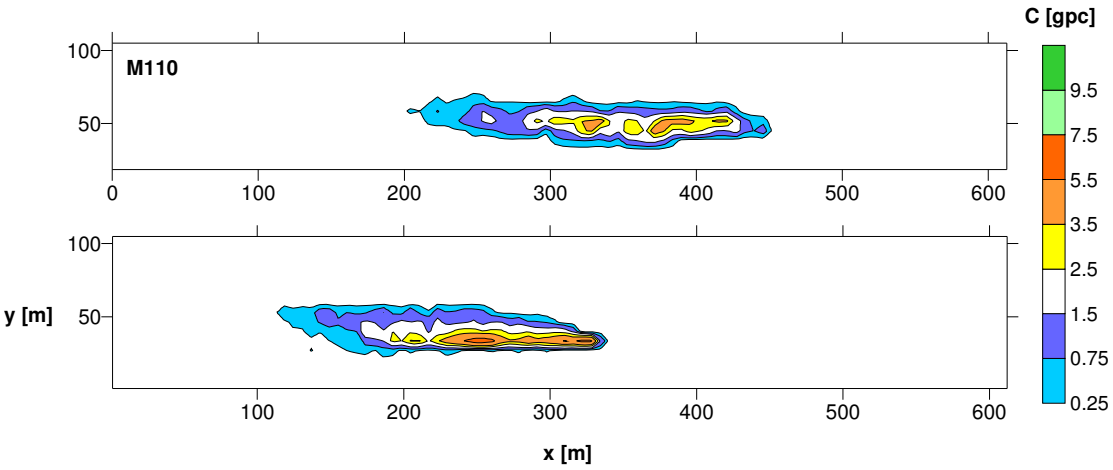

Figure 5-28. Comparison between the measured (up image) and simulated (down image) ground patterns of product concentration for the Marana 2005 drop test M110: medium viscosity, medium height drop, light breeze, right crosswind.

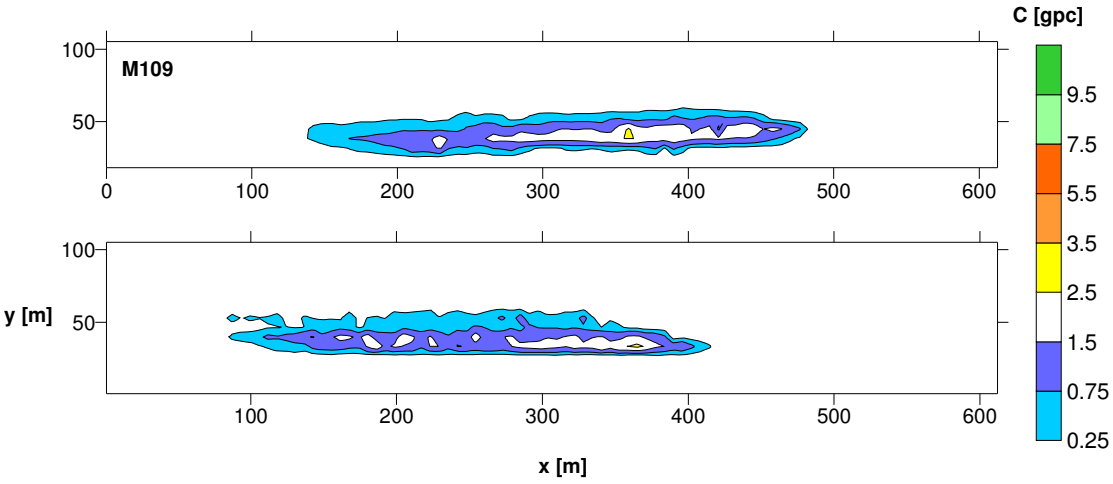

Figure 5-29. Comparison between the measured (up image) and simulated (down image) ground patterns of product concentration for the Marana 2005 drop test M109: medium viscosity, medium height drop, gentle breeze, right crosswind.

Finally, Figure 5-30 to Figure 5-32 show the model outputs in comparison to measurements for the higher viscosity trials. There is, in general, a good agreement between the shape of the patterns for each considered contour level.

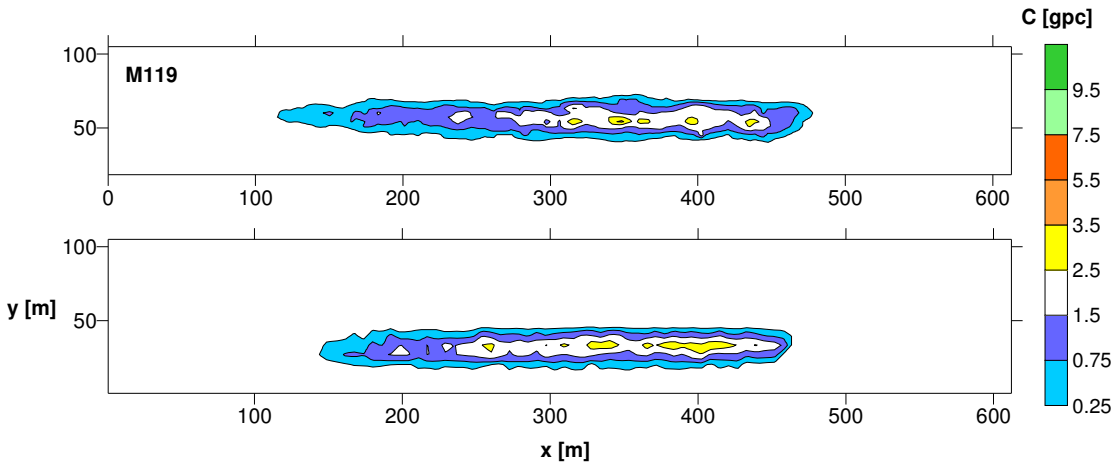

Figure 5-30. Comparison between the measured (up image) and simulated (down image) ground patterns of product concentration for the Marana 2005 drop test M119: high viscosity, medium height drop, light air, left crosswind.

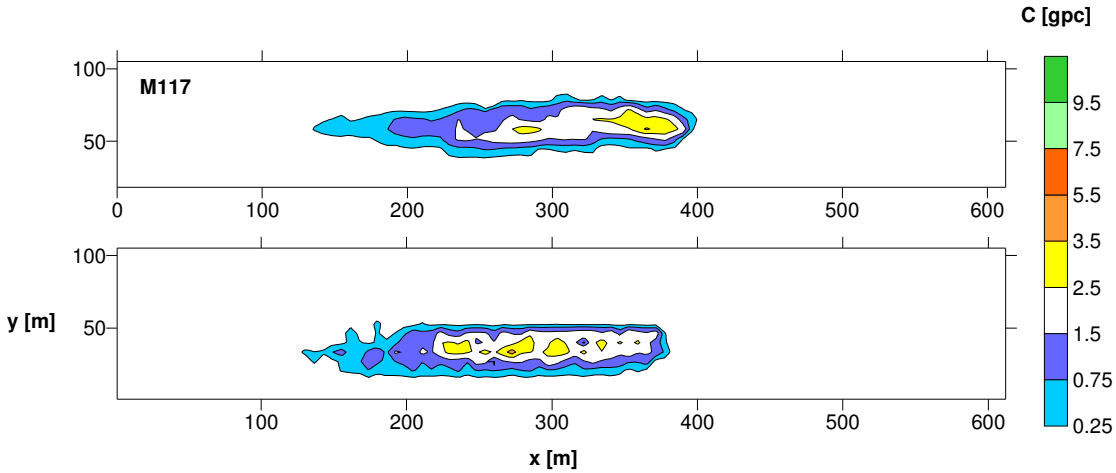

Figure 5-31. Comparison between the measured (up image) and simulated (down image) ground patterns of product concentration for the Marana 2005 drop test M117: high viscosity, high drop, light air, left crosswind.

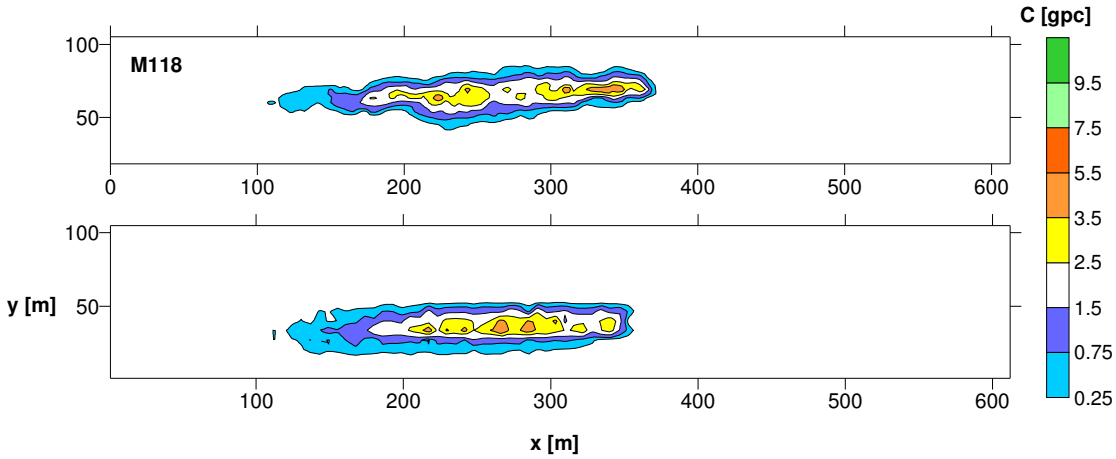

Figure 5-32. Comparison between the measured (up image) and simulated (down image) ground patterns of product concentration for the Marana 2005 drop test M118: high viscosity, medium height drop, light air, right crosswind.

In Table 5-18 and Table 5-19, the validation metrics for the intercomparison between the modelled and measured line lengths are presented. There is some fluctuation in the NMSE value, although a relation with viscosity is not obvious. Nevertheless, all the NMSE values are clearly within the expected accuracy. As pointed out in the analysis of the ground pattern contours, there is a tendency of the model to underestimate the line length values for low viscosity products, and the contrary occurs for medium viscosity retardants. For higher viscosities there is not a definite trend in the results.

Table 5-18. Statistical analysis of the ADM results for line lengths per coverage level in comparison with the experimental data for the Marana 2005 drop tests.

Product	Drop number	*NMSE*	*r*	*d* (m)	*MG* (m)	*VG* (m^2)	*FB*	*FAC2*
Water	**M128**	0.012	0.993	0.381	0.92	1.02	0.002	1.000
	M134	0.024	0.990	12.375	1.79	3.25	0.102	0.800
	M183	0.020	0.972	3.658	1.05	1.03	0.026	1.000
LV	**M114**	0.005	0.998	9.144	0.99	1.01	0.039	1.000
	M112	0.029	0.984	5.639	1.55	3.94	0.047	0.875
MV	**M120**	0.013	0.987	-4.115	1.04	1.05	-0.029	1.000
	M110	0.005	0.999	-9.144	0.68	1.89	-0.063	0.833
	M109	0.004	0.998	-3.414	1.92	9.22	-0.018	0.800
HV	**M119**	0.020	0.981	-2.804	1.06	1.21	-0.014	0.800
	M117	0.003	0.993	-1.000	0.98	1.00	-0.002	1.000
	M118	0.027	0.990	20.117	1.09	1.07	0.119	1.000

Table 5-19 presents the mean statistical metrics for the entire datasets of measured and simulated values.

Table 5-19. Statistical metrics of line lengths per coverage level for the overall Marana 2005 drop tests.

Data	μ (m)	σ (m)	*NMSE*	*r*	*d* (m)	*MG* (m)	*VG* (m^2)	*FB*	*FAC2*
Measured	161.86	107.79	0.000	1.000	0.00	1.00	1.00	0.000	1.000
ADM	159.22	102.01	0.010	0.986	2.65	1.16	1.82	0.017	0.911

The modelling outputs were also statistically evaluated in terms of the area occupied by each coverage level. The results are presented in Table 5-20. Although the good correlation between model and measurement is maintained, there is an increase of the NMSE, in particular for the low viscosity drops in which, in accordance to the line lengths analysis, an underestimation tendency is noticeable. Nevertheless, the results clearly fulfil the requirements imposed by the model acceptance criteria.

Table 5-20. Statistical analysis of the ADM results of area per coverage level in comparison with the experimental data for the Marana 2005 drop tests.

Product	Drop number	*NMSE*	*r*	*d* (m^2)	*MG* (m^2)	*VG* (m^4)	*FB*	*FAC2*
water	**M128**	0.008	0.999	-66.98	0.96	1.03	-0.022	1.000
	M134	0.006	0.999	169.72	1.91	2.53	0.067	0.600
	M183	0.063	0.999	588.7	1.41	1.18	0.182	1.000
LV	**M114**	0.035	0.994	307.11	0.98	1.02	0.077	1.000
	M112	0.392	0.980	477.07	1.33	1.71	0.310	0.750
MV	**M120**	0.030	0.990	-243.28	0.99	1.04	-0.102	1.000
	M110	0.014	0.997	5.84	0.72	3.36	0.003	0.833
	M109	0.018	0.998	-164.72	1.52	2.71	-0.058	0.800
HV	**M119**	0.058	0.998	353.35	0.84	1.20	0.124	0.800
	M117	0.007	0.998	-124.51	1.04	1.11	-0.041	1.000
	M118	0.009	0.998	92.64	1.00	1.01	0.033	1.000

The statistical metrics for the entire dataset are presented in Table 5-21. Comparing with the values shown in Table 5-19 there is, in fact, an increase in the error, resulting from the referred under-prediction. Nevertheless, nearly 90% of the results, a value similar to the one obtained in the line length validation (see Table 5-19), are within a factor of two of observations.

Table 5-21. Statistical metrics of areas per coverage level for the overall Marana 2005 drop tests.

Data	μ (m^2)	σ (m^2)	*NMSE*	*r*	*d* (m^2)	*MG* (m^2)	*VG* (m^4)	*FB*	*FAC2*
Measured	2717.1	2713.6	0.000	1.000	0.00	1.00	1.00	0.000	1.000
ADM	2588.3	2587.2	0.040	0.981	128.77	1.11	1.52	0.049	0.877

The comparison between modelled and measured line lengths per coverage level is shown in Figure 5-33. An overall tendency of ADM to keep within the expected 10% of percentage error is observed.

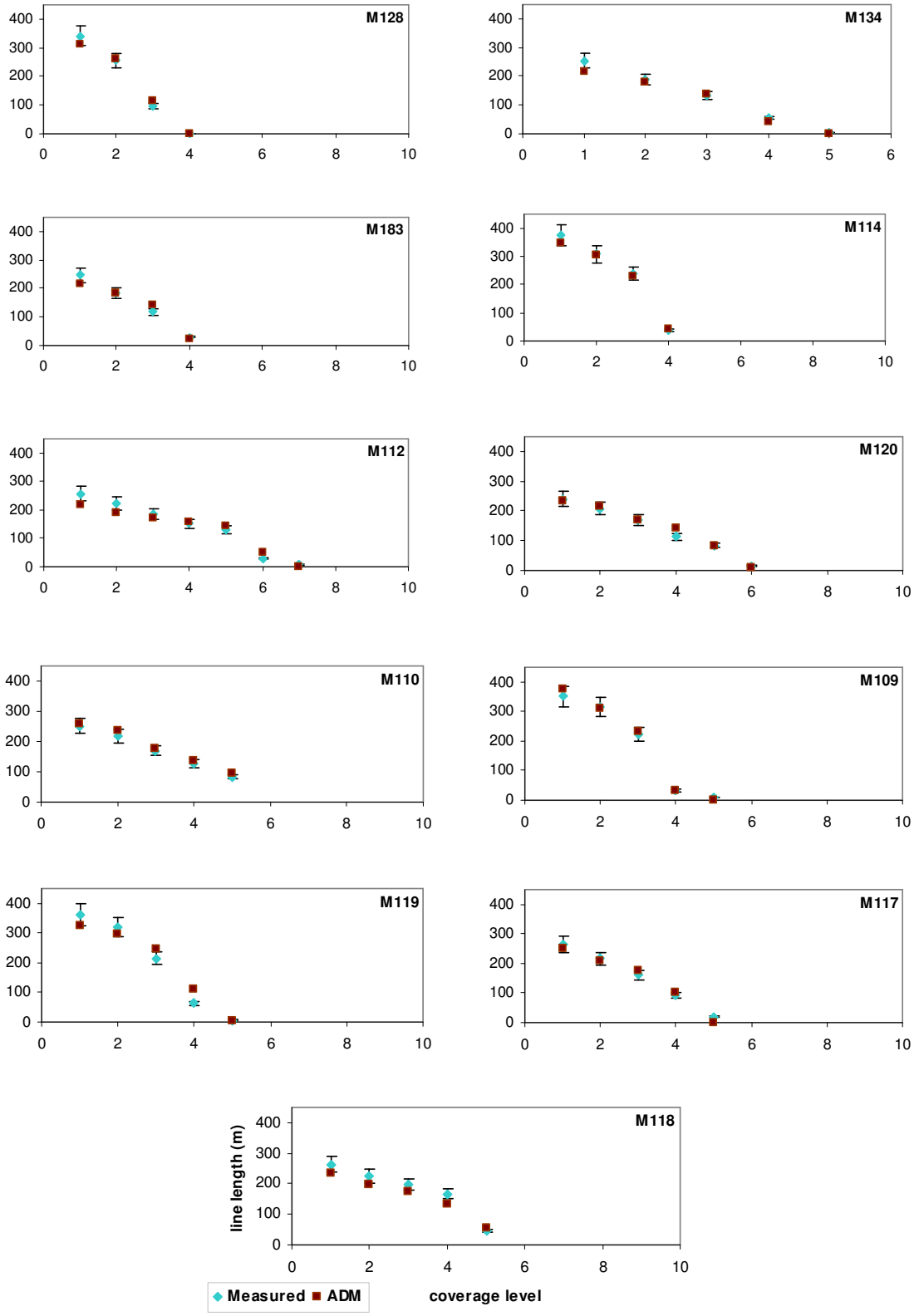

Figure 5-33. Comparison between modelled and measured line lengths per coverage level for the Marana drops. The represented coverage levels are: 0.25, 0.75, 1.5, 2.5, 3.5, 5.5, 7.5 and 9.5 gpc.

As it was shown, there is in general a good compromise between computed and experimental for the entire range of coverage levels, and contrarily to Marseille drops there is not an underestimation of line length values for mid levels. The good correlation between measured and simulated values for the wide range of viscosities is evidenced in Figure 5-34, although some few exceptions.

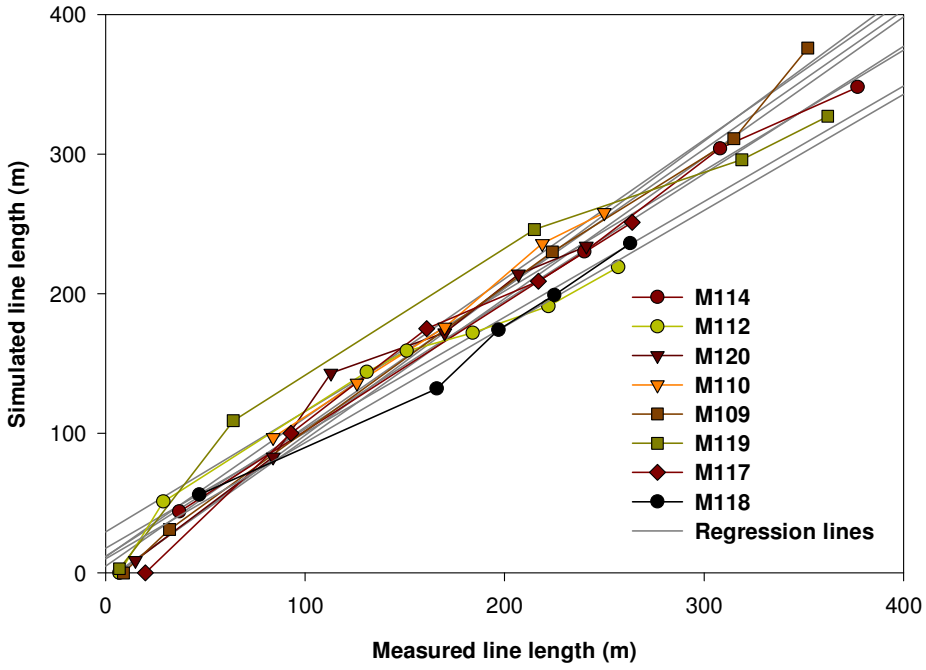

Figure 5-34. Regression analysis of the measured and simulated line lengths for the Marana drops.

The same procedure tested in Marseille drops for the validation of the simulated distribution of total volume along the *x*-axis of the grid was also applied in the analysis of Marana results. In this case, as the grid is in ft^2 and the measured concentration values are in gpc, the irregular grid was converted to a regular one in m^2 using the Kriging interpolation scheme and the volumes deposited in each new cell were converted to litres in order to be comparable with the results obtained for the Marseille cases. V_x results are given in Figure 5-35. As expected, the distributions are almost symmetric in the majority of the drops, although with some right-skewness that results from the time taken for the flow rate of the outflow from the tank to attain the maximum (and nearly constant) value, typical of constant flow delivery systems. The total length of the ground patterns is considerably higher than in Marseille because of the higher volume of product dropped and the approximately constant flow rate at the exit (longer dropping times). By comparison with the measured values the agreement can be considered very good, stressing the importance of having a detailed knowledge of the flow rate variation with time. Again,

there is some tendency of ADM to underestimate the peak value of V_x, that varies between 4% of the maximum volume in M114 and 18% in M110 (12% in average).

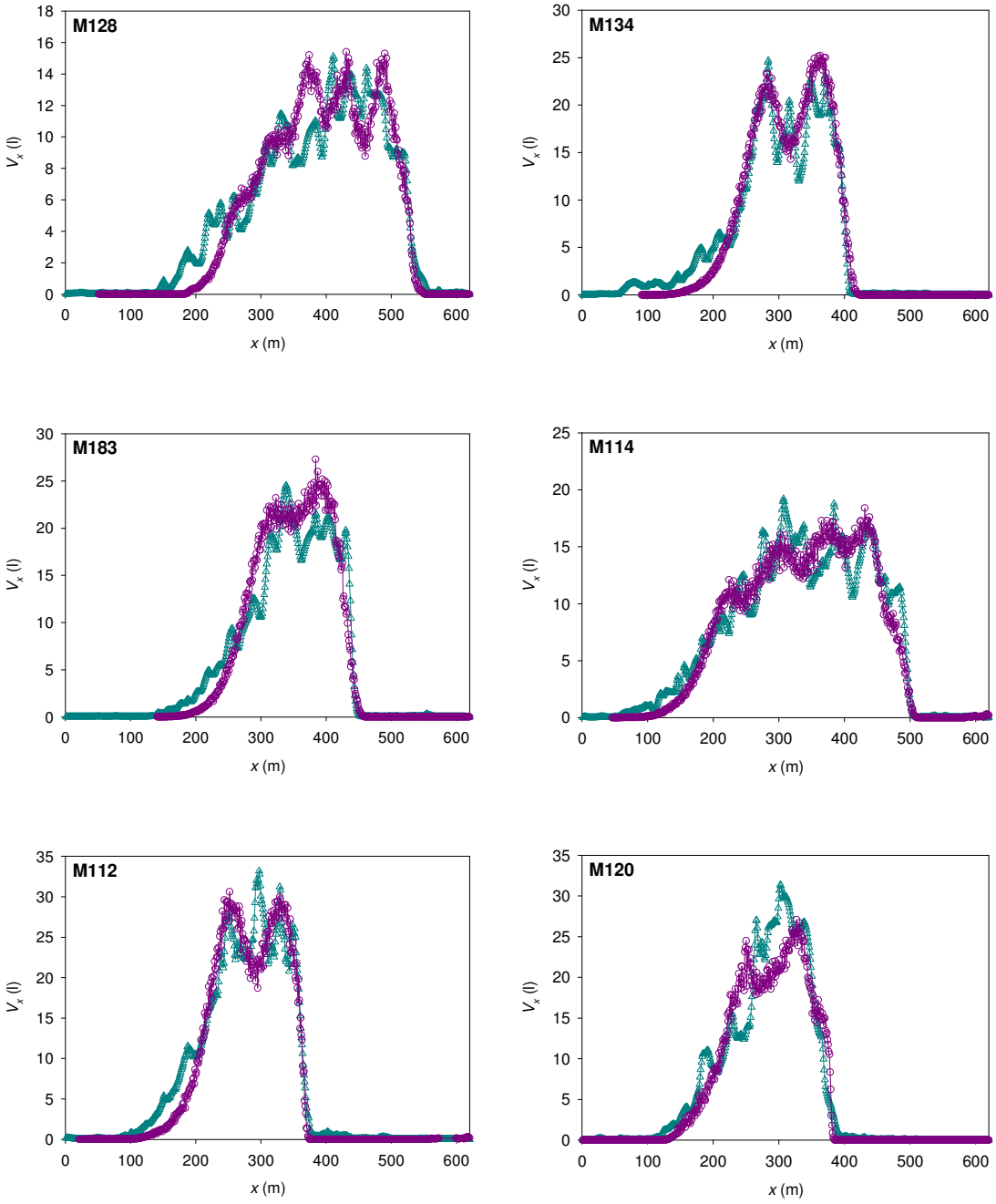

Figure 5-35. Comparison between modelled and measured values of deposited volume along the *x*-axis for the Marana drops.

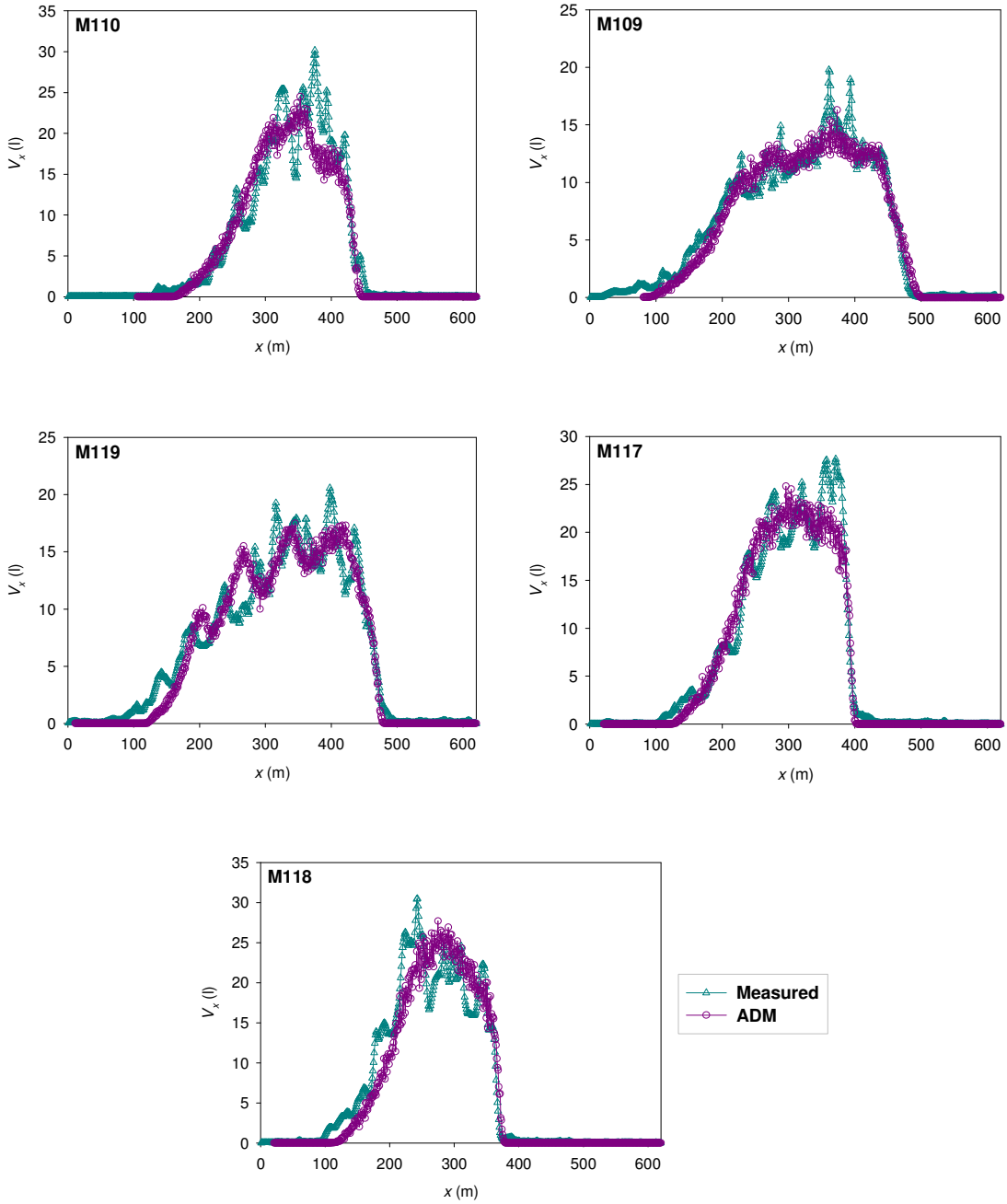

Figure 5-35 (cont.). Comparison between modelled and measured values of deposited volume along the *x*-axis for the Marana drops.

Benefiting from the knowledge of flow rate values there is an increase in the accuracy of the simulations. The difficulty found in having a good estimate of the maximum value of V_x in Marseille decreases in importance with the higher symmetry that characterises the distribution of deposited volumes along the *x*-axis in Marana drops. Nevertheless, in both cases the modelled results are, in general, very close to the measured values.

5.4. Additional analysis

In Figure 5-36, the *NMSE* of the modelled line lengths and areas of each coverage level are presented. The quality of modelling performance on predicting the length of each contour class shows no strong relation with the corresponding viscosity, although better results were obtained in the range from 700 to 1100 cP. Except for one case, there is a decreasing tendency of the *NMSE* of the simulated contour areas with the increasing viscosity.

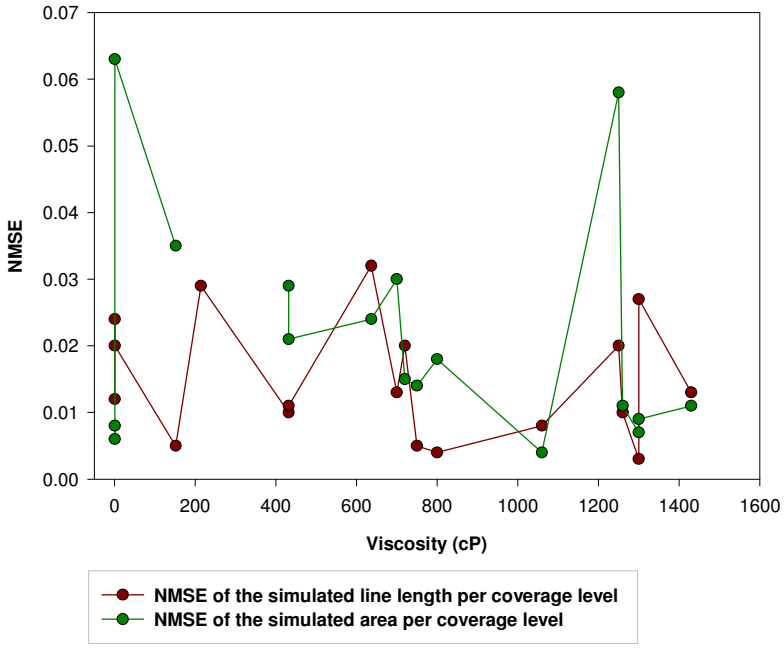

Figure 5-36. *NMSE* of the simulated length and area for each ground coverage level, considering the entire range of viscosities tested. The higher *NMSE* of the simulated area for the M112 drop (214 cP) was omitted in order to allow an easier interpretation of results. Note that three distinct products (water, FT931 and PC-XA) are represented, thus requiring some care in the analysis.

The statistical validation has shown that, in general, the results are in good agreement with observations. This conclusion is particularly important given the wide range of input conditions and the difficulty in simulating the complex dynamical behaviour of retardants in the atmosphere while maintaining the operational characteristics of the model. The good performance of ADM can also be inferred from the visual analysis of the shape of the spray cloud. As an example, Figure 5-37 graphically represents the position of droplets in the 3D space 3 s after the opening of the tank doors in the S6L3 drop. The cloud has the typical shape found in aerial drops of firefighting products (see, for instance, the initial stage in Figure 3-1). The frontal region is the jet column, which is deformed and deflected as shown in the figure as a response to the balance of drag, inertia, gravity, surface tension and

viscosity. Due to the continuous stripping of liquid ligaments and droplets from the column, there is a second main region, the spray, which has a significantly higher frontal cross section and is characterized by the presence of smaller droplets formed by secondary breakup, which have a lower terminal velocity and thus decrease the overall settling velocity of the cloud in this region as also seen in the 3D representation.

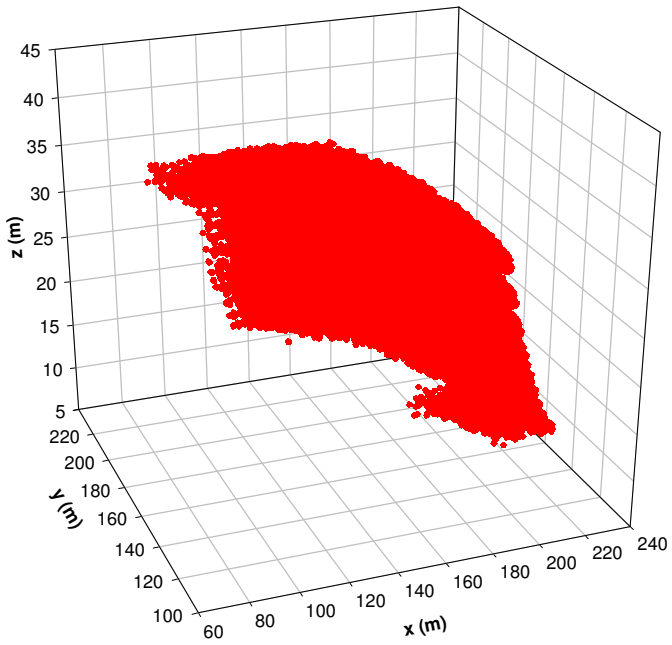

Figure 5-37. 3D position of the total number of 'marker' droplets (more than 1.04×10^5) considered in the calculation at instant t = 3s in the S6L3 drop. During the drop, the aircraft moves along the positive direction of the *x*-axis.

In its entire extension, the aerodynamic breakup of a liquid jet is an unstable process characterised by a succession of complex fluid dynamics phenomena. Due to the action of the airflow, the liquid jet is rapidly transformed into a cascade of fluid structures composed of globs and droplets as previously seen. During the fall, while the horizontal component of the liquid velocity decreases, its vertical counterpart increases due to gravity. Due to the action of the frictional force, droplets will eventually attain their terminal velocity relative to the surrounding atmosphere, unless they first reach the surface. Depending on size, droplets exhibit distinct behaviours during free-fall. The smaller ones have lower terminal velocities and are easily drifted by the action of wind. On the contrary, the horizontal distance travelled by larger droplets prior to being intercepted by the canopy or deposited at ground is mainly a result of their inertia. Moreover, due to the time needed for complete exit of the fluid from the aircraft tank and also to the distinct time needed for droplets to complete breakup, while some droplets are contacting with the surface others are still

undergoing (secondary) breakup. These mechanisms lead to size sorting, i.e., larger droplets tend to reach the surface earlier than smaller drops. The different behaviours are shown in Figure 5-38, in which the trajectories of a number of random droplets are represented for a typical drop.

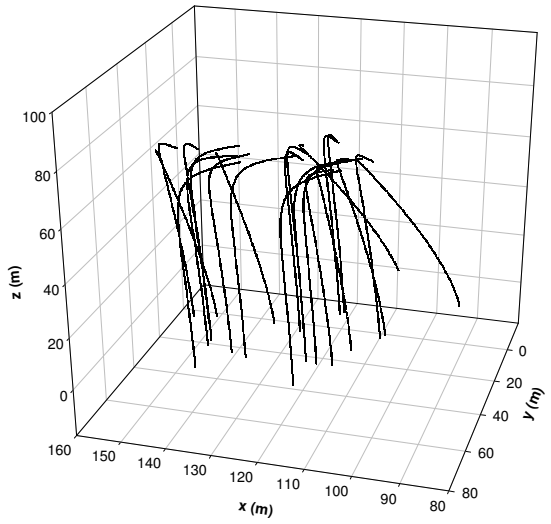

Figure 5-38. Trajectories of a number of droplets randomly selected from the S6L3 simulation.

The effect of the distinct inertia of the wide range of droplet diameters on the overall motion of the spray cloud is clearly seen in Figure 5-39. The figure shows the total 'real' number of droplets, i.e., the sum of droplets represented by each 'marker' according to Eq. 4-74). The arithmetic mean diameter was calculated individually for each computational cell (in the *xy* plane, with $z = 0$). It is shown that the response of droplets to the dynamics of breakup, and also to the velocity field that develops in the surface layer, leads to a selective dispersion of the droplets across this layer and to size sorting at ground surface. In this image, diameters that can go up to 10 mm are found at the front of the pattern. Similar range of sizes was found by the experimental analysis of Van Meter and George [1981] and the real scale measurements of Schönhuber e al. [2005]. This region is essentially constituted by droplets formed in the jet due to RT instabilities (and subsequent secondary breakup), which is in agreement with the conclusion taken by Andersen et al. [1974b] that the breakup due to RT waves is the determining factor on the effective ground pattern. On the tail of the pattern the smaller products from the secondary breakup process can be found, conjointly with droplets produced by the effect of KH waves on the jet surface (although these are extremely sensitive to wind flow conditions, and thus are easily drifted out from the grid).

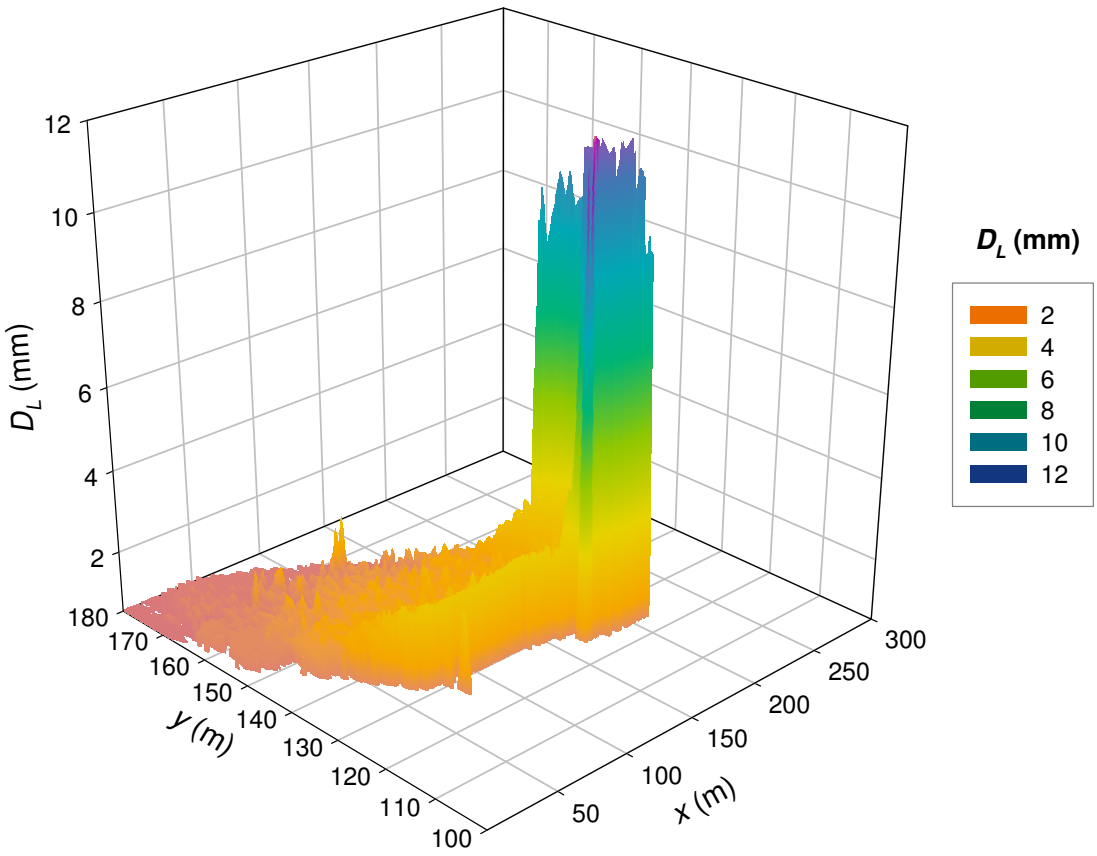

Figure 5-39. Mean diameter distribution of droplets at ground in the S6L3 drop.

The distribution of diameters at ground is not directly related to the distribution of the actual number of droplets deposited, given in Figure 5-40. Except for the lower number in the tail (which represents approximately 30% of the total length) there is a nearly homogeneous spread of droplets across the pattern. Due to the larger mass contained in larger droplets, these will have, however, a significant importance on the concentration of product at ground, causing the accumulation of product along the central axis of the pattern and at the front, as seen in Figure 5-15.

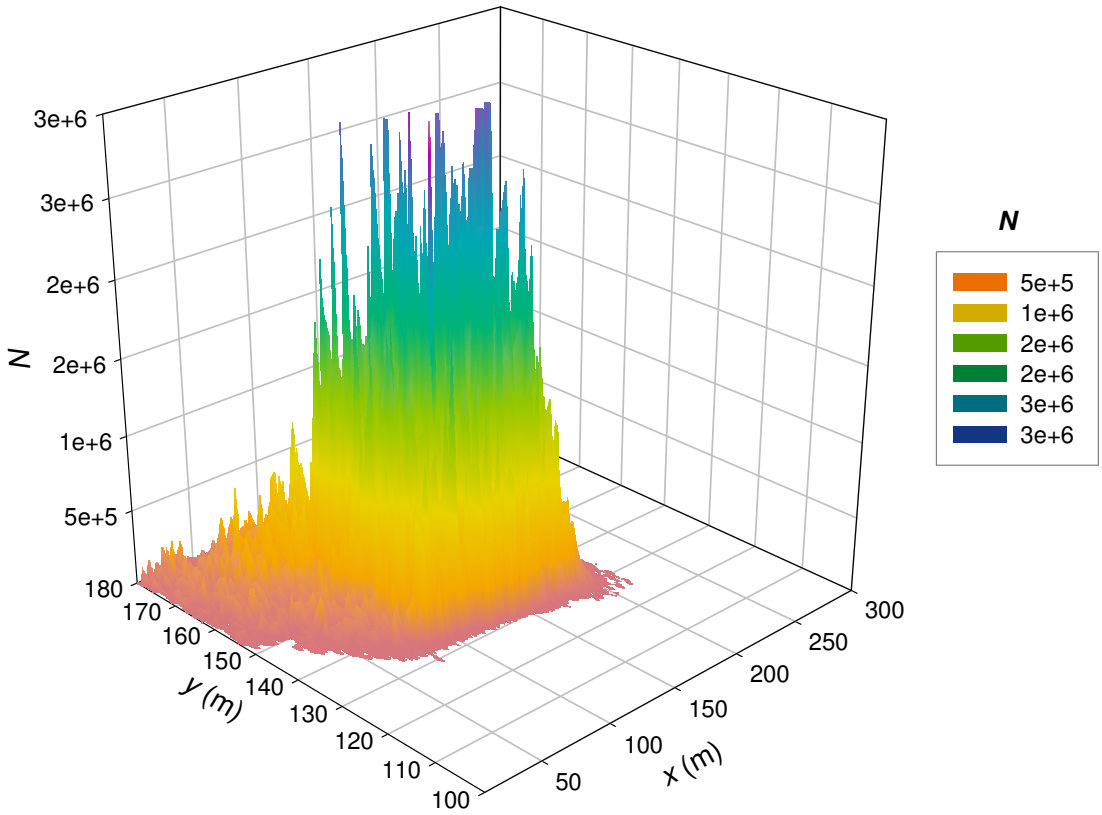

Figure 5-40. Number distribution of droplets at ground in the S6L3 drop.

These results agree with the conclusions from previous studies (e.g. Andersen et al. [1974b]) in that although the relative importance of small particles influences the drifting of the cloud the resulting ground concentration from wind stripping action promoted by KH instabilities is generally much smaller and not a meaningful part of the ground pattern. The importance of these mechanisms is, however, also dependent on the action of the wind shear. This will be the focus of the next section.

5.5. Canopy-induced airflow effect

With the objective of assessing how the vertical wind shear, particularly under the influence of a vegetative canopy, can potentially affect the trajectories of the individual droplets and the final ground contour of the spray cloud, ADM simulations for S6L3 drop were remade using different input conditions. The first step in the analysis was the definition of the vertical wind profile. This was done by selecting, from the validated profiles of section 5.1, the minimum and maximum values of wind shear, therefore corresponding to the two most extreme situations for the range of conditions studied (as can be seen in Figure 5-4c and Figure 5-5a). In order to keep coherency, the measured wind velocity (6 $m.s^{-1}$) for the S6L3 case was considered to be the velocity at the top of the canopy and the drop height is the height above the canopy top.

The contours obtained for the two situations are given in Figure 5-41. There is, as expected, a notable increase in the length of the pattern as a consequence of the higher relative velocity between the air flow and the liquid. This behaviour is a result of the largest drifting potential of the wind flow associated to the lower diameters of the droplets formed by KH instabilities during primary breakup of the jet and also during the secondary breakup stage.

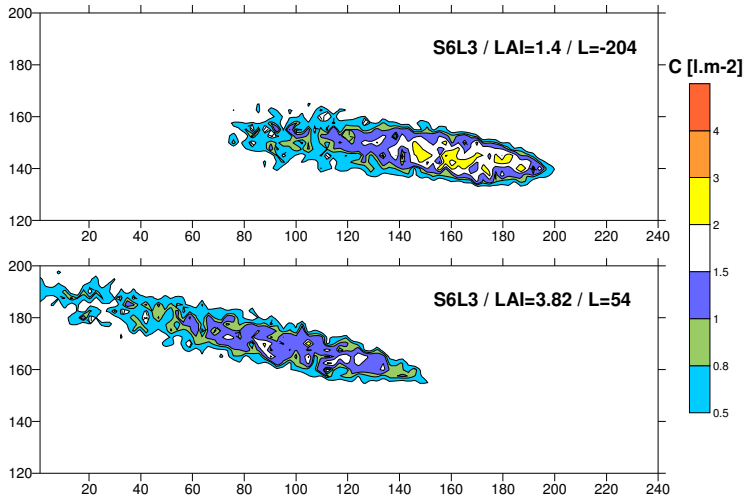

Figure 5-41. Ground pattern comparison for simulated S6L3 drop under variable LAI and atmospheric stability.

The aspects related to the potential drift of droplets under the influence of vegetative canopy-induced wind flows and diabatic atmospheric conditions were further investigated by reducing the problem to the scale of an individual droplet. Instead of analysing the entire volume of liquid dropped, this approach involved the consideration of only five droplets, with diameters between 1 and 5 mm which are

considered representative of the majority of the fluid in the spray cloud. The droplets were injected into the airflow at 30 m high above the canopy top (a typical drop height in Europe), with the following velocity: (u_0, v_0, w_0) = (40, 0, -2) m.s^{-1}. The value for u_0 represents, according to the work by Andersen et al. [1974a], the initial velocity of a droplet after being stripped from the bulk liquid and corresponds to approximately 70% of the aircraft's speed. The value for the vertical component w_0 was defined as the outflow velocity from the aircraft's tank (see section 4.4).

For the windflow, the two profiles used in the analysis shown in Figure 5-41 were again considered, representing two real extreme wind shear situations. Values of 1, 3 and 5 m.s^{-1} were defined for the wind velocity. Also the angle between the wind direction and the retardant injection was varied, in order to represent the conditions of tailwind (0º), headwind (180º) and right crosswind (90º).

The results were then analysed in terms of two parameters. The first, L1, is the difference between the maximum and the minimum horizontal distance travelled by the droplets, which represents the maximum length of the 'pattern'. The second, L2, is the mean value between the minimum and maximum travelled distances, and therefore gives an idea about the deviation of the 'cloud' relating to the release point.

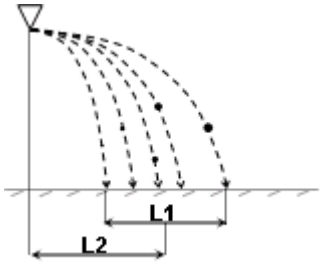

Figure 5-42. Parameters for the analysis of droplet travelled distance.

The values of L1 and L2 in each of the situations are shown in Figure 5-43. The tailwind case (0º) has a distinct behaviour from the others, particularly in the lower LAI (1.4) unstable conditions (L = -204 m). In this case, the maximum 'pattern' length (L1) is obtained for the lower wind velocity (U_h = 1 m.s^{-1}), indicating that for calm winds the trajectory of the droplet is mainly a result of its 'injection' velocity, which prevails over the flow. The length will then suddenly decrease with the increase in U_h to 3 m.s^{-1}. The trend is inverted again for the higher U_h (5 m.s^{-1}). The other profile exhibits a general increasing L1 tendency with the increase of U_h. Depending on wind flow conditions, droplets will behave distinctly depending on their inertia. In both profiles, the mean position of the 'pattern' is increased with U_h, as expected.

The headwind situation (180º), which represents the preferred direction during real drops, exhibits a linear relation for both L1 and L2 with the two profiles, indicating that with opposite winds the length and position of the 'pattern' will increase with U_h. Note, in this case, the strong inflection on trajectory given by the negative L2 values. With crosswinds (90º) the behaviour of the droplets is generally similar to the 180º case, both in the *x* and *y* directions.

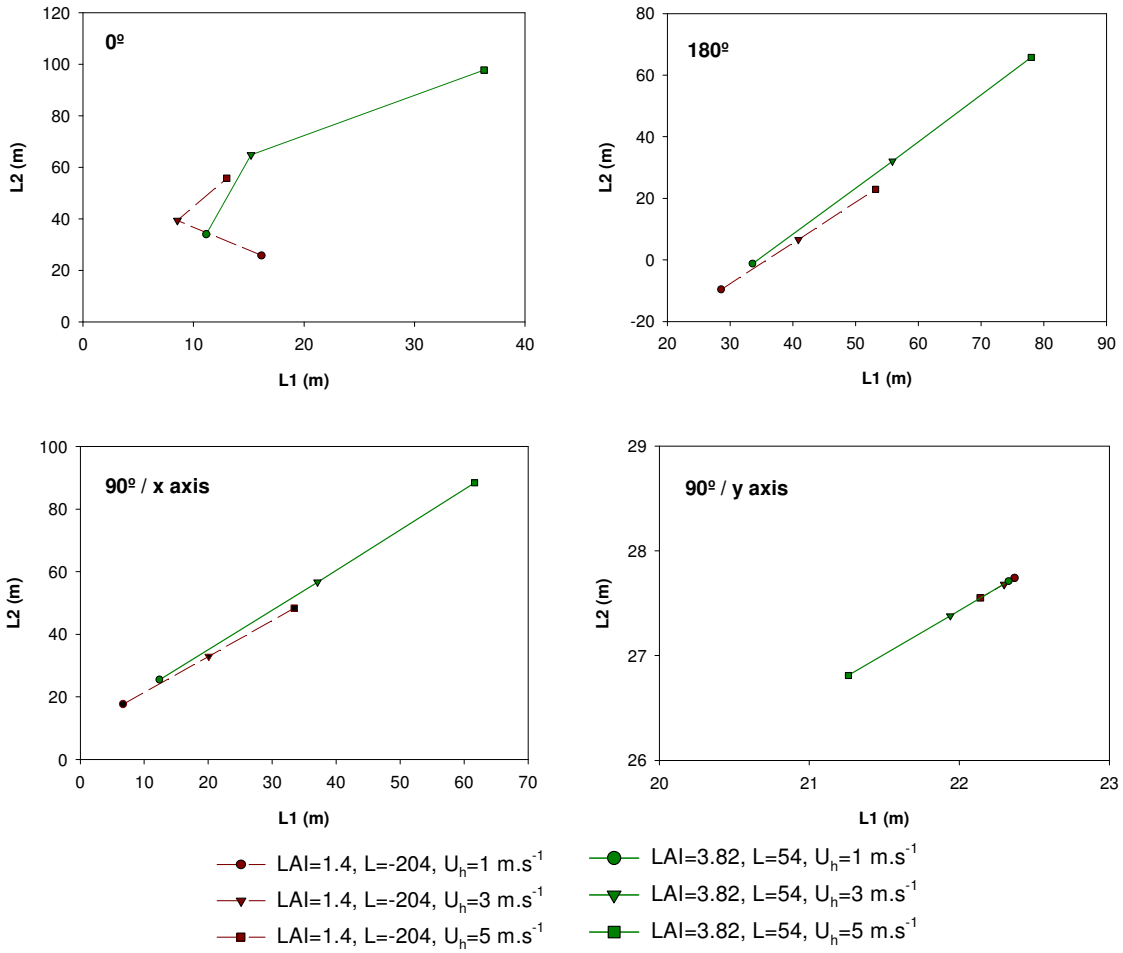

Figure 5-43. Representation of the L1 and L2 parameters in each of the study cases, for 0º, 180º and 90º wind directions.

In order to clarify the distinct behaviour of droplets when facing a wind with the same direction (relating their own velocity), the analysis was extended to two additional profiles analysed on section 5.1: L = -20 m in Duke site (LAI = 3.82, see Figure 5-4a) and L = 47 m in Tumbarumba forest (LAI = 1.4, see Figure 5-5b), which in terms of wind shear represent two intermediate situations when compared to the previously analysed. The results graphically represented in Figure 5-44 agree with the previous interpretation of Figure 5-43.

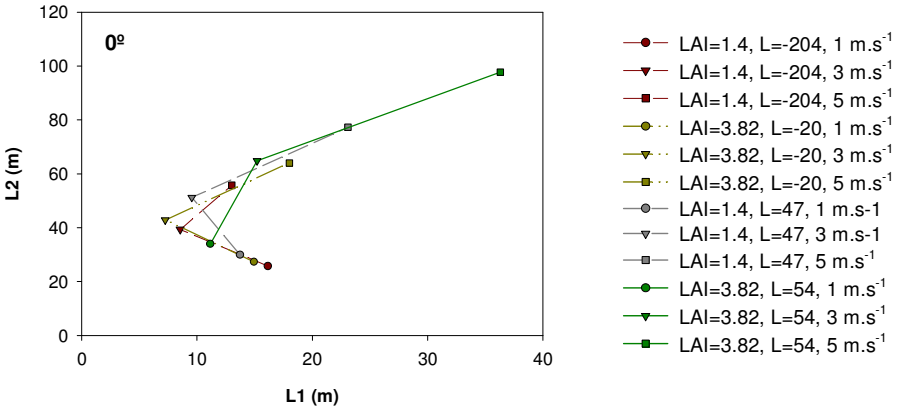

Figure 5-44. Representation of the L1 and L2 parameters for the 0º situation according to four distinct air flow conditions.

Additionally, the analysis can be focused on the distance travelled per diameter, as presented in Figure 5-45. The effect of wind flow is clearly seen in the tailwind case (0º), where with the increasing of the wind flow speed the horizontal distance travelled by droplets increases, particularly the smaller ones, which are more easily affected in their motion by the airflow. In the presence of a crosswind this behaviour is qualitatively similar. Note that the represented distance indicates the difference between the deposition and injection points (in the *x* axis) and not the effective distance travelled, thus explaining the negative values in the 180º graph. As referred, for lower wind velocities the highest distances are travelled by coarsen droplets (due to the 'injection' velocity), situation that is inverted with the increase on wind speed.

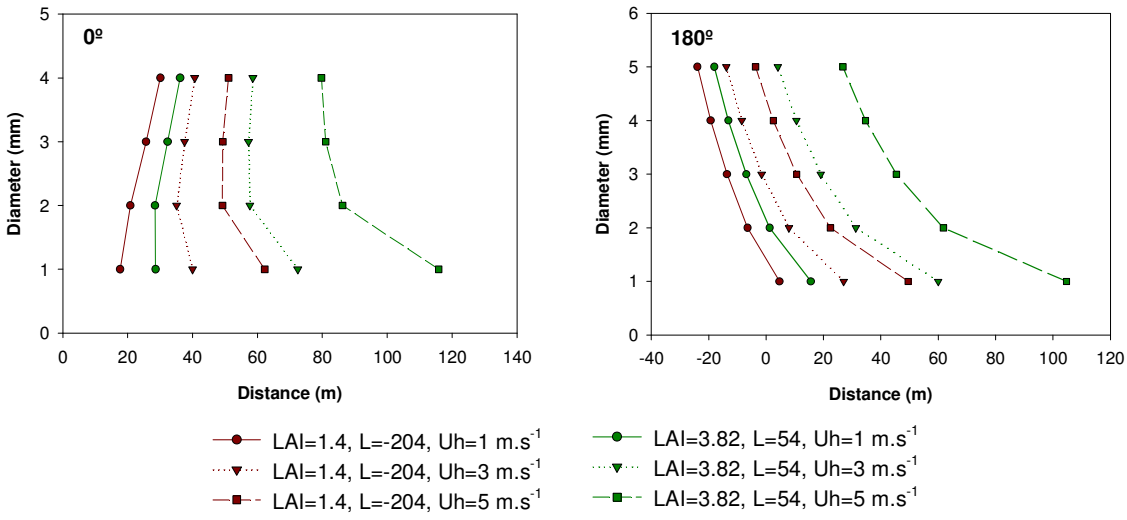

Figure 5-45. Distance travelled by each particle from its original position with different wind velocities and wind directions of 0º and 180º.

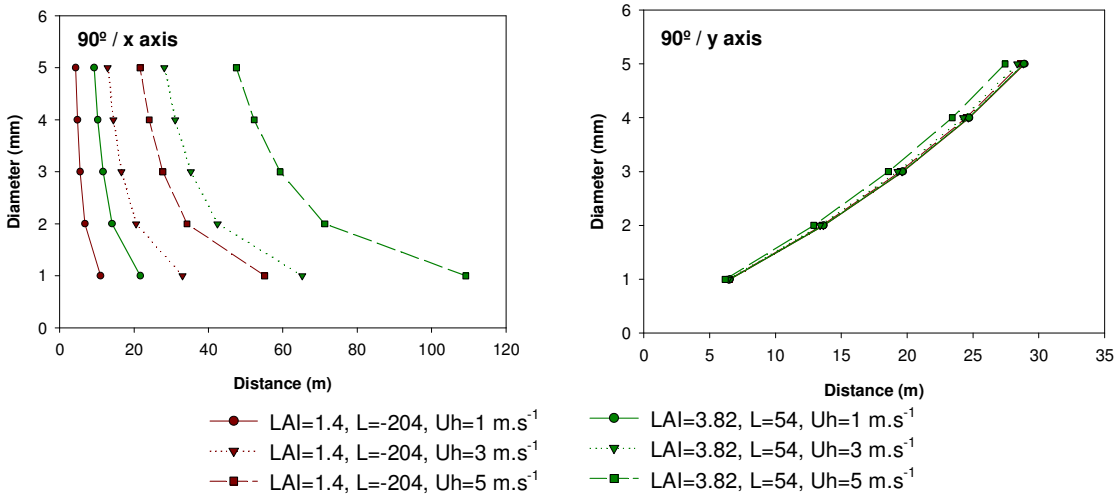

Figure 5-46.). Distance travelled by each particle from its original position with different wind velocities and wind direction of 90º.

The main conclusion from this analysis is that there is, in fact, a distinct effect of the vertical wind stress on the trajectories of the free-falling droplets depending on the diameter and on the air flow conditions, the latter varying with the canopy structure (given by LAI) and the atmospheric stability.

6. Conclusions

Fires in vegetation, in particular those occurring in the wildland-urban interface, have become a major, continuing and potentially increasing threat to human life and health, to the environment, and to the economic development of communities worldwide. In the five Southern Member States, an average value of nearly 0.5 million hectares were burned between 1980 and 2005 [EC, 2005]. Moreover, nearly 60 million hectares of forests, representing more than 50% of the former EU15 forests, were classified in 2003 as high or medium fire risk areas [EC, 2004].

The growing concern about the trend of forest fires at a global scale has led to a number of international cooperative and interdisciplinary initiatives and research programmes. These have been contributing to improved understanding of fire behaviour and the consequent impacts on ecosystems, biogeochemical cycles, atmosphere, public health and climate, and also to the development of increasingly efficient fire management techniques, involving protection (including early warning), preparedness, prevention (including prescribed burning), emergency response, restoration/rehabilitation and monitoring.

If integrated into a global firefighting strategy, the aerial drop of retardants and water can play a significant role in the overall efficiency of operations and resources in terrain within a wide range of situations. This explains the increasing use of aircraft since the 1960s, especially in the US, Australia and several European countries, and its intervention during the response stage of fire management, but also in prevention and preparedness activities.

Since on-board systems for computer-assisted drops have not yet been used operationally, the efficiency of aerial means is extremely dependent on pilot skills in dealing with fire characteristics, complex atmospheric conditions and reduced visibility. In this context, the development of numerical modelling tools can be of primary importance during training operations or real firefighting situations in the optimisation of the effectiveness of operations. Although some aerial dropping models have been developed in the 1970s by the USDA-FS and more recently under the scope of European research projects, several questions have been left open, namely those related to the aerodynamic breakup of the product or the effect of wind flows induced by vegetative canopies. A systematic and comprehensive evaluation of model performance (by comparison with experimental results from real scale dropping tests) was undertaken in the USDA-FS work. However, the technological developments attained during the last 30 years, particularly on new equipment for measuring operating conditions during flight (namely the flow rate of product during discharge), should allow for an increase the accuracy of simulations.

The main objective of the present work was the development and validation of ADM, a model for the numerical simulation of the aerial dropping of firefighting products. Capable of fulfilling some of the gaps left by previous work, the model covers several of the most important mechanisms involved in the dynamical process from the opening of tank doors to ground deposition, namely, the canopy-induced wind flow, the outflow of the liquid from the aircraft tank, the jet column bending and fracture, the primary breakup of the jet surface and column, the shape distortion and secondary breakup of the formed droplets, the gravitational settling of the droplets and the canopy interception/ground deposition of the spray cloud.

One of the objectives during ADM development was thus to consider the majority of the relevant mechanisms and phenomena involved in an aerial drop while guaranteeing the operational characteristics of the tool. The final version is a fast-running computational code, requiring approximately 1 minute CPU time in a modern computer (e.g., 3 GHz processor and 1 GB RAM) for completing a typical simulation.

Due to these characteristics and capabilities, and also the friendly-access GUI, this operational tool can potentially be used in formation, training and demonstration activities with pilots, aerial resource coordinators, civil protection personnel or general firefighters, or in the testing of the effectiveness of firefighting chemicals and delivery systems, complementing the data obtained from real scale drop tests and laboratorial experiments. The user control over the input parameters allows the effect on ground pattern to be assessed for a wide range of release scenarios, avoiding the natural variability and irreproducibility of field conditions, and a complementary understanding of the multiple interrelated phenomena involved.

One of the ADM particularities is that it accounts for the effects of vegetative canopies and atmospheric stability on the vertical wind shear and, consequently, on the breakup and deposition of droplets in the atmosphere; thus fulfilling a gap left by previous studies. As there are no measurements available that consider the aerial drop of product over forest stands, the canopy flow module was previously validated through the intercomparison with meteorological measurements in two distinct forests. Particularly in neutral stability, the agreement through the full depth of the canopy between measured and simulated values of mean wind speed is very good. Although the consideration of non-neutral conditions requires an additional effort from the model, statistical analysis has revealed a modelling performance that is within the limits defined by the acceptance criteria. In particular for stable atmosphere, some improvements on the capability of the model to simulate the mean wind flow conditions within the canopy would permit an increase in the accuracy of results. Nevertheless, the adequate response of the model to different types of canopy and a

wide range of atmospheric stability conditions, particularly if only the region above the canopy top is considered, has been shown.

ADM performance was subsequently investigated against measured data on ground concentration of product obtained during real scale drops. The delivery system type, flight parameters, meteorological conditions and product characteristics were varied in order to evaluate the model performance within a wide range of input conditions. The computed ground pattern contours have shown the features observed in the tests conducted in Marseille and Marana, namely with a ground concentration profile that starts at the tail of the pattern with a light concentration, which coincides with the instant of door opening, and increases with the increase in flow rate of product from the aircraft tanks until the effective portion of the pattern (i.e., for concentrations above 0.8 $l.m^{-2}$) is attained. The higher concentrations at the front of the pattern, with a typical elliptic contour, are particularly present in conventional delivery systems, as the one used at Marseille. With a constant flow delivery system, as in the Marana tests, there is a decrease in the maximum concentration attained, due to a more efficient ground distribution of product. This distinctive behaviour of the product as a function of the delivery system has been captured by ADM in the majority of the situations.

The simulated spatial distribution of droplets by diameters in the ground pattern is in agreement with the experimental data from Andersen et al. [1976], with a decrease in the size of droplets from the centre to the periphery of the ground pattern, and a prevalence of larger droplets in the areas of higher concentration. Due to the effect of the wind flow, droplet size and product concentration were found to be smaller on the rear side of the pattern, as expected. However, on some occasions, this drifting effect appeared to be stronger than in reality. This can be due to an underestimation of the lower classes of diameters in the DSD, which are more easily affected by air flow conditions. Also, neglecting the effect of preceding droplets on drag can be contributing to this punctual disagreement. One of the consequences is that, in some situations, the motion of droplets along the *x*-axis is under-predicted for lower liquid viscosities, resulting in shorter patterns. Other possible reasons for the origin of this behaviour can be related with some features that are not encompassed in the modelling, namely the wake induced by the flow around the jet column and how this translates to an additional source of turbulence and an effective distortion of droplet motion, particularly the finer ones. However, the underestimation of the contour length was observed mainly for concentrations lower than 0.6 $l.m^{-2}$ (1.5 gpc) with low viscosity products (μ < 214 cP). As the minimum retardant application rate required to stop a fire (despite variations in fire characteristics, meteorological conditions and vegetation) has been defined as 0.8 $l.m^{-2}$ (2 gpc) by fire agencies from the US

[George and Blakely, 1973] and Europe [Giroud et al., 2002], the referred under-prediction does not compromise the ability of the model to simulate the overall efficiency of the dropping.

In fact, the statistical validation of the results in terms of the computed length and area for a number of concentration ranges (coverage levels) indicated a generally good model performance, in particular given the wide range of input conditions assessed. The model agreement is actually within the statistical uncertainty of the cup-and-grid sampling method. Line lengths per coverage level are within a 10% error in general, with an average *NMSE* of 0.01 and a Pearson correlation coefficient above 0.9 in both Marseille and Marana drop trials. The accuracy of the simulated areas per level decreases to an average *NMSE* of 0.02 and 0.04, for the two drop trials respectively, although the good correlation remains. In all cases, nearly 90% of the results were within a factor of two of observations. Also, the *MG* was between 1.1 (for area) and 1.2 (for line length), indicating that the mean bias is clearly within the ±30% variation from the mean established by the model acceptance criteria. In all situations, all the statistical metrics fulfilled the requirements of the referred criteria.

Despite the overall good performance of the model, some aspects could be improved in the future. In particular, the spatiotemporal evolution of the mechanisms occurring during primary breakup, and the consequent impact on the ground distribution of the product, should be further investigated by wind-tunnel experimentation with liquid jets into crossflows of air, and/or by CFD modelling, with some emphasis on the potential capabilities of the VOF technique at this level. There is currently some uncertainty about the stripping of droplets from the jet surface during primary breakup, particularly in the case of a large diameter liquid jet. The parameters that define the 'injection' of these stripped droplets into the computational domain, namely the initial 3D position and the velocity, are to some extent responsible for the width of the cloud in the regions where the bulk liquid and the dense spray are located, i.e., the jet column and the near-field spray, respectively. The subsequent interaction of the formed droplets with each other and with the turbulent flow in the wake of the jet column is an important factor towards the complete understanding of the mechanisms that lead to the final ground contour of concentrations. These phenomena should be considered in future studies on the aerodynamic breakup of firefighting products.

Also the research on the effect of the non-Newtonian characteristics of retardants on breakup time and droplets sizes should be stimulated. The development of numerical approaches that could encompass the response of viscosity to shear rate would allow an increase in the understanding of fluid behaviour, particularly for those fluids showing elastic properties (as PC). These approaches should, however, be suited for

implementation into a model with operational characteristics (i.e., should not compromise the computational time). Only a systematic and detailed laboratorial analysis of the products under consideration could provide the data needed for this type of application. Nevertheless, although the linear stability theory implemented in ADM is mostly adequate for simulating the breakup of Newtonian fluids, it has shown potential to be applied also to non-Newtonian liquids apparently without significant prejudice to the overall performance of the model, even in the case of viscoelastic products, as it was evidenced by the statistical evaluation of modelling results. Additionally, other effects could be integrated in the model to describe the motion of droplets, namely the ones related to the effect of neighbouring particles on drag or the response of smaller droplets to turbulent velocity fluctuations.

The fast-running computational code implemented into ADM is an important characteristic given the interest arising from the integration of this model into a DSS that would cover all the aspects or stages involved in a forest fire situation. In fact, although several DSS were developed for supporting the process of decision making during forest fires, they usually privilege one or two of the following aspects (see, e.g., Borrego and Amorim [2007], Xanthopoulos et al. [2003]):

- fire risk: comprises the natural risk caused by factors such as vegetation, topography and meteorology; and the human risk associated to land-planning, accessibility or building protection;
- fire progression and area burned as a function of topography, vegetation characteristics and meteorological conditions;
- smoke behaviour: air quality conditions, human exposure and visibility impairment;
- optimisation of firefighting operations, helping managers to make quick and documented decisions concerning firefighting plans, according to the ground and aerial resources available in the terrain.

The integration of ADM into a DSS with the characteristics of an integrated response model for forest fire emergency situations would be a major accomplishment for the future. An integrated system with such characteristics would allow a wider applicability of ADM. As an example, the knowledge of the evolution with time of the fire line and fire intensity could be used as an essential input for understanding the effect of heat on the behaviour of the product, and thus permitting the consideration of direct attack (which is the typical procedure when using water or short-term retardants). This would necessarily oblige a number of model improvements, namely understanding how the turbulent fluxes that characterise thermally induced updrafts

influence the wind profile or even the consideration of mass transfer due to evaporation.

Again, it should be noted that the prime objective behind the development of ADM was to provide a new insight on breakup mechanisms and wind shear effects on droplet generation and motion, while maintaining the run-time on a feasible level given the limits imposed by the operational application. On the context of the existing aerial dropping models this could be interpreted as a step toward the ability to describe the complex dynamical processes determining the efficiency of firefighting products delivered by aerial means.

An integrated effort towards efficient prevention and suppression of forest fires should be strengthened at both the research and operational (in the terrain) levels. The development of powerful numerical models for operational use or as detailed research tools should be stimulated as a way to increase the common knowledge on the problem. On what relates to the research on the aerial drop of firefighting products the US has had a distinct role during the last 40 years. Due to the importance of experimental data in all stages of model development, a systematic and comprehensive collection of data on all the aspects covered by the present analysis for the specific European conditions (particularly in what relates to vegetation, delivery systems, product types and drop height) should be conducted both in the laboratory and at real scale.

7. References

Abe Y., Kizu T., Arai T., Nariai H., Chitose K. and Koyamac K., 2004. Study on thermal-hydraulic behavior during molten material and coolant interaction. Nuclear Engineering and Design 230, 277-291.

Abe Y., Matsuo E., Arai T., Nariai H., Chitose K., Koyama K. and Itoh K., 2006. Fragmentation behavior during molten material and coolant interactions. Nuclear Engineering and Design 236, 1668-1681.

Abramowitz M. and Stegun I.A., 1972. Handbook of mathematical functions with formulas, graphs and mathematical tables. National Bureau of Standards-Applied Mathematics Series 55, USA. 1046 pp.

ACRE, 2000. Final report of ACRE project - 1st January to 31st October 2000. ACRE project (contract ENV4-CT98-0729). 129 pp.

Amiro B.D., 1990. Drag coefficients and turbulence spectra within three boreal forest canopies. Boundary-Layer Meteorology 52, 227-246.

Amiro B.D., Todd J.B., Wotton B.M., Logan K.A., Flannigan M.D., Stocks B.J., Mason J.A., Martell D.L. and Hirsch K.G., 2001. Direct carbon emissions from Canadian forest fires, 1959-1999. Canadian Journal of Forest Research 31(3), 512-525.

Amorim J.H., 2003. Modelação do escoamento e da dispersão de poluentes atmosféricos em áreas urbanas. Master Thesis. University of Aveiro, Portugal. 130 pp.

Amorim J.H., Miranda A.I. and Borrego C., 2004a. Air pollutants dispersion disturbance due to urban vegetation: a porous media modelling approach to Lisbon city centre. In: Flow and transport processes in complex obstructed geometries: from cities and vegetative canopies to industrial problems. In: Proceedings of the NATO Advanced Study Institute (ASI) 980064. 4-15 May 2004. Kyiv, Ukraine.

Amorim J.H., Miranda A.I. and Borrego C., 2004b. Modelação numérica da dispersão de poluentes atmosféricos no centro de Lisboa. In: Proceedings of the 8th Conferência Nacional de Ambiente. 27-29 October 2004. Lisbon, Portugal

Amorim J.H., Miranda A.I. and Borrego C., 2005. The effect of vegetative canopy on urban air pollutants dispersion: an application to Lisbon city centre. In: Proceedings of the 14th International Symposium on Transport and Air Pollution (TAP). 1-3 June 2005. Graz, Austria. 89-98.

Amorim J.H., Miranda A.I., Borrego C. and Varela V., 2006. Recent developments on retardant aerial drop modelling for operational purposes. In: Proceedings of the V International Conference on Forest Fire Research. 27-30 November 2006. Figueira da Foz, Portugal - Forest Fire Research & Wildland Fire Safety. Viegas D.X. (Ed.), Millpress, Rotterdam. Proceedings on CD-ROM.

Amsden D.C. and Amsden A.A., 1993. The KIVA story: A paradigm of technology transfer. IEEE Transactions on Professional Communication 36(4), 190-195.

Andersen W.H., Brown R.E., Kato K.G. and Louie N.A., 1974a. Investigation of rheological properties of aerial-delivered fire retardant - Final report (8990-04). US Department of Agriculture, Forest Service (USDA-FS), Intermountain Research Station. Ogden, Utah, US. 149 pp.

Andersen W.H., Brown R.E., Louie N.A., Blatz P.J. and Burchfield J.A., 1974b. Investigation of rheological properties of aerial-delivered fire retardant extended study - Final report (8990-05). US Department of Agriculture, Forest Service (USDA-FS), Intermountain Research Station. Ogden, Utah, US. 66 pp.

Andersen W.H., Brown R.E., Louie N.A., Kato K.G., Burchfield J.A., Dalby J.D. and Zernow L., 1976. Correlation of rheological properties of liquid fire retardant with aerially delivered performance - Final report (8990-08). US Department of Agriculture, Forest Service (USDA-FS), Intermountain Research Station. Ogden, Utah, US. 95 pp.

Angeler D.G., Martín S. and Moreno J.M., 2005. Daphnia emergence: a sensitive indicator of fire-retardant stress in temporary wetlands. Environment International 31(4), 615-620.

Arcoumanis C., Khezzar L., Whitelaw D.S. and Warren B.C.H., 1994. Breakup of Newtonian and non-Newtonian fluids in air jets. Experiments in Fluids 17, 405-414.

ASTM International, 2000. Standard guide for statistical evaluation of atmospheric dispersion model performance, D 6589 – 00. ASTM International. 17 pp.

Aubrun S. and Leitl B., 2004. Development of an improved physical modelling of a forest area in a wind tunnel. Atmospheric Environment 38, 2797-2801.

Aubrun S., Koppmann R., Leitl B., Möllmann-Coers M. and Schaub A., 2005. Physical modelling of a complex forest area in a wind tunnel - Comparison with field data. Agricultural and Forest Meteorology 129(3-4), 121-135.

Ayotte K.W., Finnigan J.J. and Raupach M.R., 1999. A second-order closure for neutrally stratified vegetative canopy flows. Boundary-Layer Meteorology 90, 189-216.

Babinsky E. and Sojka P.E., 2002. Modeling drop size distributions. Progress in Energy and Combustion Science 28(4), 303-329.

Baldocchi D.D. and Meyers T.P., 1988. Turbulence structure in a deciduous forest. Boundary-Layer Meteorology 43, 345-364.

Bang K.H., Kim J.M. and Kim D.H., 2003. Experimental study of melt jet breakup in water. Journal of Nuclear Science and Technology 40(10), 807-813.

Barrios A.J.G. and Solé I.R., 2004. Air resources in the defence against forest fires. In: Proceedings of the 1st International Symposium on the Aerial Resources in Wildland Fire Suppression. 239 pp.

Beale J.C. and Reitz R.D., 1999. Modeling spray atomization with the Kelvin-Helmholtz/Rayleigh-Taylor hybrid model. Atomization and Sprays 9(6), 623-650.

Belcher S.E., Jerram N. and Hunt J.C.R., 2003. Adjustment of a turbulent boundary layer to a canopy of roughness elements. Journal of Fluid Mechanics 488, 369-398.

Bellman R. and Pennington R.H., 1953. Effects of surface tension and viscosity on Taylor instability. Quarterly of Applied Mathematics 12, 151-162.

Beyer W.H., 1987. CRC Standard Mathematical Tables, 28th Edition. CRC Press. Boca Raton, Florida, US. 674 pp.

Bi W., Potter W.D., Twardus D., Thistle H., Ghent J., Twery M. and Teske M., 2000. Aerial spray optimization. In: Proceedings of the International Conference on Artificial Intelligence, IC-AI 2000. Las Vegas, U.S. 473-480.

Bird R.B., Stewart W.E., Lightfoot E.N., 2007. Transport Phenomena. 2nd Edition. John Wiley & Sons. New York. 905 pp.

Birouk M., Azzopardi B.J., Stäbler T., 2003. Primary break-up of a viscous liquid jet in a cross airflow. Particle and Particle Systems Characterization 20, 283-289.

Blake N.J., Blake D.R., Wingenter O.W., Sive B.C., McKenzie L.M., Lopez J.P., Simpson L.J., Fuelberg H.E., Sachse G.W., Anderson B.E., Gregory G.L., Carroll M.A., Albercock G.M. and Rowland F.S., 1999. Influence of Southern hemispheric biomass burning on mid tropospheric distributions of nonmethane hydrocarbons and selected halocarbons over the remote South Pacific. Journal of Geophysical Research 104, 16213-16232.

Blakely A.D., George C.W. and Johnson G.M., 1982. Static testing to evaluate airtanker delivery performance. General Technical Report INT-78. US Department of Agriculture, Forest Service (USDA-FS), Intermountain Forest and Range Experiment Station. Ogden, Utah, US. 17 pp.

Borrego C., Tchepel O., Costa A.M., Amorim J.H. and Miranda A.I., 2003. Emission and dispersion modelling of Lisbon air quality at local scale. Atmospheric Environment 37, 5197-5205.

Borrego C., Tchepel O., Salmim L, Amorim J.H., Costa A.M. and Janko J., 2004. Integrated modelling of road traffic emissions: application to Lisbon air quality management. Cybernetics and Systems: An International journal 35(5-6), 535-548.

Borrego and Amorim, 2007. Risk and emergency modelling for environmental security: general aspects. In: Air, Water and Soil Quality Modelling for Risk and Impact Assessment. Adolf E. and Teimuraz D. (Eds.). NATO Security through Science Series – C: Environmental Security. Springer. Dordrecht. 365 pp.

Boulton A.J., Moss G.L. and Smithyman D., 2003. Short-term effects of aerially-applied fire-suppressant foams on water chemistry and macroinvertebrates in streams after natural wild-fire on Kangaroo Island, South Australia. Hydrobiologia 498(1-3), 177-189.

Brenn G., Liu Z. and Durst F., 2000. Linear analysis of the temporal instability of axisymmetrical non-Newtonian liquid jets. International Journal of Multiphase Flow 26, 1621-1644.

Browell E.V., Fenn M.A., Butler C.F., Grant W.B., Claytin M.B., Fishman J., Bachhmeier A.S., Anderson B.E., Gregory G.L., Fuelberg H.E., Bradshaw J.D., Sandholm S.T., Blake D.R., Heikes B.G., Sachse G.W., Singh H.B. and Talbot R.W., 1996. Ozone and aerosol distributions and air mass characteristics over the South Atlantic basin during burning season. Journal of Geophysical Research 101, 24043-24068.

Brunet Y., Finnigan J.J. and Raupach M.R., 1994. A wind tunnel study of air flow in waving wheat: single-point velocity statistics. Boundary-Layer Meteorology 70, 95-132.

Brunet Y. and Irvine I.R., 2000. The control of coherent eddies in vegetation canopies: Streamwise structure spacing, canopy shear scale and atmospheric stability. Boundary-Layer Meteorology 94, 139-163.

Brustet J., Vickos J., Fontan J., Podaire A. and Lavenu F., 1991. Characterisation of active fires in West African savannahs by analysis of satellite data: Landsat thematic mapper. In: Global biomass burning: atmospheric, climatic, and biospheric implications. Levine J. (Ed.). The Massachusetts Institute of Technology (MIT) Press, Massachusetts, US. 53-60.

Businger J.A., 1959. A generalization of the mixing-length concept. Journal of Meteorology 16, 516-523.

Businger J.A., Wyngaard J.C., Izumi Y. and Bradley E.F., 1971. Flux-profile relations in the atmospheric surface layer. Journal of the Atmospheric Sciences 28, 181-189.

Calabri G., 1983. Fighting fires in Mediterranean forests. Food and Agriculture Organization of the United Nations (FAO). Unasylva - An international journal of forestry and forest industries 35(141).

Calogine D., Rimbert N. and Séro-Guillaume O., 2007. Modelling of the deposition of retardant in a tree crown during fire fighting. Environmental Modelling & Software 22, 1654-1666.

Camussi R., Guj G. and Stella A., 2002. Experimental study of a jet in a crossflow at very low Reynolds number. Journal of Fluid Mechanics 454, 113-144.

CEEMACIF, 2005. Comissão Especial para o Estudo dos Meios Aéreos de Combate aos Incêndios Florestais - Final Report. 28 pp.

CEFF, 2006. Comissão Eventual para os Fogos Florestais - Relatório, July 2006. 167 pp.

CEFF, 2007. Comissão Eventual para os Fogos Florestais - 2.º Relatório, January 2007. 73 pp.

Cellier P. and Brunet Y., 1992. Flux-gradient relationships above tall plant canopies. Agricultural and Forest Meteorology 58, 93-117.

CELPA, 2002. Annual Statistics 2001. Paper Industry Association (CELPA). Lisbon, Portugal. 125 pp.

CELPA, 2003. Statistics Report 2002. Paper Industry Association (CELPA). Lisbon, Portugal. 130 pp.

CELPA, 2004. Statistics Report 2003. Paper Industry Association (CELPA). Lisbon, Portugal. 138 pp.

CELPA, 2005. Statistics Report 2004. Paper Industry Association (CELPA). Lisbon, Portugal. 108 pp.

CELPA, 2006. Statistics Report 2005. Paper Industry Association (CELPA). Lisbon, Portugal. 120 pp.

CELPA, 2007. Statistics Report 2006. Paper Industry Association (CELPA). Lisbon, Portugal. 126 pp.

Cescatti A. and Marcolla B., 2004. Drag coefficient and turbulence intensity in conifer canopies. Agricultural and Forest Meteorology 121, 197-206.

Chang J.C. and Hanna S.R., 2005. Technical descriptions and user's guide for the BOOT statistical model evaluation software package, version 2.0. 62 pp.

Chou W.H., Hsiang L-P. and Faeth G.M., 1997. Temporal properties of secondary drop breakup in the shear breakup regime. International Journal of Multiphase Flow 23, 651-669.

Cionco R.M., 1965. A mathematical model for air flow in a vegetative cover. Journal of Applied Meteorology 4, 517-522.

Conrad S.G. and Ivanova G.A., 1997. Wildfire in russian boreal forests - potential impacts of fire regime characteristics on emissions and global carbon balance estimates. Environmental Pollution 98(3), 305-313.

Cowan I.R., 1968. Mass, heat and momentum exchange between stands of plants and their environment. Quarterly Journal of the Royal Meteorological Society 94, 523-544.

Crowe C., Sommerfeld M. and Tsuji Y., 1998. Multiphase flows with droplets and particles. CRC Press. Boca Raton, Florida, US. 471 pp.

CSIRO, 2000. Fire management - Assessment of the effectiveness and environmental risk of the use of retardants to assist in wildfire control in Victoria. Research Report N.º 50. CSIRO Forestry and Forest Products. Victoria, Australia. 52 pp.

Cutini A., Matteucci G. and Scarascia Mugnozza G., 1998. Estimation of leaf area index with the Li-Cor LAI 2000 in deciduous forests. Forest Ecology and Management 105, 55-65.

Davies S.J. and Unam L., 1999. Smoke-haze from the 1997 Indonesian forest fires: effects on pollution levels, local climate, atmospheric CO_2 concentrations, and tree photosynthesis. Forest Ecology and Management 124, 137-144.

Davis J., 1959. Air drop tests: Willows, Santa Ana, Ramona 1955-1959. Res. Pap. 17382 4-60 2M SPO. US Department of Agriculture, Forest Service (USDA-FS), Pacific Southwest Forest and Range Experiment Station and the California Air Attack Coordinating Committee. 22 pp.

Dawud Y., 1999. Smoke Episodes and assessment of health impacts related to haze from forest fires: Indonesian Experience. In: Health Guidelines for Vegetation Fire Events-Background Papers. Schwela D., Goldammer J.G., Morawska L. and Simpson O. (Eds.). World Health Organization (WHO), Geneva; United Nations Environment Programme (UNEP), Nairobi; World Meteorological Organization (WMO), Geneva. WHO/UNEP/WMO Expert Task Force Meeting, 6-9 October 1998, Lima, Peru. 313-333.

De Bruin H.A.R. and Moore C.J., 1985. Zero-plane displacement and roughness length for tall vegetation, derived from a simple mass conservation hypothesis. Boundary-Layer Meteorology 31, 39-49.

Denmead O.T. and Bradley E.F., 1987. On scalar transport in plant canopies. Irrigation Science 8, 131-149.

Dennis A., Fraser M., Anderson S. and Allen D., 2002. Air pollutant emissions associated with forest, grassland, and agricultural burning in Texas. Atmospheric Environment 36, 3779-3792.

DGF, 2001. Inventário Florestal Nacional - 3ª Revisão. Direcção Geral das Florestas (DGF), Divisão de Planeamento e Estatística. Lisbon, Portugal.

DGF, 2003. Incêndios florestais 2003 (1 Janeiro a 31 de Outubro), Relatório Provisório, 3 Novembro 2003. Direcção Geral das Florestas (DGF), Divisão de Protecção e Conservação Florestal. Lisbon, Portugal. 13 pp.

DGRF, 2006. Incêndios florestais - Relatório de 2005. Direcção Geral dos Recursos Florestais (DGRF), Divisão de Defesa da Floresta contra Incêndios. Lisbon, Portugal. 26 pp.

Dziubiński M. and Marcinowski A., 2005. Comments on Reynolds number definition for the discharge of non-Newtonian liquids from tanks. Journal of Fluids Engineering 127(5), 1043-1046.

Dziubiński M. and Marcinowski A., 2006. Discharge of Newtonian and Non-Newtonian liquids from tanks. Chemical Engineering Research and Design 84(A12), 1194-1198.

EC, 2001. Forest fires in Southern Europe: Report N.º 1. Joint Research Centre, Institute for Environment and Sustainability, Land Management and Natural Hazards Unit. Official Publication of the European Commission (EC), European Communities, SPI 01.95. 40 pp.

EC, 2002. Forest Fires in Europe: 2001 fire campaign, Report N.º 2. Joint Research Centre, Institute for Environment and Sustainability, Land Management and Natural Hazards Unit. Official Publication of the European Commission (EC), European Communities, SPI.02.72. 27 pp.

EC, 2003. Forest Fires in Europe: 2002 fire campaign, Report N.º 3. Joint Research Centre, Institute for Environment and Sustainability, Land Management and Natural Hazards Unit. Official Publication of the European Commission (EC), European Communities, SPI.03.83. 35 pp.

EC, 2004a. Forest Fires in Europe: 2003 fire campaign, Report N.º 4. Joint Research Centre, Institute for Environment and Sustainability, Land Management and Natural Hazards Unit. Official Publication of the European Commission (EC), European Communities, SPI.04.124. 51 pp.

EC, 2004b. Assessment of fire damages in the EU Mediterranean Countries during the 2003 Forest Fire Campaign – Special report. Joint Research Centre, Institute for Environment and Sustainability, Land Management and Natural Hazards Unit. Official Publication of the European Commission (EC), European Communities, S.P.I.04.64. 39 pp.

EC, 2005. Forest Fires in Europe 2004, Report N.º 5. Joint Research Centre, Institute for Environment and Sustainability, Land Management and Natural Hazards Unit. Official Publication of the European Commission (EC), European Communities, S.P.I.05.147. 45 pp.

EC, 2006. Forest Fires in Europe 2005, Report N.º 6. Joint Research Centre, Institute for Environment and Sustainability, Land Management and Natural Hazards Unit. Official Publication of the European Commission (EC), European Communities, EUR 22312 EN. 53 pp.

EC, 2007. Forest Fires in Europe 2006, Report N.º 7. Joint Research Centre, Institute for Environment and Sustainability, Land Management and Natural Hazards Unit. Official Publication of the European Commission (EC). European Communities. 77 pp.

Eggers J., 1997. Nonlinear dynamics and breakup of free-surface flows. Reviews of Modern Physics 69(3), 865-929.

Eggers J., 2006. A Brief History of Drop Formation. In: Nonsmooth mechanics and analysis, theoretical and numerical advances - Chapter 14. Book Series Advances in Mechanics and Mathematics, vol. 12. Alart P., Maisonneuve O. and Rockafellar R.T. (Eds.). Springer US, 163-172.

Eggers J. and Villermaux E., 2008. Physics of liquid jets. Reports on Progress in Physics 71(3): 036601. 79 pp.

Eshbach O.W. and Souders M., 1975. Handbook of Engineering Fundamentals, 3rd Edition. Wiley, New York. 450 pp.

FAO, 2001. Global forest fire assessment 1990-2000. Forest Resources Assessment Programme - Working Paper 55. Food and Agriculture Organization of the United Nations (FAO), Forestry Department. Rome, Italy. 495 pp.

FAO, 2007a. Fire management - Global assessment 2006. A thematic study prepared in the framework of the Global Forest Resources Assessment 2005. Forestry Paper 151. Food and Agriculture Organization of the United Nations (FAO), Forestry Department. Rome, Italy. 156 pp.

FAO, 2007b. State of the World's Forests 2007. United Nations' Food and Agriculture Organization (FAO). Rome, Italy. 157 pp.

Fearnside P.M., 2000. Global warming and tropical land use change: greenhouse gas emissions from biomass burning, decomposition and soils in forest conversion, shifting cultivation and secondary vegetation. Climatic Change 46, 115-158.

Finney M.A., 1998. FARSITE: Fire Area Simulator-model development and evaluation. Research Paper RMRS-RP-4. US Department of Agriculture, Forest Service (USDA-FS), Rocky Mountain Research Station. Ogden, Utah, US. 47 pp.

Finnigan J., 2000. Turbulence in plant canopies. Annual Review of Fluid Mechanics 32, 519-571.

Finnigan J.J. and Brunet Y., 1995. Turbulent airflow in forests on flat and hilly terrain. In: Wind and Trees. Coutts M.P. and Grace J. (Eds.). Cambridge University Press. Cambridge, UK. 3-40.

Finnigan J.J. and Leuning R., 2000. Long term measurements-coordinate systems and averaging. In: Proceedings of the International Workshop for Advanced Flux Network and Flux Evaluation. 51-56.

Finnigan J.J. and Shaw R.H., 2000. A wind tunnel study of air flow in waving-wheat: An EOF analysis of the structure of the large-eddy motion. Boundary-Layer Meteorology 96, 211-255.

Forster C., Wandinger U., Wotowa G., James P., Mattis I., Althausen D., Simmonds P., O'Doherty S., Jennings S.G., Kleefeld C., Schneider J., Trickl T., Kreipl S., Jäger H. and Stohl A., 2001. Transport of boreal forest fire emissions from Canada to Europe, Journal of Geophysical Research 106 (D19), 22887-22906.

Fric T.F. and Roshko A., 1994. Vortical structures in the wake of a transverse jet. Journal of Fluid Mechanics 279, 1-47.

Fromm M.D. and Servranckx R., 2003. Transport of forest fire smoke above the tropopause by supercell convection. Geophysical Research Letters 30(10), 1542.

Fuller R.P., Wu P-K., Kirkendall K.A. and Nejad A.S., 2000. Effects of injection angle on atomization of liquid jets in transverse airflow. AIAA Journal 38(1), 64-72.

Garcia F.J. and Castellanos A., 1999. 3-D and 1-D dynamics of slender liquid jets: Linear analysis with electric field and accuracy of 1-D models near the breakup. In: Proceedings of the Conference on Electrical Insulation and Dielectric Phenomena. 17-20 October 1999. Austin, US. 346-349.

Gardiner B.A., 1994. Wind and wind forces in a plantation spruce forest. Boundary-Layer Meteorology 67, 161-186.

Garratt J.R., 1980. Surface influence on vertical profiles in the atmospheric near-surface layer. Quarterly Journal of the Royal Meteorological Society 106, 803-819.

Garratt J.R., 1983. Surface influence upon vertical profiles in the nocturnal boundary layer. Boundary-Layer Meteorology 26, 69-80.

Garratt J.R., 1992. The Atmospheric Boundary Layer. Cambridge University Press, Cambridge, UK. 316 pp.

Gayev Y.G., 2007. Variety of problems associated with canopies or EPRs. In: Flow and transport processes with complex obstructions: applications to cities, vegetative canopies and industry. Gayev Y.G. and Hunt J.C.R. (Eds.). NATO Science Series II: Mathematics, Physics and Chemistry, vol. 236. Springer. Proceedings of the NATO Advanced Study Institute on Flow and Transport Processes in Complex Obstructed Geometries: from cities and vegetative canopies to engineering problems. 5-15 May 2004. Kiev, Ukraine. 414 pp.

George, C.W. 1975. Fire retardant ground distribution patterns from the CL-215 air tanker. Research Paper INT-165. US Department of Agriculture, Forest Service (USDA-FS), Intermountain Forest and Range Experiment Station. Ogden, Utah, US. 67 pp.

George C.W. and Blakely A.D., 1973. An evaluation of the drop characteristics and ground distribution patterns of forest fire retardants. Research Paper INT-134. US Department of Agriculture, Forest Service (USDA-FS), Intermountain Research Station. Ogden, Utah, US. 59 pp.

George C.W., Blakely A.D. and Johnson G.M., 1976. Forest fire retardant research - A status report. US Department of Agriculture, Forest Service (USDA-FS), Intermountain Forest and Range Experiment Station. Ogden, Utah, US. 22 pp.

George C.W. and Johnson G.M., 1990. Developing Air Tanker Performance Guides. General Technical Report INT-268. US Department of Agriculture, Forest Service (USDA-FS), Intermountain Research Station. Ogden, Utah, US. 96 pp.

Giménez A., Pastor E., Zárate L., Planas E. and Arnaldos J., 2004. Long-term forest fire retardants: a review of quality, effectiveness, application and environmental considerations. International Journal of Wildland Fire 13, 1-15.

Giroud F., Picard C., Arvieu P. and Oegema P., 2002. An optimum use of retardant during the aerial fire fighting. In: Proceedings of the IV International Conference on Forest Fire Research. 18-23 November 2002. Luso, Portugal - Forest Fire Research & Wildland Fire Safety. Viegas D.X. (Ed.). Millpress, Rotterdam. Proceedings on CD-ROM.

Grah R.A. and Wilson C.C., 1944. Some components of rainfall interception. Journal of Forestry 42(12), 890-898.

Gromke C. and Ruck B., 2007. Influence of trees on the dispersion of pollutants in an urban street canyon - Experimental investigation of the flow and concentration field. Atmospheric Environment 41, 3387-3302.

Grover Jr. R.O., Assanis D.N. and Lippert A.M., 2004. A comparison of classical atomization models against current experimental measurements within a zero-dimensional framework. In: Proceedings of the ILASS Americas, 17th Annual Conference on Liquid Atomization and Spray Systems. May 2004. Arlington, VA, US.

Haider A. and Levenspiel O., 1989. Drag coefficient and terminal velocity of spherical and nonspherical particles. Powder Technology 58, 63-70.

Harman I. and Finnigan J., 2007. A simple unified theory for flow in the canopy and roughness sublayer. Boundary-Layer Meteorology 123(2), 339-363.

Heinselman M.L., 1978. Fire in wilderness ecosystems. In: Wilderness Management. Hendee J.C., Stankey G.H. and Lucas R.C. (Eds.). US Department of Agriculture, Forest Service (USDA-FS). Washington, DC, US. 249-278.

Hernández S.D., Pascual I.P. and Martínez J.I.V., 2007. Presente y futuro de los medios aéreos de cobertura nacional en la extinción de incendios forestales en España. Protocolos de actuación. In: Proceedings of the 4th International Wildland Fire Conference - Wildfire 2007. 13-17 May 2007. Seville, Spain. Proceedings on CD-ROM.

Hirahara H. and Kawahashi M., 1992. Experimental investigation of viscous effects upon a breakup of droplets in high-speed airflow. Experiments in Fluids 13, 423-428.

Högström U., 1996. Review of some basic characteristics of the atmospheric surface layer. Boundary-Layer Meteorology 78, 215-246.

Holdeman J., 1993. Mixing of multiple jets with a confined subsonic crossflow. Progress in Energy and Combustion Science 19, 31-70.

Holtslag A.A.M. and van Ulden A.P., 1983. A simple scheme for daytime estimates of the surface fluxes from routine weather data. Journal of Climate and Applied Meteorology 22, 517-529.

Hoyt J.W. and Taylor J.J., 1977. Waves on water jets. Journal of Fluid Mechanics 83, part 1, 119-127.

Hsi G. and Nath J.H., 1970. Wind drag within simulated forest canopies. Journal of Applied Meteorology 9(4), 592-602.

Hsiang L.-P. and Faeth G.M., 1992. Near-limit drop deformation and secondary breakup. International Journal of Multiphase Flow 18(5), 635-652.

Hsiang L.-P. and Faeth G.M., 1995. Drop deformation and breakup due to shock wave and steady disturbances. International Journal of Multiphase Flow 21(4), 545-560.

Hwang S.S., Liu Z. and Reitz R.D., 1996. Breakup mechanisms and drag coefficients of high-speed vaporizing liquid drops. Atomization and Sprays 6, 353-376.

Inamura T., Tsutagawa T., Cho S.J. and Masuya G., 2001. Numerical simulation on the behavior of a liquid jet into an air flow. Heat Transfer-Asian Research 30(6), 473-484.

Inoue E., 1963. The environment of plant surfaces. In: Environment Control of Plant Growth. Academic Press, New York. 23-32.

Irvine M.R. and Brunet Y., 1996. Wavelet analysis of coherent eddies in the vicinity of several vegetation canopies. Physics and Chemistry of the Earth 21(3), 161-165.

Irwin J.S., 1979. A theoretical variation of the wind profile law exponent as a function of surface roughness and stability. Atmospheric Environment 13, 191-194.

ITRATECH, 1999. 1st Annual report of ACRE project - Annex 5. ACRE project (contract ENV4-CT98-0729). 75-104.

Jackson P.S., 1981. On the displacement height in the logarithmic profile. Journal of Fluid Mechanics 111, 15-25.

Jonckheere I., Fleck S., Nackaerts K., Muys B., Coppin P., Weiss M. and Baret F., 2004. Review of methods for in situ leaf area index determination Part I. Theories, sensors and hemispherical photography. Agricultural and Forest Meteorology 121(1-2), 19-35.

Joseph D.D., Belanger J. and Beavers G.S., 1999. Breakup of a liquid drop suddenly exposed to a high-speed airstream. International Journal of Multiphase Flow 25, 1263-1303.

Kaimal J.C. and Finnigan J.J., 1994. Atmospheric Boundary Layer Flows: their Structure and Measurement. Oxford University Press, New York. 289 pp.

Kalabokidis K.D., 2000. Effects of wildfire suppression chemicals on people and the environment - A review. Global NEST: the International Journal 2(2), 129-137.

Kasten F. and Czeplak G., 1980. Solar and terrestrial radiation dependent on the amount and type of cloud. Solar Energy 24, 177-189.

Katul G., Oren R., Ellsworth D., Hsieh C.I., Phillips N. and Lewin K., 1997. A Lagrangian dispersion model for predicting CO_2 sources, sinks, and fluxes in a uniform loblolly pine (Pinus taeda L.) stand. Journal of Geophysical Research 102, 9309-9321.

Katul G.G. and Albertson J.D., 1998. An investigation of higher-order closure models for a forested canopy. Boundary-Layer Meteorology 89, 47-74.

Kawatani T. and Meroney R.N., 1970. Turbulence and wind speed characteristics within a model canopy flow field. Agricultural Meteorology 7, 143-158.

Kelsot R.M., Lims T.T. and Perry A.E., 1996. An experimental study of round jets in cross-flow. Journal of Fluid Mechanics 306, 111-144.

Khosla S. and Crocker D.S., 2004. CFD modeling of the atomization of plain jets in cross flow for gas turbine applications. In: Proceedings of the IGTI Turbo Expo: Combustion & Fuels, GT2004-54269. June 2004. Vienna, Austria.

Kim D., Desjardins O., Herrmann M. and Moin P., 2006. Toward two-phase simulation of the primary breakup of a round liquid jet by a coaxial flow of gas. Annual Research Briefs 2006. Center for Turbulence Research. 185-195.

Ko G.H. and Ryou H.S., 2005. Modeling of droplet collision-induced breakup process. International Journal of Multiphase Flow 31, 723-738.

Krothapalli A., Baganoff D. and Karamcheti K., 1981. On the mixing of a rectangular jet. Journal of Fluid Mechanics 107, 201-220.

Labat, 2003. Human health risk assessment: wildland fire-fighting chemicals. Labat-Anderson Incorporated. 37 pp.

Labat Environmental, 2007. Ecological risk assessment: fire-fighting chemicals. Labat Environmental. 69 pp.

Lafrance P., 1975. Nonlinear breakup of a laminar liquid jet. Physics of Fluids 18(4), 428-432.

Lasheras J.C. and Hopfinger E.J., 2000. Liquid jet instability and atomization in a coaxial gas stream. Annual Review of Fluid Mechanics 32, 275-308.

LBP, 2003. Livro Aberto do Sistema de Protecção e Socorro em Portugal. Liga dos Bombeiros Portugueses. Lisbon, Portugal. 34 pp.

Le Dantec V., Dufrêne E. and Saugier B., 2000. Interannual and spatial variation in maximum leaf area index of temperate deciduous stands. Forest Ecology and Management 134(1-3), 71-81.

Lee C.S. and Park S.W., 2002. An experimental and numerical study on fuel atomization characteristics of high-pressure diesel injection sprays. Fuel 81, 2417-2423.

Lefebvre A.H., 1989. Atomization and Sprays. Hemisphere Publishing Corporation, New York. 421 pp.

LEMTA, 2005. Modeling of dropping and atomization. Deliverable D2/D31 of ERAS project (contract EVG1-CT-2001-00039). 47 pp.

Leuning R., 2000. Estimation of scalar source/sink distributions in plant canopies using Lagrangian dispersion analysis: corrections for atmospheric stability and comparison with a multilayer canopy model. Boundary-Layer Meteorology 96, 293-314.

Leuning R., Cleugh H.A., Zegelin S.J. and Hughes D., 2005. Carbon and water fluxes over a temperate Eucalyptus forest and a tropical wet/dry savanna in Australia: measurements and comparison with MODIS remote sensing estimates. Agricultural and Forest Meteorology 129, 151-173.

Lin S.P., 2003. Breakup of Liquid Sheets and Jets. Cambridge University Press, Cambridge, UK. 269 pp.

Lin S.P. and Reitz R.D., 1998. Drop and spray formation from a liquid jet. Annual Review of Fluid Mechanics 30, 85-105.

Linne M.A., Paciaroni M., Gord J.R. and Meyer T.R., 2005. Ballistic imaging of the liquid core for a steady jet in crossflow. Applied Optics 44(31), 6627-6634.

Liu H., 2000. Science and Engineering of Droplets: Fundamentals and Applications. William Andrew Inc. 225 pp.

Liu J., Chen J.M., Black T.A. and Novak M.D., 1996. E–ε modelling of turbulent air flow downwind of a model forest edge. Boundary-Layer Meteorology 77, 21-44.

Loane I.T. and Gould J.S., 1986. Aerial suppression of bushfires: cost-benefit study for Victoria. CSIRO Division of Forest Research. Canberra, Australia. 213 pp.

Loth E., 2000. Numerical approaches for motion of dispersed particles, droplets and bubbles. Progress in Energy and Combustion Science 26, 161-223.

Lovellette G., 2004. How to conduct drop tests of aerial retardant delivery systems. Technical Report 0457-2813-MTDC. US Department of Agriculture, Forest Service

(USDA-FS), Missoula Technology and Development Center. Missoula, MT, US. 18 pp.

Lovellette G., 2005. How to conduct static tests of aerial retardant delivery systems. Technical Report 0557-2812-MTDC. US Department of Agriculture, Forest Service (USDA-FS), Missoula Technology and Development Center. Missoula, MT, US. 14 pp.

Lozanova M. and Stankov P., 1998. Experimental investigation on the similarity of a 3D rectangular turbulent jet. Experiments in Fluids 24, 470-478.

MacPherson J.I., 1967. A theoretical model for the prediction of the distribution of water released from a water bomber. Aeronautical report LR-480, National Research Council of Canada. Ottawa, Canada.

Madabhushi R.K., 2003. A model for numerical simulation of breakup of a liquid jet in crossflow. Atomization and Sprays 13, 413-424.

MAI, 2003. Livro branco dos incêndios florestais ocorridos no Verão de 2003. Ministério da Administração Interna (MAI). Lisbon, Portugal. 105 pp.

Mansour N.N. and Lundgren T.S., 1990. Satellite formation in capillary jet breakup. Physics of Fluids A 2(7), 1141-1144.

Margason R.J., 1993. Fifty years of jet in crossflow research. In: Proceedings of the AGARD Symposium on a Jet in Cross Flow (AGARD CP-534). Winchester, UK.

Marmottant P. and Villermaux E., 2004. On spray formation. Journal of Fluid Mechanics 498, 73-111.

Marshall B.J., Wood C.J., Gardiner B.A. and Belcher R.E., 2002. Conditional sampling of forest canopy gusts. Boundary-Layer Meteorology 102, 225-251.

Martins A., Cerqueira M., Ferreira F., Borrego C. and Amorim J.H., 2008. Lisbon air quality - Evaluating traffic hot-spots. International Journal of Environment and Pollution (IJEP). In press.

Mashayek F. and Ashgriz N., 1993. A height-flux method for simulating free surface flows and interfaces. International Journal for Numerical Methods in Fluids 17, 1035-1054.

Mazallon J., Dai Z. and Faeth G.M., 1999. Primary break-up of nonturbulent round liquid jets in gas cross flows. Journal of the International Institutes for Liquid Atomization and Spray Systems 9, 291-311.

McKinley G.H., 2005a. Dimensionless groups for understanding free surface flows of complex fluids. The Society of Rheology Bulletin, July 2005, 6-9.

McKinley G.H., 2005b. Visco-elasto-capillary thinning and break-up of complex fluids. Massachusetts Institute of Technology, Report N.º 05-P-04, April 2005. 49 pp.

Meroney R.N., 1968. Characteristics of wind and turbulence in and above model forests. Journal of Applied Meteorology 7(5), 780-788.

Meroney R.N., 2004. Wind tunnel and numerical simulation of pollution dispersion: A hybrid approach. Invited Lecture - Croucher Advanced Study Institute, Hong University of Science and Technology, 6-10 December 2004.

Meyers T.P. and Paw U K.T., 1986. Testing of a higher order closure model for modeling airflow within and above plant canopies. Boundary-Layer Meteorology 37, 297-313.

Miranda A. I., Borrego C. and Viegas D., 1994. Forest fire effects on the air quality. In: Proceedings of the 2nd International Conference on Air Pollution, vol. 1: Computer Simulation. Baldasano J., Brebbia C., Power H. and Zannetti P. (Eds.). Barcelona, Spain. 191-199.

Miranda A.I., Ferreira J., Valente J., Santos P., Amorim J.H. and Borrego C., 2005a. Smoke measurements during Gestosa 2002 experimental field fires. International Journal of Wildland Fire 14(1), 107-116.

Miranda A.I., Martins H., Carvalho A. and Borrego C., 2005b. Modelling smoke effects on Lisbon air quality. In: Proceedings of the 6th Fire and Forest Meteorology Symposium and the 19th Interior West Fire Council Meeting. 25-27 October 2005. Canmore, AB, Canada, US. Proceedings on CD-ROM.

Miranda A.I., Borrego C., Amorim J.H., Valente J., Santos P., Viegas D.X. and Ribeiro L., 2006. Smoke measurements in Gestosa 2004 field experiments. Abstracts of the 5th International Conference on Forest Fire Research (ICFFR). 27-30 November 2006. Figueira da Foz, Portugal – Forest Ecology and Management 234S, 158.

Miranda A., Amorim J.H., Santos P., Carvalho A.C., Tavares R., Salmim L. and Borrego C., 2007. Qualidade do ar e circulação de transportes públicos na cidade do Porto. In: Proceedings of the IX Conferência Nacional de Ambiente. 18-20 April 2007. Aveiro, Portugal. 847-854.

MMA, 2006. Los incendios forestales en España durante el año 2005. Ministerio de Medio Ambiente (MMA), Centro de Coordinación de la Información Nacional sobre Incendios Forestales. 119 pp.

MMA, 2007. Los incendios forestales en España durante el año 2006. Ministerio de Medio Ambiente (MMA), Centro de Coordinación de la Información Nacional sobre Incendios Forestales. 120 pp.

Mölder M., Grelle A., Lindroth A. and Halldin S., 1999. Flux-profile relationships over a boreal forest - roughness sublayer corrections. Agricultural and Forest Meteorology 98-99, 645-658.

Moncrieff J.B., Jarvis P.G. and Valentini R., 2000. Canopy fluxes. In: Methods in Ecosystem Science. Sala O.E., Jackson R.B., Mooney H.A. and Howarth R.W. (Eds.). Springer Verlag. Berlin, Germany. 161-180.

Monin A.S. and Yaglom A.M., 1971. Statistical Fluid Mechanics: Mechanisms of Turbulence. Vol. 1. The Massachusetts Institute of Technology (MIT) Press, Massachusetts, US. 769 pp.

Morgan A.J. and Barton I.E., 2000. Comparison of Lagrangian tracking schemes to flow over a backward facing step. Communications in numerical methods in engineering 16, 831-837.

Morsi S.A. and Alexander A.J., 1972. An investigation of particle trajectories in two-phase flow systems. Journal of Fluid Mechanics 55(2), 193-208.

Mugele R.A. and Evans H.D., 1951. Droplet size distributions in sprays. Industrial and Engineering Chemistry 43(6), 1317-1324.

Nayfeh A.H., 1970. Nonlinear stability of a liquid jet. Physics of Fluids 13(4), 841-847.

New T.H., Lim T.T. and Luo S.C., 2003. Elliptic jets in cross-flow. Journal of Fluid Mechanics 494, 119-140.

Newstead R.G. and Lieskovsky R.J., 1985. Air tanker and fire retardant drop patterns. Information Report NOR-X-273. Northern Forest Research Centre, Canadian Forestry Service. Alberta, Canada. 31 pp.

Nicolas N., 2002. Experimental study of gravity-driven dense suspension jets. Physics of Fluids 14(10), 3570-3576.

NIFC, 2007. Interagency Standards for Fire and Aviation Operations 2007. National Interagency Fire Center (NIFC). US Department of the Interior, Bureau of Land Management, Fish and Wildlife Service, and National Park Service and US Department of Agriculture, Forest Service (USDA-FS). January 2007. NFES 2724.

Novak M.D., Warland J.S., Orchansky A.L., Ketler R. and Green S., 2000. Wind tunnel and field measurements of turbulent flow in forests. Part 1: Uniformly thinned stands. Boundary Layer Meteorology 95, 457-495.

NWCG, 1997. Historical wildland firefighter fatalities 1910-1996. National Wildfire Coordinating Group (NWCG), Safety and Health Working Team. 45 pp.

NWCG, 2000. Lot acceptance, quality assurance, and field quality control for fire retardant chemicals. 6th Edition. National Wildfire Coordinating Group (NWCG). 65 pp.

NWCG, 2007a. Wildland fire accidents by type. National Wildfire Coordinating Group (NWCG), Safety and Health Working Team. 29 pp.

NWCG, 2007b. Wildland fire accidents by year. National Wildfire Coordinating Group (NWCG), Safety and Health Working Team. 25 pp.

Oegema P., 2004. Forest fire fighting chemicals: economic and R/D issues. ITRATECH. 15 pp.

Oke T.R., 1987. Boundary Layer Climates. 2nd Edition. Metheun, London, UK. 435 pp.

O'Rourke P.J. and Amsden A.A., 1987. The TAB method for numerical calculation of spray droplet breakup. SAE Technical Paper 872089.

Ortiz C., Joseph D.D. and Beavers G.S., 2004. Acceleration of a liquid drop suddenly exposed to a high-speed airstream. International Journal of Multiphase Flow 30, 217-224.

Paine R.J., 1987. User's guide to the CTDM meteorological preprocessor (METPRO) program. EPA-600/8-88-004, US Environmental Protection Agency, Research Triangle Park, NC.

Pallas N.R. and Harrison Y., 1990. An automated drop shape apparatus and the surface tension of pure water. Colloids and Surfaces 43(2), 169-194.

Park H., Yoon S.S. and Heister S.D., 2005. A nonlinear atomization model for computation of drop size distributions and spray simulations. International Journal for Numerical Methods in Fluids 48(11), 1219-1240.

Patterson M.A. and Reitz R.D., 1998. Modeling the effects of fuel characteristics on diesel engine combustion and emission. SAE 980131.

Patterson M.A., Kong S.-C., Hampson G.J. and Reitz R.D., 1994. Modeling the effects of fuel injection characteristics on diesel engine soot and NOx emissions. SAE Paper 940523.

Philpot C.W., George C.W., Blakely A.D., Johnson G.M. and Wallace Jr. W.K., 1972. The effect of two flame retardants on particulate and residue production. Research Paper INT-117. US Department of Agriculture, Forest Service (USDA-FS), Intermountain Forest and Range Experiment Station. Ogden, Utah, US.

Physick W.L. and Garratt J.R., 1995. Incorporation of a high-roughness lower boundary into a mesoscale model for studies of dry deposition over complex terrain. Boundary-Layer Meteorology 74, 55-71.

Picard C., Giroud F., Metenier J-C., Lemarchand Y. and Oegema P., 2001. Gum thickened retardant operational guidelines. Deliverable 10 of ACRE project (Contract ENV4-CT98-0729). 13 pp.

Pickler R., 1994. Aircraft and forest fire control in Canada. IFFN N.º 11 - July 1994. Bombardier Inc., Canadair Amphibious Aircraft Division.

Picot J.J.C. and Kristmanson D.D., 1997. Forestry Pesticide Aerial Spraying: Spray Droplet Generation, Dispersion and Deposition. Kluwer Academic Publishers. Netherlands.

Pilch M. and Erdman C., 1987. Use of break-up time data and velocity history data to predict the maximum size of stable fragments for acceleration-induced break-up of a liquid drop. International Journal of Multiphase Flow 13, 741-757.

Plate E.J. and Quraishi A.A., 1965. Modeling of velocity distributions inside and above tall crops. Journal of Applied Meteorology 4(3), 400-408.

Plesniak M.W. and Cusano D.M., 2005. Scalar mixing in a confined rectangular jet in crossflow. Journal of Fluid Mechanics 524, 1-45.

Plucinski M., Gould J., McCarthy G. and Hollis J., 2007. The effectiveness and efficiency of aerial fire fighting in Australia. Part I. Technical report n.º A0701. Bushfire Cooperative Research Center (CRC). 63 pp.

Pozorski J. and Minier J.-P., 1998. On the Lagrangian turbulent dispersion models based on the Langevin equation. International Journal of Multiphase Flow 24(6), 913-945.

Poggi D., Porporato A., Ridolfi L., Albertson J.D. and Katul G.G., 2004. The effect of vegetation density on canopy sublayer turbulence. Boundary-Layer Meteorology 111, 565-587.

Poo J.Y. and Ashgriz N., 1991. Variation of drag coefficients in an interacting drop stream. Experiments in Fluids 11(1), 1-8.

Pruppacher H.R., and Klett J.D., 1997. Microphysics of Clouds and Precipitation. Kluwer Academic Publishers, Dordrecht, 954 pp.

Qi J., Kerr Y.H., Moran M.S., Weltz M., Huete A.R., Sorooshian S. and Bryant R., 2000. Leaf area index estimates using remotely sensed data and BRDF models in a semiarid region. Remote Sensing of Environment 73(1), 18-30.

Quilchano C., Marañón T., Pérez-Ramos I.M., Noejovich L., Valladares F. and Zavala M.A., 2008. Patterns and ecological consequences of abiotic heterogeneity in managed cork oak forests of Southern Spain. Ecological Research 23, 127-139.

Raju M.S., 2005. Numerical investigation of various atomization models in the modeling of a spray flame. National Aeronautics and Space Administration (NASA). Report N.º E-15389. Washington, US. 15 pp.

Ranger A.A. and Nicholls J.A., 1969. The aerodynamic shattering of liquid drops. AIAA Journal 7(2), 285-290.

Raupach M.R., 1992. Drag and drag partition on rough surfaces. Boundary-Layer Meteorology 60, 375-395.

Raupach M.R. and Thom A.S., 1981. Turbulence in and above plant canopies. Annual Review of Fluid Mechanics 13, 97-129.

Raupach M.R. and Shaw R.H., 1982. Averaging procedures for flow within vegetation canopies. Boundary-Layer Meteorology 22, 79-90.

Raupach M.R., Coppin P.A. and Legg B.J., 1986. Experiments on scalar dispersion within a model plant canopy. Part I: The turbulence structure. Boundary-Layer Meteorology 35, 21-52.

Raupach M.R., Finnigan J.J., and Brunet Y., 1996. Coherent eddies and turbulence in vegetation canopies: the mixing-layer analogy. Boundary-Layer Meteorology 78, 351-382.

Rawson R., 1977. A study of the distribution of aerially applied fire retardant in softwood plantations. Fire Research Branch Report. Division of Forest Protection, Forests Commission. Melbourne, Victoria.

Rayleigh W.S., 1879. On the instability of jets. Proceedings of the London Mathematical Society 10, 4.

Reifsnyder W.E., 1973. Forest meteorology in the seventies. Bulletin of the American Meteorological Society 54(4), 326-330.

Reinhardt E., Ottmar R. and Castilla C., 2001. Smoke impacts from agricultural burning in a rural Brazilian town. Journal of the Air & Waste Management Association 51, 443-450.

Reitz R.D., 1987. Mechanisms of atomization processes in high-pressure vaporizing sprays. Atomization and Spray Technology 3, 309-337.

Reitz R.D. and Bracco F.V., 1982. Mechanism of atomization of a liquid jet. Physics of Fluids 25(10), 1730-1742.

Reitz R.D. and Diwakar R., 1987. Structure of high pressure fuel sprays. SAE Technical Paper 870598. 18 pp.

Rimbert N. and Séro-Guillaume O., 2004. Log-stable laws as asymptotic solutions to a fragmentation equation: application to the distribution of droplets in a high Weber-number spray. Physical Review E 69, 056316.

Rimbert N., Calogine D. and Séro-Guillaume O., 2002. Modelling of retardant dropping and atomisation. In: Proceedings of the IV International Conference on Forest Fire Research. 18-23 November 2002. Luso, Portugal – Forest Fire Research & Wildland Fire Safety. Viegas D.X. (Ed.). Millpress, Rotterdam. Proceedings on CD-ROM.

Robertson K., Fogarty L. and Webb S., 1997a. Firebombing effectiveness - where to from here? Fire Technology Transfer Note (FTTN), N.º 11, April 1997. New Zealand Forest Research Institute. 13 pp.

Robertson K., Fogarty L. and Webb S., 1997b. Guidelines for determining aerial drop patterns in open areas. Fire Technology Transfer Note (FTTN), N.º 12, June 1997. New Zealand Forest Research Institute. 17 pp.

Ryan M.J., 2006. CFD prediction of the trajectory of a liquid jet in a non-uniform air crossflow. Computers & Fluids 35, 463-476.

Sallam K.A., Dai Z. and Faeth G.M., 1999. Drop formation at the surface of plane turbulent liquid jets in still gases. International Journal of Multiphase Flow 25, 1161-1180.

Sauvagnargues-Lesage S., Picard C., Giroud F., Raffalli N., Xanthopoulos G., Viegas D.X., Ollero A., Arrue B., Rodriguez y Silva F. and Heikkila T., 2006. Wildland fire suppression management and planning: a state of the art. Deliverable D-09-01 of EUFIRELAB Project (contract EVR1-CT-2002-40028). 29 pp.

Schindler D., 2004. Characteristics of the atmospheric boundary layer over a Scots pine forest. Berichte des Meteorologischen Institutes der Universität Freiburg N.º 11. Freiburg, Germany. 139 pp.

Schmehl R., Klose G., Maier G. and Wittig S., 1998. Efficient numerical calculation of evaporating sprays in combustion chamber flows. In: Proceedings of the Applied Vehicle Technology Panel on Gas Turbine Engine Combustion, Emissions and Alternative Fuels. Lisbon, Portugal. 51.1-51.13.

Schönhuber M., Lammer G., Prechtl M. and Randeu W.L., 2005. Analysis of fire retardant 2DVD data. Institute of Applied Systems Technology (IAS), Joanneum Research. Graz, Austria. 97 pp.

SDTF, 1997. A summary of aerial application studies. Spray Drift Task Force (SDTF). US. 7 pp.

Seginer I., Mulhearn P.J., Bradley E.F., Finnigan J.J., 1976. Turbulent flow in a model plant canopy. Boundary-Layer Meteorology 10, 423-53.

Segletes S.B., 1998. A compact analytical fit to the exponential integral E1(x). Army Research Laboratory, ARL-TR-1758, Aberdeen. 46 pp.

Sellers P.J., Mintz Y., Sud Y.C. and Dalcher A., 1986. A simple biosphere model (SiB) for use within general circulation models. Journal of the Atmospheric Sciences 43, 505-531.

Séro-Guillaume O. and Rimbert N., 2005. On thermodynamic closures for two-phase flow with interfacial area concentration transport equation. International Journal of Multiphase Flow 31, 897-920.

Shaw R.H., Den Hartog G. and Neumann H.H., 1988. Influence of foliar density and thermal stability in profiles of Reynolds stress and turbulence intensity in a deciduous forest. Boundary-Layer Meteorology 45, 391-409.

Shaw R.H. and Schumann U., 1992. Large-eddy simulation of turbulent flow above and within a forest. Boundary-Layer Meteorology 61, 47-64.

Sherif S.A. and Pletcher R.H., 1989. Measurements of the thermal characteristics of heated turbulent jets in cross flow. ASME Journal of Heat Transfer 111, 897-903.

Simmons H.C., 1977. The correlation of drop-size distribution in fuel-nozzle sprays. Journal of Engineering for Gas Turbines and Power 99, 309-319.

Smith S.H. and Mungal M.G., 1998. Mixing, structure and scaling of the jet in crossflow. Journal of Fluid Mechanics 357, 83-122.

Spangler C.A., Hilbing J.H. and Heister S.D., 1995. Nonlinear modeling of jet atomization in the wind-induced regime. Physics of Fluids 7(5), 964-971.

Spichtinger N., Wenig M., James P., Wagner T., Platt U. and Stohl A., 2001. Satellite detection of a continental scale plume of nitrogen oxides from boreal forest fires. Geophysical Research Letters 28(24), 4579-4582.

Stechishen E. and Murray W.G., 1988. Effectiveness of foam as a fire suppressant. pp. 123-136. In: Proceedings of the 1st Interior West Fire Council Annual Meeting and Workshop on the Art and Science of Fire Management. 24-27 October 1988. Kananaskis Village, Alberta, Canada. Forestry Canada, Information Report NOR-X-309. 333 pp.

Stechishen E., 1976. Cascading Fire-Trol 931 fire retardant into a jack pine stand. Information Report FF-X-58. Forest Fire Research Institute, Canadian Forestry Service. Ottawa, Canada. 18 pp.

Storr G.J. and Behnia M., 1999. Experiments with large diameter gravity driven impacting liquid jets. Experiments in Fluids 27, 60-69.

Strickland B.G., 1984. Reducing the cost of fire retardants. In: Proceedings of the 2nd International Scientific-Technical Symposium on Progress in Fighting Fires and Catastrophes from the Air. March 1984. Bremen, Germany. Deutscher Gemeindeverlag - Verlag W. Kohlhammer. 268 pp.

Stroppiana D., Boschetti M., Confalonieri R., Bocchi S. and Brivio P.A., 2006. Evaluation of LAI-2000 for leaf area index monitoring in paddy rice. Field Crops Research 99, 167-170.

Stull R.B., 1988. An Introduction to Boundary Layer Meteorology. Kluwer Academic Publishers. Dordrecht, The Netherlands. 666 pp.

Su H.-B., Shaw R.H., Paw U K.T., Moeng C.-H. and Sullivan P.P., 1998. Turbulent statistics of neutrally stratified flow within and above a sparse forest from large-eddy simulation and field observations. Boundary-Layer Meteorology 88, 363-97.

Su T.F., Patterson M.A., Reitz R.D. and Farrell P.V., 1996. Experimental and numerical studies of high pressure multiple injection sprays. SAE Technical Paper 960861, Society of Automotive Engineers. Warrendale, PA.

Suter A., 2000. Drop testing airtankers: a discussion of the cup-and-grid method. Technical Report. 0057-2868-MTDC. US Department of Agriculture, Forest Service (USDA-FS). Missoula Technology and Development Center. Missoula, MT, US. 14 pp.

Suter A., 2003. Aerial delivery systems - User information. Conventional aerial delivery systems. US Department of Agriculture, Forest Service (USDA-FS), Wildland Fire Chemical Systems (WFCS). 2 pp.

Suter A., 2006. Aerial delivery systems - User information. Modular Aerial Fire Fighting System (MAFFS). US Department of Agriculture, Forest Service (USDA-FS), Wildland Fire Chemical Systems (WFCS). 1 pp.

Swanson D.H. and Helvig T.N., 1973. High-altitude retardant drop mechanization study. Final report, vol. 1. Contract 26-2888, 30 April 1973, Honeywell Inc., Government and Aeronautical Products Division. Hopkins, Minnesota, US.

Swanson D.H. and Helvig T.N., 1974. Extended high-altitude retardant drop mechanization study. Final report, contract 26-2888, 10 January 1974, Honeywell Inc., Government and Aeronautical Products Division. Hopkins, Minnesota, US.

Swanson D.H., Luedecke A.D., Helvig T.N. and Parduhn F.J., 1975. Development of user guidelines for selected retardant aircraft. Final report, contract 26-3332, 15 February 1975, Honeywell Inc., Government and Aeronautical Products Division. Hopkins, Minnesota, US. 167 pp.

Swanson D.H., Luedecke A.D., Helvig T.N. and Parduhn F.J., 1977. Supplement to development of user guidelines for selected retardant aircraft. Final report, contract 26-3332, April 1977, Honeywell Inc., Government and Aeronautical Products Division. Hopkins, Minnesota, US. 88 pp.

Swanson D.H., Luedecke A.D. and Helvig T.N., 1978. Experimental tank and gating system (ETAGS). Final report, contract 26-3425, 1 September 1978, Honeywell Inc., Government and Aeronautical Products Division. Hopkins, Minnesota, US. 62 pp.

Tanner F.X., 1998. Liquid jet atomization and droplet breakup modeling of non-evaporating diesel fuel sprays. SAE Technical Paper 970050.

Tanner F.X., 2003. A cascade atomization and drop breakup model for the simulation of high-pressure liquid jets. SAE Paper 2003-01-1044.

Tansey K., Grégoire J-M., Pereira J.M.C., Defourny P., Leigh R., Pekel J-F., Barros A., Silva J., van Bogaert E., Bartholomé E. and Bontemps S., 2007. L3JRC - A global, multi-year (2000-2007) burnt area product (1 km resolution and daily time steps). In: Proceedings of the Remote Sensing and Photogrammetry Society Annual Conference 2007. 11-14 September 2007. Newcastle upon Tyne, UK.

Teske M.E., Bowers J.F., Rafferty J.E. and Barry J.W., 1993. FSCBG: an aerial spray dispersion model for predicting the fate of released material behind aircraft. Environmental Toxicology and Chemistry 12, 453-464.

Teske M.E., Bird S.L., Esterly D.M., Ray S.L. and Perry S.G., 1997. A user's guide for AgDRIFT 1.0: a tiered approach for the assessment of spray drift of pesticides. Technical Note N.º 95-10. Continuum Dynamics, Inc. Princeton, NJ.

Teske M.E., Kaufman A.E. and Johnson G.M., 1999. Collapsing bucket drop test data with a Lagrangian model. In: Proceedings of the ILASS Americas 12th Annual Conference on Liquid Atomization and Spray Systems. May 1999. Indianapolis, US.

Teske M.E. and Thistle H.W., 2004. A library of forest canopy structure for use in interception modelling. Forest Ecology and Management 198(1-3), 341-350.

Thom A.S., 1971. Momentum absorption by vegetation. Quarterly Journal of the Royal Meteorological Society 97, 414-428.

Thom A.S., Stewart J.B., Oliver H.R. and Gash J.H.C., 1975. Comparison of aerodynamic and energy budget estimates of fluxes over a pine forest. Quarterly Journal of the Royal Meteorological Society 101, 93-105.

Tomé M., 2004. Modelação da nuvem de retardante químico: Optimização no combate aos fogos florestais. Ph.D. Dissertation. University of Aveiro, Department of Environment and Planning. Aveiro, Portugal. 196 pp.

Tomé M. and Borrego C., 2002. Fighting wildfires with retardants applied with airplanes. In: Proceedings of the IV International Conference on Forest Fire Research. 18-23 November 2002. Luso, Portugal – Forest Fire Research & Wildland Fire Safety. Viegas D.X. (Ed.). Millpress, Rotterdam. Proceedings on CD-ROM.

Torres D.J. and Trujillo M.F., 2006. KIVA-4: an unstructured ALE code for compressible gas flow with sprays. Journal of Computational Physics 219(2), 943-975.

UA/NTUA/CEREN, 2005. An assessment of the impacts on the air of the use of retardants. University of Aveiro (UA), National Technical University of Athens (NTUA), Centre d'Essais et de Recherche de l'Entente (CEREN). Deliverable D25 of ERAS Project (contract EVG1-CT-2001-00039).

Uchijima Z. and Wright J.L., 1964. An experimental study of air flow in a corn plant-air layer. Bulletin of the National Institute of Agricultural Sciences (Japan), Ser. A. 11, 19-65.

USDA-FS, 2001. History of smokejumping. National smokejumper training guide – Chapter 1. US Department of Agriculture, Forest Service (USDA-FS). 15 pp.

USDA-FS, 2007a. Long-term retardant, wildland firefighting; Specification 5100-304c; June 1, 2007. US Department of Agriculture, Forest Service (USDA-FS). 29 pp.

USDA-FS, 2007b. Specification for fire suppressant foam for wildland firefighting (Class A foam); Specification 5100-307a; June 1, 2007. US Department of Agriculture, Forest Service (USDA-FS). 32 pp.

USDA-FS, 2007c. Specification for water enhancers (gels) for wildland firefighting; Specification 5100-306a; June 1, 2007. US Department of Agriculture, Forest Service (USDA-FS). 39 pp.

USEPA, 1999. User's guide for the AERMOD meteorological pre-processor (AERMET) - Revised draft. US Environmental Protection Agency (USEPA), Office of Air Quality Planning and Standards. Research Triangle Park, North Carolina, US. 273 pp.

Valente F., 1999. Intercepção da precipitação em povoamentos florestais esparsos. Modelação do processo e características aerodinâmicas dos cobertos molhados. Ph.D. Dissertation. Universidade Técnica de Lisboa, Instituto Superior de Agronomia. Lisbon, Portugal. 172 pp.

Van Meter W.P., 1983. Using rheology to estimate short-term retardant droplet sizes. Research Note INT-327. US Department of Agriculture, Forest Service (USDA-FS), Intermountain Forest and Range Experiment Station. Ogden, Utah, US. 13 pp.

Van Meter W.P. and George C.W., 1981. Correlating laboratory air drop data with retardant rheological properties. Research Paper INT-278. US Department of Agriculture, Forest Service (USDA-FS), Intermountain Forest and Range Experiment Station. Ogden, Utah, US. 12 pp.

Vandersall H.L., 1994. Air attack: retardants, rheology and some new options. International Journal of Wildland Fire 4(1), 45-51.

Varga C.M., Lasheras J.C. and Hopfinger E.J., 2003. Initial breakup of a small-diameter liquid jet by a high-speed gas stream. Journal of Fluid Mechanics 497, 405-434.

Vélez R. (Ed.), 2000. La Defensa Contra Incendios Forestales. Fundamentos Y Experiencias. McGrawHill. Madrid, Spain. 1360 pp.

Vich G. and Ledoux M., 1997. Investigation of a liquid jet in a subsonic cross flow. In: Proceedings of the ICLASS. 23-30.

Wang D.P., 1968. Finite amplitude effect on the stability of a jet of circular cross-section. Journal of Fluid Mechanics 34(2), 299-313.

Ward D., Rothermel R. and Bushey C., 1993. Particulate matter and trace gas emissions from the Canyon Creek Fire of 1988. In: Proceedings of the 12th Fire and Forest Meteorology. Georgia, US. Society of American Foresters (Eds.). 62-76.

Warren C.R. and Adams M.A., 2001. Distribution of N, Rubisco and photosynthesis in *Pinus pinaster* and acclimation to light. Plant, Cell and Environment 24, 597-609.

Watson D.J., 1947. Comparative physiological studies in the growth of field crops. I. Variation in net assimilation rate and leaf area between species and varieties, and within and between years. Annals of Botany 11, 41-76.

Weiss M., Baret F., Smith G.J., Jonckheere I. and Coppin P., 2004. Review of methods for in situ leaf area index (LAI) determination. Part II. Estimation of LAI, errors and sampling. Agricultural and Forest Meteorology 121, 37-53.

Wesely M.L. and Hicks B.B., 2000. A review of the current status of knowledge on dry deposition. Atmospheric Environment 34, 2261-2282.

WFCS, 2007. Wildland fire chemical products - Effect on structures. US Department of Agriculture, Forest Service (USDA-FS), Wildland Fire Chemical Systems (WFCS). 1 pp.

WHO 2007. The world health report 2007 - A safer future: global public health security in the 21st century. World Health Organization (WHO). Geneva, Switzerland. 72 pp.

WHO/UNEP/WMO 1999. Health guidelines for vegetation fire events - Guideline document. Schwela D., Goldammer J.G., Morawska L., Simpson O. (Eds.). World Health Organization (WHO), Geneva; United Nations Environment Programme (UNEP), Nairobi; World Meteorological Organization (WMO), Geneva. WHO/UNEP/WMO Expert Task Force Meeting, 6-9 October 1998, Lima, Peru.

Wilson J.D., 1988. A second order closure model for flow through vegetation. Boundary-Layer Meteorology 42, 371-392.

Wilson N.R. and Shaw R.H., 1977. A higher order closure model for canopy flow. Journal of Applied Meteorology 16, 1198-1205.

Wilson J.D., Ward D.P., Thurtell G.W. and Kidd G.E., 1982. Statistics of atmospheric turbulence within and above a corn canopy. Boundary-Layer Meteorology 24, 495-519.

Wotowa G. and Trainer M., 2000. The influence of Canadian forest fires on pollutant concentrations in the United States. Science 288, 324-328.

Wright J.L. and Lemon E.R., 1966. Photosynthesis under field conditions. VIII. Analysis of windspeed fluctuation data to evaluate turbulent exchange within a corn crop. Agronomy Journal 58, 255-261.

Wu P.-K., Ruff G.A. and Faeth G.M., 1991. Primary breakup in liquid/gas mixing layers. Atomization and Sprays 1, 421-440.

Wu P.-K., Tseng L.-K. and Faeth G.M., 1992. Primary breakup in gas/liquid mixing layers for turbulent liquids. Atomization and Sprays 2, 295-317.

Wu P.-K. and Faeth G.M., 1993. Aerodynamic effects on primary breakup of turbulent liquids. Atomization and Sprays 3, 265-289.

Wu P.-K. and Faeth G.M., 1995. Onset and end of drop formation along the surface of turbulent liquid jets in still gases. Physics of Fluids A7, 2915-2917.

Wu P.-K., Miranda R.F. and Faeth G.M., 1995. Effects of initial flow conditions on primary breakup of nonturbulent and turbulent round liquid jets. Atomization and Sprays 5, 175-196.

Wu P.K., Kirkendall K.A., Fuller R.P. and Nejad A.S., 1997. Breakup processes of liquid jets in subsonic crossflows. Journal of Propulsion and Power 13, 64-73.

Xanthopoulos G., 2003. Chemicals against forest fires: infrastructure and application means, new technologies. In: Proceedings of the International Seminar for the Use of chemicals, retardants and foams, in forest fire fighting from the air and on the ground. 23-25 October 1995. Rethymno, Crete, Greece. (Extended and improved in 2003 as part of the ERAS research project) 16 pp.

Xanthopoulos G., 2007. Forest fire related deaths in Greece: confirming what we already know. In: Proceedings of the 4th International Wildland Fire Conference - Wildfire 2007. 13-17 May 2007. Seville, Spain. Proceedings on CD-ROM.

Xanthopoulos G., Varela V., Fernandes P., Ribeiro L. and Guarnieri F., 2003. Decision support systems and tools: a state of the art. Deliverable D-06-02 of EUFIRELAB project (contract EVR1-CT-2002-40028). 41 pp.

Xanthopoulos G., Ghosn D. and Kazakis G., 2005. Weathering effects of wind and of rain on fire retardant. Part I: Evaluation of forest fire retardant removal from forest fuels by rainfall. Deliverable D 12 - Part I of ERAS project (contract EVG1-CT-2001-00039).

Yarin A.L., 1993. Free Liquid Jets and Films: Hydrodynamics and Rheology. Longman Scientific & Technical and Wiley & Sons. Harlow, New York. 446 pp.

Yoon S.S. and Heister S.D., 2003. Categorizing linear theories for atomizing round jets. Atomization and Sprays 13, 499-516.

Yu H. and Girimaji S.S., 2005. Near-field turbulent simulations of rectangular jets using lattice Boltzmann method. Physics of Fluids 17, 125106-1–125106-17.

Websites:

url 1. http://www.wildlandfire.com

url 2. http://www.euspaceimaging.com

url 3. http://www.fire.uni-freiburg.de/emergency/ger.htm

url 4. http://www.martinmars.com

url 5. http://www.ericksonaircrane.com

url 6. http://www.302aw.afrc.af.mil

url 7. http://www.boeing.com

url 8. http://www.phoschek.com

url 9. http://www.firetrolcanada.com

url 10. http://www.icl-perfproductslp.com

url 11. http://www.biogema.fr

url 12. http://www.wildsentry.org

url 13. http://www.garrco.com

url 14. http://ehasl.cvmbs.colostate.edu

url 15. http://c-h2oecology.env.duke.edu/site/images.html

url 16. http://www.cmar.csiro.au/ozflux/monitoringsites/tumbarumba/index.html

url 17. http://www.tracker-france.com

A. Annex

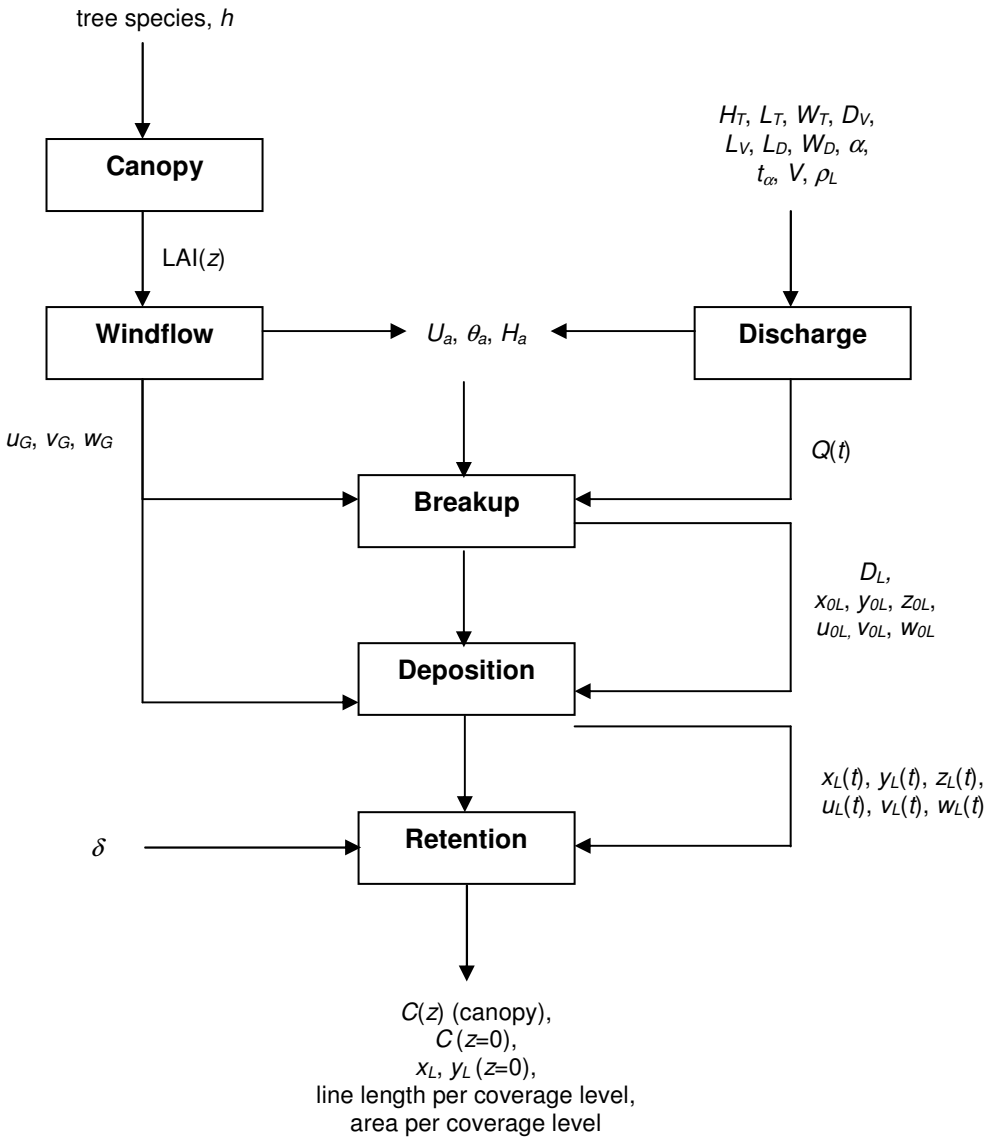

Figure A-1. ADM fluxogram showing the different modules and the main input data, data transferred between modules and output data.

Table A-1. Retardant classification based on viscosity range and application conditions and objective [Vandersall, 1994].

Retardant type	Viscosity range (cP)	Situation
No viscosity (water-like)	< 60	Gentle terrain Low drop height (15 – 30 m) Low wind conditions Slow moving fire Light fuel loading Fire in tundra, peat and duff Mop-up
Low viscosity	60 – 250	Gentle terrain Low drop height (30 – 60 m) Low to medium wind conditions Ground firebeneath overstory Standing grassy fuel Moderate fuel loading Mixed fuels including duff Evaluate alternative to water-like
Medium viscosity	250 – 1000	Broken terrain Higher drop height (60 – 75 m) Higher wind conditions Brush below understory Ladder fuels Evaluate alternative to high viscosity
High viscosity	> 1000	Extreme conditions in: - topography - drop height (> 75 m) - wind conditions - fire intensity - fuels characteristics and loading MAFFS operations

Table A-2. Field and wind-tunnel measurements of flows on different types of canopies.

Reference	Canopy type
Field measurements on natural canopies	
Baldocchi and Meyers [1988], Shaw et al. [1988]	deciduous forests
Denmead and Bradley [1987], Amiro [1990]	pine forests
Raupach et al. [1996]	eucalypt forests
Amiro [1990]	aspen forests
Amiro [1990], Gardiner [1994]	spruce forests
Wilson et al. [1982], Meyers and Paw U [1986]	corn canopies
Wind-tunnel measurements on artificial canopies	
Plate and Quraishi [1965], Kawatani and Meroney [1970]	wood pegs and plastic strips
Meroney [1968], Hsi and Nath [1970]	artificial plastic trees
Seginer et al. [1976]	rods
Raupach et al. [1986]	rigid strips
Brunet et al. [1994]	aeroelastic wheat model
Novak et al. [2000]	spruce artificial tree branches
Marshall et al. [2002]	aeroelastic spruce model trees
Aubrun and Leitl [2004], Aubrun et al. [2005]	model of a typical European forest made of a mesh of metallic rings
Gromke and Ruck [2007]	models of idealized street-canyon urban trees with varying permeability

Table A-3. Parameters describing sampled canopies of *Pinus pinaster* Ait., *Eucalyptus globulus* Labill. and *Quercus suber* L.

Site location	Species	Height (m)	*LAI* ($m^2.m^{-2}$)	Age (years)	Plantation	Stands density (ha^{-1})	Reference
Wickepin, SW Australia (32º78´S, 117º56'E)	*Pinus pinaster* Ait.	10	1.6	12	-	500	Warren and Adams [2001]
Le Bray, SW France (44º43´N, 0º46´W)		13.5	2.8	19	Managed	-	Irvine and Brunet [1996]
		15	2.7	21			
		15.6	2.6	22			
		16.3	3.5	25			
Sabres, SW France (44º12´N, 0º42´W)		24	2.1	40	-	-	
Pinhal da Carrasqueira (38º50´N, 8º51´W)		23.9	2.7	59	Unmanaged	312	Valente [1999]
Herdade de Espirra (38º38´N, 8º36´W)	*Eucalyptus globulus* Labill.	16.5	3.2	6	-	983	
Tiradero site, Los Alcornocales Natural Park, S Spain (36º9´46´´N, 5º35'39''W)	*Quercus suber* L.	-	2.26	-	-	-	Quilchano et al. [2008]
Buenas Noches site, Los Alcornocales Natural Park, S Spain (36º22´56´´N, 5º34'57''W)			1.64				
Panera site, Los Alcornocales Natural Park, S Spain (36º31´54´´N, 5º34'29''W)			1.84				

Table A-4. Statistical parameters for the assessment of modelling performance. S_i is the i^{th} simulated value; M_i is the i^{th} measured value and x is the quantity under analysis [Abramowitz and Stegun, 1972; ASTM International, 2000; Chang and Hanna, 2005].

Statistical parameters	Equation	Model acceptance criteria [s]	Ideal values	Units
Average bias	$d = \overline{d_i} = \overline{M_i - S_i}$	—	—	[x]
Geometric mean bias	$MG = \exp\left(\overline{\ln M_i} - \overline{\ln S_i}\right)$	$0.7 < MG < 1.3$	1.0	[x]
Geometric variance	$VG = \exp\left[\overline{(\ln M_i - \ln S_i)^2}\right]$	$VG < 4$	1.0	[x^2]
Fractional bias	$FB = \dfrac{\sum_i (M_i - S_i)}{0.5 \cdot \sum_i (M_i + S_i)}$	$\lvert FB \rvert < 0.3$	0.0	—
Normalized mean squared error	$NMSE = \dfrac{\overline{(M_i - S_i)^2}}{\overline{M}\,\overline{S}}$	NMSE < 1.5	0.0	—
Percentage error	$\delta x = \left(\dfrac{M_i - S_i}{M_i}\right) \times 100$	$\lvert \delta x \rvert < 10$	0.0	%
Pearson correlation coefficient	$r = \dfrac{\sum (M_i - \overline{M})(S_i - \overline{S})}{\left[\sum (M_i - \overline{M})^2 \cdot \sum (S_i - \overline{S})^2\right]^{1/2}}$	Undefined	1.0	—
Factor of two	$FAC2$: fraction of data that satisfy : $0.5 \le \dfrac{S_i}{M_i} \le 2.0$	$FAC2 > 0.5$	1.0	—

[s] The limit values for all the criteria presented, except for the percentage error, represent typical thresholds on air quality modelling studies [Chang and Hanna, 2005]. The 10% limit defined for the modulus of the percentage error has been used as a quality requirement by the USDA-FS for aerial dropping models [R. Becker, pers. communication]. When comparing to the limit value defined for NMSE, the 10% maximum is a much more stringent performance criterion for a model to satisfy.